

Remaining Strength Assessment of Deteriorating Energy Pipelines

by

© Bipul Chandra Mondal

A thesis submitted to the

School of Graduate Studies

in partial fulfillment of the requirement for the degree of

Doctor of Philosophy (Civil Engineering)

Faculty of Engineering & Applied Science

Memorial University of Newfoundland

October 2018

St. John's, Newfoundland, Canada

ABSTRACT

Pipelines are extensively used as the most economic means of transporting oil and gas. The steel pipelines have been widely used for these applications due to the high strength to weight ratio of the material, resulting in lower material cost. These pipelines are subjected to corruptions during the service life, resulting in the reduction of wall thicknesses. The prediction of the remaining strength of a corroded pipeline is required for fitness-for-purpose assessment. For the prediction of the remaining strength, different models were developed based on simplified results of analysis and/or empirical fits to limited experimental data which are expressed in terms of burst pressure. The established design codes adopt simplified design equations for the burst pressure prediction for corroded pipelines. However, the burst pressures predicted using the simplified equations are not consistent with the burst test results and results obtained from rigorous finite element (FE) analyses. Besides, the pipelines are often subjected to axial force and bending moment. The effects of the axial force and bending moment on the burst pressure are not rationally accounted. In this research, the axial forces and bending moments experience by energy pipelines are first examined considering a case of offshore pipelines. The improved burst pressure models are then developed for pipelines with and without the axial forces and bending moments. The existing models of burst pressures for deteriorated-steel pipelines are investigated to determine the contributing parameters to the burst pressures. The Folias factor and flow stress are identified as the major parameters contributing to the burst pressures of the corroded pipelines. A detailed study, based on FE analysis using Abaqus, has been carried out to develop a new method of defining the Folias factor and to

develop an improved model for burst pressure prediction for a corroded pipeline. The finite element analysis is then extended to develop the new interaction rules for the pipelines subjected to multiple patches of the corrosion defects. The FE analysis is used to develop failure loci for burst pressure prediction for pipelines subjected to axial forces and bending moments. Corroded pipelines often suffer from the stress corrosion cracking (SCC) when the pipelines in corrosive environments are subjected to high tensile stresses. The SCC occurs at a stress intensity factor well below the fracture toughness of the material. The effects of the SCC and the crack propagation in the deteriorating pipelines cannot be captured using standard FE modeling techniques. It is proposed to employ fracture mechanics to determine the remaining strengths of pipelines containing corrosion defects or crack-like defects or corrosion with crack-like defects.

ACKNOWLEDGEMENTS

First of all, I would like to take the opportunity to acknowledge the contributions of many individuals whose helps were instrumental in completion of this thesis. I would like to express my sincere and heartfelt gratitude to **Dr. Ashutosh Sutra Dhar** for his proper guidance and valuable suggestions, sincere supervision and co-operation throughout the research work.

I would also like to thank my supervisory committee members, **Dr. Amgad Hussein** and **Dr. Seshu Adluri**, for their valuable comments. The supports provided from a fellow PhD student, **Mr. Hieu Chi Phan** during analysis are acknowledged.

I would like to thank Husky Energy for helping me at different stages during my research work by providing some valuable information about the seabed, offshore Newfoundland.

The funding provided by President's Doctoral Student Investment Fund, School of Graduate Studies, Innovate NL (former Research and Development Corporation of NL) and Mitacs-Accelerate Internship Program are gratefully acknowledged.

I would like to dedicate this thesis to my father Late **Mr. Binod Behari Mondal** who passed away on February 3, 2016 when I was in the second year of my PhD program at MUN. Finally, I would like to express my deep sense of gratitude and indebtedness to my mother, my wife, my son and my little daughter for their encouragements, patience and moral supports throughout the tenure of the research work.

Table of Contents

ABSTRACT.....	ii
ACKNOWLEDGEMENTS	iv
Chapter 1	1
Introduction	1
1.1 Background.....	1
1.2 Rationale for the current study	5
1.3 Research Objectives and Scope	6
1.4 Outline of the Research Methodology	7
1.5 Organization of the Thesis.....	10
Chapter 2.....	12
Literature Review	12
2.1 General.....	12
2.2 Existing Burst Pressure Models.....	13
2.2.1 Folias Factor.....	18
2.2.2 Evaluation of Burst Pressure Models.....	19
2.3 Interaction of Multiple Corrosion Defects.....	21
2.4 Pipelines Subjected to Axial force and Bending Moment.....	25
2.5 Application of Fracture Mechanics	29

Chapter 3	33
Loading Conditions Experienced by Surface-Laid Offshore Pipeline.....	33
3.1 Introduction	33
3.2 Seabed Profile.....	37
3.3 Shape of Initial Imperfection	38
3.4 FE Analysis.....	40
3.5 Effects of Seabed Profile	45
3.5.1 Initial Shapes of Pipelines.....	45
3.5.2 Effect of Initial Shape	45
3.5.3 Installation Stress	49
3.6. Parametric study	51
3.6.1 Flexural Stiffness of Pipeline.....	51
3.6.2 Seabed Soil Parameters.....	52
3.6.3 Temperature and Pressure Loads	53
3.7. Optimum Height of Imperfection	58
3.8 Internal Forces Developed during Upheaval Buckling	60
3.8.1 Axial Force and Bending Moment.....	60
3.9. Summery	61
Chapter 4.....	65

Finite-Element Evaluation of Burst Pressure Models for Corroded Pipelines.....	65
4.1 Introduction	65
4.2 Burst Pressure Models	67
4.3 Finite Element Modeling (FEM)	68
4.3.1 Geometry and Boundary Conditions	68
4.3.2 Material Modeling	71
4.3.3 Validation of FEM	73
4.4 Stress/Strain Localization	76
4.5 Comparison of Burst Pressures.....	78
4.6 Folias Factor	82
4.7 Summary.....	85
Chapter 5	87
Improved Folias Factor and Burst Pressure Models for Corroded Pipelines	87
5.1 Introduction	87
5.2 Folias Factor	91
5.3 FE Model Development.....	94
5.4 Folias Factor from FE Analysis.....	99
5.5 Determination of Model Constants/Model Parameters	100
5.6 Evaluation of the Developed Models for the Folias Factor	103

5.7 Revision of Burst Pressure Model	104
5.7.1 Comparison with Design Codes.....	108
5.7.2 Comparison with Burst Test Results.....	109
5.8 Summary.....	110
Chapter 6.....	116
Interaction of multiple corrosion defects on burst pressure of pipelines	116
6.1 Introduction	116
6.2 Interaction Rule	118
6.3 Finite Element Analysis.....	122
6.3.1 FE Model	122
6.3.2 Material Parameters	125
6.3.3 Validation of FE Model	128
6.4 Results and Discussions.....	131
6.4.1 Interaction of corrosion patches.....	131
6.4.1.1 Pipe Geometry.....	135
6.4.1.2 Locations of Corrosion Patches.....	136
6.4.1.3 Depth of Corrosion Patches	136
6.4.2 New Interaction Rule	139
6.5 Summary.....	143

Chapter 7	145
Burst Pressure of Corroded Pipelines Considering Combined Axial Forces and Bending Moments	145
7.1 Introduction	145
7.2 FE Model	148
7.2.1 Material Model.....	152
7.2.2 Failure Criteria	153
7.2.3 Validation of FE Model	154
7.3 Effects of Axial Force or Bending Moment	156
7.4 Development of Failure Loci.....	161
7.4.1 Corrosion Depth.....	163
7.4.2 Corrosion Length	165
7.4.3 Pipe Dimensions	166
7.5 Failure Loci.....	167
7.7 Summary.....	169
Chapter 8	173
Burst Pressure Assessment of Corroded Pipelines using Fracture Mechanics Criterion	173
8.1 Introduction	173

8.2 FE Model Development.....	179
8.2.1 Pipe Geometry	179
8.2.2 Material Model.....	184
8.3 <i>J</i> -integral based Burst Pressure Assessment.....	186
8.3.1 Crack-in-corrosion (CIC) defect	186
8.3.2 Corrosion only defect.....	188
8.3.3 Comparison with Existing Burst Pressure Models	195
8.3.4 Pipeline containing Crack-Like Defect.....	196
8.4 Parametric Study on CIC pipe	199
8.4.1 Effect of Crack Depth	202
8.4.2 Effect of Crack Length.....	206
8.9 Summary.....	208
Chapter 9.....	211
Conclusion and Future Work	211
9.1 Overview	211
9.1.1 Forces Experienced by Surface-Laid Offshore Pipelines	212
9.1.2 Existing Burst Pressure Models	212
9.1.3 Improved Burst Pressure Models.....	213
9.1.4 Interaction of multiple corrosion defects	214

9.1.5 Effects of Axial Forces and Bending Moments	215
9.1.6 Application of Fracture Criterion.....	216
9.2 Recommendations for Future Work	217
9.2.1 Effect of Loads.....	217
9.2.2 Interacting Defects	217
9.2.3 Application of Fracture Mechanics.....	218
9.2.4 Study on Buried Pipelines.....	218
References	219
Appendix I.....	231
Appendix II	238
Appendix III	248

List of figures

Figure 1.1: Offshore Pipelines (Guo et al. 2014).....	2
Figure 1.2: Multiple corrosions on inner surface of a pipe wall (Sykes 2012).....	4
Figure 2.1: Comparison of Folias factors obtained from FE analysis and design codes ..	21
Figure 2.2: Failure Locus for Combined Internal Pressure and Bending Moment (Chauhan and Swankie 2010)	27
Figure 2.3: Evaluation of H_I (DNV-RP-F101 2015).....	29
Figure 3.1: Seabed profile from offshore Newfoundland.....	39
Figure 3.2: Effect of soil model on the upheaval buckling [$H=1000$ mm, $t=18.3$ mm] ..	42
Figure 3.3: Pipeline placed at the crest of the seabed prop.....	44
Figure 3.4: Comparison of initial shapes of pipe.....	46
Figure 3.5: Effect of initial shapes on upheaval buckling	48
Figure 3.6: Effect of installation stress on critical temperature and critical pressure.....	50
Figure 3.7: Effect of flexural stiffness of pipeline.....	52
Figure 3.8: Effect of foundation soil properties on upheaval buckling	54
Figure 3.9: Pipe deflection with different method of idealization.....	56
Figure 3.10: Effect of imperfection height on upheaval buckling behavior.....	57
Figure 3.11: Relation between temperature and pressure with respect to out of straightness.....	59
Figure 3.12: Forces in pipe wall at the crest of undulation.....	62
Figure 3.13: Forces in pipe wall for different imperfection heights	63
Figure 4.1: Idealization of corrosion.....	70

Figure 4.2: Finite element mesh	72
Figure 4.3: Stress-strain relations for pipe materials (Pipe A, C and D)	73
Figure 4.4: Burst Pressure Calculation using FEM (Pipe A1).....	75
Figure 4.5: Effect of the edge shape of corrosion [$D=324\text{mm}$, $d/t=0.40$, $l=528\text{mm}$].....	76
Figure 4.6: Deformation of cross-section at the mid-section of corroded area [Deformation is exaggerated by 50 times]	77
Figure 4.7: Contours of von Mises stress and principal plastic strain ($D=324\text{mm}$, $d/t=0.70$, $l/D= 1.63$ and internal pressure = $0.66P_{burst}$).....	78
Figure 4.8: Comparison of burst pressures	80
Figure 4.9: Comparison of burst pressure reduction factors.....	81
Figure 4.10: Folias factors	84
Figure 5.1: Comparison of Folias factors obtained from FE analysis and design codes (After Mondal and Dhar 2016a)	90
Figure 5.2: Typical Finite Element Mesh	95
Figure 5.3: von Mises stress and the location of failure	98
Figure 5.4: Variations of the Folias factor	100
Figure 5.5: Comparison of Folias factors	105
Figure 5.6: Folias factors with depth of corrosion defect	106
Figure 5.7: Comparison of burst pressure predicted using the proposed model and FE results	108
Figure 5.8: Comparison of burst pressure obtained from different models.....	110
Figure 5.9: Comparison of proposed burst pressure model with test results	112

Figure 6.1: Type 1 Interaction (Redrawn after DNV-RP-F101)	119
Figure 6.2: Type 2 Interaction (Redrawn after DNV-RP-F101) 2015)	120
Figure 6.3: Type 3 Interaction (Redrawn after DNV-RP-F101)	120
Figure 6.4: Edge condition of corrosion patch	123
Figure 6.5: Stress-strain relation of pipe material (API 5L X60)	127
Figure 6.6: Effect of material model on burst pressure	127
Figure 6.7: A typical finite element mesh.....	128
Figure 6.8: Failure location of pipe containing single corrosion defect	130
Figure 6.9: Location of failure observed in a full-scale pipe test (After Benjamin et al. 2005)	130
Figure 6.10: Effect of interaction of longitudinally and diagonally spaced corrosion patches ($l=60\text{mm}$, $w=20^\circ$, $d/t=0.50$)	133
Figure 6.11: Effect of interaction of circumferentially spaced corrosion patches ($l=60\text{mm}$, $w=20^\circ$, $d/t=0.50$)	134
Figure 6.12: Effect of corrosion depth on interaction ($D= 300\text{ mm}$, $l=60\text{ mm}$, $w=20$ degree).....	138
Figure 6.13: Distribution of von Mises stress through wall thickness.....	139
Figure 6.14: New Interaction Rule	141
Figure 6.15: Comparison of burst pressures with various interaction rules	143
Figure 7.1: Typical sectional view of corrosion patch (after Mondal and Dhar 2017b)	149
Figure 7.2: Quarter Model of Pipe with Boundary Conditions	150
Figure 7.3: Application of loadings on FE model	151

Figure 7.4: Typical meshing of FE model	152
Figure 7.5: True stress–strain data for API X65 steel (Oh et al. 2007)	153
Figure 7.6: Burst Pressure Calculation Using FEA	156
Figure 7.7: Effects of axial force and bending moment on burst pressure	159
Figure 7.8: Evaluation of DNV-RP-F101 (2015)	161
Figure 7.9: Comparison of failure locus developed by current study with Liu et al. (2009)	163
Figure 7.10: Effect of corrosion depth on failure locus	164
Figure 7.11: Effect of corrosion length on failure locus	165
Figure 7.12: Effect of pipe dimensions on failure locus	167
Figure 7.13: Failure Locus for d/t for 0.2	170
Figure 7.14: Failure Locus for d/t for 0.5	170
Figure 7.15: Failure Locus for d/t for 0.8	171
Figure 8.1: Arbitrary contour for the definition of J -integral	176
Figure 8.2: Measurement of crack tip opening displacement, δ	176
Figure 8.3: Sectional view of pipe with crack-in-corrosion (CIC) defect (Not to scale)	181
Figure 8.4: Sectional view of pipe with corrosion defect (Not to scale)	182
Figure 8.5: Half model of full pipeline with boundary conditions and loading	185
Figure 8.6: Typical meshing of FE model	186
Figure 8.7: True stress–strain curve of pipe steel, after Bedairi et al. (2012).....	187

Figure 8.8: Comparison of J -integral obtained from the current study and those from Bedairi et al. (2012)	190
Figure 8.9: Crack growth in corrosion only defect from XFEM	192
Figure 8.10: J -integral for pipe with corrosion only defect under internal pressure	193
Figure 8.11: Burst pressure estimation based on $J=51 \text{ kJ/m}^2$ criterion	194
Figure 8.12: Comparison of Burst Pressures	198
Figure 8.13: Schematic diagram of crack-like defect	199
Figure 8.14: Comparison of J -integral for corrosion defect and crack-like defect.....	200
Figure 8.15: Cross-section of pipe with CIC defect	201
Figure 8.16: Comparison of blunt crack and V-notch crack in CIC defect	201
Figure 8.17: Crack-like defect with sharp edge	202
Figure 8.18: J -integral of CIC defect with sharp crack edge and smooth crack edge ...	203
Figure 8.19: J -integral for pipe with CIC defect of different crack depths	204
Figure 8.20: Variation of J -integrals with crack depths of pipe with CIC defect.....	205
Figure 8.21: Effect of crack depth on burst pressure of pipe with CIC defects.....	207
Figure 8.22: J -integral of pipe with CIC defect with different crack lengths.....	208
Figure 8.23: Effect of crack dimensions on burst pressure of a pipe with CIC defect ..	209

List of tables

Table 2.1: Interaction Rules	23
Table 2.2: Parameters for calculating H_I	28
Table 3.1: Material Properties.....	43
Table 4.1: Pipe geometry and corrosion dimensions	71
Table 4.2: Mechanical properties of pipe materials	72
Table 4.3: Validation of burst pressure calculations.....	74
Table 4.4: Summary of burst pressures.....	79
Table 5.1: Models of Burst Pressure provided by codes.....	88
Table 5.2: Geometric Parameters of FE models	96
Table 5.3: Material Parameters used (API 5L X60 grade steel)	97
Table 5.4: FE database of burst pressures for corroded pipelines	101
Table 5.5: Model Parameters	103
Table 5.6: Database of Burst Test of Corroded Pipes.....	113
Table 6.1: Interaction Rule.....	121
Table 6.2: Pipes dimensions and corrosion geometries	124
Table 6.3: Material Properties.....	126
Table 6.4: Burst pressures for different edge conditions	132
Table 7.1: Material parameters of API X65 Steel (Oh et al. 2007)	153
Table 7.2: Dimensions of pipe and corrosion for FEM validation (Oh et al. 2007)	155
Table 7.3: Dimensions of pipe and corrosion defect after Liu et al. (2009)	158
Table 7.4: Parameters for calculation of H_I	160

Table 7.4: Dimensions of Pipe “A” and Pipe “B”	166
Table 8.1: Pipe dimensions and defect geometries	183
Table 8.2: Properties of Pipe Steel (Bedairi et al. 2012).....	185
Table 8.3: Dimensions of pipe and corrosion geometries used (after Bedairi et al. 2012)	191
Table 8.4: Comparison of Burst Pressures	195
Table 8.5: Dimensions of pipe and corrosion geometries.....	197

List of symbols

D, D_0 = Outer diameter of pipe

D_i = Inner diameter of pipe

L = Length of pipe used in FEA

t = Wall thickness

d = depth of corrosion defect

d_c = Crack depth

l = length of corrosion defect

l_c = Crack length

c, w = width of corrosion defect

H = Height of probe

θ = Change of temperature

y = Vertical deflection of pipe

r_y = radius of plastic zone around the crack tip

σ_Y = Specified minimum yield strength (*SMYS*)

σ_U = Specified minimum tensile strength (*SMTS*)

σ_{flow}, S_{flow} = Flow stress

σ_{ref} = Reference stress used for creep and plastic consideration

σ_t = Axial tensile stress

σ_a = Axial stress

σ_A = Axial stress developed by axial force, F_Z

σ_B = Axial stress developed by bending moment, M_X

ρ = Density of material

E = Young's Modulus of elasticity of pipe material

ν = Poisson's ration

ϵ_u = Strain at failure

α = Thermal expansion coefficient

β, n = Material constants used in Ramberg-Osgood equation

P_0 = Failure pressure of intake pipe

P = Failure pressure of pipe with defects

F_Z = Axial force

M = Bulging stress magnification factor/Folias factor

M_X = Bending moment

$$\lambda = \sqrt[4]{\frac{3(1 - \nu^2)l^4}{D^2 t^2}}$$

$f_e(\lambda)$ = Extensional coefficient

$f_b(\lambda)$ = Bending coefficient

$$\chi(\lambda) = \frac{\sigma_{bending}}{\sigma_{hoop}}$$

S_l = Longitudinal spacing between adjacent corrosion patches

S_c = Circumferential spacing between adjacent corrosion patches

$(S_l)_{lim}$ = Maximum longitudinal spacing between adjacent corrosion patches above which the corrosion patches are treated as single isolated patches

$(S_c)_{lim}$ = Maximum circumferential spacing between adjacent corrosion patches above which the corrosion patches are treated as single isolated patches

FE= Finite Element

FEA= Finite Element Analysis

FEM= Finite Element Model

RMSD= Root-mean-square-deviation

P_{com} = Burst pressure of corroded pipe subjected to combined loadings

P_o = Burst pressure of intake pipeline

M_{com} = Moment capacity of corroded pipe subjected to combined loadings

M_o = Moment capacity of intake pipeline

F_{com} = Axial force capacity of corroded pipe subjected to combined loadings

F_o = Axial force capacity intake pipeline

CHAPTER 1

Introduction

1.1 Background

The offshore and onshore oil and gas development activities have been growing rapidly over the last few decades to meet the global energy demands. Pipelines play a very important role in these activities through transporting the products of hydrocarbon from the wellheads to the platforms, between the platforms, and to the end users. Pipelines are also used for transporting municipal water and waste water, and for other industrial applications. Pipelines are made of different materials including steel, pre-stressed concrete and polymers. Steel pipelines are widely used in the oil and gas industries due to the high strength to weight ratio of the material, resulting in lower material cost. The size of the commonly used pipelines varies from 100 mm to 1500 mm (Mohitpour et al. 2003). The diameter to thickness ratios of the pipelines range from 10 to 75 (Guo et al. 2014). Depending on the thicknesses, the pipelines are classified as thick pipelines or thin pipelines. During analysis and design, separate assumptions are used for thick pipelines and thin pipelines. The network of pipelines used in the offshore oil and gas industries consists of several segments. Depending on the purposes, the pipelines, used at different segments, are classified as flowlines, infilled flowlines and export pipelines (Guo et al. 2014). The flowlines transport oil and/or gas from satellite subsea well to subsea manifolds to production facility platforms. These flowlines also transport water or chemicals from production facility platforms to injection wellheads. The infilled flowlines transport oil

and/or gas between production facility platforms. The export pipelines transport oil and/or gas from production facility platforms to onshore. The networking system of the above mentioned flowlines is schematically shown in Figure 1.1.

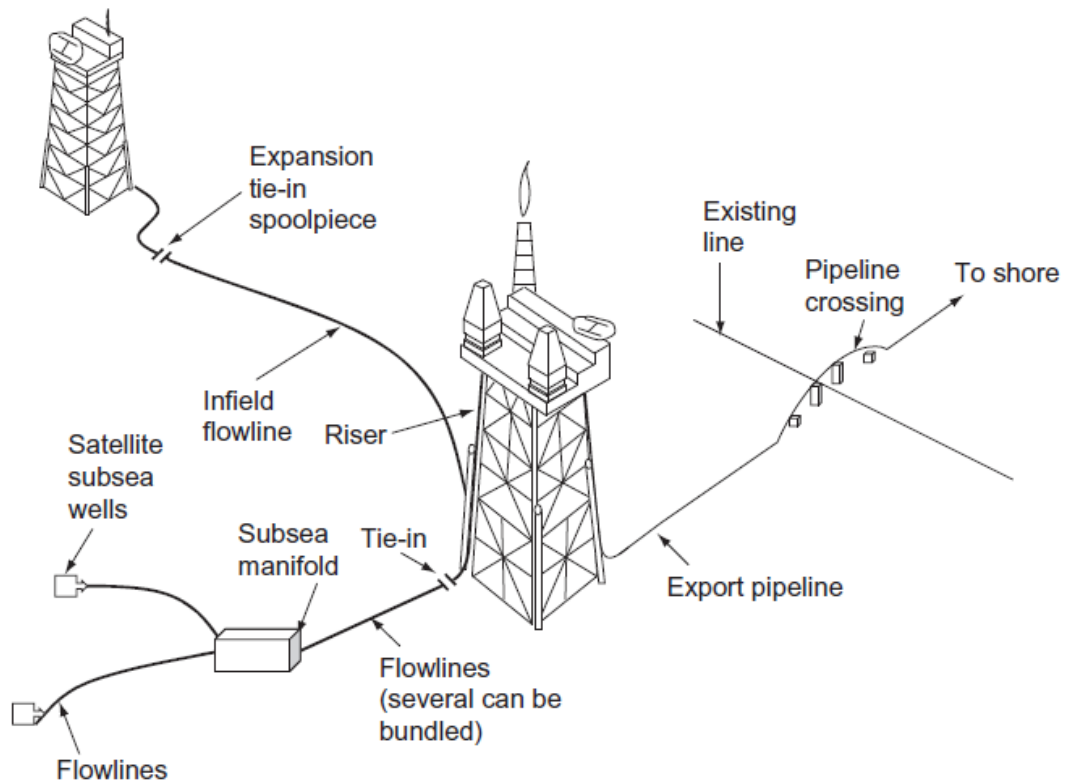


Figure 1.1: Offshore Pipelines (Guo et al. 2014)

The internal pressure exerted by the transported oil and/or gas is the primary loading in a pipeline during operation. Sometimes, the oil is transported with high temperature to avoid the consolidation of wax in oil and to ease of flow of oil through the pipelines. The temperature develops compressive axial force in the pipe wall when the pipeline is restrained in the longitudinal direction.

The unburied offshore pipelines are sometimes laid on the seabed having undulations in the vertical profile. The offshore pipelines may run over props on the seabed. The buried offshore pipelines are also subjected to undulations on the bed of the trench. These bed undulations lead to initial imperfections (out-of-straightness) of the laid pipelines. The initial imperfection causes the development of bending moment and axial force in the pipeline. The offshore pipelines are often operated at a high internal pressure and a high temperature (HPHT) for ease of transportation of the oil. The HPHT causes upheaval buckling and/or lateral buckling of a surface laid pipeline with the initial imperfection. Pipelines undergoing the bucklings are subjected to high bending moments and axial forces, in addition to the high internal pressures. The effects of these complex loading conditions should be properly identified for the structural integrity assessments of the pipelines. However, only the internal pressure is commonly considered for the structural integrity assessment of pipelines (ASME B31G 2012).

The pipelines are exposed to corrosive environments through the routes and carry corrosive subjects, causing wall corrosions during the service life. According to CEPA (2017), corrosion is the lead cause of oil and gas transmission pipelines failure, followed by manufacturing/construction defects and cracking. The corrosion defects may be aligned along a circumferential direction and/or a longitudinal direction of the pipelines. It has been demonstrated that the longitudinal extend of a defect has greater effect on the structural performance, in terms of burst pressure, than the circumferential extent of the defect (e.g., DNV-RP-F101 2015, CSA Z-662-15). The defect depth has been identified as the most influential geometric parameter of a defect on the remaining strength of a corroded pipeline

(DNV-RP-F101 2015). The circumferential extend (defect width) has been reported to have the minimum effect on strength reduction (Chiodo and Ruggieri 2009).

The pipeline may contains multiple corrosion defects spaced along the circumferential direction and/or the longitudinal direction of the pipeline as shown in Figure 1.2. When the multiple corrosion defects interact with each other under the applied loads, these are termed as interacting defects. The existing design codes (e.g., ASME B31G 2012, DNV-RP-F101 2015, CSA Z-662-15 2015) define the limiting distances between the defects, beyond which the defects do not interact. For the interacting defects, the remaining strength of a pipeline is evaluated considering a single defect with modifying the depth of the overall defect.

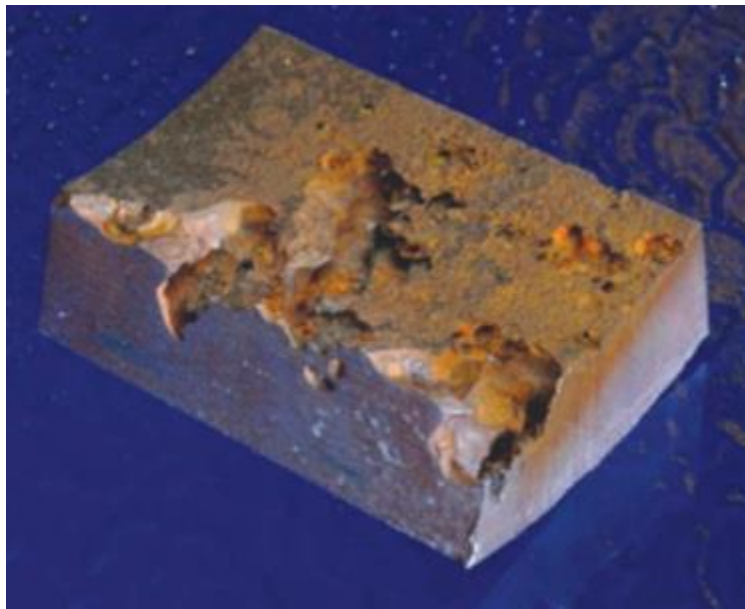


Figure 1.2: Multiple corrosions on inner surface of a pipe wall (Sykes 2012)

The pipe-walls may contain other flaws including cracks, gauge defects at the welding, non-uniform wall thickness, and ovality of cross-section. When the pipelines with tensile loadings are subjected to corrosive mediums then cracks are developed in the pipe wall at a stress intensity factor lower than the fracture toughness of the material. This phenomenon is known as stress corrosion cracking (SCC). The crack-like defects are more damaging than other flaws. A crack-like defect causes high stress concentration near the crack tip/crack front that leads to reduce the strength of the pipeline. Similar to corrosion defects, the cracks may be aligned along the circumferential direction and/or the longitudinal direction of the pipeline. The circumferential cracks are more detrimental when the pipelines are subjected to bending loading or tension loading, resulting in higher longitudinal stress in the pipe-walls. The effects of longitudinal cracks are more significant when the pipelines are subjected to an internal pressure, leading to the higher circumferential stresses.

1. 2 Rationale for the current study

The fitness-for-purpose of the corroded pipelines are assessed using burst pressure models available in the existing design codes (e.g., ASME B31G 2012, DNV-RP-F101 2015, CSA Z-662-15 2015, BS 9710 2013). The design codes provide simplified models for burst pressure predictions for corroded pipelines. Most of the existing burst pressure models neglect the presence of axial forces and bending moments experienced by the pipelines. However, the pipelines crossing various ground and operating conditions may experience axial forces and bending moments of various magnitudes (Taylor et al. 2015).

The burst pressure models should account for the effects of the axial forces and bending moments to properly assess the remaining strength of the pipelines.

In the existing methods, no specific guideline is provided to assess the pipelines having cracks or crack-like defects. The current research focuses on addressing the limitations discussed above toward developing an improved method for the assessment of the remaining strength of deteriorating pipelines.

1. 3 Research Objectives and Scope

The overall objective of the research is to develop the improved model for predicting the remaining strengths of deteriorating pipelines with particular focus to offshore energy pipelines. The level of axial forces and bending moments experienced by an offshore pipeline is first examined using finite element modelling. A case of offshore pipeline is considered for the assessment of the axial force and bending moments. Existing models for assessing the remaining strengths of deteriorating pipelines are then evaluated to develop the improved methods for FFS (fitness-for-service) assessments of the pipelines. A fracture mechanics approach is employed to assess the pipelines subjected to crack or crack-like defects. Specific objectives of this research are to:

- (i) Examine the loading conditions experienced by the offshore pipelines subjected to high temperature and/or high internal pressure.
- (ii) Evaluate existing burst pressure models and identify the contributing parameters to the burst pressure of a deteriorating pipeline.

- (iii) Develop an improved burst pressure model.
- (iv) Develop the new interaction rules for pipelines with multiple corrosion defects.
- (v) Evaluate the remaining strengths of corroded pipelines subjected to combined loadings including axial force, bending moment and internal pressure.
- (vi) Examine the effects of crack-like defects and crack-in-corrosion (CIC) defects using fracture mechanics criterion.

1.4 Outline of the Research Methodology

The following presents a brief outline of the methodologies undertaken to achieve the above objectives. A more detail discussion on the research methodologies and results are provided in the subsequent chapters.

Literature review: Existing literature on the remaining strength assessments of offshore energy pipelines is thoroughly reviewed.

Loads on offshore pipelines: Performance of a pipeline depends on the internal forces such as axial forces and bending moments in addition to internal pressure. The offshore pipelines laid on the seabed experience internally developed forces due to upheaval buckling resulting from high temperature and/or high operating pressure. The internal forces in pipelines subjected to upheaval buckling are investigated using large deformation finite element modelling techniques. A version of the work has been published in an Elsevier's journal, *Applied Ocean Research*, Vol. 66(2017), 146-155. Preliminary

findings from this work were presented in the *69th Canadian Geotechnical Conference* (GeoVancouver2016), Vancouver, B.C., 2–5 October 2016.

Evaluation of existing burst pressure models: Burst pressure models available in the existing design codes and literature are evaluated using rigorous finite element analyses. Based on this study, the key parameters responsible for the discrepancies observed in the existing burst pressure models are identified. This work has been published in an ASME journal, *Journal of Pressure Vessel Technology*, Vol. 139 (2016), 021702-1. Preliminary findings from this work were presented in two conferences: one at *34th International Conference on Ocean, Offshore and Arctic Engineering*, St. John's, NL, May 31- June 5, 2015 and the other at *IBC Energy's 6th Annual Conference*, St. John's, NL, April 14-15, 2015.

Development of the improved burst pressure model: The finite element modelling techniques are employed to conduct a parametric study with various pipe diameters and the shapes of corrosion geometries. Using the results of finite element analyses, the improved close-form equations for the Folias factor and for the burst pressure are developed for corroded pipelines. The work has been published in an ASME journal, *Journal of Pressure Vessel Technology*, Vol. 140(2018), 011702-1-9.

Interaction rules for multiple corrosion defects: Burst pressure for a pipeline with multiple corrosion defects is assessed considering each size of corrosion patches independently but separated by a distance from each other. The current design codes provide design equations for calculate the limiting distances beyond which the defects act

independently. These design equations do not include the depth of corrosion into consideration. However, it has been demonstrated that the limiting distance can be different depending on the defect depth. The effects of the defect depth and the arrangement of the defects on the interaction of multiple corrosion defects are investigated using finite element analyses, ending to the development of the new interaction rules. This study has been published in a CSCE journal, *Canadian Journal of Civil Engineering*, Vol. 44(2017): 589-597. Preliminary findings from this study were presented in *CSCE Annual Conference*, 1-4 June, 2016.

Corroded pipelines subjected to combined loadings: The above studies on the remaining strengths of corroded pipelines examine the pipelines under internal pressure only. However, as demonstrated in Mondal and Dhar (2017a & 2017b), the axial forces and bending moments are developed in the offshore pipelines. The effects of axial forces and bending moments on the burst pressures of corroded pipelines are examined using finite element analysis to develop simplified design methods.

Cracking in corroded pipelines: The corroded pipelines often suffer from stress corrosion cracking (SCC) when the pipelines in corrosive environments are subjected to high tensile stresses. A SCC occurs at a stress intensity factor well below the fracture toughness of the material. The effect of a SCC and the crack propagation in deteriorating pipelines cannot be captured using standard FE modeling techniques. It is proposed to employ fracture mechanics criterion to determine the remaining strengths of the pipelines containing crack-like defects. The investigations of pipelines with crack-like defects are conducted using fracture mechanics approach.

1.5 Organization of the Thesis

This thesis is organized in nine chapters.

Chapter 1 includes a discussion on the research background, objectives of the research and an outline of the methodology.

Chapter 2 provides a discussion on the literature review relating to the burst pressures of defected (corroded or cracked) pipelines subjected to different loadings, including the pipelines with multiple corrosion defects.

Chapter 3 presents the study to investigate the loadings experienced by the offshore energy pipelines during installation and operation.

Chapter 4 presents the study to evaluate the burst pressure models for corroded pipelines available in the existing design codes. The factors contributing to the discrepancies in the burst pressure models are identified and are discussed in this chapter.

Chapter 5 presents a study to investigate the contributing factors identified in Chapter 4 and to develop the improved model for burst pressure calculation of a corroded pipeline subjected to the internal pressure.

Chapter 6 presents a study to evaluate the existing interaction rules for a pipeline containing multiple corrosion defects. Based on the study, the improved interaction rules are developed.

Chapter 7 presents a study to account for the effects of bending moments and axial forces on the burst pressures of corroded pipelines.

In **Chapter 8**, burst pressure evaluation, using fracture mechanics criterion, is presented.

The burst pressures of pipelines containing corrosion only defects or crack-in-corrosion defects are examined.

Chapter 9 presents the overall conclusion of the thesis and the recommendations for future work.

All references reviewed in this study are given after Chapter 9.

CHAPTER 2

Literature Review

2.1 General

The major design consideration for a pipeline is the internal pressure containment where the pipeline is designed to carry the maximum internal pressure without failure. The capacity of a pipeline to carry the internal pressure is termed as “burst pressure”. The burst pressure of a pipeline depends on the pipe diameter, wall thickness and the strength of the material. The offshore pipelines are often subjected to axial forces and bending moments in addition to the internal pressures. The strength of a pipeline is also affected by these loads.

The corrosion is the primary cause of failure of a liquid pipeline and is the secondary cause of failure of a natural gas transmission pipeline and a distributing pipeline (Chauhan and Swankie 2010). A corrosion causes reduction of wall thickness locally. The corrosion defects can be of different shapes and with different orientations (along the longitudinal direction, circumferential direction and/or oblique direction), which affect the remaining strengths of the corroded pipelines. Pipelines experiencing tensile stresses in corrosive mediums are subjected to stress corrosion cracking that reduces the strengths of pipelines more significantly. The remaining strengths of the deteriorating pipelines subjected to corrosion and stress corrosion cracking should be determined for the fitness-for-purpose (FFP) assessments of the pipelines. This research focuses on developing the

improve methods for assessing the strengths of the deteriorating pipelines. This chapter presents a review of literature pertaining to the loading conditions of offshore pipelines followed by the current state of knowledge on the deteriorating pipelines subjected to those loadings.

2.2 Existing Burst Pressure Models

Several models of burst pressure for corroded pipelines are available in the literature. However, no single model was reported to predict the burst pressure accurately in general (Zhu and Leis 2012). The commonly used models include modified ASME B31G (2012), CSA Z662-15 (2015), DNV-RP-F101 (2015), LPC-1 (Swankie et al. 2012), Shell 92 (Zhou and Huang 2012), BS 7910 (2013) and RSTRENGTH (Kiefner and Vieth 1989). The models are briefly described below. The following parameters are consistently used for all of the models described below.

D : Outer diameter of pipeline

t : Wall thickness

d : Depth of corrosion defect

l : Length of corrosion defect

w : Width of corrosion defect

σ_y : Specified Minimum Yield Strength of the pipe material (*SMYS*)

σ_u : Specified Minimum ultimate Tensile Strength of the pipe material (*SMTS*)

S_{flow} : Flow stress

P_o : Pressure resistance of defect free pipeline

P : Burst pressure of corroded pipeline

M : Bulging stress magnification factor/Folias factor

Modified ASME B31G:

The modified ASME B31G code was developed through modification of the original ASME B31G code. The irregular longitudinal profile of a corroded area is replaced by an equivalent rectangular section having a depth of 0.85 times the maximum depth (d_{max}). The maximum stress capacity of the material is expressed by a flow stress, S_{flow} , which is taken as $1.1 \sigma_y$ or average of σ_y and σ_u , to account for the strain hardening effects.

In the modified ASME B31G code, the burst pressure is expressed as (Equation 2.1):

$$P = \frac{2t}{D} S_{flow} (= 1.1\sigma_y) \left[\frac{1 - 0.85 \frac{d_{max}}{t}}{1 - 0.85 \frac{d_{max}}{tM}} \right] \quad (2.1)$$

In Equation 2.1, M is termed as the Folias factor, accounting for the effects of geometry of the defect, and is given by Equation 2.2 or 2.3 depending on the defect length.

The Folias factor is discussed in details in section 2.2.1.

$$\text{For } \frac{l^2}{Dt} \leq 50$$

$$M = \sqrt{1 + 0.6275 \frac{l^2}{D \cdot t} - 0.003375 \frac{l^4}{D^2 t^2}} \quad (2.2)$$

For $\frac{l^2}{Dt} > 50$

$$M = 0.032 \frac{l^2}{Dt} + 3.30 \quad (2.3)$$

CSA Z662-15:

The CSA Z662-15 code uses similar equations as those in the modified ASME B31G code, except that the average depth (d_{avg}) of the corroded area is used instead of $0.85d_{max}$. The flow stress is used as $0.9\sigma_u$ for material with the yield strength greater than 241 MPa, which is the case for most pipe materials. The burst pressure in the CSA Z662-15 codes is given by (for $\sigma_y > 241$ MPa) Equation 2.4:

$$P_c = \frac{2t}{D} (0.9\sigma_u) \left[\frac{1 - \frac{d_{avg}}{t}}{1 - \frac{d_{avg}}{tM}} \right] \quad (2.4)$$

The Folias factor in this model is same as the one used in the modified ASME B31G.

DNV-RP-F101:

In the DNV RP-F101 code, the maximum depth of corrosion and ultimate tensile strength of the material are used. Partial safety factors are recommended for the material property and corrosion depth. A factor of 1.05 is used in the equation that was developed based on comparison of the model with laboratory test results. The model used in the DNV-RP-F101 code is given by Equation 2.5.

$$P = \frac{2t}{D-t} (1.05\sigma_u) \left[\frac{1 - \frac{d_{max}}{t}}{1 - \frac{d_{max}}{tM}} \right] \quad (2.5)$$

As seen in Equation 2.5, an average pipe diameter is used in the burst pressure model. The Folias factor in this model is given by Equation 2.6.

$$M = \sqrt{1 + 0.31 \left(\frac{l}{\sqrt{Dt}} \right)^2} \quad (2.6)$$

LPC-1:

The LPC-1 method also uses the ultimate tensile strength of the pipe material, the maximum depth of the corrosion and the average pipe diameter, as in the DNV-RP-F101 method. The model for the burst pressure in the LPC-1 code is given by Equation 2.7:

$$P = \frac{2t}{D-t} \sigma_u \left[\frac{1 - \frac{d_{max}}{t}}{1 - \frac{d_{max}}{tM}} \right] \quad (2.7)$$

The Folias factor in this equation is same as the DNV-RP-F101 code given above.

Shell 92:

The burst pressure according to the Shell 92 method is given by Equation 2.8.

$$P = \frac{2t}{D-t} (0.90\sigma_u) \left[\frac{1 - \frac{d_{max}}{t}}{1 - \frac{d_{max}}{tM}} \right] \quad (2.8)$$

The Folias factor in this method is expressed by Equation 2.9.

$$M = \sqrt{1 + 0.80 \left(\frac{l}{\sqrt{Dt}} \right)^2} \quad (2.9)$$

BS 7910 (2013):

In this code, the corroded area is represented by a rectangular section with the maximum depth and the maximum length of a corrosion. The flow stress is defined as the reference stress which is the mean of yield strength and ultimate tensile strength. The equation of burst pressure in this codes is (Equation 2.10):

$$P = \frac{2t}{D - t} \sigma_{ref} \left[\frac{1 - \frac{d_{max}}{t}}{1 - \frac{d_{max}}{tM}} \right] \quad (2.10)$$

Where, the equation of Folias factor is similar to the DNV-RP-F101 code.

RSTRENGTH:

The model of burst pressure in the RSTRENGTH method is similar to modified ASME B31G code, except the definition of flow stress. In RSTRENGTH, a 69 MPa (10 ksi) is added to the SMYS to determine the flow stress. The model of burst pressure in the RSTRENGTH code is express as (Equation 2.11):

$$P = \frac{2t}{D} S_{flow} (= \sigma_y + 69) \left[\frac{1 - 0.85 \frac{d_{max}}{t}}{1 - 0.85 \frac{d_{max}}{tM}} \right] \quad (2.11)$$

Where the equation of Folias factor is similar to modified ASME B31G code.

2.2.1 Folias Factor

Each of the models discussed above includes a parameter called “Folias Factor”. The term “Folias Factor, M ” is used to describe the bulging effect of a shell surface that is thinner in wall thickness than the surrounding shell. It measures the stress concentration at the tip of a crack with expansion under an internal pressure. The factor was first derived analytically by Folias (1964) considering a surface crack along the axis of a cylindrical shell. The general form of the factor is given by Equation 2.12 (Folias 1973).

$$M = f_e(\lambda) + f_b(\lambda)\chi(\lambda) \quad (2.12)$$

where,

$$\lambda = \sqrt[4]{\frac{3(1-\nu^2)l^4}{D^2t^2}}$$

$f_e(\lambda)$ = extensionl coefficient

$f_b(\lambda)$ = bending coefficient

$$\chi(\lambda) = \frac{\sigma_{bending}}{\sigma_{hoop}}$$

When the cylindrical shell is subjected to the internal pressure only, the simplified expression of the factor is reduced to Equation 2.13.

$$M = \sqrt{1 + 0.317\lambda^2} \quad (2.13)$$

The Folias factor was investigated by several researchers to apply it for the determination of the remaining strengths of corroded pipelines. The expression of the

Folias factor was modified and incorporated in the design codes (e.g., modified ASME B31G, DNV-RP-F101, BS 7910, CSA Z662-15). The modified ASME B31G, CSA Z662-15 and RSTRENGTH codes define the corrosion defects into two types, such as short defects and long defects. The expressions of the Folias factor recommended in these codes for the short and the long defects are given by Equations 2.2 and 2.3, respectively. The DNV-RP-F10 and the BS 7910 codes do not distinguish the short defects and long defects. A single equation is recommended for the Folias factor (Equation 2.6).

2.2.2 Evaluation of Burst Pressure Models

The burst pressure models discussed above have two components in general: one component is outside the bracket and the other component is inside the bracket. The component outside the bracket indicates the burst pressure of an intake pipeline and the component inside the bracket, known as burst pressure reduction factor (BPRF), measures the reduction of a burst pressure due to the presence of defect in the pipe wall. The burst models vary from each other with respect to the burst pressure of the intake pipeline (the term outside the bracket) and the burst pressure reduction factor (the term inside the bracket). As a result, different burst pressure models provide significantly variable failure probabilities of corroded pipelines even with the same defect dimensions (Hasan et al. 2011). Researchers are working to identify the limitations of the existing models and to develop the improved burst pressure models. Based on experimental results of 460 mm diameter and 8 mm thick pipelines, Chen et al. (2015) reported that the ASME B31G and the DNV-RP-F101 methods underestimate the failure pressures of corroded pipelines. However, Swankie et al. (2012) reported the results of 80 full-scale burst tests for a number

of pipelines with diameters ranging from 88.9 mm to 168.3 mm, where the modified ASME B31G method provided un-conservative estimations for 35% of the pipelines and conservative estimations for 50% of the pipelines tested. Majority of their predictions using the LPC-1 method was also found to be un-conservative with respect to the test results. Using FE analysis, Mondal and Dhar (2015) have found that a pipeline designed using the modified ASME B31G method would provide a factor of safety less than the design factor of safety. The modified ASME B31G method was found to provide un-conservative burst pressures for pipelines with multiple corrosion patches as well (Dhar and Mondal 2015). The model errors in several existing models were found to affect the burst probability assessments by several order of magnitudes (Zhou and Zhang 2015). An improved burst pressure model is therefore required for the assessments of the remaining strengths of corroded pipelines.

In this research, the key parameters contributing to the discrepancies in the existing models are identified and an improved burst pressure model has been developed. It has been identified that the expressions for the Folias factor do not include the defect depth, whereas defect depth was found to influence the factor. Figure 2.1 compares the Folias factors calculated using the equations in the modified ASME B31G and DNV-RP-F101 codes with those calculated using FE analysis (After Mondal and Dhar 2016). Figure 2.1 plots M^2 as a function of $l^2/(Dt)$, since the factors in the design codes are expressed as a square root of a function of $l^2/(Dt)$. In this figure, the FE method calculates different M for different d/t ratios with the same $l^2/(Dt)$. For $l^2/(Dt)$ of around 90, two data points are widely

scattered, one with $M^2 = 53.15$ for $d/t = 0.2$ and the other with $M^2 = 156$ for $d/t=0.7$. An improved equation for the Folias factor is developed from the current study.

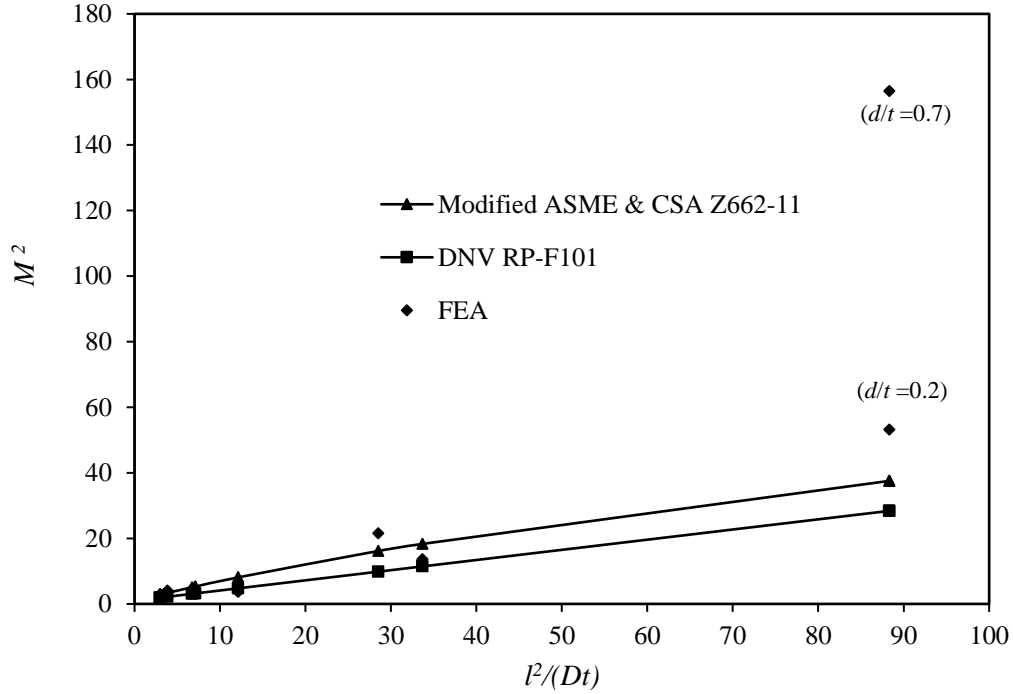


Figure 2.1: Comparison of Folias factors obtained from FE analysis and design codes

2.3 Interaction of Multiple Corrosion Defects

Corrosion in a pipeline may occur in a single patch or in multiple patches. For multiple corrosion patches, strength of the pipeline can be assessed considering a single patch only, if the corrosion patches are farther apart and do not interact with each other. For interacting defects, the burst pressure is calculated based on an entire corroded area inclusive of the corrosion patches. Different design codes such as DNV-RP-F101 (2015), CSA Z662-15 (2015), ASME B31G (2012) provide different interaction rules to determine

the limit of interacting distance using different criteria (Table 2.1). The maximum distance between the patches up to which the patches interact with each other is termed as the limit of interacting distance.

The interaction rules state about the limiting distances along the circumferential direction and longitudinal direction, $(S_c)_{lim}$ and $(S_l)_{lim}$, respectively, between two successive corrosion patches beyond which the effect of interaction of the adjacent patches is negligible. Three basic types of interacting corrosion defects are generally considered, which are termed as Type 1, Type 2 and Type 3, respectively (Kiefner and Vieth 1990).

All of the three types of interactions are described in details in Chapter 6. The following definitions are consistently used in the interaction rules.

S_l : longitudinal spacing between adjacent corrosion patches

S_c : circumferential spacing between adjacent corrosion patches

$(S_l)_{lim}$: maximum longitudinal spacing between adjacent corrosion patches above which the corrosion patches are treated as single isolated patches

$(S_c)_{lim}$: maximum circumferential spacing between adjacent corrosion patches above which the corrosion patches are treated as single isolated patches

The current design codes (e.g. DNV-RP-F101, modified ASME B31G, CSA Z662-15) recommend the limiting distances (spacing), $(S_c)_{lim}$ and $(S_l)_{lim}$, in terms of different parameters. The DNV-RP-F101 code expresses the spacing in terms of pipe dimensions (diameter and thickness). The modified ASME B31G and CSA Z662-15 codes express the

spacings in terms of pipe wall thickness and the dimension of corrosion patches, respectively.

Table 2.1: Interaction Rules

Source	Longitudinal limit $(S_l)_{lim}$	Circumferential limit $(S_c)_{lim}$	Criteria for interaction
DNV-RP-F101 (2015)	$2\sqrt{Dt}$	$360 \sqrt{\frac{t}{D}}$ (degree)	$S_l \leq (S_l)_{lim}$ $S_c \leq (S_c)_{lim}$
ASME B31G (2012)	$3t$	$3t$	$S_l \leq (S_l)_{lim}$ $S_c \leq (S_c)_{lim}$
CSA Z662-15 (2015)	Minimum(l_m to l_n)	Minimum(l_m to l_n)	$S_l \leq (S_l)_{lim}$ $S_c \leq (S_c)_{lim}$
Kiefner and Vieth (1990)	Minimum($6t, l_m$ to l_n)	Minimum($6t, w_m$ to w_n)	$S_l \leq (S_l)_{lim}$ $S_c \leq (S_c)_{lim}$
Pipeline Operator Forum (2005)	25.4 mm (1 inch)	$6t$	$S_l \leq (S_l)_{lim}$ $S_c \leq (S_c)_{lim}$

The interacting corrosion defects are treated as a single defect for calculating the burst pressure. The ASME B31G (2012) code recommends using a length equals to the total length of corrosion group, l_{mn} , and a depth equals to the maximum depth in the group, d_{max} . The width of the corrosion defect is not included in the ASME B31G model. The DNV-RP-F101 code also uses the length similar to that recommended in the ASME method. The depth for the corrosion group in the DNV-RP-F101 code is calculated using Equation 2.14.

$$d_{mn} = \frac{\sum_{i=m}^{i=n} d_i l_i}{l_{mn}} \quad (2.14)$$

Here, d_i and l_i are the maximum depth and length, respectively, of the i^{th} corrosion of the interacting corrosion group (as shown in Figure 6.3).

Li et al. (2016) reported that, for same defect sizes and configurations, the different design codes provide different results of interactions between corrosion defects. They revisited the interaction rules for a pipeline of 458.8 mm diameter with multiple corrosion patches using finite element analysis. Based on the study, the new interaction rules were proposed. Al-Owaisi et al. (2016) investigated the interaction of two shapes of corrosion defects for a 508 mm diameter pipe using finite element analysis. It was concluded that the shapes and locations of the defects influence the burst pressures of pipelines containing interacting defects.

Most of the studies on the interactions of corrosion patches focused on pipelines with diameters of around 460 mm (Fu and Batte 1999, Silva et al. 2007, Benjamin et al. 2016, Li et al. 2016). The limiting distances for interactions are expressed in terms of pipe diameter and/or wall thickness of the pipeline. The effect of the depth of corrosion is not included in the interaction rules. Silva et al. (2007) however showed that corrosion depths may affect the interaction rules. In this research, the interaction rules for a wide range of pipe diameters and corrosion depths are examined to develop the new interaction rules for pipelines with multiple corrosion patches.

2.4 Pipelines Subjected to Axial force and Bending Moment

Although the primary load for a pipeline is the internal pressure, the pipelines particularly in offshore environment are subjected to additional loads causing axial forces and longitudinal bending moments (Liu et al. 2009). The additional loadings could be the result of formation of free spans, specially for unburied pipeline, and temperature difference. The free span can impose bending moment, whereas the temperature difference can causes axial force and bending moment in the pipe wall. The burst pressure of a pipeline is affected by the axial forces and the bending moments. Wang et al. (2016) demonstrated that the burst pressure for a flawless pipeline is reduced due to the presence of bending moment. Axial tension was also found to reduce the burst pressure of defect free stainless steel pipes (Lasebikan and Akisanya 2014). Chen et al. (2015) and Ye et al. (2016) developed semi-empirical equations for the pipelines with an infinitely long corrosion defect. The solutions would underestimate the capacities of the pipelines with shorter corrosion patches.

Liu et al. (2009) investigated the burst pressures of pipelines with corrosion patches subjected to bending moment or axial compressive force using finite element analysis. Using the results of analysis, interaction diagrams were developed to relate the internal pressure (burst pressure) with bending moment or with the axial force for pipelines with diameters of 203.2 mm to 914.4 mm. Chauhan and Swankie (2010) also examined the burst pressures of corroded pipelines subjected to compressive forces or bending moments and developed interaction diagrams for pipelines with defect depths of 20% to 80% of wall thickness. For an example, Figure 2.2 shows the interaction diagrams when the pipelines

are subjected to bending moments and internal pressures. In the figure, M_A indicates the applied moment to the corroded pipeline and P_A indicates the burst pressure of the corroded pipeline with M_A , whereas M_0 and P_0 indicate the moment capacity and burst pressure of defect-free pipeline, respectively. The figure shows that the bending moment capacity is not affected by the corrosion defect when the pipeline is subjected to bending moment only (i.e., $M_A/M_0 = 1$), even with the defect depth of 80% of wall thickness that may not be consistent with the test result, specially for larger corrosion width. The figure also shows that when the pipeline is subjected to internal pressure only, the pipeline with d/t of 20% has the burst pressure similar to that of intake pipeline (i.e., $P_A/P_0 = 1$) and the pipeline with d/t of 50% has the burst pressure equals to 95% of burst pressure of the intake pipeline (i.e., $P_A/P_0 = 0.95$). These burst pressures are significantly different from the burst pressures obtained by the burst pressure models available in the literatures (e.g., ASME, CSA, DNV, BS). Moreover, the studies conducted by Liu et al. (2009) and Chauhan and Swankie (2010) did not consider the effect of simultaneous axial force and bending moment on the burst pressure.

The DNV-RP-F101 (2015) accommodated the effect of axial force and bending moment on the burst pressures of corroded pipelines by applying an additional factor (H_I) to the burst pressures of the pipelines without axial force and bending moment. The factor is defined by Equation 2.15, where ξ , γ_m , γ_d , σ_L , ε_d and $\text{StD}[d/t]$ indicate usage factor, partial safety factor for longitudinal corrosion, partial safety factor for corrosion depth, total longitudinal stress, fractile factor for corrosion depth and standard deviation of the measured corrosion depth, respectively. The effect of bending moment is accounted in

calculating the total longitudinal stress. The ratio of hoop stress to longitudinal stress, due to burst pressure, was assumed as 2 during developing the equation (Bjornoy et al. 2001).

$$H_1 = \frac{1 + \frac{\sigma_L}{\xi \sigma_u A_r}}{1 - \frac{\gamma_m}{2\xi A_r} \frac{1 - \gamma_d \left(\frac{d}{t}\right)^*}{1 - \gamma_d \frac{1}{M} \left(\frac{d}{t}\right)^*}} \quad (2.15)$$

$$\text{where, } A_r = 1 - \frac{dw}{\pi D t} \text{ and } \left(\frac{d}{t}\right)^* = \frac{d}{t} + \varepsilon_d \text{StD} \left[\frac{d}{t}\right]$$

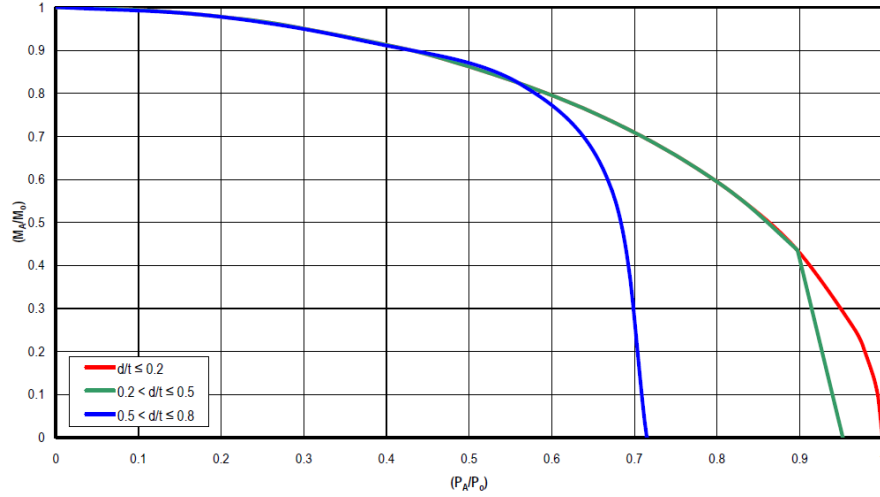


Figure 2.2: Failure Locus for Combined Internal Pressure and Bending Moment (Chauhan and Swankie 2010)

The DNV provides the H_I for three safety classes, such as Low Safety Class, Medium Safety Class and High Safety Class. Two safety classes, Medium Safety Class and High Safety Class, are evaluated here using the information about the pipe dimensions and material properties, given in Table 2.2. The evaluations are shown in Figure 2.3, where H_I is evaluated with respect to different longitudinal compressive stresses. The longitudinal stresses are expressed in terms of material ultimate strength, σ_u . For any axial compressive

stress, the H_I should be less than one. But, Figure 2.3 shows that when the pipeline is subjected to low compressive stress (i.e., $\sigma_L/\sigma_u = 0.31$ and 0.34 for high safety class and medium safety class, respectively), the H_I becomes greater than one. The H_I greater than one indicates that the burst pressure of the pipeline under the axial compressive stress is greater than the burst pressure of the pipeline without axial compressive stress. Therefore, the DNV recommendation, specially under low compressive stress, should be applied carefully for the determination of burst pressures of pipelines subjected to combined loadings.

Table 2.2: Parameters for calculating H_I

Parameter	Safety Class: Medium	Safety Class: High
Material Ultimate Strength, σ_u (MPa)	563.8	563.8
Pipe Diameter, D (mm)	762	762
Wall Thickness, t (mm)	17.5	17.5
Defect Depth, d (mm)	8.75	8.75
Defect Length, l (mm)	100	100
Defect Width, w (mm)	50	50
Usage Factor, ξ	0.85	0.80
Partial Safety Factor, γ_m	0.88	0.82
Partial Safety Factor, γ_d	1.28	1.32
Standard Deviation, $\text{StD}[d/t]$	0.08	0.08
Fractile Value, ε_d	1.0	1.0

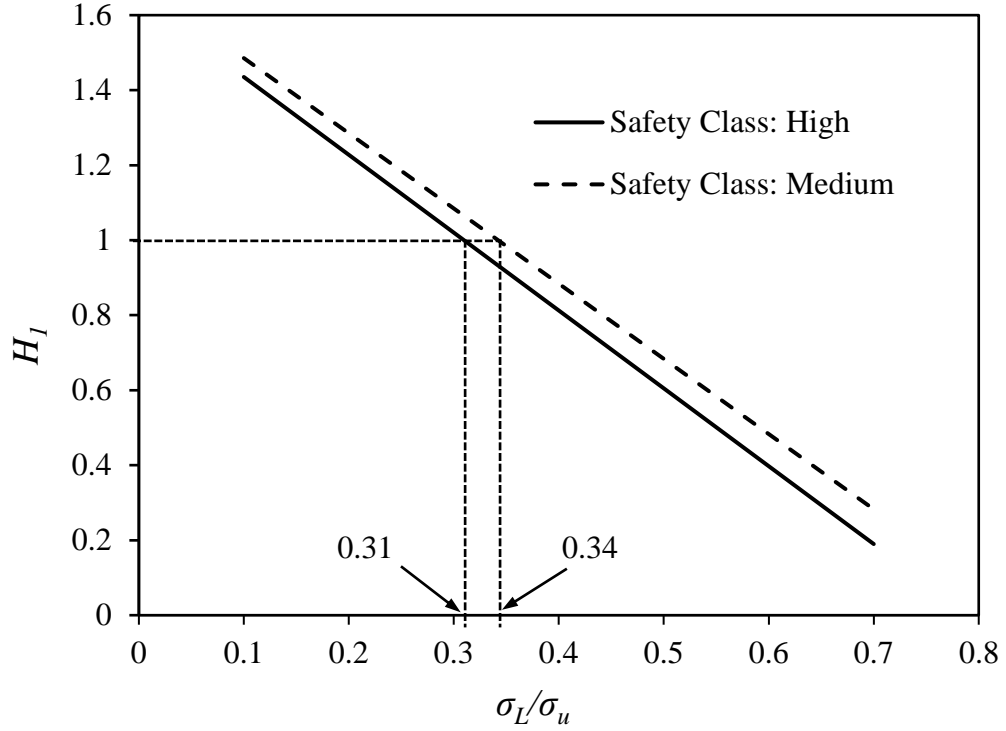


Figure 2.3: Evaluation of H_I (DNV-RP-F101 2015)

In this research, the burst pressures of corroded pipelines subjected to axial forces and bending moments are investigated to develop a simplified design method. The axial forces and bending moments experienced by the offshore pipelines are first investigated considering the seabed conditions of offshore Newfoundland. The interaction diagrams between internal pressures and bending moments with different constant axial forces are then developed.

2.5 Application of Fracture Mechanics

Pipelines with corrosion defects are generally analyzed using the continuum mechanics approach. In the continuum mechanics approach, the failure of a pipeline is

assumed when the equivalent von Mises stresses through the ligament (i.e., minimum thickness at the corroded zone) of the pipeline reach to the ultimate strength of the pipe material. The von Mises stress at the outer surface of the ligament reaches the ultimate strength first, particularly for a large depth of corrosion, which then extends to the inner surface (Liu et al. 2009, Mondal and Dhar 2018). When the von Mises stress on the outer surface reaches to the ultimate strength, the stress is assumed to remain constant at this point while the stress increases at every other point in the pipe wall with the increase of internal pressure. However, when the von Mises stress at any point exceeds the ultimate strength, a crack might initiate at that point where the stress will be reduced to zero. The crack initiation and its propagation are not considered in continuum modelling. Thus, the continuum modelling approach may over-predict the pipeline strength. The crack initiation and crack propagation during loading can be better modelled using fracture mechanics.

In fracture mechanics, the strength of a material against cracking is determined by the fracture toughness of the material. The fracture toughness can be defined by four parameters, such as stress intensity factor (K), strain energy release rate (G), J -integral (J) and crack tip opening displacement (δ). All of these terms are explained in Chapter 8 in details. The critical values of the above four parameters corresponding to crack initiation are known as fracture toughness (i.e., K_c , G_c , J_c and δ_c , respectively). For a beam subjected to concentrated load at the center, K is given by Equation 2.16 where P , B , W , a , and $f(a/W)$ indicate the applied load, specimen thickness, specimen width, crack length and geometry function, respectively (Zhu and Joyce 2012). The expression of geometry function depends on the types of specimens and loading.

$$K = \frac{P}{B\sqrt{W}} f\left(\frac{a}{W}\right) \quad (2.16)$$

The strain energy release rate, G , is defined as Equation 2.17, where π indicates the potential energy under the applied loading (Gdoutos 2005). It measures the energy available for an increment of a crack. The J -integral is given as in Equation 2.18, where Γ is an arbitrary curve around the tip of a crack, w is the strain energy density, T_i is the components of the traction vector, u_i is the displacement vector components, ds is the length increment along the contour, and x and y are the rectangular coordinates with the y direction taken normal to the crack line and the origin is at the crack tip (Zhu and Joyce 2012). The crack tip opening displacement, δ is the gap between the crack surfaces measured at a certain distance behind the crack tip. The above terminologies are described in details in Chapter 8.

$$G = -\frac{\partial \pi}{\partial a} \quad (2.17)$$

$$J = \oint_{\Gamma} \left(w dy - T_i \frac{\partial u_i}{\partial x} ds \right) \quad (2.18)$$

The stress intensity based fracture toughness, K_c , is generally used for brittle materials that follows linear elastic fracture mechanics principles. The nonlinear fracture mechanics are used for ductile materials where the critical point of the structure undergoes significant yielding before the stress intensity factor reaches to K_c . The existing design practices for cracked pipelines are based on stress intensity factor. But the effects of yielding, due to plastic properties of ductile pipeline, on the fracture toughness are not

considered separately. Using the equation of failure assessment curve (FAC) provided by Milne et al. (1988), Yang et al. (2016) developed an analytical model of elastic fracture toughness by quantifying the K_c of ductile pipeline. Using this model, the linear elastic fracture mechanics can be applied to determine the failure criteria of ductile pipelines. However, the determination of the stress intensity factor and the J -integral for pipelines subjected to corrosion defects are the most critical components of applying the fracture mechanics. In this research, XFEM (Extended Finite Element Method) features available in Abaqus have been used for the assessment of crack propagation in corroded pipelines.

CHAPTER 3

Loading Conditions Experienced by Surface-Laid Offshore Pipeline

3.1 Introduction

Pipelines traversing large distance are often subjected to axial force and bending moments in addition to the internal pressure. The magnitude of the axial force and bending moments may be significant which has not been extensively investigated. Particularly, the offshore pipeline transporting oil with high internal pressure and high temperature (HPHT) experiences high compressive force normal to the pipe cross-section when the pipeline is constrained along longitudinal direction. The pipeline buckles laterally, vertically or obliquely when this compressive force exceeds the critical buckling force. As a result, high bending moments may be caused in the longitudinal direction. Theory and laboratory-scale experiments demonstrate that the high internal pressure alone can cause upheaval buckling (Palmar and King 2008) which may induce longitudinal bending moment. The surrounding soil offers resistance to buckling of the pipeline, which is greater against lateral buckling than the upheaval buckling (Liu and Yan 2013, DNV-RP-F101 2007 and Wang et al. 2011). Thus, upheaval buckling are sometimes expected to occur. The objective of the study presented in this chapter is to investigate the axial forces and bending moments in pipelines considering a case of upheaval buckling of an offshore pipeline. A site of offshore Newfoundland is selected where the installation of a surface laid pipeline is proposed by an offshore oil company (i.e. Husky Energy).

The upheaval buckling of a subsea pipeline is greatly affected by the initial imperfection (out-of-straightness) of the pipeline (Wang et al. 2011, Zeng et al. 2014, Shi et al. 2013, Karampour et al. 2013 and Liu et al. 2012). The initial imperfection may be due to the imperfection of the existing seabed, manufacturing defect, or installation of the pipelines. The imperfection of the seabed may be influenced by trenching during installation. The behavior of the pipeline during buckling is governed by the amplitude (Liu et al. 2015, Karampour et al. 2013, Liu et al. 2012 and Run et al. 2013) and the shape (DNV-RP-F101 2007, Zeng et al. 2014 and Karampour et al. 2013) of the imperfection.

For the structural stability assessments of pipelines subjected to upheaval buckling, several analytical solutions were developed for critical buckling forces using beam formulations with assumed shapes of localized imperfections (Zeng et al. 2014, Liu et al. 2012, Hobbs 1984, Palmer and King 2008 and Zhang and Duan 2015). For simplicity in analysis, different idealized shapes of initial imperfections were assumed in the development of the analytical solutions. The idealized shapes include those of Taylor and Tran (1996), who developed empathetic models from mathematical reasoning for three different types of imperfections, such as “basic contact undulation”, “isolated prop” and “infilled prop”. Palmer and King (2008) employed sinusoidal imperfection shape for a pipeline, and defined it using two parameters such as imperfection height and imperfection length. However, researchers have demonstrated that the imperfection geometry of a pipeline in the seabed is much more complex than the idealized shapes, which has significant effect on the critical buckling load. Zeng et al. (2014) investigated the pipelines with sinusoidal and other polynomial shaped imperfections using finite element analysis

and showed that the imperfection shapes significantly influence the critical buckling force where the critical buckling force is defined by the force that results the initiation of buckling of the pipeline. The study indicates the necessity of considering realistic imperfection shape for the assessment of upheaval buckling for a subsea pipeline.

Mondal and Dhar (2016) conducted a two-dimensional (2D) finite element (FE) analysis to investigate the effect of a seabed condition on the upheaval buckling behavior of a surface laid offshore pipeline using a commercially available software “Abaqus”. The pipeline is modeled using 2D pipe element (Abaqus element type “PIPE21H”) and the seabed is modeled using plane strain element (Abaqus element type “CPEG8R”). The node-to-surface interaction with frictional coefficient of 0.40 is applied between the pipeline and the seabed. The frictional coefficient is selected from literature based on soil type (Liu et al. 2014). As the pipeline is modeled using 2D element, the internal pressure could not be applied directly during the FE analysis. The effect of the internal pressure is incorporated indirectly through increasing an equivalent amount of pipe temperature calculated using Equation 3.1 (after Karampour et al. 2013).

$$\Delta T_p = \frac{pD(1 - 2\nu)}{4tE\alpha} \quad (3.1)$$

Where ΔT_p is the temperature change required to result in the same effect as that of an internal pressure of p . The other parameters in the equation such as D , t , E , α and ν correspond to pipe outer diameter, pipe wall thickness, modulus of elasticity, coefficient of thermal expansion and Poisson’s ratio, respectively. Equation 3.1 is based on the

assumption of fully restrained longitudinal expansion of the pipeline, which is expected for pipelines undergoing upheaval buckling. The longitudinal expansion of an offshore pipeline is inhibited by the friction between the pipeline and the seabed soil (Taylor and Gan 1986 and Craveiro and Neto 2016). The pipelines are also anchored using rock dump over a length that restrains the axial movement (Palmer and King 2008). Mondal and Dhar (2016) revealed that the local seabed condition affects the upheaval buckling behavior. The initial shape of the pipeline with the local seabed profile was different from the idealized shapes recommended in the design codes. The temperature required to initiate upheaval buckling (i.e., critical buckling temperature/force) was also found to be less for the pipeline affected by the local seabed profile, implying that the critical buckling temperature based on the idealized initial shapes might be unconservative with respect to the 2D FE calculation. It is however to be noted that the two-dimensional idealization in FE analysis is unable to account for the 3D settlement of the pipeline into the foundation soil that may occur during upheaval buckling. The applicability of idealization of the internal pressure with an equivalent temperature also requires evaluation. As a result, the predications using 2D idealization remain questionable. Liu et al. (2014) earlier reported discrepancies in the results of 2D and 3D analyses for global buckling in offshore pipelines. Three-dimensional (3D) analysis is therefore employed in this study.

In the current study, 3D FE analysis is used to the upheaval buckling and the internal forces (axial forces and bending moments) in offshore pipelines. The initial shape of an unburied pipeline laid on an imperfect seabed is developed by the FE modelling. The developed shape is compared with the existing models for the initial imperfection

(Karampour et al. 2013 and Taylor and Tran 1996). The upheaval buckling behavior of the pipeline subjected to pressure and temperature is then investigated. A parametric study is conducted to investigate the effects of imperfection geometry, pipe cross-sectional property and seabed soil conditions on the upheaval buckling and the internal forces. A remedial measure against upheaval buckling is also considered through management of seabed imperfection.

3.2 Seabed Profile

A real seabed profile of offshore Newfoundland in Canada is first considered for this study. The seabed profile and the geotechnical information of the subsea soil along a potential pipeline project were obtained through a collaboration with Husky Energy. Figure 3.1 shows the seabed profile over the length of 350 m from a reference point. A length of 350 m is employed in the analysis based on a preliminary study revealing that this length is sufficient for the analysis of the upheaval buckling. Figure 3.1 represents profile with respect to the depth of water. The figure also shows elevation of the seabed profile with respect to an arbitrary datum located at 76 m below the water surface. It reveals that the seabed is irregular and has an upward prop of about 2.2 m height between the distance of 150 m and 250 m. A pipeline laid on this seabed will develop an initial shape of imperfection that will be governed by the shape of the seabed, stiffness of the seabed and the flexural rigidity of the pipeline.

3.3 Shape of Initial Imperfection

Several different idealized profiles for subsea pipeline exist in the literature to represent the initial shape of pipeline imperfection. Taylor and Tran (1996) proposed the shape of an initial imperfection for an isolated prop of the seabed imperfection (Equation 3.2).

$$y = \frac{q}{72EI} \left[2L_o \left(\frac{L_o}{2} - x \right)^3 - 3 \left(\frac{L_o}{2} - x \right)^4 \right] \quad (3.2)$$

Where,

y = height above the lowest point

H = maximum height of imperfection

L_o = wave length of imperfection = $5.8259 \left(H \frac{EI}{q} \right)^{\frac{1}{4}}$

x = distance measured from the symmetric point of imperfection

q = submerged otherwise self-weight of pipeline per unit length

I = moment of inertia of pipe section

E = modulus of elasticity of pipe material

For an infilled prop imperfection where the pipeline is perfectly fitting with the seabed, the proposed shape of imperfection is as given by Equation 3.3 (Taylor and Tran 1996):

$$y = H \left[0.707 - 0.26176 \frac{\pi^2 x^2}{L_o^2} + 0.293 \cos \left(\frac{2.86\pi x}{L_o} \right) \right] \quad (3.3)$$

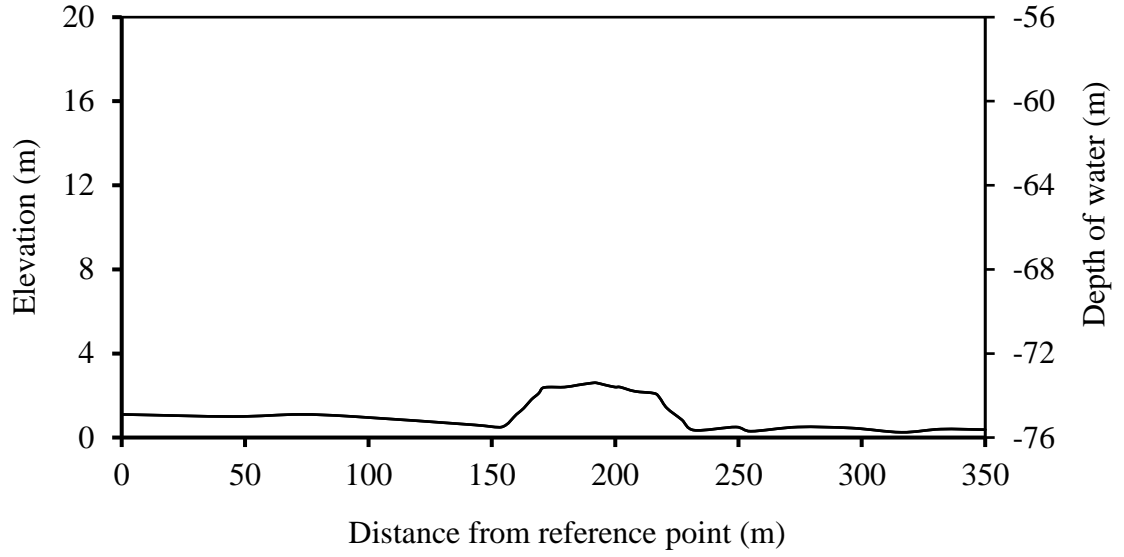


Figure 3.1: Seabed profile from offshore Newfoundland

Palmer and King (2008) employed the sinusoidal profile of an imperfection (Equation 3.4) to develop the universal design curve for upheaval buckling.

$$y = \frac{H}{2} \left[1 + \cos \left(\frac{2\pi x}{L_o} \right) \right] \quad (3.4)$$

Karampour et al. (2013) used two other imperfection shapes (Equations 3.5 and 3.6) to account for possible undulations of the seabed.

$$y = H \left(8 \frac{x}{L_o} + 1 \right) \left(\frac{2x}{L_o} - 1 \right)^4 \quad (3.5)$$

$$y = H \left[\frac{32}{3} \left(\frac{x}{L_o} \right)^2 + 6 \left(\frac{x}{L_o} \right) + 1 \right] \left(1 - \frac{2x}{L_o} \right) \quad (3.6)$$

The seabed profile shown in Figure 3.1 is assumed to result in the infilled prop type imperfection (or basic contact undulation) of the pipeline. The shapes given in Equation 3.3 to 3.6 would thus represent the idealized initial shape, which are investigated here for comparison. However, the initial shape given by Equation 3.4 is used to model the pipeline imperfection for the parametric study.

In the above idealized imperfection shapes, only Equation 3.2 includes a term for flexural rigidity (EI) of the pipeline. The effects of soil stiffness are not incorporated in any of the equations above. A FE modelling technique is used here to investigate the effect of pipe flexural rigidity and seabed soil stiffness on upheaval buckling of pipelines.

3.4 FE Analysis

The purposes of the FE analysis presented in this study are threefold. In step 1, the initial shape of imperfection of a pipeline is investigated. The pipeline is allowed to fall on an elastic continuum seabed under gravity to obtain the initial shape of imperfection. In step 2, the upheaval buckling associated with the increase of temperature and/or internal pressure is investigated. The effects of upheaval buckling on the pipeline with an initial shape of imperfection obtained from the FE analysis and those obtained from idealized imperfection shapes are compared. It is to be noted that the upheaval buckling prediction using the idealized imperfection shape neglects the residual stress in the pipeline resulting from pipeline installation. The effect of residual stress resulting from falling pipeline to the seabed under the gravity load is included in the analysis. In Step 3, a remedial measure against upheaval buckling is investigated.

A commercially available FE software “Abaqus” is used in this study. The pipeline and the seabed is modeled using 8-noded linear brick element with reduced integration and hourglass control option (Abaqus element type “C3D8R”). The outer diameter (D) and wall thickness (t) of the pipeline are 219.1 mm and 18.3 mm, respectively. A wall thickness of 8 mm is also considered to study the effect of flexural stiffness of the pipeline. The sheathing on pipeline is not considered in this study. The seabed is extended sufficiently along the transverse direction to avoid the effect of boundary condition. The surface-to-surface interaction between the pipeline and seabed is used. The seabed soil is generally assumed as an elastic material. The effect of soil plasticity is found to be less significant on the upheaval buckling of the surface laid pipeline, as demonstrated in Figure 3.2. This is due to fact that the seabed soil does not undergo significant deformation during upheaval buckling of the surface laid pipeline. The pipelines mostly move in upward direction. Figure 3.2 plots the buckling amplitude against temperature considering an elastic and an elasto-plastic seabed. The Mohr-Coulomb model is used to account for the soil plasticity. The soil parameters are estimated based on the information from a geotechnical investigation report for the site. The soil at the site (very dense gravelly sand) is considered highly permeable and the drained condition is simulated. A study is conducted with a seabed domain thickness of 2 m and 3 m to investigate the effect of seabed domain thickness on the FE simulation of the pipeline responses. No significant difference on the upheaval buckling is found for the two thicknesses. A thickness of 2 m is therefore used in the FE modelling.

The bilinear elastic material model is used for the steel pipe material. However, the effects of bilinear material model is expected to be negligible for the study presented here, since the pipe stress during upheaval buckling is not significantly higher (often less) than the yield strength. The material parameters used in the general analysis are listed in Table 3.1 based on typical values for steel and the soil encountered at the site of offshore Newfoundland (“Soil friction angle” 2013 and “Table of ultimate friction factors for dissimilar materials” 2017). However, a wide range of soil parameters are considered (numbers in parenthesis) to investigate the effect of these parameters. Since the effect of soil plasticity was insignificant on the pipe response, constant values of the angle of internal friction and the dilation angle are used.

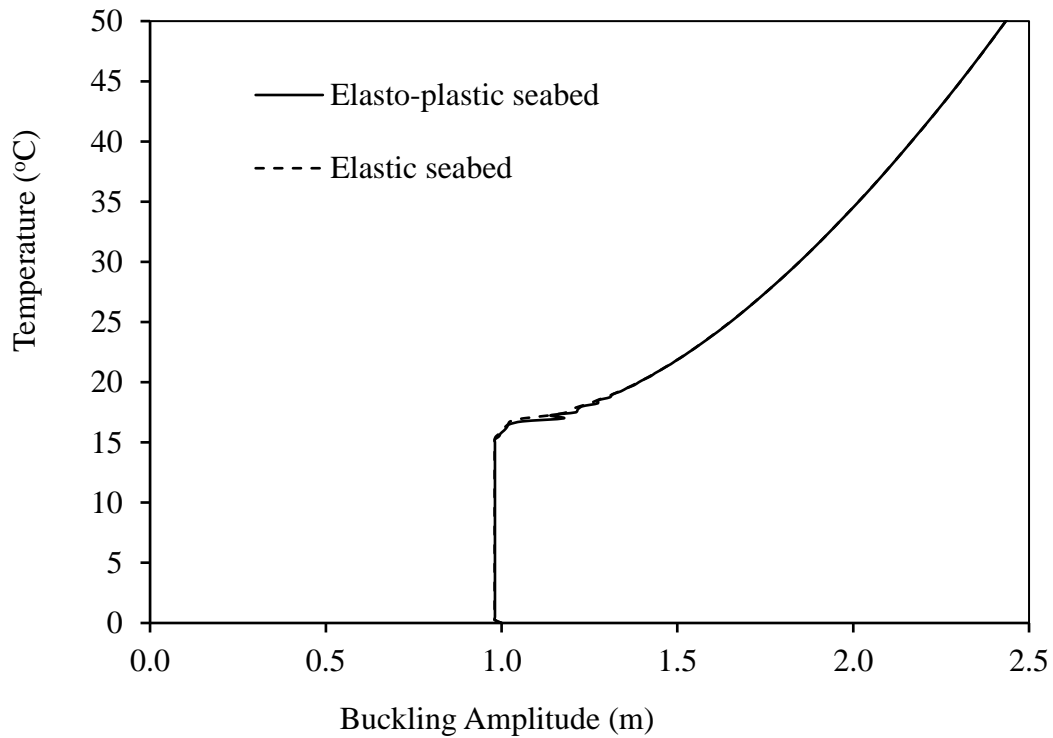


Figure 3.2: Effect of soil model on the upheaval buckling [$H=1000$ mm, $t=18.3$ mm]

Table 3.1: Material Properties

Property	Steel	Soil
Submerged Density, ρ' (kg/m ³)	6850	600
Modulus of Elasticity, E (MPa)	207000	40 (10, 300)
Poisson's Ratio, ν	0.30	0.25
Specified Minimum Yield Strength, σ_Y (MPa)	450	---
Specified Minimum Tensile Strength, σ_U (Mpa)	535	---
Total strain at ultimate strength, ϵ_U	0.043	---
Thermal expansion coefficient, α (m/m/°C)	1.17x10 ⁻⁵	---
Friction angle (°)	---	42
Dilation angle (°)	---	15
Coefficient of friction	0.40 (0.20, 0.80)	

Analysis is performed in different steps using automatic time increment in each step. The dynamic implicit method is used for the analysis, which is computationally efficient (less time required) with respect to the dynamic explicit method. The implicit and explicit methods are found to provide similar results (Liu et al. 2014). The modelling approach used in each step of analysis is elaborated below.

Step 1: The pipeline is first placed horizontally at the crest level of the upward prop on the seabed (Figure 3.3). The pipeline is then allowed to deform under gravity load. At this level of analysis, the pipe deformation at the crest of the prop is restrained. The nonlinearities in geometry and material are included in the analysis. Geometric nonlinearity using Abaqus command allows updating the equilibrium equations considering the

deformed state of the models. Material nonlinearity analysis from soil plasticity is also considered.

Step 2: The temperature and/or pressure of the pipeline having an initial shape with imperfections at the seabed temperature is increased to investigate the upheaval buckling. Applied temperature is thus increased with respect to ambient seabed temperature. For the simulation, the pipe ends are fully restrained by maintaining the constant deformations developed by self-weight of the pipeline (i.e., the deformations developed by Step 1). The pipeline between the ends is set free to move and/or rotate. The initial shape obtained from the FE analysis in Step 1 is first investigated. A pipeline with an idealized imperfection (Equation 3.3 to 3.6) is also considered.

Step 3: In this step, the relation of the prop height on the initiation of upheaval buckling is investigated under different temperature loads and pressure loads.

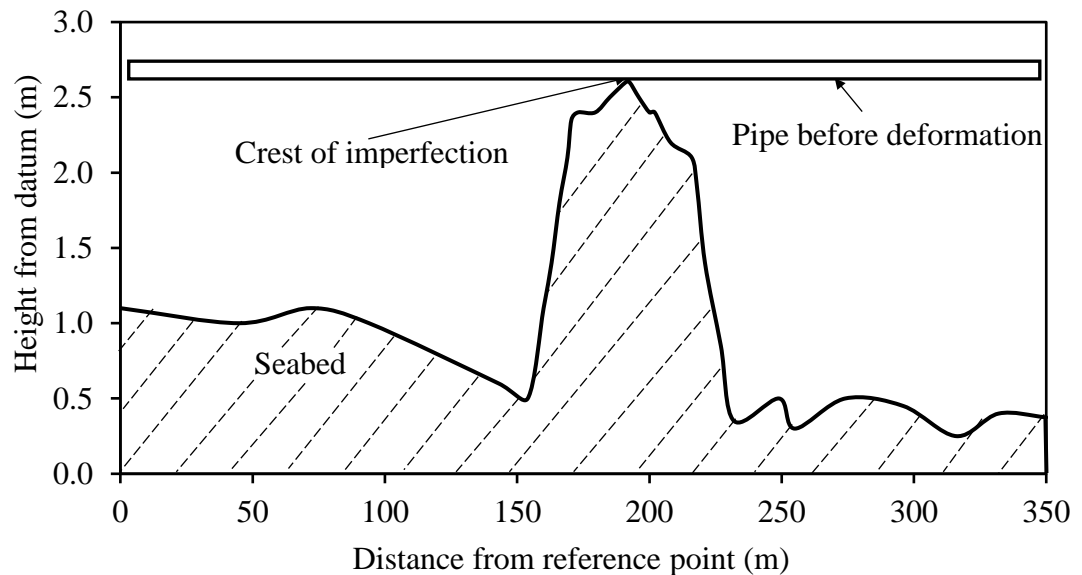


Figure 3.3: Pipeline placed at the crest of the seabed prop

The result of dynamic analysis of snap-through buckling is often influenced by the time period used in each step (Wang et al. 2015). A preliminary study is carried out to determine the optimum step time. Based on the study, a time step is selected that corresponds to a loading rate of 0.25MPa/sec or 0.25°C/sec.

3.5 Effects of Seabed Profile

3.5.1 Initial Shapes of Pipelines

Figure 3.4 compares the shapes of initial imperfections derived using the idealized shapes (Equation 3.3 to 3.6) and from FE analysis. For the idealized shapes, a wavelength, L_o , of 96 m is used for a height of imperfection, H , of 2.2 m. The wavelength is assumed from 144.5 m to 240.5 m along the length of the pipeline (Figure 3.1).

The comparison in Figure 3.4 indicates that the differences of the initial shapes given by Equation 3.3 to 3.6 are not significant. However, the idealized initial profiles differ from that obtained from the FE analysis. The FE analysis accounts for the real shape of the seabed. The seabed profile is also included in the figure. In Figure 3.4, the shapes from the FE analysis match the shape of the seabed except around the prop. The pipeline appears to be penetrated/ settled into the flexible seabed under the gravity load. The seabed embedment could not be simulated using 2D analysis (Mondal and Dhar 2016).

3.5.2 Effect of Initial Shape

Figure 3.5 shows the effects of seabed imperfection on the pipeline upheaval buckling due to temperature load. The results obtained based on an initial shape obtained from FE analysis and the one given by Equation 3.4 (idealized shape) are compared in the

figure. The idealized shape was obtained for an imperfection height of 2.20 m and wavelength of 96 m. The maximum longitudinal stress and the maximum deflection at the crest of imperfection are plotted in Figure 3.5. The compressive stress is plotted along the positive y-axis.

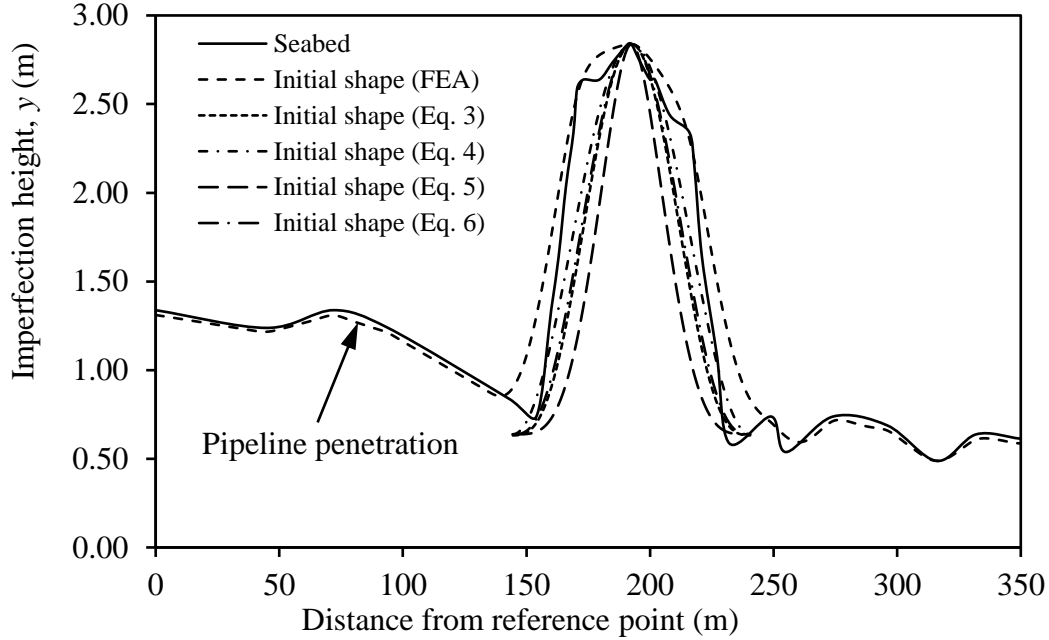


Figure 3.4: Comparison of initial shapes of pipe

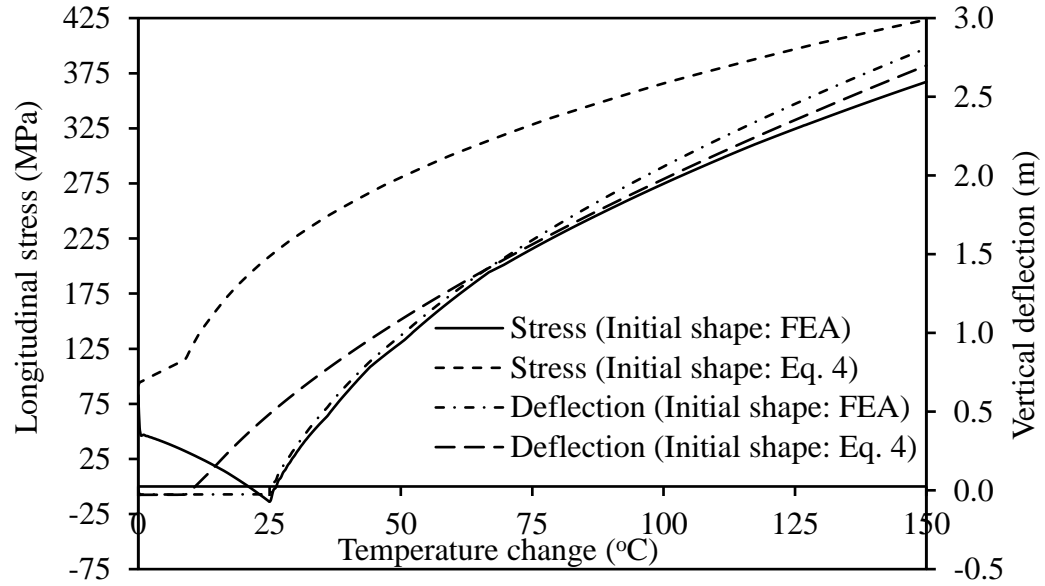
In Figure 3.5 (a), the pipe deflections against the rise of temperature are not significant up to the temperature required to initiate upheaval buckling (i.e., critical buckling temperature). Beyond the critical buckling temperature, the pipe deflection increases at a higher rate. Figure 3.5 (a) indicates that the critical buckling temperature calculated based on simplified idealization of the initial shape (Equation 3.4) is around 10.25°C while the temperature based the initial shape obtained from the FE analysis is around 25°C. The idealized profile thus provides a much conservative estimate of the buckling initiation temperature. At very high temperature (beyond 75°C), the two curves

for pipe deflections become close to each other, indicating that the pipeline deformation is independent on the initial shape beyond that temperature. However, the simplified idealization of the initial shape results in the calculation of a significantly high longitudinal stress in the pipe wall. The longitudinal stress calculated based on the idealized shape is consistently higher in Figure 3.5 (a) than the stress calculated using the FE based initial shape.

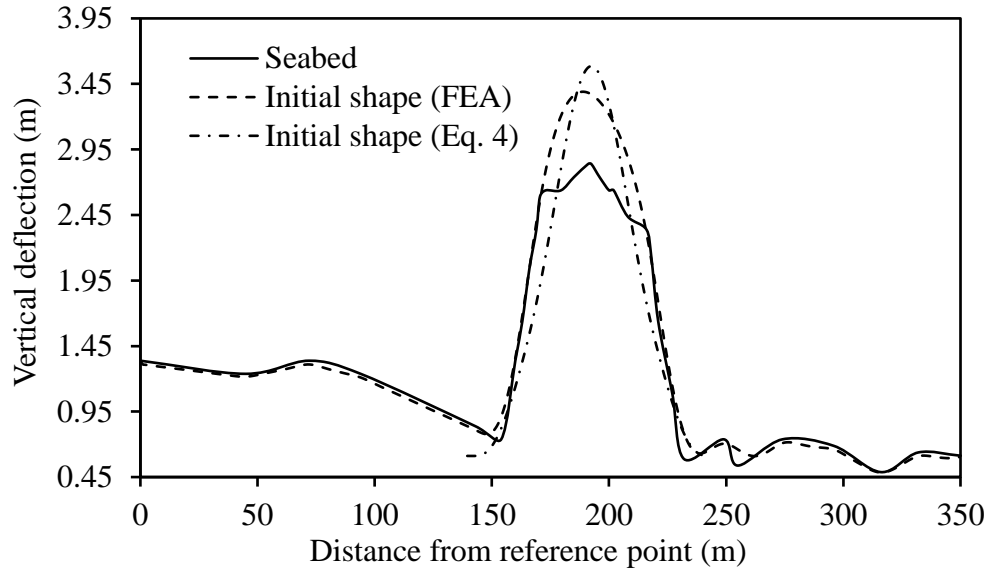
In Figure 3.5 (a), no snap-through instability is observed, which is attributed to the high amplitude of initial imperfection (i.e., 2.2 m) for the pipelines investigated. Run et al. (2013) demonstrated that snap-through instability occurs for only small amplitudes of initial imperfection (i.e., up to 100 mm). They did not observe any snap type deformations for an initial imperfection of 300 mm height. However, the buckling amplitude increases with a higher rate at a temperature around 15°C to 20°C (Run et al. 2013), similar to that observed in the current study.

Figure 3.5 (b) shows the vertical deflection along the length of pipeline at a temperature of 35°C, which is greater than the critical buckling temperature (10.25°C or 25°C). Due to the presence of local undulations on the seabed, the shape of the pipeline profile obtained from the FE analysis is not symmetric about the crest. As a result, the location of the maximum deflection varies around the crest and is not always at the crest of the initial shape. The decrease in the longitudinal stress at the crest in Figure 3.5 (a) with temperature up to the critical buckling temperature (i.e., 25°C) is attributed to the variation of the location of the maximum deflection. The longitudinal stress increases consistently

with temperature beyond critical buckling temperature when the effect of the local seabed feature is insignificant. For analysis with an idealized initial shape, the profile is assumed to be symmetric about the crest. Therefore, the maximum deflection is always at the crest of the initial profile and the longitudinal stress increases consistently with temperature.



(a) Longitudinal stress and vertical deflection



(b) Vertical deflection along the length of pipeline at 35°C

Figure 3.5: Effect of initial shapes on upheaval buckling

The above comparison implies that the initial shape of a pipeline influences the upheaval buckling behavior of the pipeline. The simplified idealization of the initial profile is found to provide conservative (lower) estimations of critical buckling temperature and unconservative estimations of the pipe wall stress.

3.5.3 Installation Stress

During installation of a subsea pipeline on an undulated seabed or an uneven trenched bottom, stresses develop in the pipe wall. The stress is defined herein as installation stress or initial stress. The effect of the installation stress on the upheaval buckling behavior is often neglected when the pipeline is assumed to have an initial shape given in the simplified equation (i.e., Equation 3.4).

The initial stress condition is simulated here using the FE analysis to investigate its effects. In order to account for the initial stress condition, an idealized seabed is first developed using Equation 3.4. The pipeline is then laid on the seabed under gravity, as discussed in section 3.4. The resulting initial shape of the pipeline was found to match with the shape of the idealized seabed. The temperature and/or pressure load are then applied to the pipeline. To model a pipeline without installation stress (i.e. initially unstressed), the seabed and pipeline are modelled according to the shape given by Equation 3.4. The pipeline is then subjected to the loads.

Figure 3.6 shows the maximum deflection of the pipeline due to temperature load or pressure load. The imperfection height of 2.2 m is considered to develop the idealized seabed. The initial non-zero (negative) deflection in Figure 3.6 is the penetration of the

pipeline into the seabed under the gravity load. It can be seen in the figure that the critical buckling temperature and the critical buckling pressure are influenced by the initial stress conditions. The critical buckling temperatures with initially unstressed and initially stressed conditions are 7.25°C and 10.25°C, respectively. The critical buckling pressures of the pipeline are 19.5 MPa and 27.0 MPa, respectively. The critical buckling temperature and pressure are thus underestimated for the pipelines with no initial stress. For the pipeline considered, the critical buckling temperature and the pressure are underestimated by 41% and 38%, respectively. Neglecting of the installation stress would thus provide over conservative estimation of the buckling behavior.

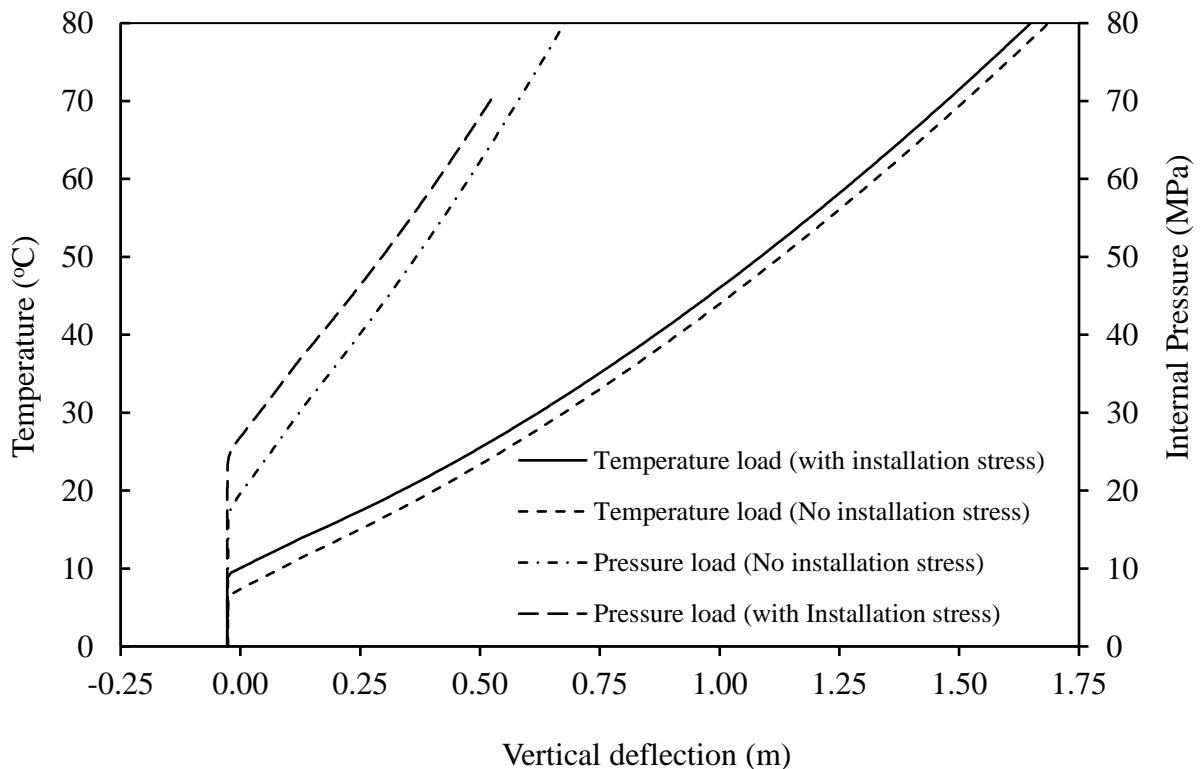


Figure 3.6: Effect of installation stress on critical temperature and critical pressure

3.6. Parametric study

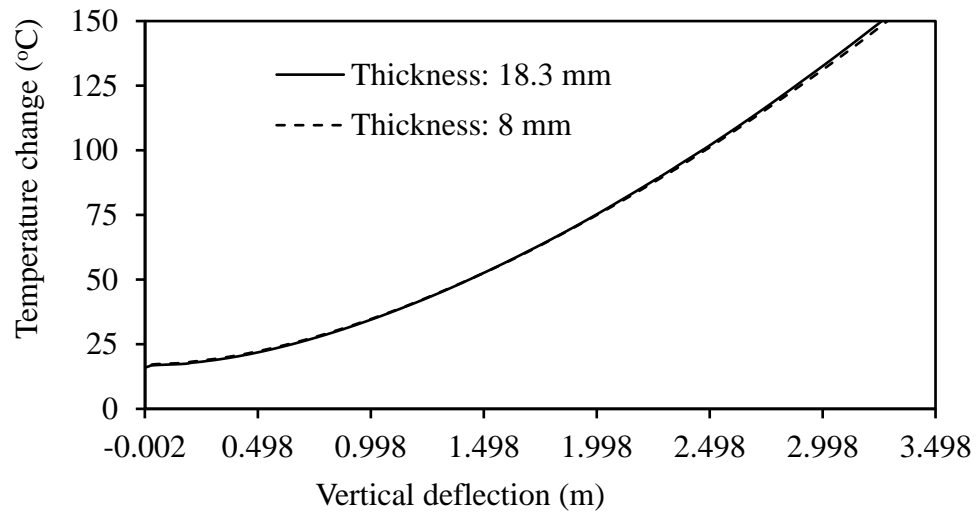
A parametric study is conducted to identify the effects of flexural stiffness of the pipeline, soil conditions and the loading types on the upheaval buckling of the pipeline. The parametric study is conducted for an idealized seabed profile that is expected to provide an initial shape of the pipeline recommended in the design codes (i.e., Equation 3.4). The pipeline laying on the seabed is simulated to account for the installation stress on the pipe wall, as discussed above. An idealized profile with an imperfection height of 1 m and wavelength of 96 m is considered.

3.6.1 Flexural Stiffness of Pipeline

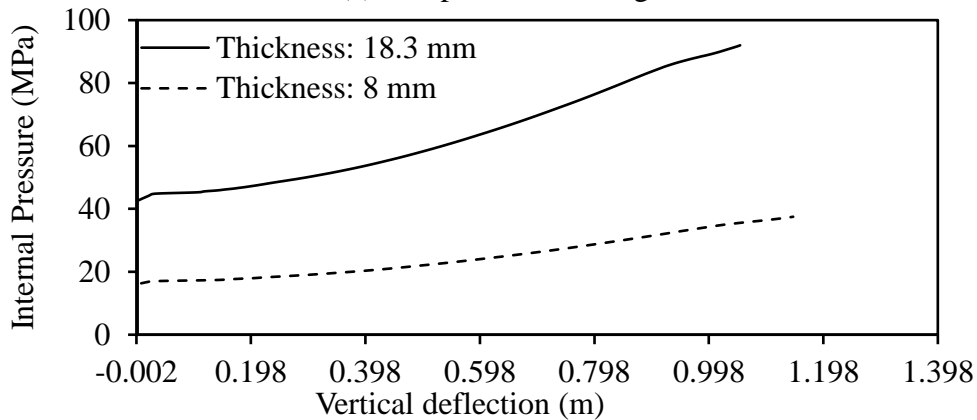
Two different wall thicknesses (i.e., 8 mm and 18.3 mm) for a 219.1 mm diameter pipelines are considered to investigate the effects of the flexural stiffness of the pipeline. Moments of inertia for the pipelines are calculated to be $29.60 \times 10^6 \text{ mm}^4$ and $58.67 \times 10^6 \text{ mm}^4$, respectively. Figure 3.7 shows the maximum deflection of the pipeline (at the crest of the imperfection) due to temperature load and pressure loads. As seen in Figure 3.7 (a), the upheaval buckling behavior under temperature load is not affected by the pipeline stiffness for the two pipe thicknesses considered. However, under the loading of internal pressure, the critical buckling pressure is higher for the pipeline with higher flexural stiffness as shown in Figure 3.7 (b). Due to the increase of the wall thickness from 8 mm to 18.3 mm (increase of the flexural stiffness from $29.60 \times 10^6 \text{ mm}^4$ to $58.67 \times 10^6 \text{ mm}^4$), the critical buckling pressure is increased from 16 MPa to 42.5 MPa (about 166%).

3.6.2 Seabed Soil Parameters

The effects of stiffness and strength parameters of subsea soil on the upheaval buckling of pipeline are investigated using FE modelling. A seabed condition consisting of granular soil is considered. The granular soil condition is encountered at the seabed of offshore Newfoundland. The analysis was conducted with typical lower bound and upper bound values of the friction coefficients between the pipeline and the seabed soil (after, Hobbs 1984).



(a) Temperature loading



(b) Pressure loading

Figure 3.7: Effect of flexural stiffness of pipeline

Figure 3.8 plots the maximum pipe deflections with temperature for a lower bound and an upper bound values of soil modulus, E_s (i.e., 10 MPa and 300 MPa) and the interface friction, f (0.2 and 0.8) for granular soil. Two idealized imperfections obtained using Equation 3.4 with imperfection height (H) of 1000 mm and 400 mm and a wavelength of 96 m are examined. In Figure 3.8, pipe deflection shows a sudden jump at the critical buckling temperature (around 35°C) for the imperfection height of 400 mm, while the rate of deflection suddenly increase at the critical temperature (around 15°C) for the imperfection height of 1000 mm. As discussed earlier, for the pipeline with high imperfection height (i.e., 1000 mm), no snap through buckling occurs. As a result, the sudden jump is not observed. For the pipe with 400 mm of imperfection height, a snap through buckling is expected. The snap through buckling process involves transformation of the strain energy of the system into the kinetic energy that stabilized after a short period of fluctuation (Wang et al. 2015), which is seen at the deflection of around 1.25 m. Figure 3.8 reveals that the critical buckling temperature is not affected significantly by the seabed soil conditions for the surface laid pipeline considered. The critical buckling temperature appears to depend predominantly on the height of imperfection.

3.6.3 Temperature and Pressure Loads

The upheaval buckling of an offshore pipeline is caused by the high pressure and high temperature during operation. The current practice of accounting for the effect of the internal pressure is to apply an equivalent temperature that is calculated from the pressure using Equation 3.1. However, the study presented above reveals that the behavior of the pipeline could be different under the temperature and the pressure loads. As a result, the

approach of using equivalent temperature for the pressure load may not always be applicable. The effects of the temperature and pressure loads are studied here with applications of the temperature and the internal pressure to the pipe using 3D FE analysis. To date, the effect of high pressure on the upheaval buckling has not been studied with direct application of internal pressure.

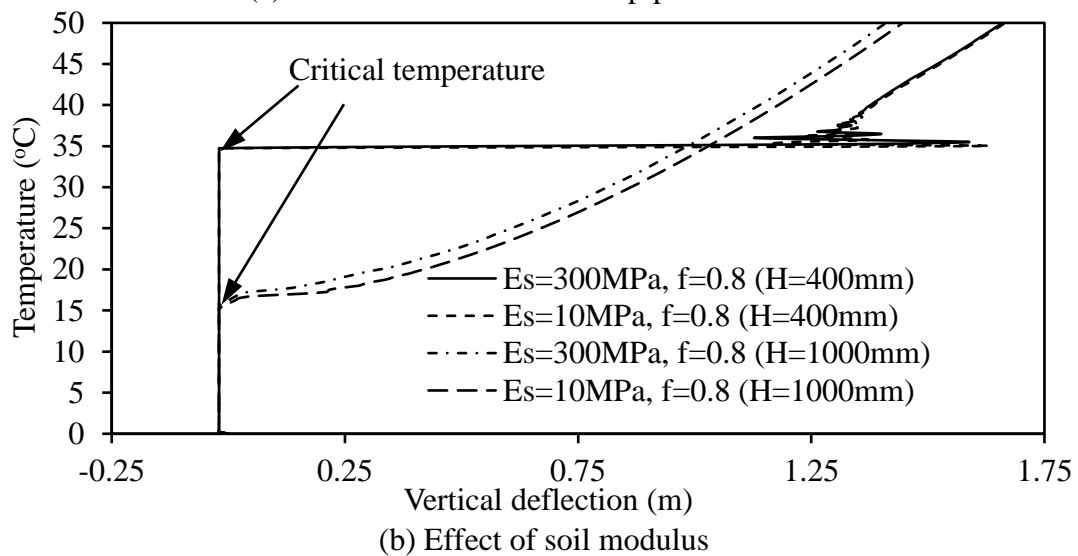
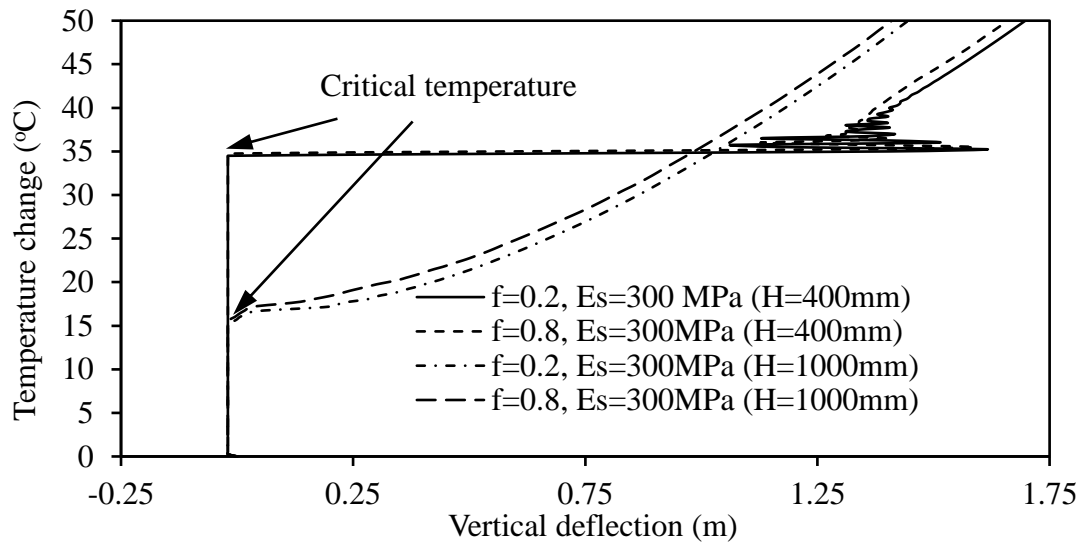


Figure 3.8: Effect of foundation soil properties on upheaval buckling

The validity of the assumption of representing a pressure load by an equivalent temperature load is first examined. A pipeline subjected to 35°C of temperature and 20 MPa of internal pressure is considered. The pipeline is subjected to an imperfection (Equation 3.4) with a height of 400 mm and wavelength of 96 m. The analyses are performed with the applications of each of the loads independently and with representation of the pressure by an equivalent temperature (Equation 3.1). The equivalent temperature corresponding to a pressure of 20 MPa is calculated to be 10°C that results in a total temperature load of 45°C for the pipe. The analysis is also performed with back-representation of the temperature by an equivalent internal pressure using Equation 3.1. The total equivalent pressure of the pipeline is calculated to be 91 MPa. The results of analyses with the three approaches of idealization are compared in Figure 3.9. As shown in the figure, the maximum pipe deflections calculated using the different approaches of the idealization are different. The maximum deflection calculated using equivalent temperature is higher than the deflection calculated using actual loading condition with application of temperature and internal pressure. Idealization of the pressure load by an equivalent temperature would thus provide a conservative estimate of the pipeline behavior. On the other hand, idealization of temperature load by an equivalent pressure would provide unconservative estimation of the pipe deflection. The calculated maximum pipe deflection is significantly less when using the equivalent pressure (Figure 3.9).

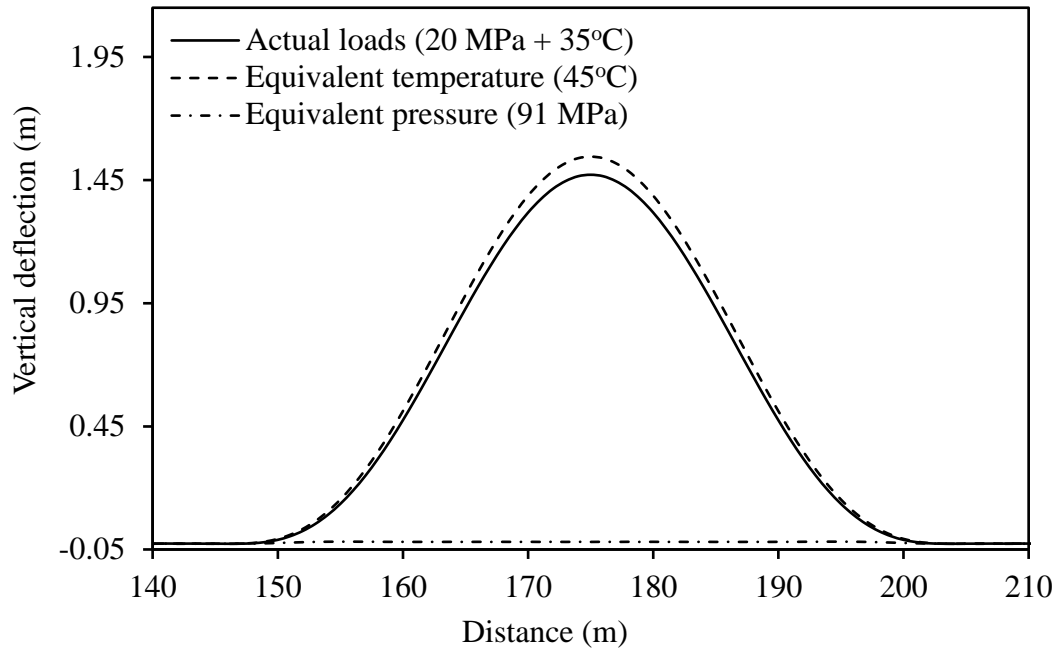


Figure 3.9: Pipe deflection with different method of idealization

The comparison of results from different approaches of modelling the temperature and pressure loads reveals that idealization of the pressure load using equivalent temperature and vice versa may not be applicable for analysis of the upheaval buckling.

Apparently, no buckling is expected with an equivalent internal pressure of 91 MPa with the level of imperfection considered (Figure 3.9). However, for a higher level of imperfection, a pressure load may also initiate upheaval buckling. Figure 3.10 shows the results of analysis conducted with different heights (amplitudes) of initial imperfection under the temperature and pressure loads independently. In Figure 3.10, “T” and “P” in the parentheses correspond to the temperature and pressure loads, respectively. The deflection amplitude of the pipeline is plotted against the temperature and the pressure in the figure. The figure reveals that only internal pressure can cause upheaval buckling if the amplitude

of the imperfection is high. The rate of pipe deflection suddenly increases at the pressures of 25 MPa, 45 MPa, 65 MPa and 90 MPa for the imperfection height of 2200 mm, 1000 mm, 600 mm and 400 mm, respectively. Thus, the critical buckling pressure increases with the decrease of the height of the imperfection (dashed line).

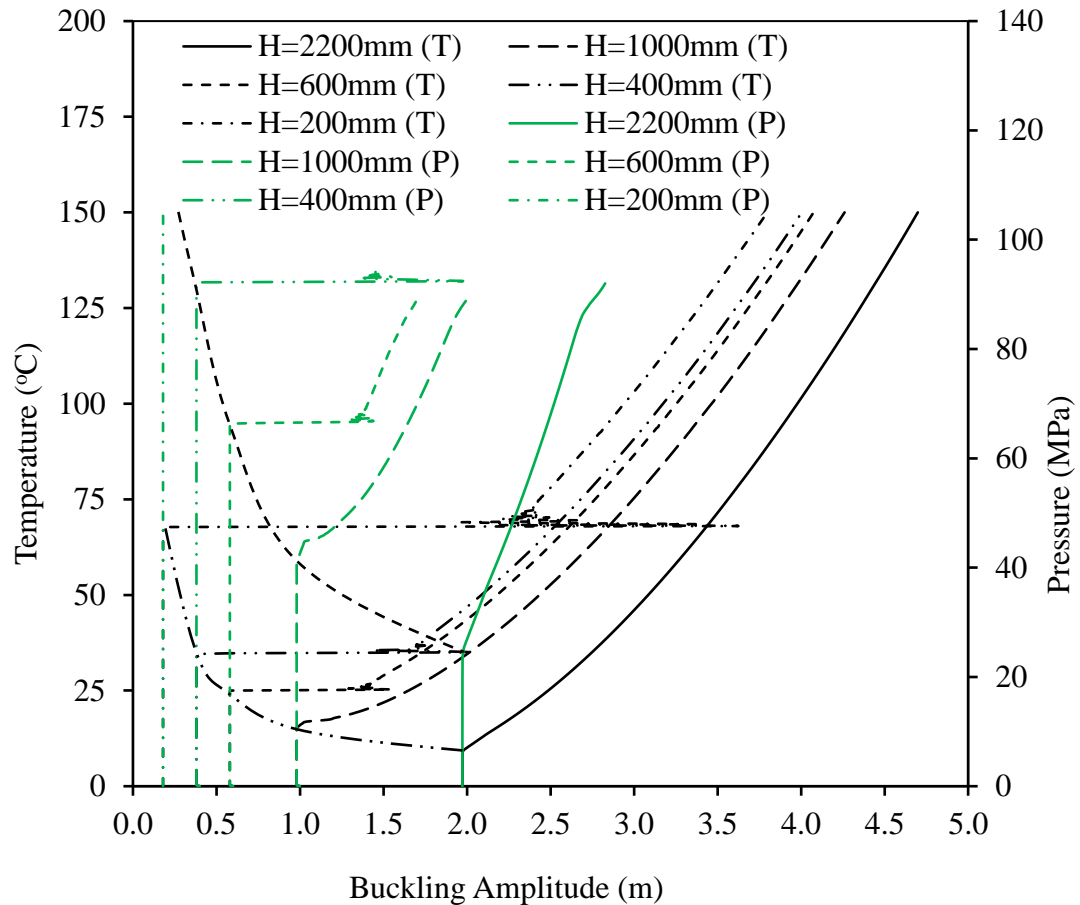


Figure 3.10: Effect of imperfection height on upheaval buckling behavior

For an imperfection of 200 mm height, the critical buckling pressure is not reached within an internal pressure of 100 MPa. As expected, the critical buckling temperature also increases with the decrease of the height of the imperfection (dash-dot line). The height of the imperfection can therefore be controlled to increase the critical buckling temperature

and pressure in order to minimize the upheaval buckling, if the method is economically viable. In the following section, a method is proposed to optimize the height of imperfection as a measure to control upheaval buckling.

3.7. Optimum Height of Imperfection

The seabed profile along the route of the pipeline may include features (i.e., imperfections) of different heights that influence the shape of the initial imperfection of the pipeline. As demonstrated in the above study, the shape of the imperfection significantly affects the behavior of pipeline subjected to upheaval buckling. The critical buckling temperatures and/or pressures would be lower for the pipeline traversing over higher features. The pipelines traversing over higher features are therefore prone to upheaval buckling at lower temperatures and/or internal pressures. In this regard, the height of the features or imperfections could be reduced through excavation to increase the safety of the pipeline to a manageable level. The design height of the imperfection would depend on the operating temperature and pressure of the pipeline. Pipelines under different operating conditions are investigated using 3D FE analysis to develop a design chart for selection of the optimum imperfection height based on the anticipated operating condition of the pipeline. The critical buckling temperatures are calculated for different operating pressures of the pipeline under four different imperfection geometries. A pipeline with a diameter of 219.1 mm and wall thickness of 18.3 mm is considered for this study. The geometry of the imperfection is expressed as the ratio of height (h) and wavelength (L) of the pipeline imperfection.

Figure 3.11 presents the design chart relating the critical buckling temperature with the operating pressure for the pipeline with four different conditions of imperfection. It reveals that the critical buckling temperature decreases linearly with the operating pressure of the pipeline for each of the imperfections. With reduction of h/L , the critical buckling temperature is increased. The design chart in Figure 3.11 could be used to determine the optimum imperfection height to manage pipeline stability against upheaval buckling.

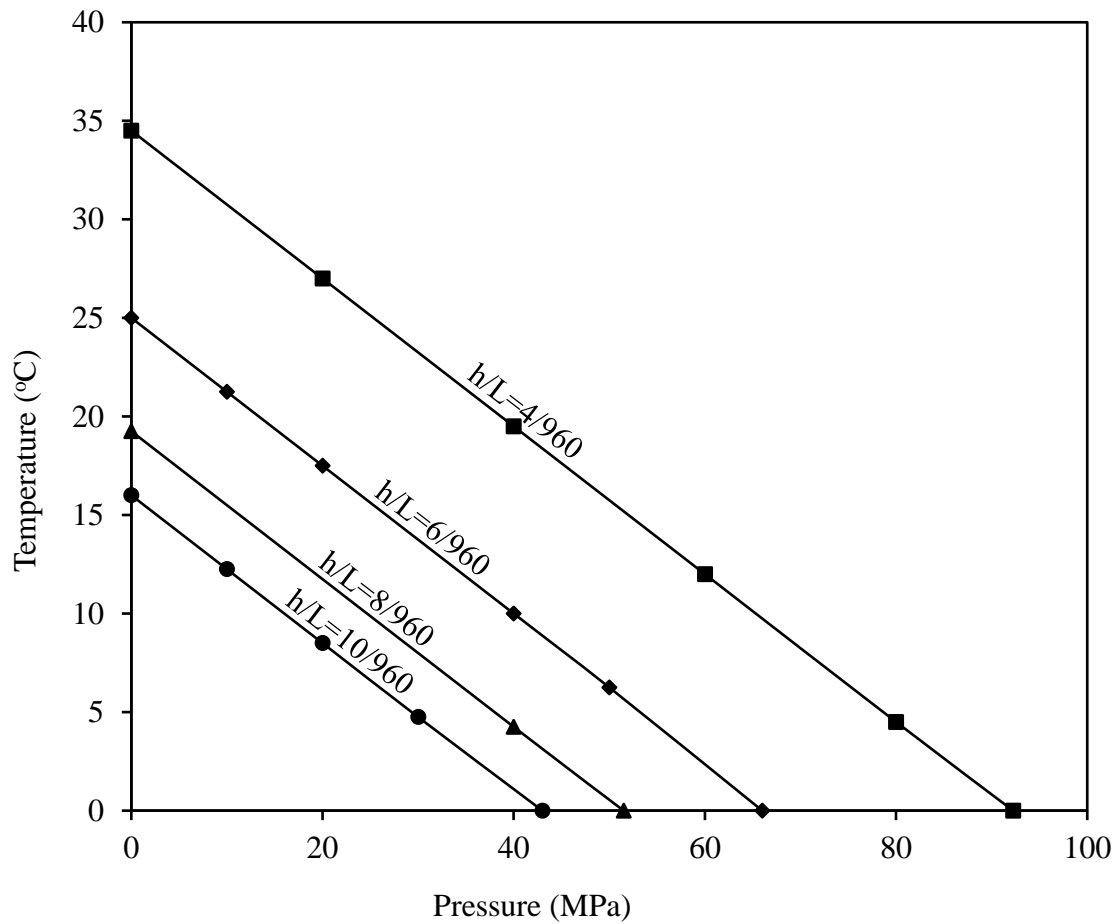


Figure 3.11: Relation between temperature and pressure with respect to out of straightness

3.8 Internal Forces Developed during Upheaval Buckling

3.8.1 Axial Force and Bending Moment

Due to the upheaval buckling, bending moments and axial forces are developed in the pipe wall. The effect of upheaval buckling on the axial force and moment are investigated using an idealized seabed profile with the imperfection height or prop height of 2200 mm (Equation 3.4). The maximum bending moments and the axial forces developed in the pipe wall, located at the crest of seabed profile, with the increase of operating temperature are shown Figure 3.12. The results of analysis for pipelines with installation stresses and without installation stresses are plotted in the figure. The critical buckling temperature for the imperfection height of 2200 mm is 10.25°C (from Figure 3.10). The Figure 3.12 shows that the significant amount of axial compressive force and bending moment are developed in the pipeline cross-section at the initiation of upheaval buckling (i.e., at 10.25°C). The figure also shows that the maximum axial force and the bending moment are affected significantly by the installation stress. For the operating temperature considered, the maximum axial compression of around 230 kN and the maximum bending moment of around 55 kN-m are calculated.

In addition to installation stress, the height of imperfection also affects the axial force and bending moment developed in the pipe wall subjected to temperature load. The effect of imperfection height on the forces is shown in Figure 3.13 using three imperfection heights of 400 mm, 1000 mm and 2200 mm. The installation stress is considered for the results presented in this figure. The critical buckling temperatures for the imperfection heights of 400 mm, 1000 mm and 2200 mm are 34.5°, 16° and 10.25°, respectively (Figure

3.10). The maximum axial compressive force corresponding to these critical buckling temperatures are 985 kN, 417 kN and 185 kN, respectively, whereas the maximum bending moment corresponding to these critical buckling temperatures are 11 kN-m, 30 kN-m and 53 kN-m, respectively (Figure 3.13).

3.9. Summery

The subsea pipeline operated at HPHT is subjected to upheaval buckling. The upheaval buckling is influenced by several factors including initial imperfection, soil properties, loading type and pipe stiffness. The 3D FE models are developed using Abaqus software to study the upheaval buckling and its effects on developing axial forces and bending moments in the pipe cross-section. A real seabed profile of offshore Newfoundland in Canada is examined. The idealized shape of imperfections are also considered for comparison. A method is proposed to determine the optimum height of an imperfection for different load combinations. Based on the analysis, the following conclusions can be drawn:

- The initial shape of pipeline subjected to gravity load depends on the shape of the seabed profile and differs from the idealized shapes recommended in the design codes/literature. The initial shape should be properly modelled to predict the pipeline behavior in upheaval buckling.
- For the pipeline and seabed condition considered, the critical buckling temperature is underestimated by the idealized shape of imperfection. The installation stress on the pipeline is also found to influence the critical buckling loads on the pipelines. For the

pipeline with no installation stress, the critical buckling temperature and the critical buckling pressure are underestimated.

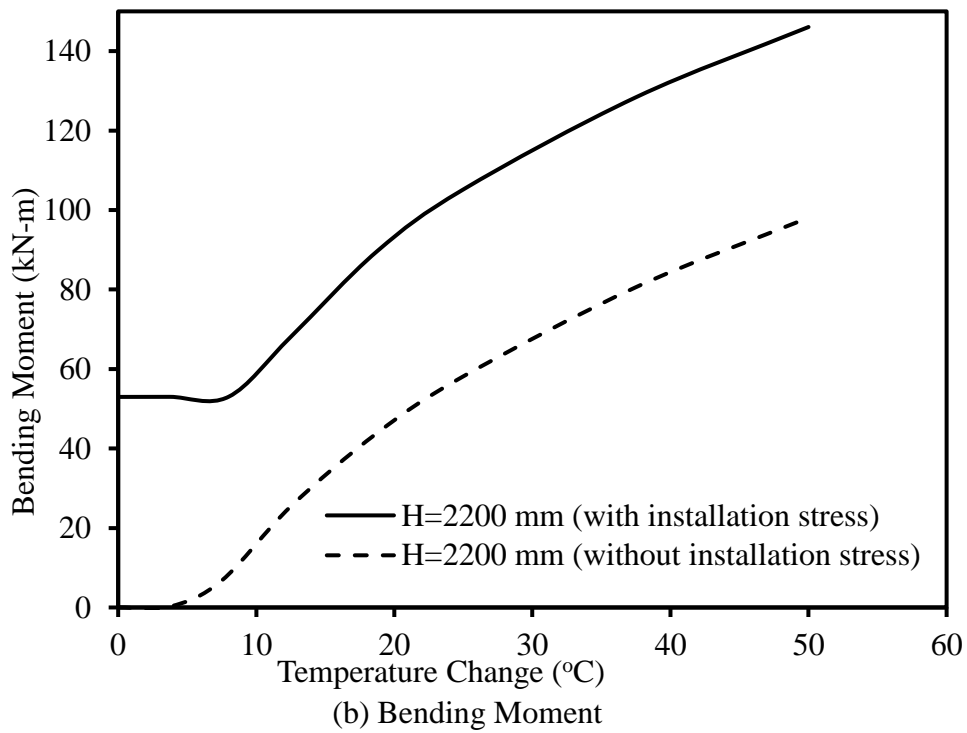
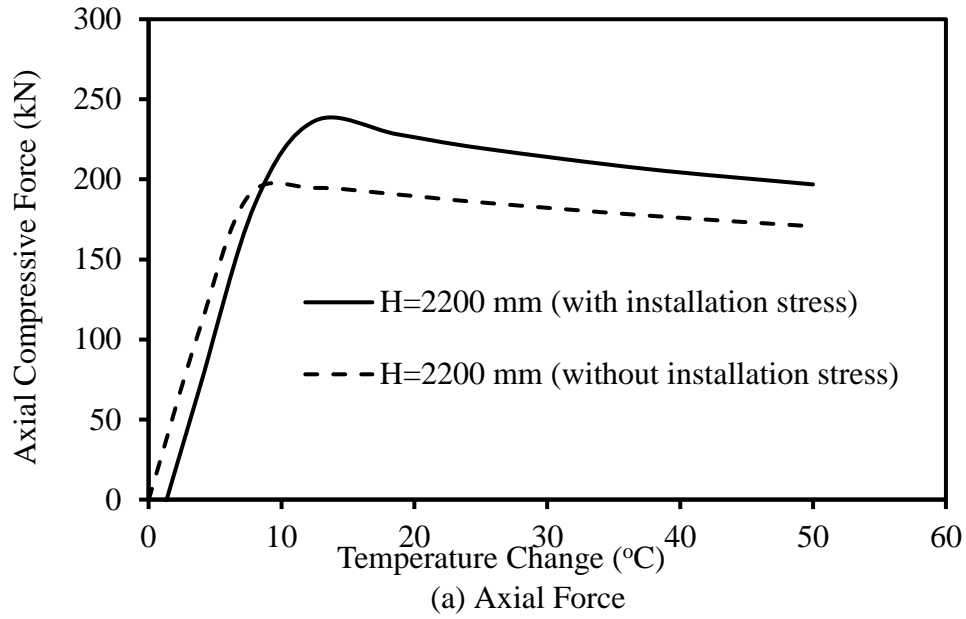


Figure 3.12: Forces in pipe wall at the crest of undulation

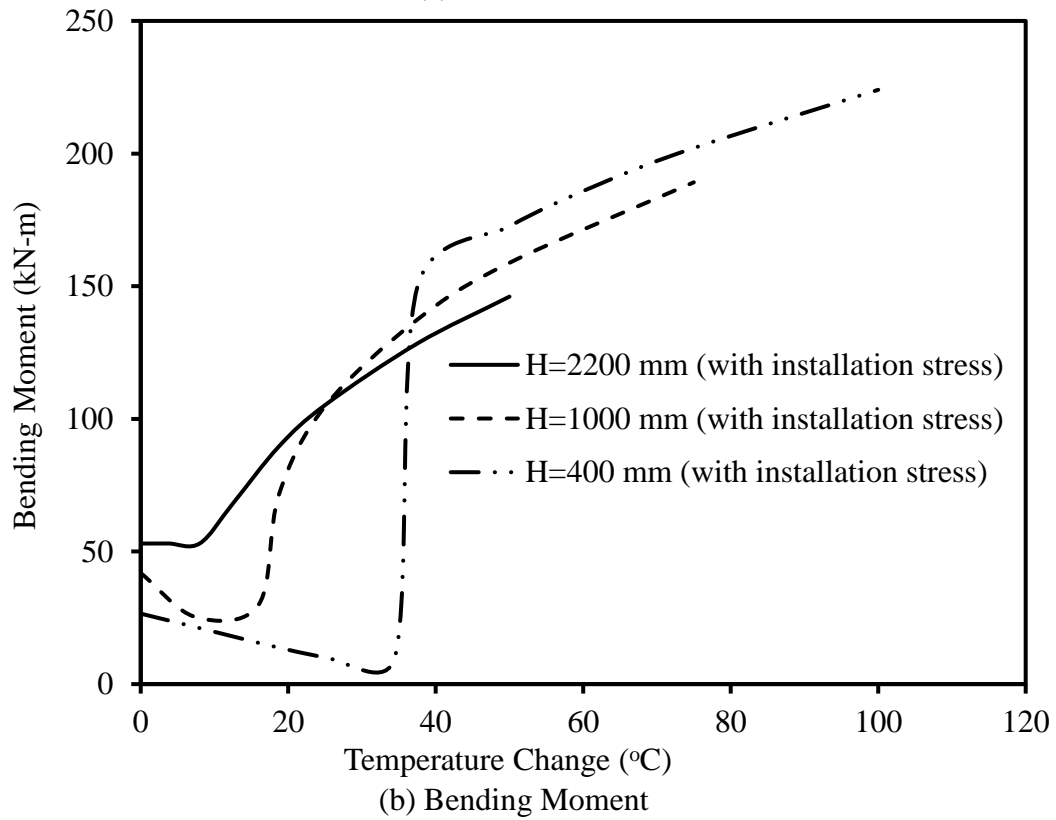
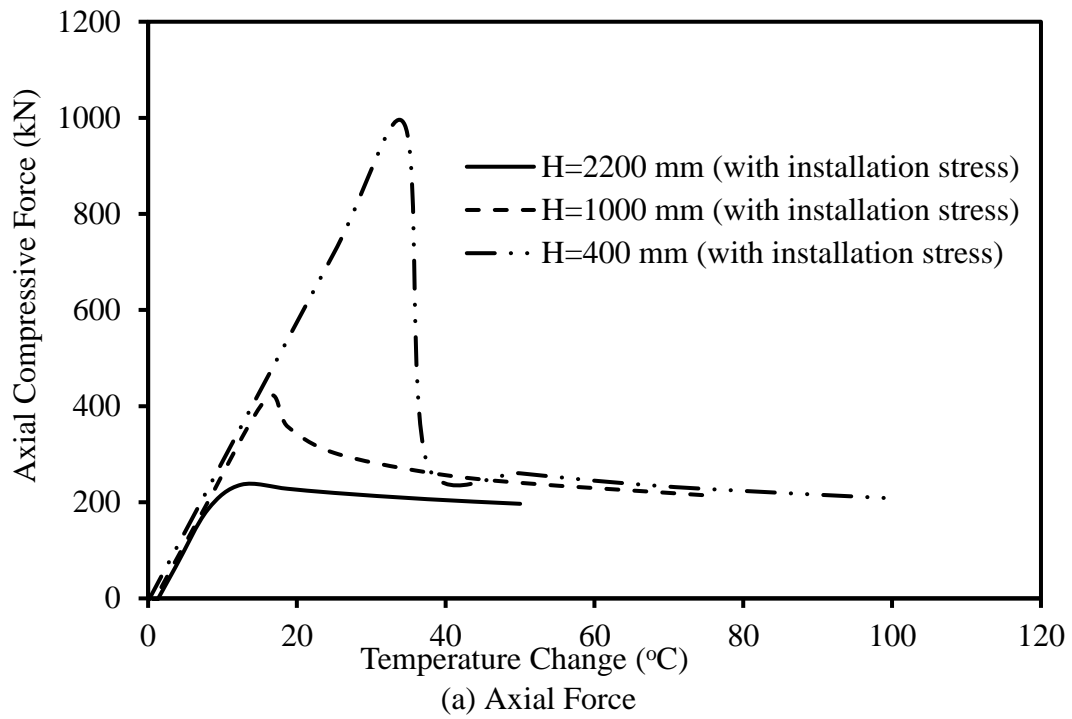


Figure 3.13: Forces in pipe wall for different imperfection heights

- The effects of soil stiffness and pipe-soil interface friction on the upheaval buckling behavior of the surface-laid pipe are not significant. The flexural stiffness of the pipeline has less effect on the critical buckling temperature and has significant effect on the critical buckling pressure. Critical buckling temperature and critical buckling pressure decreases with the increase of the imperfection height.
- Idealization of the pressure load using equivalent temperature and vice versa is not always applicable for the analysis of upheaval buckling of the pipeline. The temperature-pressure interaction diagram can be developed for the assessment of critical loads under the effect of combined loads. A design chart using the interaction diagram is developed to determine the optimum height of a seabed feature to control upheaval buckling.
- The temperature increase in the offshore pipeline laid on an uneven seabed causes the development of internal forces in the pipe cross-section such as axial compressive force and bending moment. The internal forces are maximum at the location of maximum prop height or imperfection height.
- As the offshore pipelines are operated at high temperature and high pressure, the pipelines will be subjected to the load combination of externally applied internal pressure and internally developed axial compressive force and bending moment. Therefore, the strength of the pipelines should be assessed considering the combined effects of axial compressive force, bending moment and the internal pressure.

CHAPTER 4

Finite-Element Evaluation of Burst Pressure Models for Corroded Pipelines

4.1 Introduction

Pipelines play a very important role in the oil and gas industry through transporting the products from the wellheads to the platforms, between the platforms, and to the end users. Steel pipelines have been widely used for these applications due to the high strength to weight ratio of the material, resulting in lower material cost. Pipelines with diameters ranging from 100 mm to over 1500 mm are commonly used (Mohitpour et al. 2003). The oil and gas pipelines are often operated at high internal pressures. The burst pressure generally controls the structural design and safe operation for the high pressure pipelines.

The predictive models for burst pressures for unflawed cylindrical vessels have been developed over the last several decades to accurately predict the failure pressures at plastic collapses of the pipelines. Researchers are working toward improving the burst pressure model, since no single model was found to be accurate in general (Zhu and Leis 2012). On the other hand, the steel pipelines those were laid many years ago are subjected to corrosion. Three common types of corrosion that occurs in the steel pipelines include local corrosion, general corrosion, and pitting corrosions. The corrosion results in different patterns of defects on the pipe wall. The types and the patterns of the corrosion defects significantly affect the internal pressure containment (i.e. burst pressure) of corroded

pipelines. A reliable burst pressure model for the corroded pipelines is required to ensure the structural integrity of the pipelines and avoid catastrophic failures.

A number of design models currently exist to determine the remaining strengths of corroded pipelines (e.g. Modified ASME B31G, CSA Z662-15, DNV, LPC-1, Shell 92). The remaining strength in these models is expressed as the burst pressure as a function of pipe diameter, non-corroded wall thickness, depth of corrosion, longitudinal length of corrosion, and the original strength of the pipe material. Hasan et al. (2011) evaluated several burst pressure models using statistical methods and revealed that different burst models in the design standards/codes provide significantly variable failure probabilities even with the same defect dimensions. Evaluation of several design models using finite element analysis and laboratory burst tests also showed inconclusive results. As mentioned earlier, Chen et al. (2015) revealed, based on experimental results of 460 mm diameter and 8 mm thick pipelines, that the ASME B31G and DNV-RP-F101 methods underestimate the failure pressures of corroded pipelines. However, Swankie et al. (2012) reported the result of 80 full-scale burst tests for a number of pipes with diameters ranging from 88.9 mm to 168.3 mm where the modified ASME B31G method provided unconservative estimation for 35% of the pipes and conservative estimation for 50% of the pipes tested. Majority of their predictions using the LPC-1 method was also found to be unconservative with respect to the test results. Mondal and Dhar (2015) have recently evaluated the modified ASME B31G design model using three-dimensional finite element analysis and found that a pipeline designed using the modified ASME B31G method would provide a factor of safety less than the design factor of safety. The modified ASME B31G method

was found to provide un-conservative burst pressures for pipelines with multiple corrosion patches as well (Dhar and Mondal 2015).

The objective of this study is to identify the strengths and limitations of different existing burst pressure models toward developing an improved burst pressure model for corroded pipelines. Three-dimensional finite element (*FE*) method is used to investigate the failure mechanism of pipelines and to evaluate the burst pressures models.

4.2 Burst Pressure Models

The burst pressure is defined as the internal pressure causing plastic collapse of the pipeline. As discussed earlier, a number of burst pressure models were developed for unflawed and corroded pipelines those are incorporated in different design codes/standards. The models in the modified ASME B31G (2012), CSA Z662-15 (2015), DNV-RP-F101 (2015), LPC-1 and Shell 92 (Hasan et al. 2011) codes are discussed earlier (see section 2.2), as these are evaluated in the current research. These models express the burst pressures as a function of the material flow stress, the defect area projected on the longitudinal plane through the pipe wall thickness direction and the Folias factor as well as pipe geometric parameters (i.e. diameter and wall thickness).

The burst pressure models discussed in Chapter 2 (section 2.2) reveal that the models vary from each other in terms of the definitions of the flow stresses, corrosion depths and Folias factors. For an idealized thin-wall pipeline with uniform corrosion thickness and elastic-perfectly plastic material, all terms in the burst pressure equations in different design codes would be the same except the Folias Factor. Thus, the definition of

the Folias factor is likely to be the major cause of variability of the burst pressures predicted by various methods. The finite element analysis is used in this research to investigate the variability in the burst pressure models.

4.3 Finite Element Modeling (FEM)

A commercially available finite element (FE) software, Abaqus/Explicit, is used for the analysis of the corroded pipelines. Abaqus/Explicit is effective in modelling the problems with large nonlinearity. Large non-linear stress distribution is expected in the wall of corroded pipelines.

4.3.1 Geometry and Boundary Conditions

For the analysis, the length of the pipeline was chosen sufficiently long with respect to the corrosion dimensions and the pipe diameter to avoid any boundary effects. Fekete and Varge (2012) revealed that the boundary effects of a corroded pipeline are minimized if the boundary is located at a distance of L_{min} from the corrosion location, where L_{min} is expressed in terms of pipe diameter, wall thickness and corrosion dimensions as below (Fekete and Varga 2012):

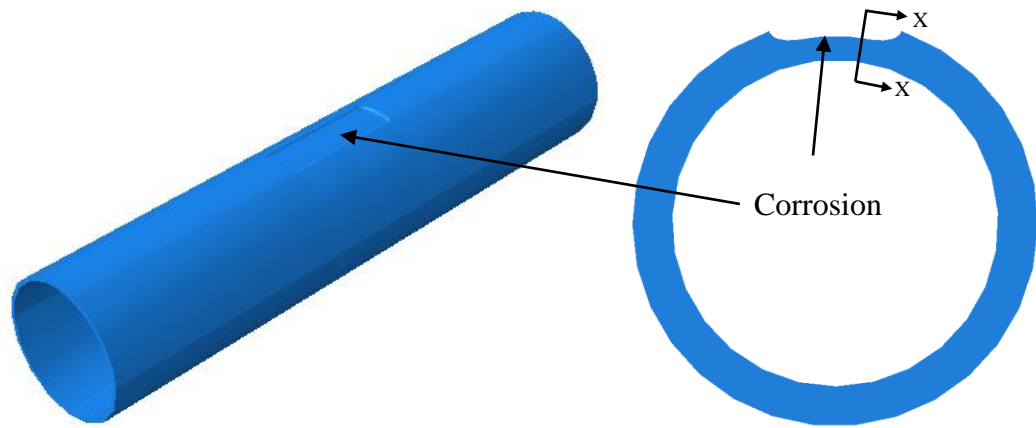
$$L_{min} = \frac{l}{2} + \frac{d}{t} \sqrt{D \cdot t \cdot l} \quad (4.1)$$

The lengths of the pipelines in the finite element models are chosen to be longer than L_{min} . The analyses with fully-restraint boundary condition (fixed support) and only longitudinal restraint at the pipe ends were carried out to investigate the effects of boundary conditions on the behaviour of corroded pipelines. The analyses showed insignificant

variations in the stresses within the corroded zone for the two types of boundary conditions. The stress/strain within the corroded zone is expected to be influenced less significantly by the boundary conditions at the pipeline ends than by the restraint offered by the uncorroded part of the wall near the corroded zone (Diniz et al. 2006). Fully restraint boundary conditions are used at the ends of the pipeline for this study.

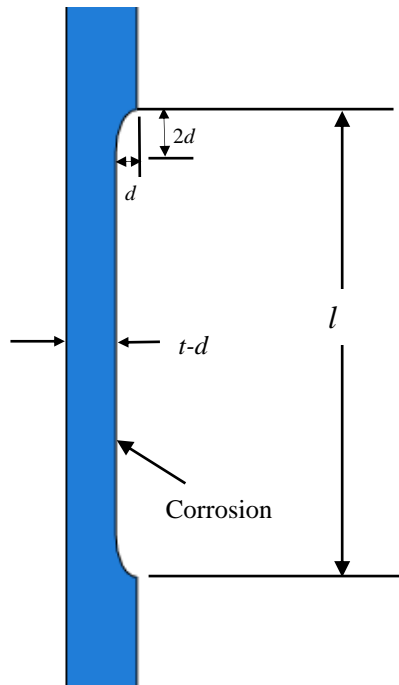
The corrosion is represented as a rectangular patch of thin area on the outer surface located at the mid-length of the pipelines (Figure 4.1). The elliptical shapes with a ratio of the major to minor axis of 2 are fitted at the edges of the corrosion zone to provide smooth interface (Figure 4.1 (c)), since high stress concentration is expected for corrosion defects with sharp edges (Figure 4.1 (d)). The analyses are also carried out for corroded pipelines with sharp edged defects to investigate the extents of the stress concentration.

Four pipe sizes (pipes A, B, C and D) are selected for the analysis. The burst test information for these pipelines are available in the literature (DNV-RP-F101 2015, Diniz et al. 2006 and Oh et al. 2007). The finite element model is first validated through simulation of the burst test result. The model is then extended for a parametric study. For the parametric study, the depth of corrosion (d) is varied from 20% to 70% of pipe wall thickness. The length of corrosion (l) is varied from 0.262 to 1.63 times the outer diameter of pipeline. Two circumferential widths (c) of corrosion (i.e. 95.3 mm and 50 mm) were selected based on the information of test samples which give c/t ratio 2.857 to 9.78. The details of pipeline information and corrosion geometries considered in this study are provided in Table 4.1. The numbers to A, B and C are used to indicate a corrosion geometry used for the parametric study.

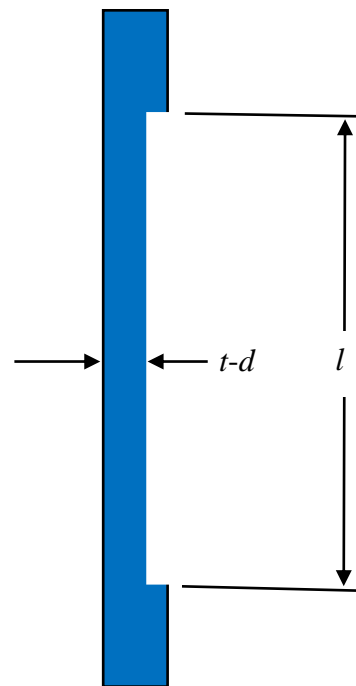


(a) Corrosion on pipe surface

(b) Cross-section with smooth edge



(c) Longitudinal section (X-X) with smooth edge



(d) Longitudinal section (X-X) with sharp edge

Figure 4.1: Idealization of corrosion

For the finite element mesh, fine mesh is used within the zone where stress concentration was expected and coarse mesh is used where uniform stress was expected. Stress concentration is generally expected within and around the corroded area of the pipelines. Thus, the fine mesh is applied within and in the vicinity of the corroded zone and the coarse mesh is applied away from the corroded area. Figure 4.2 shows a typical finite element mesh used in the analysis. The pipe domain was modelled using eight-node continuum element (Abaqus element “C3D8R”). Automatic time increment was chosen for the solution process in Abaqus.

Table 4.1: Pipe geometry and corrosion dimensions

Pipe Identification	D (mm)	t (mm)	d/t	l/D	c/t	L (mm)	Shape of edge
A1	324	9.74	0.70	1.63	9.785	1500	Elliptical
A2	324	9.74	0.70	0.926	9.785	1500	Elliptical
A3	324	9.74	0.70	0.463	9.785	1500	Elliptical
A4	324	9.74	0.20	1.63	9.785	1500	Elliptical
B1	508	14.6	0.70	0.984	6.527	2000	Sharp
B2	508	14.6	0.70	0.591	6.527	2000	Elliptical
B3	508	14.6	0.70	0.295	6.527	2000	Elliptical
C1	762	17.5	0.50	0.394	2.857	2300	Sharp
C2	762	17.5	0.50	0.262	2.857	2300	Sharp
C3	762	17.5	0.25	0.262	2.857	2300	Sharp
D	914.4	25.4	0.40	0.328	3.752	2000	Elliptical

4.3.2 Material Modeling

The material model for the analysis is determined from the test results of stress–strain relations for the pipe materials reported in the literature. Mechanical parameters such as yield strength, ultimate tensile strength, modulus of elasticity, failure strain for these

materials (pipes A, B, C and D) are available in DNV-RP-F101 (2015), Diniz et al. (2006), Fekete and Varga (2012) and Oh et al. (2007). This information is used to develop elastic-perfectly plastic, non-linear and/or bilinear stress–strain models for the FE analysis. The pipe material parameters are shown in Table 4.2. Corresponding stress–strain relations for pipes A, C and D are shown in Figure 4.3.

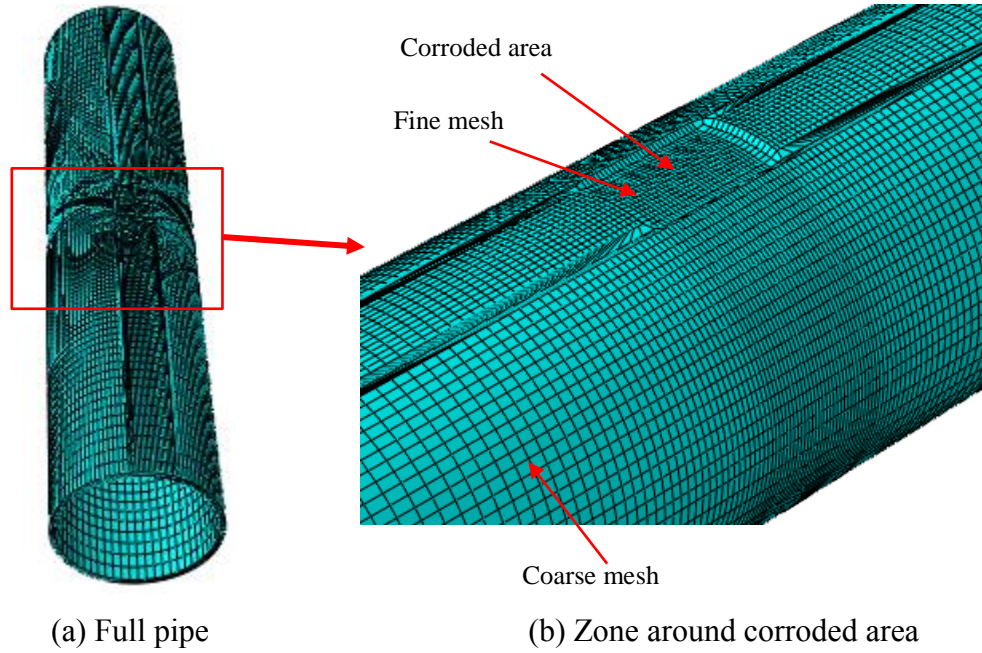


Figure 4.2: Finite element mesh

Table 4.2: Mechanical properties of pipe materials

Pipe ID	Steel Grade	σ_y (MPa)	σ_u (MPa)	E (GPa)	ν	ε_u	Reference
A, D	API X60	452	542	210	0.3	0.043	Fekete and Varga (2012), Diniz et al. (2006)
B	API X60	414	600	210	0.3	0.095	Diniz et al. (2006)
C	API X65	465	564	210.7	0.3	0.061	Oh et al. (2007)

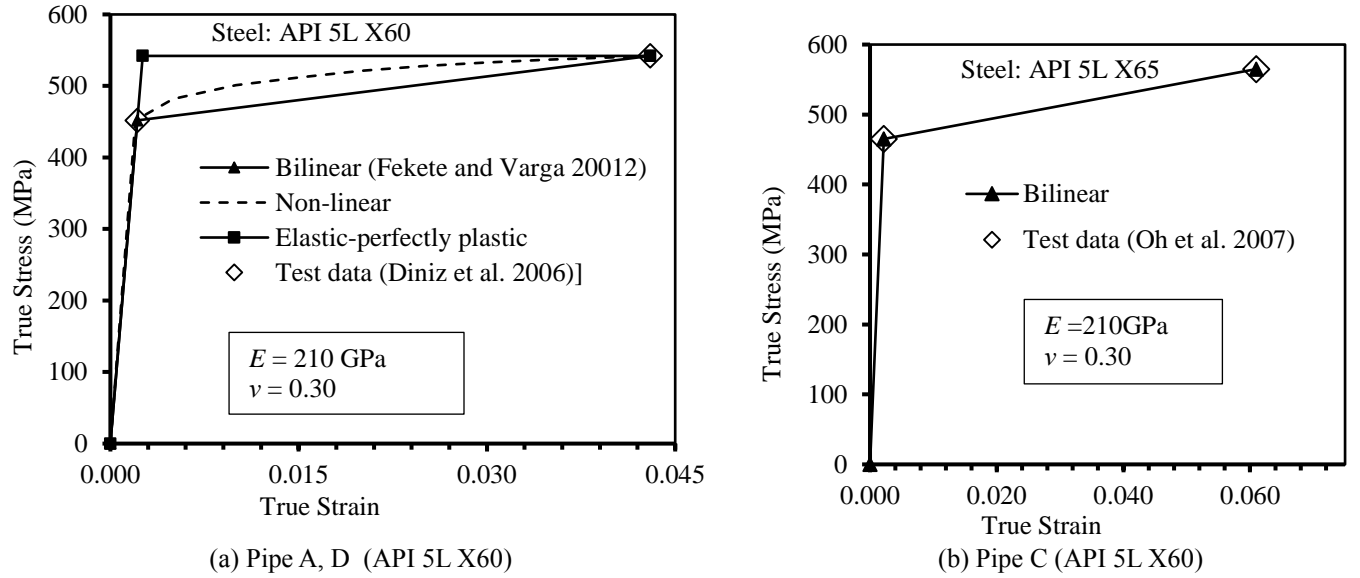


Figure 4.3: Stress-strain relations for pipe materials (Pipe A, C and D)

4.3.3 Validation of FEM

Figure 4.4 shows a comparison of the results of finite element analysis with the burst test results for pipe “A”. The finite element analyses with non-linear material model, bilinear elastic material model and elastic perfectly plastic material model are included in the figure. For the elastic perfectly plastic model, yield strength of the material is taken same as the ultimate tensile strength to simulate the experimental burst pressure, which corresponds to ultimate failure of the pipeline.

Figure 4.4 plots the pipeline internal pressure and the maximum plastic strain on the pipe wall as a function of lateral deflection of pipe wall (a point on the outer surface) at the centre point of the corroded area. In the figure, the maximum internal pressure with the non-linear material model is reached at a plastic strain equal to the failure strain of the

material (plastic strain corresponding to true ultimate tensile strength) (i.e. 0.041), as expected. The internal pressures corresponding to the failure strain of the material are taken as the burst pressures from the analyses with the non-linear and the bilinear material models. The burst pressures of the pipelines are calculated to be 11.63 MPa, 11.43 MPa and 11.61 MPa with non-linear, bilinear and elastic-perfectly plastic material models, respectively. The burst pressure for the pipe from full-scale laboratory test is 11.30 MPa (Diniz et al. 2006), which is within 3% of the finite element calculations. The bilinear material and elastic perfectly plastic models appear to provide almost the same burst pressure (within 2%) as that of non-linear material model. The bilinear model is used for the rest of the analysis presented here to avoid the additional computational time required for the non-linear based model. The burst pressures from the finite element analysis and those from full-scale laboratory tests (DNV-RP-F101 2015, Diniz et al. 2006 and Oh et al. 2007) are given in Table 4.3 for comparison.

Table 4.3: Validation of burst pressure calculations

Pipe ID	D (mm)	t (mm)	d (mm)	P _{test} (MPa)	P _{FEA} (MPa)
A1	324	9.74	6.818	11.30 (Diniz et al. 2006)	11.43
B1	508	14.6	10.220	14.60 (Diniz et al. 2006)	13.26
C1	762	17.5	8.750	19.80 (Oh et al. 2007)	18.11
C2	762	17.5	8.750	21.76 (Oh et al. 2007)	20.44
C3	762	17.5	4.375	24.11 (Oh et al. 2007)	24.33
D	914.4	25.4	10.160	---	25.12

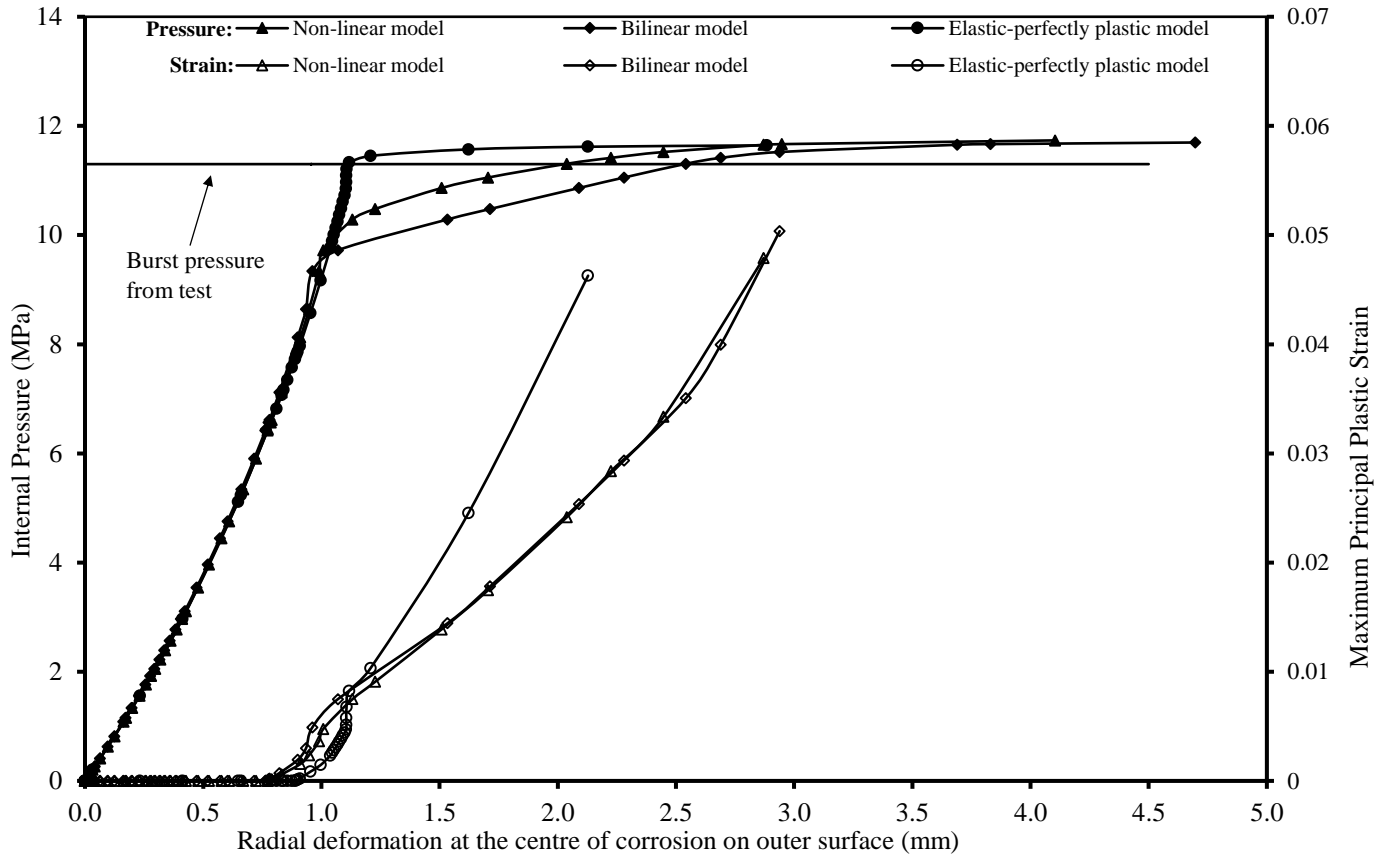


Figure 4.4: Burst Pressure Calculation using FEM (Pipe A1)

In the analysis presented in Figure 4.4, smooth elliptical edge is considered for the corrosion defect. Analysis is also performed to investigate the burst pressure for a pipeline with the sharp edged defect (Figure 4.5). However, the effect of the edge shape is found to be insignificant on the burst pressure. The smooth-edge corrosion is therefore used for the analysis presented herein.

Figure 4.5 presents the results of analysis for a 324 mm diameter pipe with 9.74 mm wall thickness (Pipe A). The corrosion dimensions are $d = 3.896$ mm, $l = 528$ mm and

$c = 95.3$ mm. The burst pressures of 22.50 MPa and 22.44 MPa are obtained for sharp-edged and smooth-edged (elliptical) corruptions, respectively.

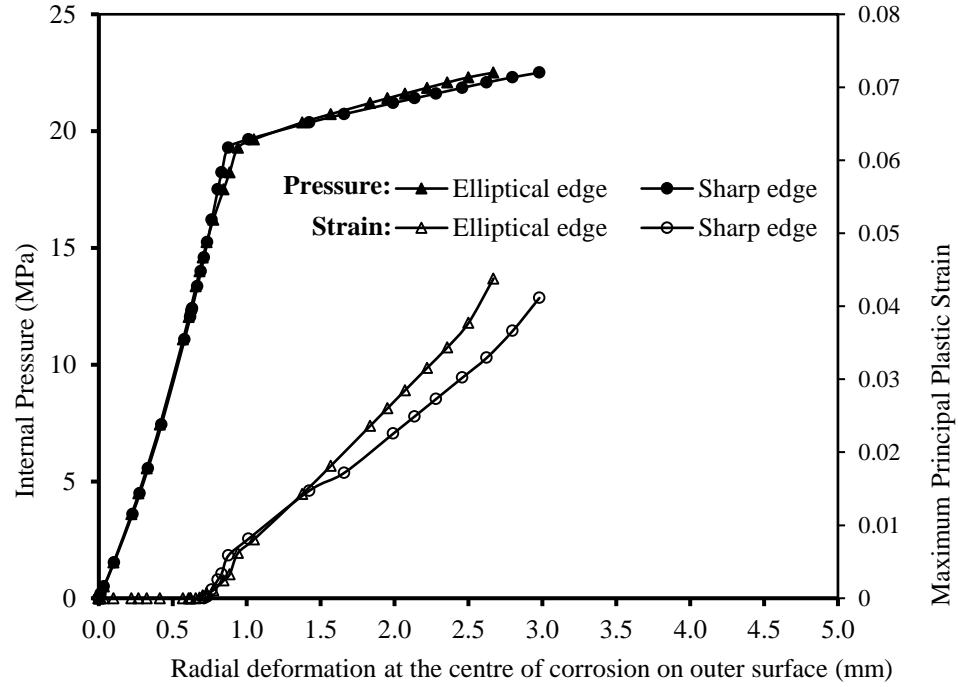


Figure 4.5: Effect of the edge shape of corrosion [$D=324\text{mm}$, $d/t=0.40$, $l=528\text{mm}$]

4.4 Stress/Strain Localization

The deformations of the cross-section of a corroded pipeline (pipe A) at the mid-section of the corroded area (and pipe) are plotted in Figure 4.6. The deformations are plotted at an internal pressure of 7.5 MPa (66% of the burst pressure) at which plastic strain initiates for this pipeline (Figure 4.4).

Figure 4.6 shows non-uniform deformation of the pipe cross-section, while a uniform cross-sectional deformation is expected for defect free pipelines. The deformation is higher near the corrosion zone, which is associated with stress/strain

localization/concentration within that zone. The stress/strain localization resulted in the development of plastic strains at few elements within the corroded area of the pipeline under the internal pressure of 7.5 MPa. Figure 4.7 shows the contour of von Mises stresses and maximum plastic strains at that internal pressure. As shown in Figure 4.7, the maximum von Mises stress is located near the edges of the corroded area. The plastic strain thus initiates on the elements at the edges that extends to the other elements with increase of the internal pressure.

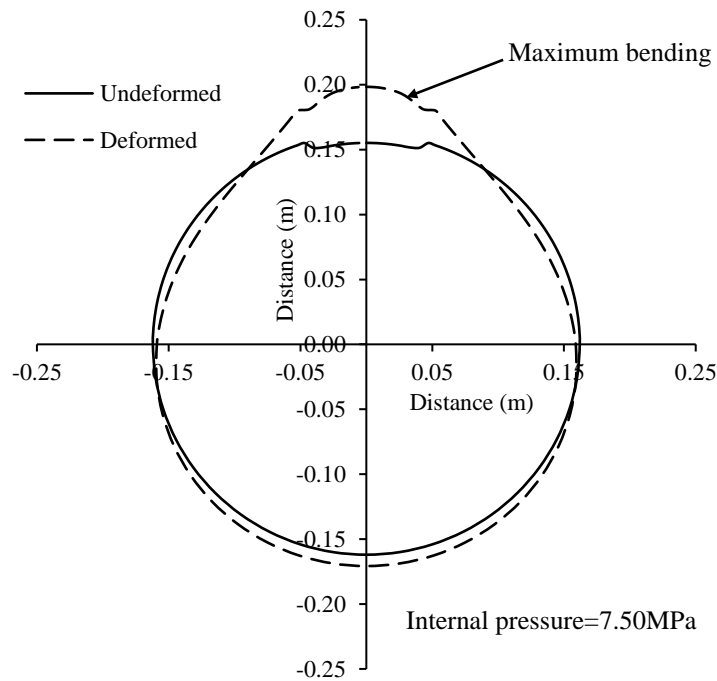


Figure 4.6: Deformation of cross-section at the mid-section of corroded area [Deformation is exaggerated by 50 times]

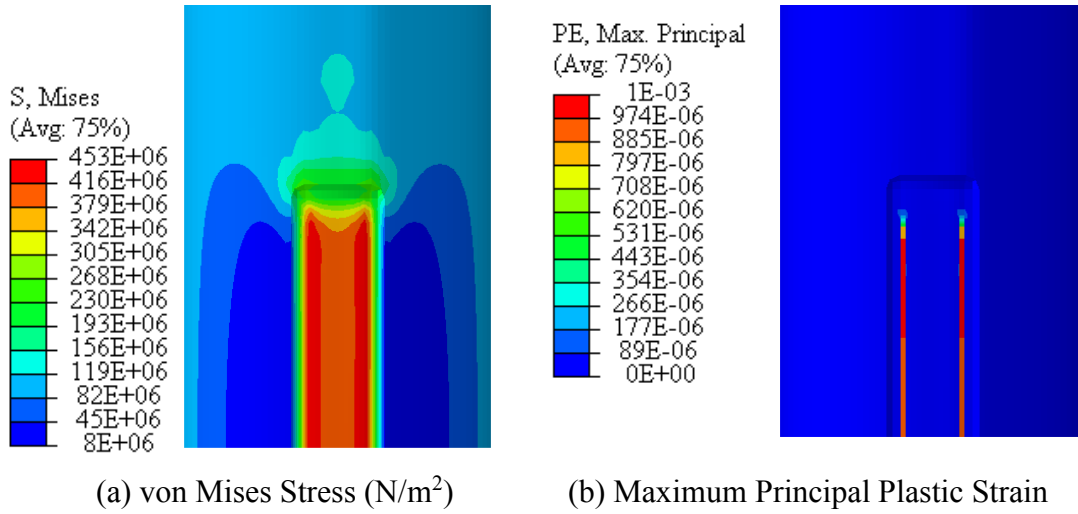


Figure 4.7: Contours of von Mises stress and principal plastic strain ($D=324\text{mm}$, $d/t=0.70$, $l/D= 1.63$ and internal pressure $= 0.66P_{burst}$)

4.5 Comparison of Burst Pressures

A comparison of the burst pressures calculated using different design codes and the finite element methods with the test results from published literature are shown in Table 4.4. Figure 4.8 plots the experimental burst pressures and those given by design codes against the burst pressure obtained from the finite element analysis. The finite element analysis appears to provide a lower bound of the experimental burst pressures in Figure 4.8. The DNV-RP-F101 code provides an upper bound estimations of the experimental burst pressures for a range of burst pressures (from 13.3 MPa to 20.4 MPa) and unconservative estimations beyond that range. The burst pressures from the LPC-1 method are close to the 1:1 line in Figure 4.8, indicating that the method matches with the finite element calculations, particularly for burst pressures less than 25 MPa. At the burst pressure of 30 MPa, the LPC-1 method provides a conservative estimations. The modified

ASME method provides unconservative estimations for burst pressures less than 12.7 MPa and conservative estimations for higher burst pressures. The CSA Z662-15 and Shell 92 codes generally provide overly conservative estimations.

Table 4.4: Summary of burst pressures

Pipe ID	Pressure capacity (MPa)						
	P_{test}	P_{FEA}	P_{ASME}	P_{CSA}	P_{DNV}	$P_{\text{LPC-1}}$	$P_{\text{Shell 92}}$
A1	11.30	11.43	13.41	9.46	12.18	11.60	9.89
A2	---	12.71	14.21	10.21	13.62	12.97	10.59
A3	---	16.64	16.33	12.28	17.37	16.54	12.43
A4	---	29.59	25.52	24.35	29.32	27.93	24.78
B1	14.60	13.26	12.31	10.67	14.10	13.43	11.05
B2	---	16.96	13.40	11.93	16.47	15.68	12.20
B3	---	24.65	16.34	15.59	22.48	21.41	15.42
C1	19.80	18.11	16.65	14.96	19.45	18.52	14.87
C2	21.76	20.44	18.05	16.61	21.75	20.71	16.37
C3	24.11	24.33	21.16	20.73	25.46	24.25	20.70
D	---	25.12	22.37	20.83	26.71	25.44	20.84

The LPC-1 method appears to provide most reasonable calculations of the burst pressures among the methods discussed above for the ranges of pipelines investigated. The modified ASME and the DNV-RP-F101 methods are less reliable since the methods can provide both conservative and unconservative burst pressures. However, Swankie et al. (2012) demonstrated that the LPC-1 method provides both conservative and unconservative burst pressures for small diameter pipes. They recommended not using the LPC-1 method and the modified ASME method to assess the remaining strength for small diameter pipes (diameter < 150 mm).

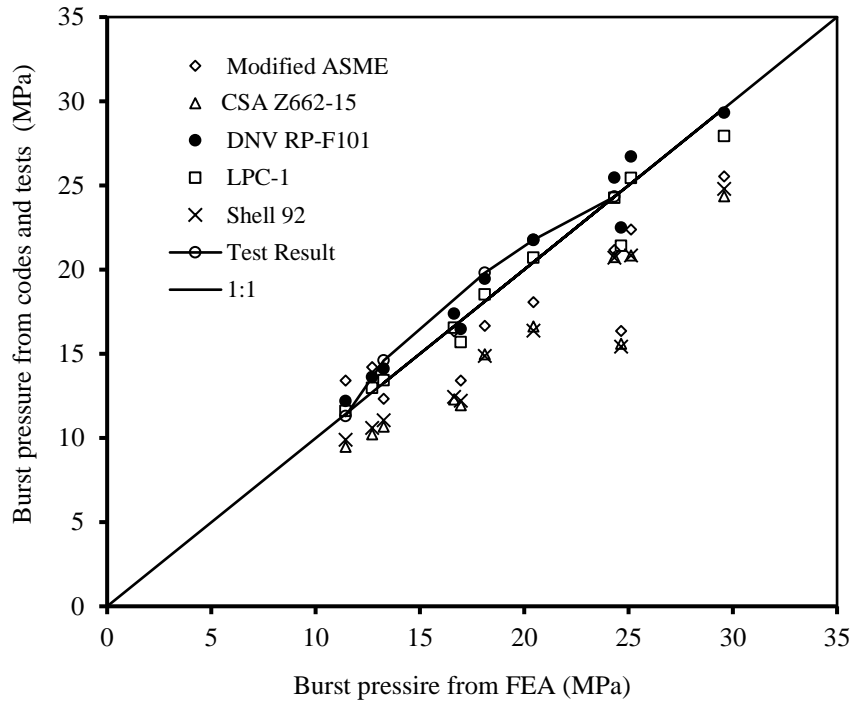


Figure 4.8: Comparison of burst pressures

The differences in the estimations of burst pressures by the different codes are attributed to the terms within parenthesis in the burst pressures equations (i.e. Equations 2.1 to 2.9), since the terms outside the parenthesis correspond to the burst pressures of flawless pipelines. The term within the parenthesis is herein called as “burst pressure reduction factors”. The burst pressure reduction factors from different methods are compared in Figure 4.9. The factors from the finite element analysis are calculated as the ratio of the burst pressures of defected pipelines to the burst pressures of flawless pipelines.

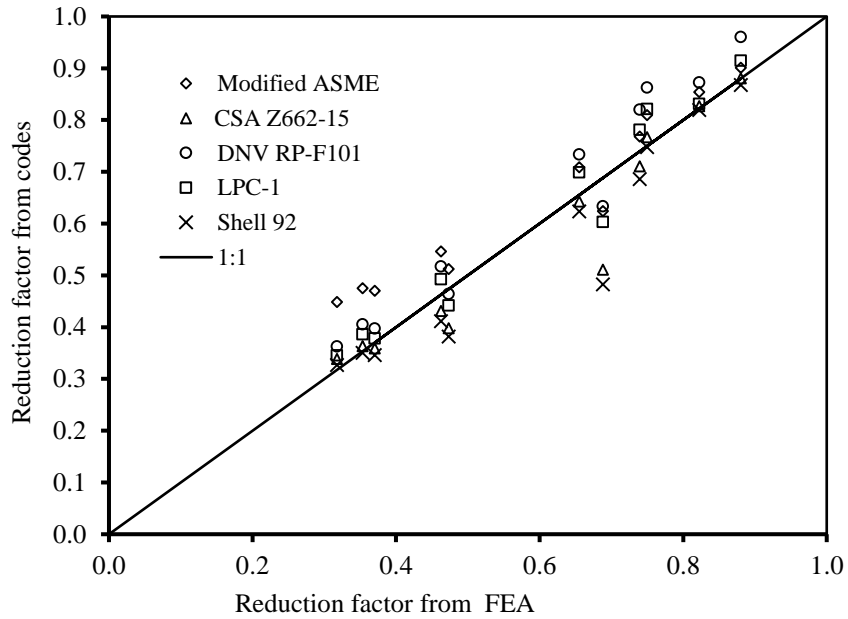


Figure 4.9: Comparison of burst pressure reduction factors

The burst pressure reduction factors from the DNV-RP-F101 code are generally higher than the finite element calculations (Figure 4.9). This may be the reason for over-estimation of the burst pressures in this method with respect to the finite element calculations (as seen in Figure 4.8). Besides, the DNV-RP-F101 code uses the flow stress as $1.05\sigma_u$, in calculation of burst pressure. The method with flow stress equal to σ_u might provide burst pressures closer to the finite element calculations. The burst pressure reduction factors from the LPC-1 method are close to the 1:1 line. This is consistent with the burst pressures obtained using the method (Figure 4.8). The LPC-1 method uses ultimate tensile strength, σ_u , as the flow stress in the calculation of the burst pressure.

The modified ASME method provides higher burst pressure reduction factors in Figure 4.9. This explains the over-estimation of the burst pressures by the method for lower

burst pressures (Figure 4.8). The under-estimations of the burst pressure for higher burst pressure range may be attributed to the flow stress used in this method. As discussed earlier, the flow stress in the modified ASME method is taken as $1.1\sigma_y$, which is less than the ultimate tensile strength, σ_u , of the material. The CSA Z662-15 and Shell 92 codes provide the burst pressure reduction factors close to the 1:1 line, except for few points where the factors are below the 1:1 line. The under-estimation of burst pressure in these methods is likely due to the use of the flow stress of $0.9\sigma_u$, which is less than the ultimate tensile strength.

4.6 Folias Factor

The comparison presented above reveals that the discrepancies in the calculated burst pressures by different codes are likely due to the difference in the definitions of the flow stress and the burst pressure reduction factor. The flow stress is a strength parameter of the pipe material whereas the burst pressure reduction factor is a geometric parameter, which is related to the geometries of the defects. Individual contribution of the strength parameter and the geometric parameter need to be identified in order to develop improved burst pressure prediction models. However, laboratory burst tests provide burst pressures of the test pipes under the combined effects of material strength, defect geometry and any internal flaws, if presents. It is not possible to separate the contribution of each parameter from the results of laboratory tests. In this regard, finite element analysis could be used to determine the individual contribution of each parameter through a parametric study.

In the finite element analysis presented in this study, material parameters of the actual pipe materials are used that are obtained from published literature. The geometric parameter is separated from the results of finite element analysis as discussed below.

The equations for the burst pressure in different codes appear to follow a general form as in Equation 4.2.

$$P = P_0 \left[\frac{1 - \frac{d}{t}}{1 - \frac{d}{tM}} \right] \quad (4.2)$$

Where ‘ P ’ is the burst pressure of corroded pipeline, “ P_0 ” is the burst pressure for flawless pipeline, “ d ” is the depth of defect, “ t ” is the pipe wall thickness and “ M ” is the Folias factor.

As mentioned earlier, Folias factor is likely the major parameter causing the variability in the burst pressures predicted by various methods. Different equations are used in different codes to define the Folias factor. Equation 4.2 can be rearranged to obtain an expression for the Folias factor as below (Equation 4.3):

$$M = \frac{\frac{Pd}{tP_0}}{\frac{P}{P_0} + \frac{d}{t} - 1} \quad (4.3)$$

Equation 4.3 is used to calculate the Folias factor from the result of finite element analysis. The Folias factor, M , from finite element analysis are compared with those obtained from various codes in Figure 4.10. Figure 4.10 plots M^2 as a function of $l^2/(Dt)$, since the factors in the design codes are expressed as a square root of a function of $l^2/(Dt)$.

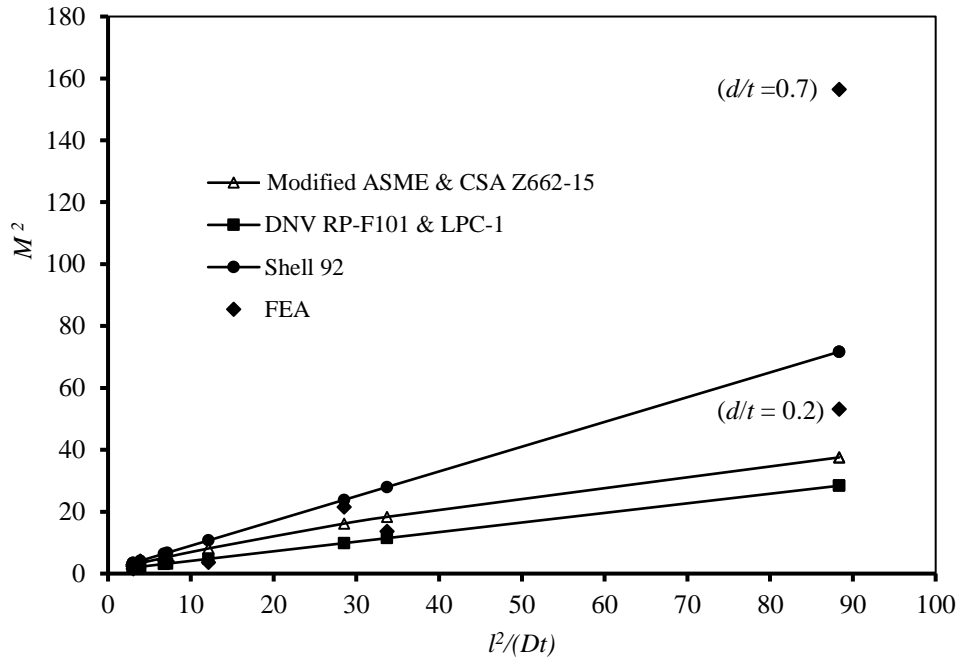


Figure 4.10: Folias factors

As expected, a linear correlation is observed in Figure 4.10 for all of the design codes including the modified ASME code that include a second order term in the equation for the Folias factor (i.e. $l^4/(Dt)^2$). The contribution of the second order term appears to be negligible for the analysis presented.

The data from the finite element calculations are scattered in Figure 4.10. It appears that other parameters such as corrosion depth may have effects on the Folias factor in addition to $l^2/(Dt)$. For $l^2/(Dt)$ of around 90, two data points are widely scattered, one with $M^2 = 53.15$ for $d/t = 0.2$ and the other with $M^2 = 156$ for $d/t=0.7$. However, contribution of corrosion depth or d/t is not incorporated in the calculation of the Folias factor in the

current design codes. Further research is therefore anticipated in this regard to develop an improved burst pressure model for corroded pipelines.

4.7 Summary

Several burst pressure models recommended in the design codes/standards are evaluated in this study using finite element analysis. Laboratory test results from published literature are used for validation of the finite element models. The study reveals that the calculated burst pressures using different codes/standards vary significantly. Among these, the DNV-RP-F101 code provided upper bound estimation of the experimental burst pressures for a range of burst pressures (from 13.3 MPa to 20.4 MPa) and unconservative estimations beyond that range. The burst pressures from the LPC-1 method are close to the finite element calculation. The modified ASME method provided conservative and unconservative estimations of the burst pressures. The modified ASME method showed conservative results for higher burst pressures. The CSA Z662-15 and Shell 92 codes provided overly conservative estimations. The LPC-1 method thus appears to provide most reasonable calculation of the burst pressures among the methods discussed herein for the ranges of pipes investigated.

The discrepancies in the calculated burst pressures by different codes are attributed to the different definitions of the flow stress and the burst pressure reduction factor in the codes. The flow stress is a strength parameter of the pipe material, whereas the burst pressure reduction factor is a geometric parameter. While it is difficult to separate the contribution of strength parameters and geometric parameters from the results of laboratory

tests, the finite element analysis could be used to determine the individual contribution of each parameter.

The Folias factor is identified as the major parameter contributing to the geometric parameter (i.e., burst pressure reduction factor). A finite element evaluation of the Folias factor revealed that the factor depends on other parameter such as defect depth in addition to the parameters currently considered in the design codes (i.e. $l^2/(Dt)$). Further research is recommended to incorporate the effect of defect depth in the calculation of the Folias factor.

CHAPTER 5

Improved Folias Factor and Burst Pressure Models for Corroded Pipelines

5.1 Introduction

Pipelines are extensively used as the most economic means of transporting oil and gas. Steel pipelines have been widely used for these applications due to the high strength to weight ratio of the material, resulting in lower material cost. These pipelines are subjected to corrosion over the service life, resulting in the reduction of wall thickness. The prediction of the remaining strength of a corroded pipeline is required for fitness-for-purpose assessment. For the prediction of the remaining strength, different models were developed based on simplified results of analysis and/or empirical fits to limited experimental data. A few of these models were developed through industry specific study, e.g. RSTRENGTH (Kiefner and Vieth 1989), and are not readily available in the public domain. The established design codes i.e. ASME B31G (2012), DNV-RP-F101 (2015), BS 7910 (2013), CSA Z662-15 (2015) adopt simplified design equations for the prediction of remaining strengths of corroded pipelines. The equations adopted in different codes are summarized in Table 5.1. However, researchers have demonstrated that pipeline strengths predicted using the existing design methods are not consistent with the burst test results and results obtained from rigorous finite element (FE) analysis.

Mondal and Dhar (2016) critically investigated different existing burst pressure models to demonstrate the differences among the models and to identify the source of the

inconsistencies in the prediction of the burst pressures. It is revealed that the burst pressures in these models (Table 5.1) are expressed in general in terms of the maximum stress capacity of material expressed as a flow stress, σ_{flow} , the defect area projected on the longitudinal plane through pipe wall thickness and the Folias factor, in addition to pipe geometric parameters (i.e. diameter and wall thickness), as shown in Equation 5.1.

Table 5.1: Models of Burst Pressure provided by codes

Code	Burst Pressure Model	Depth of defect	Equation for M
ASME B31G (2012)	$P = \frac{2t}{D} \sigma_{flow} \left(\frac{1 - 0.85 \frac{d}{t}}{1 - 0.85 \frac{d}{tM}} \right)$	$d = d_{max}$	Equation 5.4 or 5.5
DNV-RP-F101 (2015)	$P = \frac{2t}{D - t} (1.05 \sigma_u) \left(\frac{1 - \frac{d}{t}}{1 - \frac{d}{tM}} \right)$	$d = d_{max}$	Equation 5.6
BS 9710 (2013)	$P = \frac{2t}{D - t} \sigma_{ref} \left(\frac{1 - \frac{d}{t}}{1 - \frac{d}{tM}} \right)$	$d = d_{max}$	Equation 5.6
CSA Z662-15 (2015)	$P = \frac{2t}{D} \sigma_{flow} (= 0.90 \sigma_u) \left(\frac{1 - \frac{d}{t}}{1 - \frac{d}{tM}} \right)$	$d = d_{avg}$	Equation 5.4 or 5.5

$$P = \frac{2t}{D} \sigma_{flow} \left[\frac{1 - \frac{d}{t}}{1 - \frac{d}{tM}} \right] \quad (5.1)$$

As seen in Table 5.1, the burst pressure models in the design codes differ from each other in the definitions of flow stress, depth of corrosion defect and the Folias factor. For example, the flow stress in the Modified ASME B31G code uses $1.1 \sigma_y$ or average of σ_y and σ_u to account for the strain hardening effects, while the DNV-RP-F10 code use 1.05

σ_u . It is to be noted that the flow stress (the maximum stress capacity of material) is independent of the shape of the corrosion defect and is also applicable for a pipeline without any corrosion defect (flawless pipe). Mondal and Dhar (2016a) expressed the terms outside the parenthesis in Equation 5.1 as the burst pressure of flawless pipes and the terms within parenthesis as “burst pressure reduction factor” that account for the reduction of the burst pressure due to corrosion. They proposed to consider these terms separately toward developing an improved burst pressure model.

For the burst pressure reduction factor, the Modified ASME B31G code recommends using of the depth as 0.85 times the maximum depth (d_{max}), while the DNV-RP-F101 recommends using the maximum depth. However, for a corrosion defect with a uniform depth (which is most commonly used in the laboratory burst test and in FE modelling), the depth recommended in each of the codes is necessarily the same. Thus, the only parameter contributing to the burst pressure reduction is the Folias factor.

A few different equations are currently used to calculate the Folias factor in the design codes (Table 5.1) where it is expressed in terms of $l^2/(Dt)$. Mondal and Dhar (2016a) revealed that none of the expressions is capable of predicting the burst pressure reduction correctly. They identified that the expressions for the Folias factor do not include the defect depth, whereas defect depth was found to influence the factor. Figure 5.1 compares the Folias factors calculated using the equations in ASME B31G and DNV-RP-F10 codes with those calculated using FE analysis (After Mondal and Dhar 2016a). Figure 5.1 plots M^2 as a function of $l^2/(Dt)$, since the factors in the design codes are expressed as a square root of a function of $l^2/(Dt)$. In this figure, the FE method calculates different M for different d/t

ratios with the same of $l^2/(Dt)$. For $l^2/(Dt)$ of around 90, two data points are widely scattered, one with $M^2 = 53.15$ for $d/t = 0.2$ and the other with $M^2 = 156$ for $d/t=0.7$. The study demonstrates the necessity of developing an improved model for correctly calculating the Folias factor.

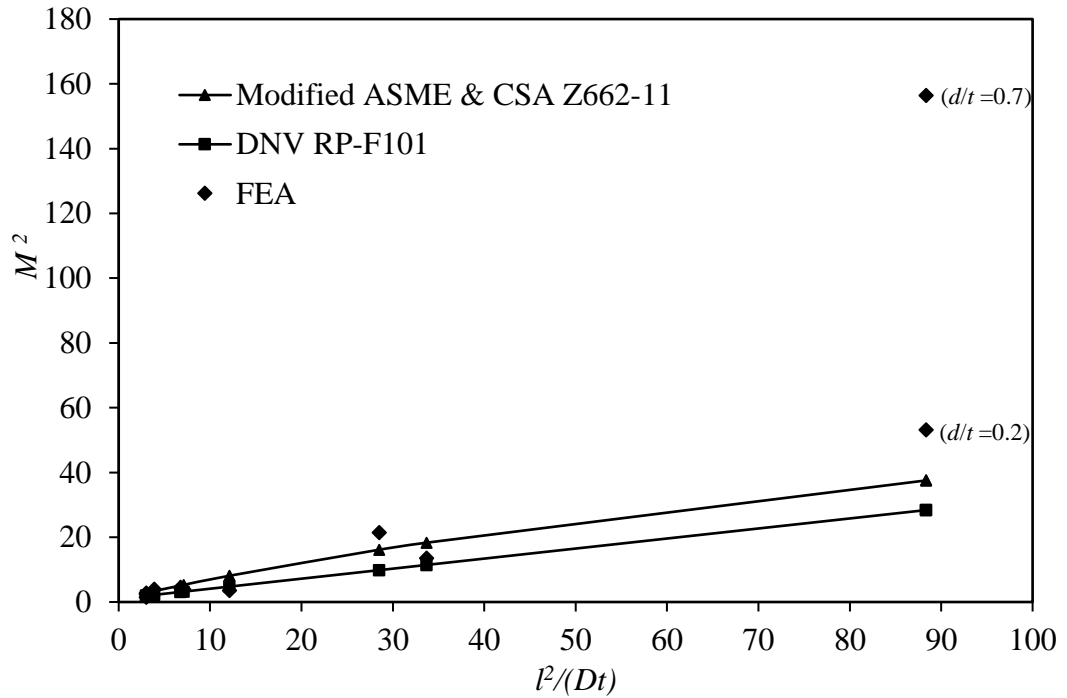


Figure 5.1: Comparison of Folias factors obtained from FE analysis and design codes (After Mondal and Dhar 2016a)

In this study, an improved burst pressure model for corroded pipeline is developed considering the components of the burst pressure of flawless pipe and the Folias factor separately. The new model is proposed for the Folias factor accounting for the effects of d/t ratio. The model constants (i.e., coefficients and exponents) are determined based on a database developed using FE analysis. A series of FE analyses are conducted with different pipe dimensions and different defect geometries to develop the database. A revision of the

existing model for the component of burst pressure of flawless pipeline is also proposed that provides a better estimation of the burst pressure for the corroded pipelines with respect to the results of finite element analysis and laboratory burst tests.

5.2 Folias Factor

The term “Folias Factor, M” is used to describe the bulging effect of a shell surface that is thinner in wall thickness than the surrounding shell. It measures the stress concentration at the tip of a crack with expansion under internal pressure. The factor was first derived analytically by Folias (1964) considering a surface crack along the axis of a cylindrical shell. The general form of the factor is given by Equation 5.2 (Folias 1973).

$$M = f_e(\lambda) + f_b(\lambda)\chi(\lambda) \quad (5.2)$$

Where,

$$\lambda = \sqrt[4]{\frac{3(1 - \nu^2)l^4}{D^2t^2}}$$

$f_e(\lambda)$ = extensional coefficient

$f_b(\lambda)$ = bending coefficient

$$\chi(\lambda) = \frac{\sigma_{bending}}{\sigma_{hoop}}$$

When the cylindrical shell is subjected to internal pressure only, the simplified expression of the factor is reduced to Equation 5.3.

$$M = \sqrt{1 + 0.317\lambda^2} \quad (5.3)$$

The Folias factor was investigated by several researchers to apply it to the determination of the remaining strength of corroded pipelines. The expression of the Folias factor was modified and incorporated in the design codes (e.g., ASME B31G 2012, DNV-RP-F10 2015, BS 7910 2013, CSA Z662-15 2015). The ASME B31G and CSA Z662-15 codes define the corrosion defects into two types such as short defects and long defects. Different expressions of the Folias factor are used for the short and the long defects, separately. Equation 5.4 and Equation 5.5 present the expressions recommended in the ASME B31G and CSA Z662-15 codes.

For $\frac{l^2}{Dt} \leq 50$

$$M = \sqrt{1 + 0.6275 \frac{l^2}{Dt} - 0.003375 \frac{l^4}{D^2 t^2}} \quad (5.4)$$

For $\frac{l^2}{Dt} > 50$

$$M = 0.032 \frac{l^2}{Dt} + 3.30 \quad (5.5)$$

The DNV-RP-F10 and BS 7910 codes do not distinguish short and long corrosion defects. A single equation is recommended for the Folias factor (Equation 5.6).

$$M = \sqrt{1 + 0.31 \left(\frac{l}{\sqrt{Dt}} \right)^2} \quad (5.6)$$

The structures of the equations used in different codes for Folias factor are thus different from each other. The equations are expressed in terms of $l^2/(Dt)$ and do not include the depth of the defect. Keeping the similarities in the structures of equations, two new models for Folias factor, M_1 and M_2 , are proposed in this study, as shown in Equation 5.7 and 5.8, incorporating the depth of corrosion defect.

$$M_1 = \sqrt{1 + k_1 \left(\frac{l^2}{Dt} \right)^{k_2} \left(\frac{d}{t} \right)^{k_3}} \quad (5.7)$$

$$M_2 = \sqrt{1 + k_1 \left(\frac{l^2}{Dt} \right)^{k_2} \left(\frac{d}{t} \right)^{k_3} + k_4 \left(\frac{l^4}{D^2 t^2} \right)^{k_5} \left(\frac{d^2}{t^2} \right)^{k_6}} \quad (5.8)$$

In Equation 5.7 and 5.8, the constants k_1 , k_2 and k_3 or k_1 , k_2 , k_3 , k_4 , k_5 and k_6 are known as model parameters (k_i). The optimum values of model parameters are determined through the application of Least Square Estimation method using the FE database developed in this study.

5.3 FE Model Development

The Abaqus/Standard module is used in this study for the calculation of burst pressures of corroded pipelines. The Abaqus is one of the commonly used software for the analysis of pipelines. It has the capability of modelling the non-linear deformation during yielding of corroded pipeline under high pressure.

A rectangular area with constant depth (flat at the bottom) located on the outer surface of a pipeline is considered for idealization of the corroded area (corrosion patch). The edges of the corrosion patch are perpendicular to each other and/or to the pipe surface (i.e., sharp edge). Mondal and Dhar (2016a, 2016b) showed that the burst pressures with different edge conditions (i.e. smooth edge or sharp edge) of corroded areas are not significantly different. However, the development and analysis of the FE model of a corroded pipeline with smooth edge of corroded area is complicated and time consuming.

The existing literature reveals that the failure behavior of corroded pipelines mainly depends on the maximum depth and the longitudinal extent of the corroded area. The length and the depth of corrosion defect are therefore varied for the study presented here. The length of the defect is varied from 60 mm to 580 mm and the depth is varied from 20% to 80% of the wall thickness. A constant circumferential extent (c) of the defect subtending an angle of 20° at the centre of pipe cross-section is considered. This circumference extent is arbitrarily chosen from a range of corrosion widths commonly considered in published literature (Diniz et al. 2006, Li et al. 2016 and Oh et al. 2007). However, the circumferential width has negligible effect on the burst pressures of defected pipelines (Chiodo and

Ruggieri 2009). The pipe sizes are varied over a wide range from 300 mm to 914.4 mm of diameter. Only the pipelines under the load of internal pressure are considered.

Eight-noded continuum element with reduced integration (Abaqus element “C3D8R”) is used to model the pipe domain. A mesh sensitivity analysis is conducted to determine the optimum size of mesh to have no significant change of the burst pressure for further reduction of mesh size. The fine mesh is applied within and around the corroded area where stress concentration is expected. The coarse mesh is applied away from the corroded area where uniform stress is expected. An appropriate gradient is used in the transition zone of coarse to fine mesh that yields the mesh sizes from 4 mm to 17.75 mm. Three layers are applied through the minimum thickness at the corroded area of the pipelines. Figure 5.2 shows a typical finite-element mesh used in the analysis.

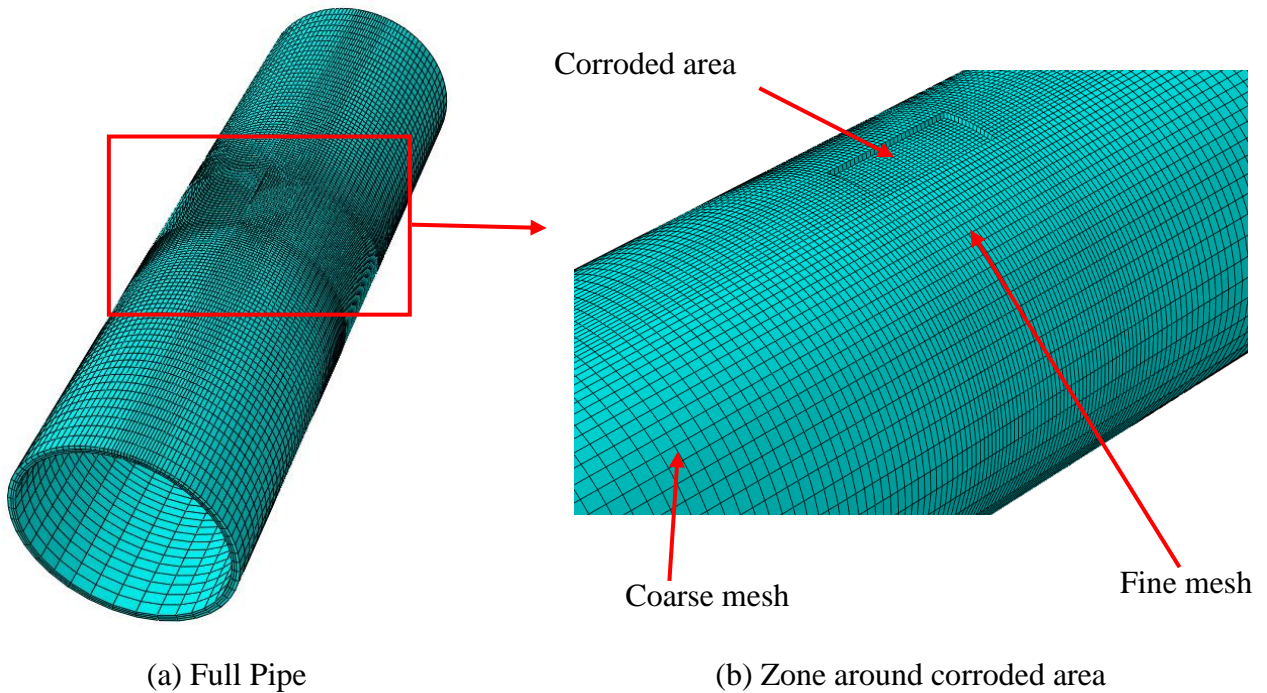


Figure 5.2: Typical Finite Element Mesh

Sufficiently long pipeline models are developed for the analysis to avoid the effects of boundaries on the pipe response. Fekete and Varge (2012) demonstrated that the minimum length of the pipeline required to avoid the boundary effects depends on the corrosion dimensions and the pipe diameter. The length of a pipe model is chosen to be longer than the minimum length recommended in Fekete and Varge (2012). Table 5.2 summaries the geometric parameters of the FE models. Further detail of the FE modelling approach is available elsewhere (Mondal and Dhar 2016a, 2016b).

Table 5.2: Geometric Parameters of FE models

Outer diameter, D (mm)	Thickness, t (mm)	Defect length, l (mm)	Defect depth, d/t (%)	Minimum length (mm)	Length in FE model, L (mm)
300	10	60-580	20-80	2691	3000
324	9.74	150-528	20-70	2335	2500
500	15	60-580	20-80	3917	4000
762	25.4	60-580	20-80	5941	6000
762	17.5	150-528	20-70	4243	4500
914.4	25.4	300	40	2412	2500

The stress–strain relation for ductile steel is non-linear beyond the yield stress. The non-linear response is often expressed using a bilinear response in FE modelling to save computational time. Mondal and Dhar (2016a) investigated the effect of non-linear and bilinear stress–strain relationship of a pipe material on the burst pressure of a corroded pipeline. They have shown that the FE model with non-linear material properties provides only 2% higher burst pressure than the FE model with bilinear material properties. A bilinear stress–strain relationship of the pipe material is used in this study to avoid

additional computation time required for the analysis with non-linear stress–strain relation.

The material properties of API 5L X60 grade steel is considered (Table 5.3).

Table 5.3: Material Parameters used (API 5L X60 grade steel)

Property	Value
Density, ρ (kg/m ³)	7850
Young's Modulus, E (GPa)	210
Poisson's Ratio, ν	0.30
Yield Strength, σ_Y (MPa)	452
True Ultimate Tensile Strength, σ_U (MPa)	542
Total strain at failure, ε_U	0.043

The failure of the pipeline is assumed when the von Mises equivalent stress throughout the wall thickness reaches the true ultimate strength of the pipe material. The pressure corresponding to this level of stress is defined as the burst pressure. The von Mises stress around the corroded zone for a pipeline is examined as shown in Figure 5.3. Figure 5.3 plots the contour of von Mises stress corresponding to failure of a 300 mm diameter pipeline with the corrosion dimensions of $l = 60$ mm, $c=20^\circ$ and d/t of 0.50. It shows that the von Mises stress reaches to the ultimate strength of the pipe material (i.e., 542 MPa) along a line almost parallel to the edge of the corrosion patch in longitudinal direction. This is similar to the failure mechanism observed in a full-scale pipe test with an artificial corrosion patch (Benjamin et al. 2005). The von Mises stress along the failure plane is almost the same (as the ultimate strength) on the inner and outer surface of the pipe.

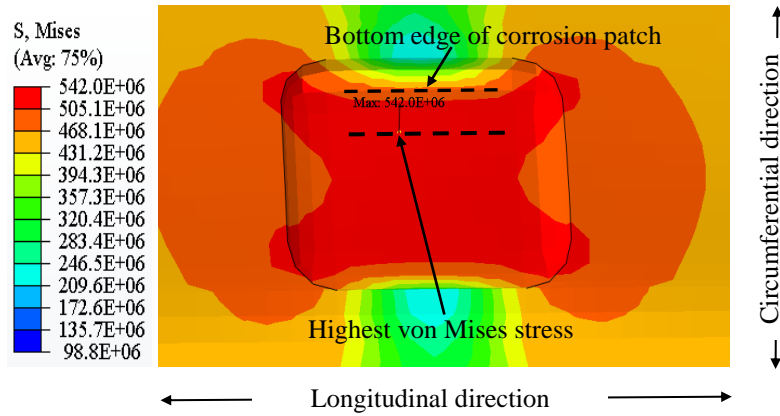


Figure 5.3: von Mises stress and the location of failure

Test results on the burst pressures of corroded pipelines with parameters (Table 5.2) for specific pipe materials are not available in the literature for a wide range of pipe dimensions for validation of the FE models. Diniz et al. (2006) conducted a burst test of a corroded pipe and determined the parameters of the pipe material using laboratory tests. The burst test results and material parameters of Diniz et al. (2006) were used to validate a FE model for burst pressure prediction of the corroded pipeline (Mondal and Dhar 2016a). The validated FE model is used here to develop the database of burst pressure presented in this study (Table 5.4). The burst pressures from FE models of un-corroded pipelines, developed in this study, are also compared with those obtained from thin-wall pressure vessel theory. The results are in agreement within about 3.5%. Corrosion defects are then applied to the pipelines in the validated FE models.

5.4 Folias Factor from FE Analysis

Folias factor is a geometric parameter used to account for the geometry of wall defects on the reduction of burst pressure. To obtain the Folias factor from the burst pressure, the burst pressure of a corroded pipeline is expressed as (after Mondal and Dhar 2016a):

$$P = P_o \left(\frac{1 - \frac{d}{t}}{1 - \frac{d}{tM}} \right) \quad (5.9)$$

Where ‘ P ’ is the burst pressure of a corroded pipeline, ‘ P_o ’ is the burst pressure for the flawless pipeline, ‘ d ’ is the depth of defect, ‘ t ’ is the pipe wall thickness and ‘ M ’ is the Folias factor. The equation can be rearranged to obtain an expression for the Folias factor as below (Equation 5.10):

$$M = \frac{\frac{Pd}{tP_o}}{\frac{P}{P_o} + \frac{d}{t} - 1} \quad (5.10)$$

Figure 5.4 shows the Folias factors calculated from the results of FE analysis using Equation 5.10 against the defect depths for three pipe sizes (i.e., 300 mm, 500 mm and 762 mm) and two defect lengths (i.e., 60 mm and 120 mm). The figure indicates that the Folias factor is higher for the pipelines with smaller diameters. For the pipelines with the same diameter, the factor is higher for longer defects. The Folias factor decreases in general with

the increase of defect depth. However, existing design codes do not include the defect depth in calculating the Folias factor, which has been addressed in the current research.

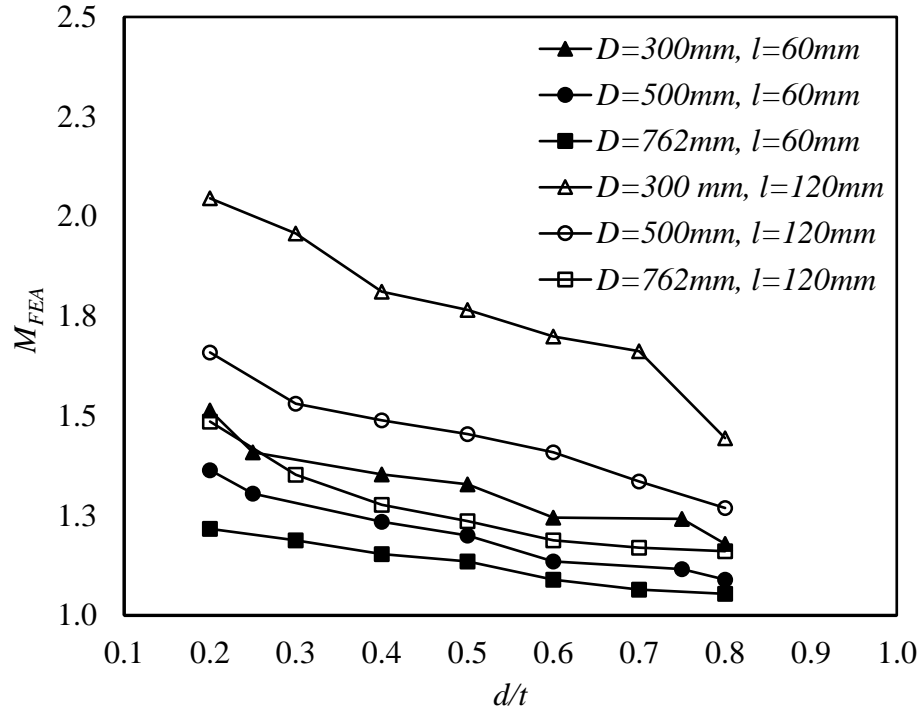


Figure 5.4: Variations of the Folias factor

5.5 Determination of Model Constants/Model Parameters

The value of constants (model parameters) for the Folias factor in Equation 5.7 and 5.8 are determined using a database developed using FE analysis. A database of 95 burst pressures with different pipe dimensions and defect geometries is developed as shown in Table 5.4. The table includes burst pressure data available in Phan et al. (2017). The database covers a wide range of pipe diameters, defect lengths including short defect, long defect and ultra-long defect as per Li et al. (2016).

Table 5.4: FE database of burst pressures for corroded pipelines

D (mm)	t (mm)	d (mm)	l (mm)	d/t	P (MPa)	D (mm)	t (mm)	d (mm)	l (mm)	d/t	P (MPa)
300	10	2	60	0.2	36.87	500	15	3	420	0.2	30.31
300	10	2.5	60	0.25	36.47	500	15	3	500	0.2	30.10
300	10	4	60	0.4	34.07	500	15	3	580	0.2	29.91
300	10	5	60	0.5	32.07	500	15	7.5	300	0.5	21.35
300	10	6	60	0.6	30.87	500	15	7.5	420	0.5	20.00
300	10	7.5	60	0.75	25.25	500	15	7.5	500	0.5	19.50
300	10	8	60	0.8	24.87	500	15	7.5	580	0.5	19.20
300	10	2	120	0.2	35.47	500	15	10.5	300	0.7	14.30
300	10	3	120	0.3	33.07	500	15	10.5	420	0.7	12.70
300	10	4	120	0.4	30.80	500	15	10.5	500	0.7	12.20
300	10	5	120	0.5	27.90	500	15	10.5	580	0.7	11.85
300	10	6	120	0.6	24.73	762	25.4	5.08	60	0.2	38.41
300	10	7	120	0.7	20.73	762	25.4	7.62	60	0.3	37.57
300	10	8	120	0.8	17.93	762	25.4	10.16	60	0.4	36.85
300	10	2	300	0.2	33.60	762	25.4	12.7	60	0.5	35.85
300	10	2	420	0.2	33.25	762	25.4	15.24	60	0.6	35.73
300	10	2	500	0.2	33.17	762	25.4	17.78	60	0.7	35.13
300	10	2	580	0.2	33.10	762	25.4	20.32	60	0.8	33.29
300	10	5	300	0.5	21.90	762	25.4	5.08	120	0.2	37.09
300	10	5	420	0.5	21.15	762	25.4	7.62	120	0.3	36.09
300	10	5	500	0.5	20.95	762	25.4	10.16	120	0.4	35.05
300	10	5	580	0.5	20.85	762	25.4	12.7	120	0.5	33.69
300	10	7	300	0.7	13.80	762	25.4	15.24	120	0.6	32.41
300	10	7	420	0.7	13.05	762	25.4	17.78	120	0.7	29.97
300	10	7	580	0.7	12.60	762	25.4	20.32	120	0.8	25.81
300	10	7	500	0.7	12.80	762	25.4	5.08	300	0.2	35.50
324	9.74	6.82	528	0.7	11.43	762	25.4	5.08	420	0.2	34.75
324	9.74	6.82	300	0.7	12.71	762	25.4	5.08	500	0.2	34.35
324	9.74	6.82	150	0.7	16.64	762	25.4	5.08	580	0.2	34.05
324	9.74	1.95	528	0.2	29.59	762	25.4	12.7	300	0.5	27.00
324	9.74	3.90	528	0.4	22.44	762	25.4	12.7	420	0.5	24.60
324	9.74	3.90	300	0.4	23.30	762	25.4	12.7	500	0.5	23.55

Table 5.4: Continued

D (mm)	t (mm)	d (mm)	l (mm)	d/t	P (MPa)	D (mm)	t (mm)	d (mm)	l (mm)	d/t	P (MPa)
324	9.74	3.90	150	0.4	25.40	762	25.4	12.7	580	0.5	22.85
500	15	3	60	0.2	33.66	762	25.4	17.78	300	0.7	20.15
500	15	3.75	60	0.25	33.31	762	25.4	17.78	420	0.7	17.50
500	15	6	60	0.4	31.87	762	25.4	17.78	500	0.7	15.65
500	15	7.5	60	0.5	30.77	762	25.4	17.78	580	0.7	14.80
500	15	9	60	0.6	30.47	762	17.5	12.25	528	0.7	9.99
500	15	11.25	60	0.75	27.35	762	17.5	7	528	0.4	17.77
500	15	12	60	0.8	27.01	762	17.5	3.5	528	0.2	22.95
500	15	3	120	0.2	32.67	762	17.5	12.25	300	0.7	12.84
500	15	4.5	120	0.3	31.27	762	17.5	7	300	0.4	19.52
500	15	6	120	0.4	29.46	762	17.5	3.5	300	0.2	23.76
500	15	7.5	120	0.5	27.36	762	17.5	12.25	150	0.7	17.60
500	15	9	120	0.6	25.03	762	17.5	7	150	0.4	22.25
500	15	10.5	120	0.7	22.63	762	17.5	3.5	150	0.2	24.66
500	15	12	120	0.8	19.43	914.4	25.4	10.16	300	0.4	25.12
500	15	3	300	0.2	30.95	-	-	-	-	-	-

The Folias factors from the burst pressures are then calculated using Equation 5.10, which are used in Equation 5.7 and 5.8 to determine the model constants (or model parameters). The model parameters are determined through minimization of the sum of the square of errors using Differential Evolution (DE) method. In this method, the material parameters are obtained through a direct search approach to improve the candidate solutions with regards to the objective function (Storn and Price 1997). The method is suitable for optimization of discontinuous function or problems with more than one local minimum (Vincenzi et al. 2013). Details of DE algorithm are available in Phan et al (2017).

Table 5.5 shows the values of constants for two different models for the Folias factor (i.e., M_1 and M_2) along with the coefficient of determination (i.e. R^2). The values of

coefficient of determination are very high (≈ 0.97), indicating that the models fit well with the FE database. The resulting models of Folias factors obtained from this investigation are shown in Equation 5.11 and 5.12, respectively.

$$M_1 = \sqrt{1 + 0.523 \cdot \left(\frac{l^2}{Dt}\right)^{1.324} \times \left(\frac{d}{t}\right)^{0.845}} \quad (5.11)$$

$$M_2 = \sqrt{1 + 0.278 \cdot \left(\frac{l^2}{Dt}\right)^{0.447} \times \left(\frac{d}{t}\right)^{-0.718} + 0.337 \cdot \left(\frac{l^4}{D^2 t^2}\right)^{0.717} \times \left(\frac{d^2}{t^2}\right)^{0.504}} \quad (5.12)$$

Table 5.5: Model Parameters

Model	k_1	k_2	k_3	k_4	k_5	k_6	R^2
M_1	0.523	1.324	0.845	-	-	-	0.9667
M_2	0.278	0.447	-0.718	0.337	0.717	0.504	0.9725

5.6 Evaluation of the Developed Models for the Folias Factor

Figure 5.6 plots the Folias factors calculated using Equation 5.11 and 5.12 against those obtained from FE analysis. In the figure, the data points lie on and around the 1:1 line with a root-mean-square-deviation (RMSD) coefficient of determination of 0.54269667 and 0.49299725, indicating a good correlation between the developed models of Folias factor and the FE calculations. Thus, both equations (M_1 and M_2) appear to calculate similar values of the factor. However, due to the higher coefficient of

determination, model M_2 is proposed in this study and hence only used for the comparison presented below.

The capability of the proposed model in capturing the effect of corrosion defect depth is demonstrated in Figure 5.6 (drawn on Figure 5.1). The Folias factors calculated using different methods are compared in the figure for different defect geometries. As the equations for the Folias factor in the existing design codes do not include a term for the depth of defect, M^2 calculated using this equation increases linearly with $l^2/(Dt)$ for DNV-RP-F10 code and almost linearly for ASME B31G and CSA Z662-15 codes. For a particular $l^2/(Dt)$, M^2 is constant and independent of the defect depth. However, results of the FE reveal that M^2 can be different for the same $l^2/(Dt)$, depending on the defect depth. The proposed model for M reasonably simulates the M calculated using FE analysis. For $l^2/(Dt)$ of around 90, M^2 calculated for two d/t ratios from the FE analysis and the proposed model are closer.

5.7 Revision of Burst Pressure Model

The generalized burst pressure model for corroded pipeline (Equation 5.9) includes a term corresponding to the burst pressure of intake pipe (P_o) and a term corresponding to burst pressure reduction due to the corrosion defect. The existing design codes employ Barlow's thin wall pressure vessel theory to calculate the burst pressure of an intake pipeline. The burst pressure for the intake pipeline is revised here based on the theory of thick-wall cylinder (Hearn 1997). The maximum circumferential stress for a thick-wall cylinder subjected to an internal pressure is given by (Equation 5.13):

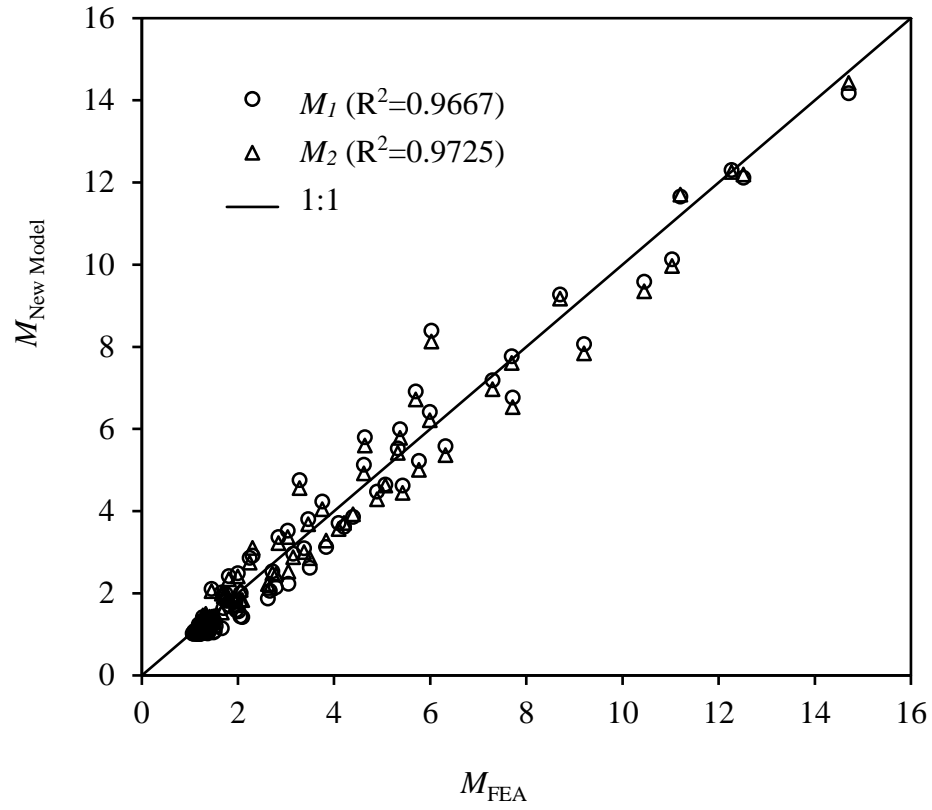


Figure 5.5: Comparison of Folias factors

$$\sigma = P_o \frac{D_o^2 + D_i^2}{D_o^2 - D_i^2} \quad (5.13)$$

Where P_o is the internal pressure, D_o is the outer diameter, and D_i is the inner diameter of the pipeline. Denoting the outer diameter as D and expressing the inner diameter as $D-2t$, Equation 5.13 can be rewritten as (Equation 5.14):

$$\sigma = P_o \frac{2D^2 - 4Dt + 4t^2}{4Dt - 4t^2} \quad (5.14)$$

Equation 14 can be rearranged as (Equation 5.15):

$$\sigma = P_o \frac{2D^2 \left\{ \left(1 - 2\frac{t}{D} \right) + 2\left(\frac{t}{D} \right)^2 \right\}}{4D^2 \left\{ \frac{t}{D} - \left(\frac{t}{D} \right)^2 \right\}} \quad (5.15)$$

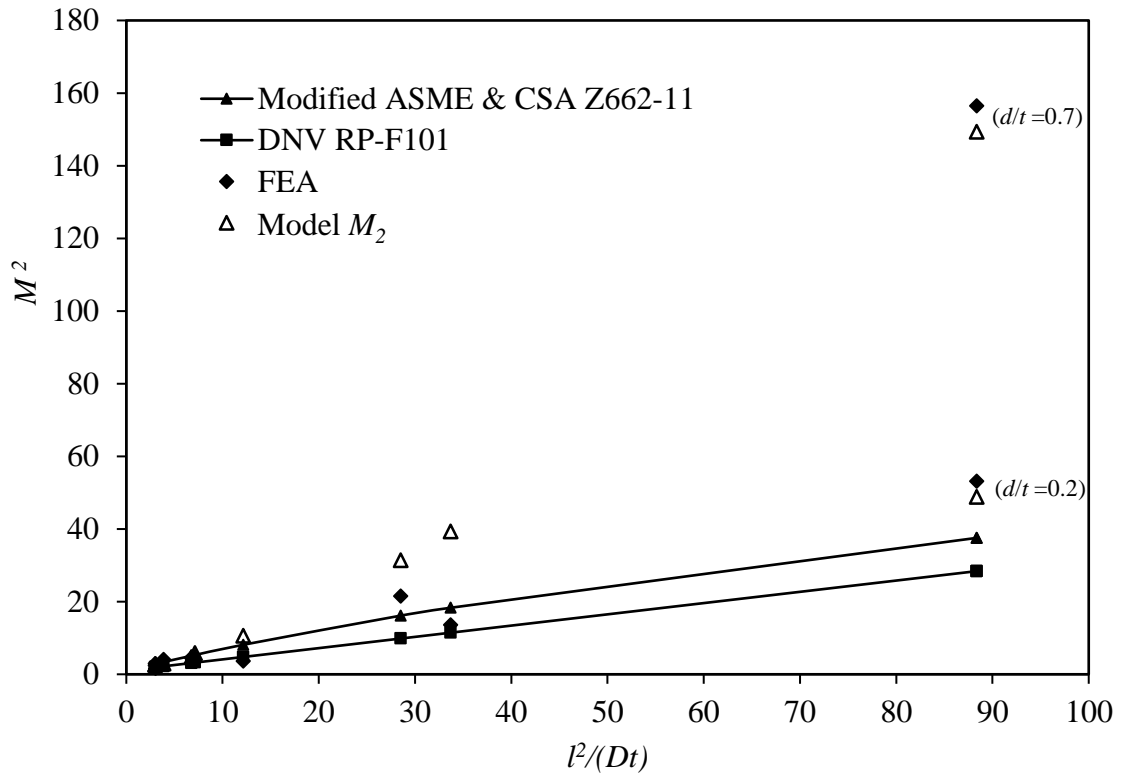


Figure 5.6: Folias factors with depth of corrosion defect

Neglecting the higher order terms of t/D , the equation can be written as (Equation

5.16):

$$\sigma = P_o \frac{1 - 2\frac{t}{D}}{2\frac{t}{D}} = P_o \frac{D - 2t}{2t} \quad (5.16)$$

Considering the hoop stress at failure equal to the ultimate strength of the material, σ_u , the expression of burst pressure for an intake pipeline is (Equation 5.17):

$$P_o = \frac{2t}{(D - 2t)} \sigma_u \quad (5.17)$$

Including the burst pressure reduction factor in Equation 5.17, the burst pressure of a corroded pipeline can be expressed as (Equation 5.18):

$$P = \frac{2t}{(D - 2t)} \sigma_u \left(\frac{1 - \frac{d}{t}}{1 - \frac{d}{tM}} \right) \quad (5.18)$$

The proposed burst pressure model for a corroded pipeline is evaluated through comparison with the burst pressure calculated using the model and FE analysis, as shown in Figure 5.7. In Figure 5.7, the data points lie around 1:1 line, indicating that the proposed model predicts the burst pressure very closely to FE results. The model provides lower bound values of burst pressures with respect to FE results.

5.7.1 Comparison with Design Codes

Burst pressures calculated using different codes are compared with FE calculations in Figure 5.8. The figure shows that the DNV-RP-F10 code over-predicts the burst pressure with respect to FE calculations, while the CSA Z662-15 and BS 7910 codes consistently under-predict the burst pressures. The ASME B31G over-predicts up to a burst pressure of around 20 MPa, beyond which it under-predicts the burst pressure. The proposed model consistently provides lower bound estimation of the burst pressure.

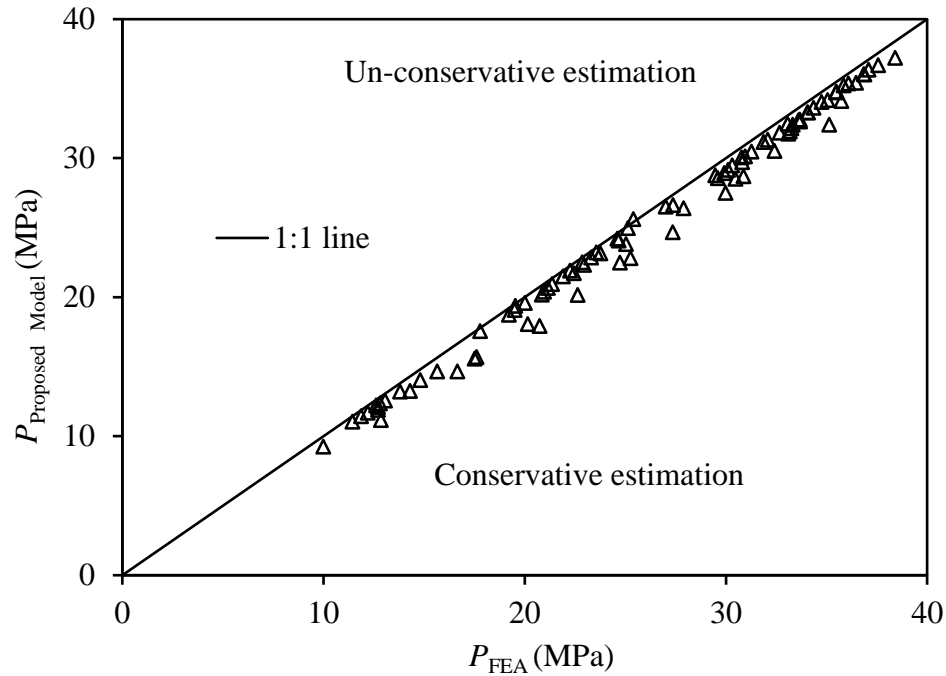


Figure 5.7: Comparison of burst pressure predicted using the proposed model and FE results

The root-mean-square-deviation (RMSD) for each model of burst pressure with respect to the burst pressure obtained by FE analysis are calculated as shown in the legend

of Figure 5.8. The proposed model is found to provide the lowest RMSD indicating that the model performs better than the existing models. Among the existing codes, the DNV-RP-F101 provides the lowest RMSD value while the CSA Z662-15 code provides the highest RMSD value. The DNV-RP-F101 code is therefore expected to provide better estimation of the burst pressure for corroded pipelines.

5.7.2 Comparison with Burst Test Results

To evaluate the proposed burst pressure model with the test results, a database of burst test of intake and corroded pipe is developed using the test result of burst pressure available in the public domain. Table 5.6 shows a database of 86 burst tests obtained from different sources. The sources of data are provided in the last column of the table. The material properties presented in the table such as yield strength and ultimate strength are apparently based on limited tests and were not determined from the specimen extracted from pipe samples. The information about the yield strength of pipe material is not available for the data collected from Ma et al. (2013). The test data covers a wide range of steel strength from low to high grades of steel (i.e. X42 to X80 grade).

The comparison of burst pressures predicted by the proposed burst pressure model with the test results are shown in Figure 5.9. The burst pressures of the test samples are calculated using the pipe dimensions and corrosion dimensions as given in Table 5.6. The data points are scattered in the figure, indicating that the test results are variable. The variability in test results may be attributed to material non-homogeneity, non-uniform wall thickness and pipe diameter.

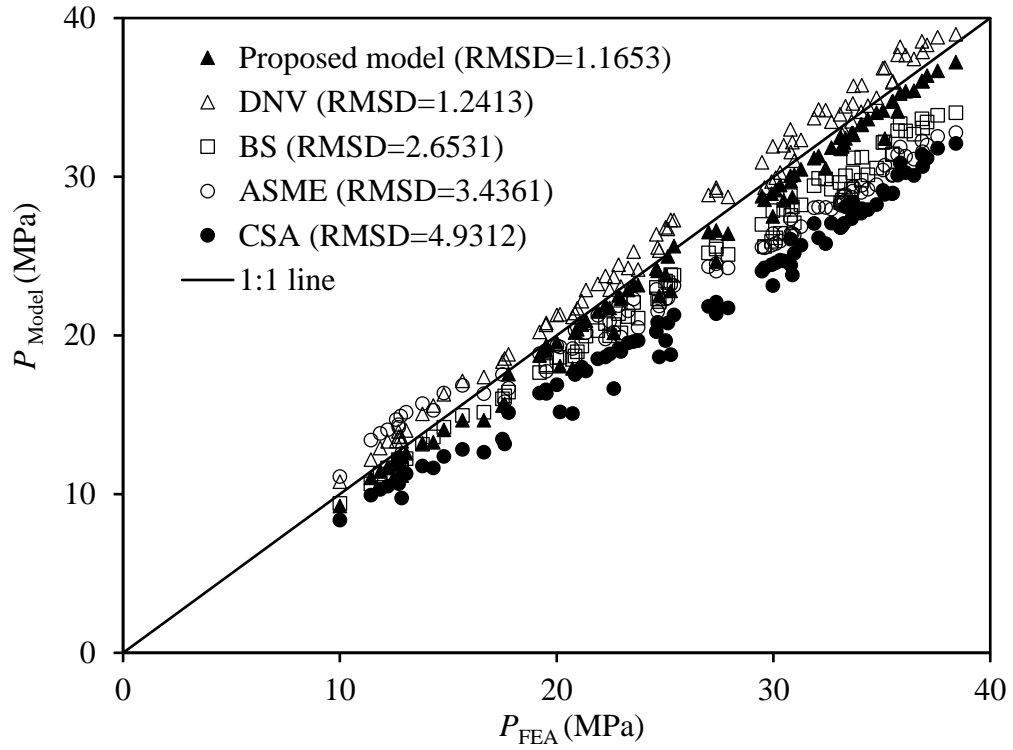


Figure 5.8: Comparison of burst pressure obtained from different models

Figure 5.9 indicates that the proposed burst pressure model provides a reasonable lower bound (conservative) estimate of the burst pressures with respect to the test results.

5.8 Summary

An improved burst pressure model for corroded pipelines is developed in this study. Two components of the model, such as the burst pressure of a flawless pipeline and a reduction factor for the corrosion defect, are separately considered for the development of the model. The Folias factor is considered as the major parameter contributing to the burst pressure reduction factor. An improved equation for the Folias factor is developed

incorporating the defect depth in the equation. The equations for the Folias factor in current design codes do not include the defect depth. However, the authors' earlier research demonstrated the importance of including the defect depth in the calculation of the Folias factor.

A revision of the burst pressure for flawless pipe is developed based on the theory of the thick-wall cylinder. The proposed burst pressure model with new equations for the burst pressure of the flawless pipeline and Folias factor reasonably simulates the burst pressure from FE analyses and full-scale burst tests. The following conclusions are also drawn from this study:

- The Folias factor decreases with pipe size and increases with the increase of corrosion defect length. The factor also decreases with the increase of defect depth. The proposed equation for the Folias factor can reasonably capture the effect of pipe size, defect length and defect depth.
- The burst pressure equation developed based on the theory of thick-wall cylinder provides an improvement in the burst pressure model for pipelines.
- For the pipelines considered, the DNV-RP-F10 code over-predicts the burst pressure with respect to the FE calculation. The CSA Z662-15 and BS 7910 codes under-predicts the burst pressure. The ASME B31G code over-predicts the burst pressure up to a pressure of around 20 MPa and under-predict beyond this pressure. The proposed model provides reasonable lower bound estimations of the burst pressures obtained from FE analyses.

- The laboratory burst test results can be scattered due to material non-homogeneity, a non-uniform wall thickness and pipe diameters.
- Although the proposed model has been developed based on the data developed using finite element analysis for the particular type of pipe material, the model provides a lower bound estimation of the burst pressure obtained from laboratory tests for a wide range of pipe materials.

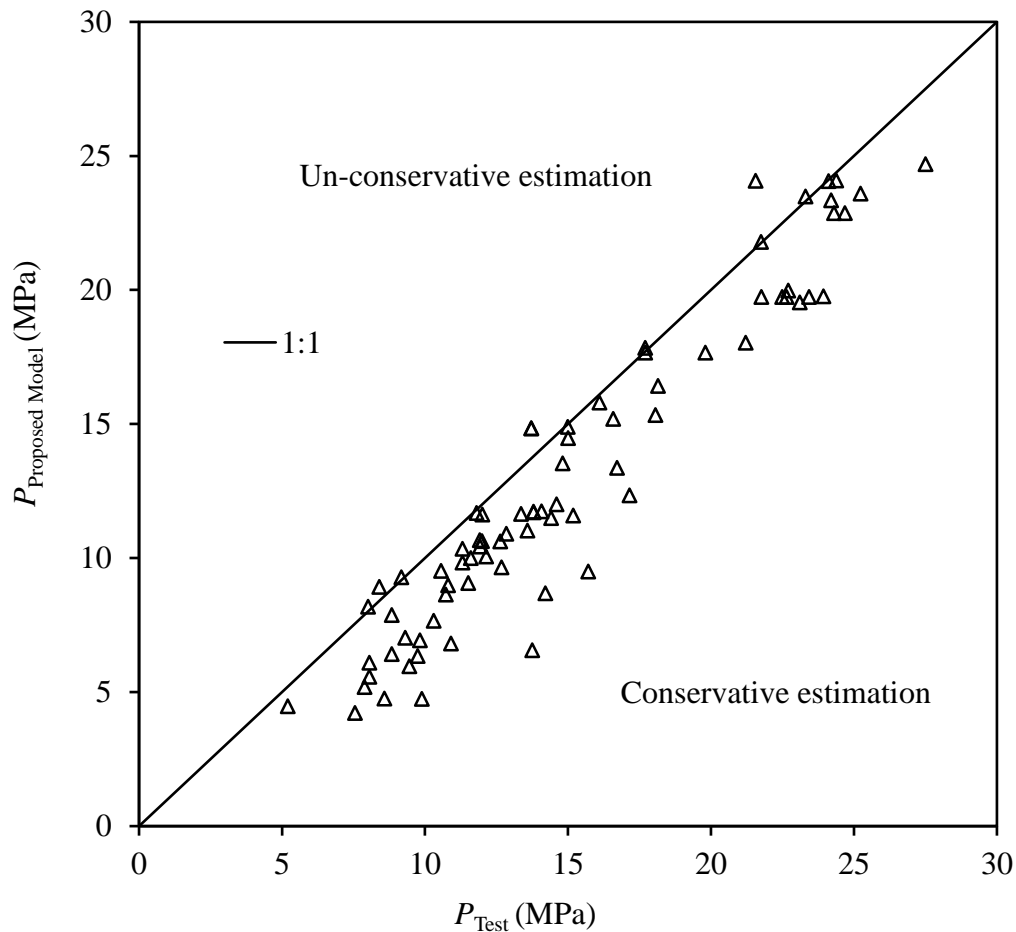


Figure 5.9: Comparison of proposed burst pressure model with test results

Table 5.6: Database of Burst Test of Corroded Pipes

Grade	D (mm)	t (mm)	d (mm)	l (mm)	σ_y (MPa)	σ_u (MPa)	P_{Test} (MPa)	Source
X46	323.6	8.5	0.0	0.0	356.4	469.3	25.1	Cronin and Pick (2000)
X46	323.6	8.6	0.0	0.0	356.4	469.3	24.4	
X46	324.1	8.5	0.0	0.0	356.4	469.3	25.0	
X46	321.6	8.3	0.0	0.0	356.4	469.3	22.5	
X46	323.6	8.7	0.0	0.0	356.4	469.3	23.9	
X46	324.1	8.4	0.0	0.0	356.4	469.3	23.3	
X46	323.9	8.6	0.0	0.0	356.4	469.3	24.5	
X52	273.1	5.3	0.0	0.0	388.7	502.2	17.2	
X46	323.3	8.6	2.2	63.5	356.4	469.3	24.4	
X46	323.1	8.6	3.0	203.2	356.4	469.3	23.1	
X46	323.1	8.6	2.7	61.0	356.4	469.3	25.2	
X46	323.6	8.6	3.3	144.8	356.4	469.3	23.9	
X46	323.6	8.6	2.7	127.0	356.4	469.3	21.7	
X46	323.1	8.5	2.2	50.8	356.4	469.3	21.6	
X52	273.1	5.2	1.9	408.9	388.7	502.2	16.7	
X52	273.1	5.3	1.7	139.7	388.7	502.2	18.1	
-	273.1	8.3	4.0	241.3	409.3	481.1	21.2	
X52	611.4	6.6	3.3	901.7	402.5	534.5	9.4	
X52	612.5	6.4	3.6	1432.6	402.5	534.5	7.9	
X52	611.5	6.4	2.6	1371.6	402.5	534.5	9.8	
X42	273.3	5.0	3.3	182.9	350.6	453.8	13.7	
X42	273.0	4.7	2.6	48.3	350.6	453.8	13.8	

Table 5.6: Continued

Grade	D (mm)	t (mm)	d (mm)	l (mm)	σ_y (MPa)	σ_u (MPa)	P_{Test} (MPa)	Source
X42	273.5	4.8	1.6	30.5	350.6	453.8	13.7	Cronin and Pick (2000)
X42	273.1	4.9	2.2	101.6	350.6	453.8	15.2	
X42	273.9	4.9	1.6	45.7	350.6	453.8	15.0	
X42	274.1	5.0	2.2	124.5	350.6	453.8	13.3	
X42	274.4	4.6	2.7	66.0	350.6	453.8	12.7	
X42	274.1	5.0	2.7	38.1	350.6	453.8	14.8	
X42	274.5	4.8	2.1	157.5	350.6	453.8	12.6	
X46	323.9	5.1	3.7	99.1	372.7	472.4	9.7	
X55	506.7	5.7	3.0	132.1	462.3	587.3	10.7	
X55	505.0	5.7	3.3	462.3	462.3	587.3	8.1	
X55	508.0	5.7	3.8	619.8	462.3	587.3	8.6	
X55	508.0	5.7	3.8	533.4	462.3	587.3	9.9	
X55	508.0	5.7	3.0	416.6	462.3	587.3	10.9	
X55	508.3	5.6	3.4	596.9	462.3	587.3	8.0	
X55	508.0	5.6	2.5	170.2	462.3	587.3	11.5	
X46	863.6	9.6	3.6	213.4	400.2	508.0	10.8	
X46	863.6	9.5	3.0	185.4	400.2	508.0	10.6	
X46	863.6	9.4	4.6	91.4	400.2	508.0	9.2	
X60	324	9.79	6.99	500	452	542	11.99	Diniz et al. (2006)
X60	324	9.74	7.14	528	452	542	11.3	
X60	324	9.8	7.08	256	452	542	14.4	
X60	324	9.66	6.76	306	452	542	14.07	
X60	324	9.71	6.93	350	452	542	13.58	
X60	324	9.71	6.91	395	452	542	12.84	
X60	324	9.91	7.31	433	452	542	12.13	
X60	324	9.94	7.22	467	452	542	11.92	
X60	324	9.79	6.99	484	452	542	11.91	
X60	508	14.8	9.7	500	414	600	15.8	
X60	508	14.6	10.35	500	414	600	14.6	

Table 5.6: Continued

Grade	D (mm)	t (mm)	d (mm)	l (mm)	σ_y (MPa)	σ_u (MPa)	P_{Test} (MPa)	Source
X65	762	17.5	4.375	200	464.5	563.8	24.11	Oh et al. (2007)
X65	762	17.5	8.75	200	464.5	563.8	21.76	
X65	762	17.5	13.125	200	464.5	563.8	17.15	
X65	762	17.5	8.75	100	464.5	563.8	24.3	
X65	762	17.5	8.75	300	464.5	563.8	19.8	
X65	762	17.5	8.75	200	464.5	563.8	23.42	
X65	762	17.5	8.75	200	464.5	563.8	22.64	
X65	762	17.5	8.75	100	464.5	563.8	24.68	
X65	762	17.5	8.75	200	464.5	563.8	22.48	
X65	762	17.5	8.75	300	464.5	563.8	17.7	
X65	762	17.5	8.75	400	464.5	563.8	18.14	
X65	762	17.5	8.75	600	464.5	563.8	16.57	
X80	459	8	3.75	40	589	731	24.2	Freire et al. (2006)
X80	457	8.1	5.40	39.6	601	684	22.7	
X65	762	17.5	8.75	50	464.5	563.8	27.5	Kim et al. (2004)
X65	762	17.5	8.75	900	464.5	563.8	15	
X80	1219	19.89	15.41	605.72	641	740	9.3	Chen et al. (2015) and Sadasue et al. (2004)
X80	1219	19.89	7.44	605.72	641	740	17.7	
X80	1219	19.89	1.77	607.74	641	740	23.3	
X80	1219	13.79	10.78	588.37	641	740	5.2	
X80	1219	13.79	5.45	589.4	641	740	12	
X80	1219	13.79	1.54	586.42	641	740	16.1	
X42	272.97	4.67	2.62	48.26	-	453.86	13.79	Ma et al. (2013)
X42	273.53	4.78	1.63	30.48	-	453.86	13.71	
X42	529	9	4.7	350	-	415	8.83	
X42	529	9	4.7	160	-	415	15.7	
X42	529	9	5.3	150	-	415	14.2	
X60	508	6.6	2.62	381	-	598.9	11.3	Ma et al. (2013)
X60	508	6.7	2.66	1016	-	601	11.6	
X60	508	6.4	3.46	899.2	-	672.5	8	
X60	508	6.4	2.18	899.2	-	672.5	11.8	
X60	508	6.4	3.18	1000.8	-	672.5	8.4	
X60	720	8	4.3	180	-	535	10.3	
X60	720	8	4.4	320	-	535	8.83	
X60	720	8	6.2	180	-	535	7.55	

CHAPTER 6

Interaction of multiple corrosion defects on burst pressure of pipelines

6.1 Introduction

The pipelines are used for transporting hydrocarbons, municipal water and waste water, and for other industrial applications. The pipelines are often exposed to corrosive environments causing wall corruptions. The corrosion reduces the strength of the pipeline significantly and may lead to premature failure. A prediction of the remaining strength of a corroded pipeline is required to assess the structural integrity of the pipeline.

The corrosion in pipeline may occur in a single patch or in multiple patches. The effects of corrosion patches on the strength of pipeline are extensively investigated (Ma et al. 2013, Oh et al. 2007, Diniz et al. 2006). The pipe strength is generally expressed in terms of the burst pressure which is the internal pressure at the plastic collapse of the pipeline. The researchers are still contributing to the improvement of the burst pressure model for determining the remaining strength of corroded pipelines more accurately for level-1 and/or level-2 assessments.

For multiple corrosion patches, the burst pressure is calculated based on only a single patch if the patches are located further apart and do not interact with each other. For interacting defects, the burst pressure is conservatively calculated based on an entire defected area inclusive of the corrosion patches. In this regards, the interaction rules are employed to determine if the interaction between the defects occurs. Different interaction

rules are adopted in the design codes such as DNV (2015), CSA (2015), ASME (2012) and others. However, the criteria used in the codes are different from each other. Benjamin et al. (2016) and Li et al. (2016) reported that for same defect sizes and configurations, the design codes provide different results of interactions between corrosion defects. A revision of the interaction rules is therefore required to validate the interaction criteria used in the design codes.

Li et al. (2016) have recently revisited the interaction rules for a pipeline with multiple corrosion patches using finite element analysis. The pipe diameter and wall thickness were 458.8 mm and 8.1 mm, respectively. They investigated three patterns of defect colonies (of a defect) with five different geometries. The defect lengths (l) considered were 36.9 mm, 272.6 mm and 436.1 mm to represent short and long defects. The widths (w) of the defects were 31.9 mm and 72.1 mm. The depths of the defects were 30%, 50% and 66% of the pipe wall thickness. Based on the study, new interaction rules were proposed. The limiting distance between the corrosion patches in the longitudinal direction is expressed in terms of $\sqrt{(Dt)}$, where D is the pipe diameter and t is wall thickness. The circumferential spacing is expressed in terms of pipe diameter or wall thickness depending on the length of corrosion defects.

Al-Owaisi et al. (2016) investigated the interaction of two identical corrosion patches for a 508 mm diameter pipe and with 8.9 mm wall thickness. They studied the effects of two shapes of corrosion defects (circular and curved boxed) on the interaction of corrosion patches. The size of a circular defect was 35 mm in diameter and that of a curved

boxed defect was 35 mm \times 35 mm. The study was limited to defects penetrating 50% of pipe wall thickness. It was concluded that the shapes and locations of the defects influence the burst pressure of pipelines containing interacting defects. However, the limiting spacing of interaction of the defects was not extensively investigated in this research.

Most of the studies on the interactions of corrosion patches focused on pipelines with diameter of around 460 mm (Fu and Batte 1999, Silva et al. 2007, Benjamin et al. 2016, Li et al. 2016). The limiting distances for interactions are expressed in terms of pipe diameter and/or wall thickness of the pipeline. The effect of the depth of corrosion is not included in the interaction rules. Silva et al. (2007), however, showed that the corrosion depths may affect the interaction rules.

In this research, corrosion patches are investigated using finite element analysis for pipelines with different diameters considering the effects of corrosion depths. A parametric study based on finite element analysis is conducted to investigate the effects of interactions of multiple corrosion patches on the burst pressure of corroded pipelines. Based on the investigation, the new interaction rules are proposed incorporating the corrosion depths.

6.2 Interaction Rule

An interaction rule is employed to account for the interaction of multiple corrosion patches in the calculation of the burst pressure. The interaction rule states the limiting distances along the circumferential and longitudinal directions, $(S_c)_{lim}$ and $(S_l)_{lim}$, respectively, between two successive corrosion patches beyond which the effect of

interaction of the adjacent patches is negligible. Three basic types of interacting corrosion defects are generally considered, which are termed as Type 1, Type 2 and Type 3, respectively (Kiefner and Vieth 1990). In Type 1 interaction, the projections of two or more corrosion patches overlap in the longitudinal direction when projected onto a longitudinal plane passing through the wall thickness, as shown in Figure 6.1. The corrosion patches are separated in the circumferential direction (at distances of S_{c1} , S_{c2} ... S_{cn} etc.). In Type 2, corrosion patches are separated in the longitudinal direction also (at distances of S_{l1} , S_{l2} ... S_{ln} etc.) as shown in Figure 6.2. The Type 3 corresponds to a larger corroded area with localized deeper zones as shown in Figure 6.3.

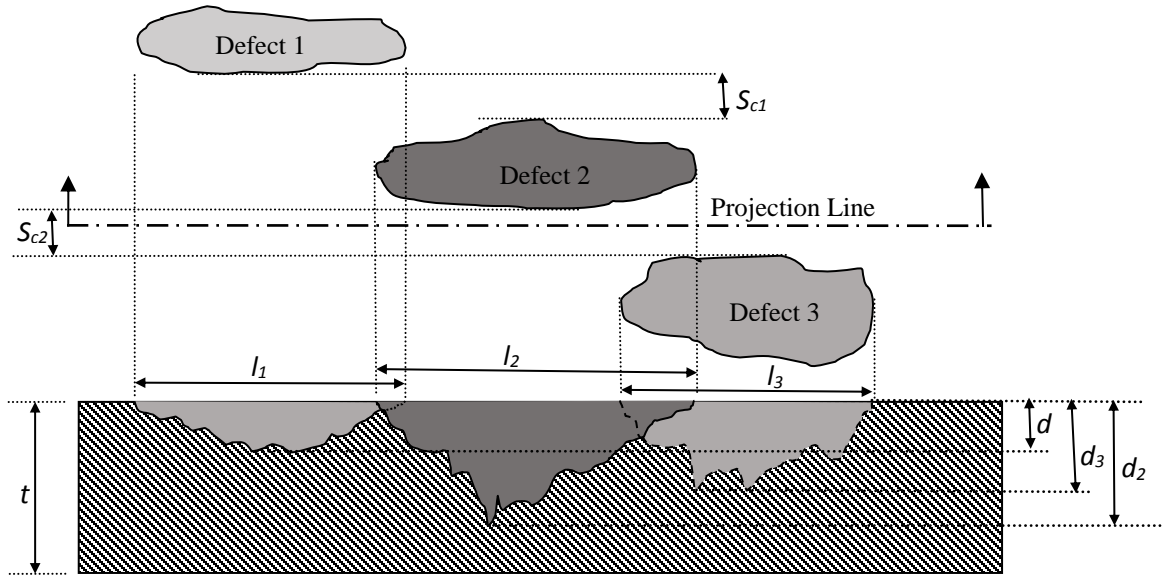


Figure 6.1: Type 1 Interaction (Redrawn after DNV-RP-F101)

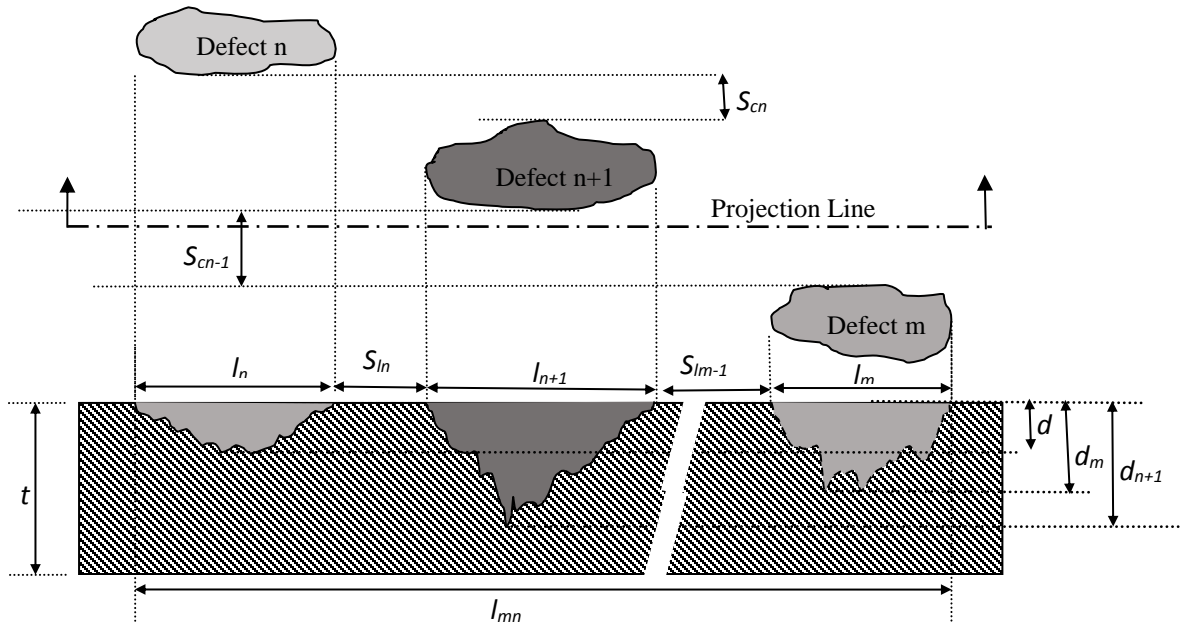


Figure 6.2: Type 2 Interaction (Redrawn after DNV-RP-F101)

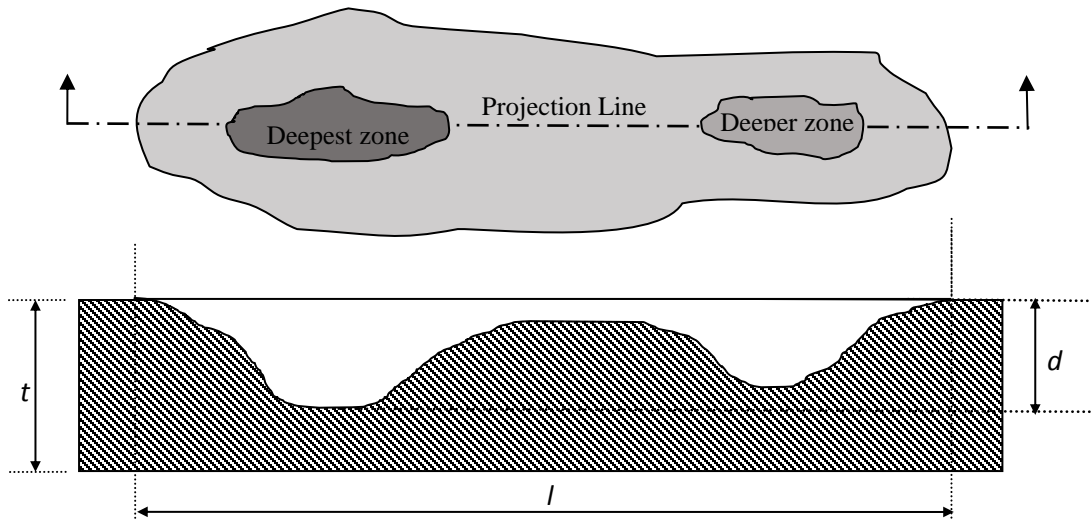


Figure 6.3: Type 3 Interaction (Redrawn after DNV-RP-F101)

The design codes (e.g. DNV, ASME, CSA) recommend the limiting distances (spacing), $(S_c)_{lim}$ and $(S_l)_{lim}$, in terms of different parameters. The DNV code expresses the spacing in terms of pipe dimensions (diameter and thickness). The ASME B31G and CSA

Z662-15 codes express the spacing in terms of pipe wall thickness and the lengths of corrosion patches, respectively. The Table 6.1 provides a summary of different recommendations for the spacing and the criteria for interaction between the patches. The effect of interaction between the defects occurs when $S_l \leq (S_l)_{lim}$ or $S_c \leq (S_c)_{lim}$.

Table 6.1: Interaction Rule

Source	Longitudinal limit, $(S_l)_{lim}$	Circumferential limit, $(S_c)_{lim}$	Criteria for interaction
DNV RP-F101 (2015)	$2\sqrt{Dt}$	$360 \sqrt{\frac{t}{D}}$ (degree)	$S_l \leq (S_l)_{lim}$ $S_c \leq (S_c)_{lim}$
ASME B31G (2012)	$3t$	$3t$	$S_l \leq (S_l)_{lim}$ $S_c \leq (S_c)_{lim}$
CSA Z662-15 (2015)	$Minimum(l_m \text{ to } l_n)$	$Minimum(l_m \text{ to } l_n)$	$S_l \leq (S_l)_{lim}$ $S_c \leq (S_c)_{lim}$
Kiefner and Vieth (1990)	$Minimum(6t, l_m \text{ to } l_n)$	$Minimum(6t, w_m \text{ to } w_n)$	$S_l \leq (S_l)_{lim}$ $S_c \leq (S_c)_{lim}$
Pipeline Operator Forum (2005)	25.4 mm (1 inch)	$6t$	$S_l \leq (S_l)_{lim}$ $S_c \leq (S_c)_{lim}$

The interacting corrosion defects are treated as a single defect for calculating the burst pressure. The ASME B31G (2012) code recommends using a length equal to the total length of the corrosion group, l_{mn} and a depth equals to the maximum depth in the group, d_{max} . The width of the corrosion defect is not included in the ASME B31G model. The DNV code (DNV-RP-F101 2015) also uses the length similar to that recommended in the ASME method. The depth for the corrosion group in the DNV code is calculated using Equation 6.1.

$$d_{mn} = \frac{\sum_{i=m}^{i=n} d_i l_i}{l_{mn}} \quad (6.1)$$

Here, d_i and l_i are the maximum depth and length, respectively, of the i^{th} corrosion of the interacting corrosion group, as shown in Figure 6.1.

6.3 Finite Element Analysis

The FE analysis provides a powerful tool for modelling complex problems with non-linear material responses. Among the commercially available software for FE analysis, Abaqus is one of the commonly used software for analysis of pipelines. Abaqus has the capability of modelling the non-linear deformation during yielding of a corroded pipeline under high pressure. Abaqus/Standard module is used in this study for calculation of burst pressure of corroded pipelines with multiple corrosion defects.

6.3.1 FE Model

The pipe domain is modelled using eight-noded continuum element (Abaqus element “C3D8R”). Although the actual geometry of a corrosion patch is very complex, the existing literature shows that the failure behavior of corroded pipelines mainly depends on the maximum depth and the longitudinal extent of the corroded area. A rectangular area with a constant depth (flat at the bottom) is therefore considered, even though it is an idealized corrosion patch. The corrosion defects are created on the external surface of the pipe wall, as shown in Figure 6.4. The sharp edge and smooth (curved) edge (Figure 6.4) are considered for the investigation of the effects of the edge conditions of the corrosion

patches on the burst pressure. An ellipse with a ratio of the major to minor axis of 2 is fitted to produce the curved edge (after Mondal and Dhar 2016a, Mondal and Dhar 2016c).

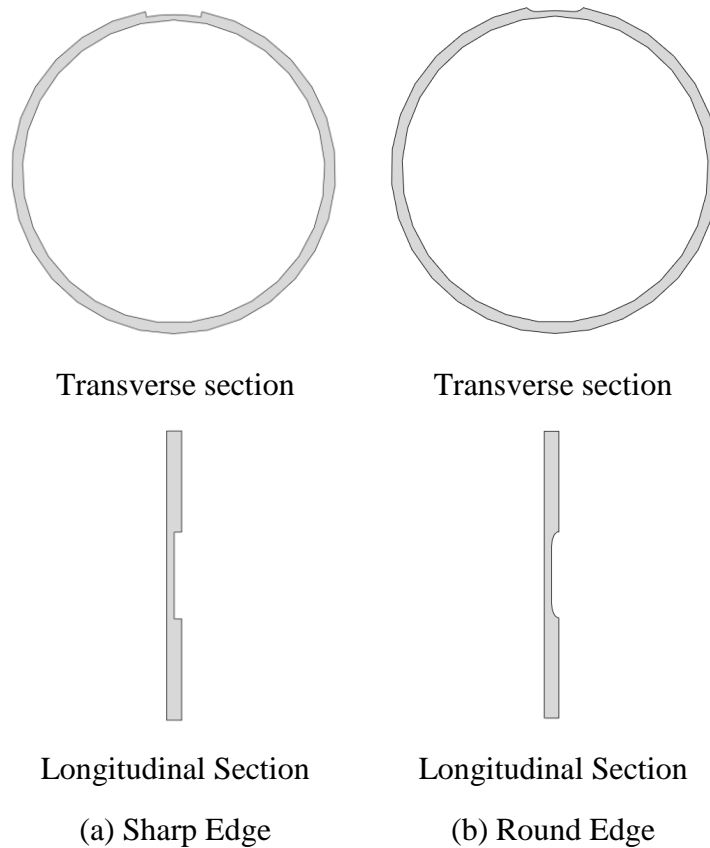


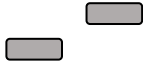

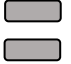


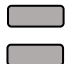





Figure 6.4: Edge condition of corrosion patch

To investigate the interaction of different corrosion patches, 154 numbers of 3D Finite Element Models are developed for pipelines with diameters of 300 mm, 500 mm and 762 mm for analysis. The spacing between two identical sizes of patches is varied independently along the longitudinal, circumferential and oblique directions of pipelines. A pipeline with a single defect of that size is termed as the base defect (BD). The models with the base defects are called BD-1, BD-2 and BD-3 for 300 mm, 500 mm and 762 mm

diameter pipeline, respectively. The dimensions of the corrosion defects and the pipelines considered in the FE analysis are summarized in Table 6.2. The parameters are selected based on the typical values used in the previous research (Ma et al. 2013, Oh et al. 2007, Diniz et al. 2006).

Table 6.2: Pipes dimensions and corrosion geometries

Model ID	Corrosion arrangement	D (mm)	t (mm)	d/t	l (mm)	w (°)	S_l (times t)	S_c (times t)
A	Un-corroded	300	10	-	-	-	-	-
BD-1		300	10, 15	0.20, 0.25, 0.30, 0.40, 0.50, 0.60, 0.70, 0.75, 0.80	60, 120	20	-	-
C		300	10, 15	0.20, 0.25, 0.30, 0.40, 0.50, 0.60, 0.70, 0.75, 0.80	60	20	0-14	-
D		300	10	0.50	60	20	0-10	0-10
E		300	10	0.50	60	20	3 (overlap)	0-10
F		300	10	0.50	60	20	-	0-6
G	Un-corroded	500	15	-	-	-	-	-
BD-2		500	15	0.20, 0.25, 0.40, 0.50, 0.60, 0.75, 0.80	60, 120	20	-	-
H		500	15	0.20, 0.25, 0.40, 0.50, 0.60, 0.75, 0.80	60	20	0-14	-
I		500	15	0.50	60	20	-	0-6
J	Un-corroded	762	25.4	-	-	-	-	-
BD-3		762	25.4	0.20, 0.30, 0.40, 0.50, 0.60, 0.70, 0.80	60, 120	20	-	-
K		762	25.4	0.20, 0.30, 0.40, 0.50, 0.60, 0.70, 0.80	60	20	0-16	-
L		762	25.4	0.50	60	20	-	0-6

The efficiency of FE analysis could be achieved by applying simplified boundary conditions (such as symmetric condition) to the model. It is, however, difficult to apply simplified boundary condition to the pipelines containing unsymmetric corrosion patches such as Model D and E in Table 6.2. For this reason, fully-restrained boundary conditions at the ends of the pipelines are applied. To avoid the effect of boundary conditions within the corroded zone, the pipelines of sufficient lengths (longer than minimum length as recommended in Fekete and Varge 2012) are considered. Outward radial pressure is applied to the inner surface of the pipeline to simulate the internal pressure. Automatic time increment is chosen for the solution process.

6.3.2 Material Parameters

The Stress–strain relation for ductile steel is non-linear beyond the yield stress. The non-linear response is often expressed using bilinear response in FE modelling to save computational time. Figure 6.5 shows the non-linear and bilinear relation of API 5L X60 steel (Fekete and Varge 2012, Mondal and Dhar 2016a). To determine the effect of using the bilinear material model over the non-linear properties on the burst pressure, a finite element model of a pipeline with 300 mm of diameter and 10 mm wall thickness is analyzed. A corrosion with 60 mm of length, 20 degree circumferential extent and 0.50 of d/t ratio was considered. Figure 6.6 shows the variation of von Mises equivalent stress for the pipeline against internal pressure at two points, one on the outer surface and the other on the inner surface of the corroded area. An outer point and an inner point on the same section through the wall thickness were selected to represent the state of stress throughout the ligament. During analysis, the stress reached the true ultimate strength at these points

first. This condition is assumed as the failure criterion in this study, as discussed later. Beyond the yield limit, the stresses at these points are somewhat different for the two different material models (Figure 6.6). The stresses reach the true ultimate strength (i.e., 542 MPa) of the material at the internal pressure of 32.50 MPa and 33.60 MPa for bilinear and non-linear material models, respectively. The internal pressures thus differ by about 3.3% for the two material models. The error due to the material model will be further reduced by the normalization of results. The burst pressures of the pipelines with multiple corrosion patches are normalized with the burst pressure for a pipeline with single corrosion patch (termed herein as the burst pressure with base defect). The bilinear material model is therefore used in the FE models presented here to avoid additional computational time with the non-linear model. The material properties used in the analysis are shown in Table 6.3.

Table 6.3: Material Properties

Property	Value
Density, ρ (kg/m ³)	7850
Young's Modulus, E (GPa)	210
Poisson's Ratio, ν	0.30
Yield Strength, σ_Y (MPa)	452
True Ultimate Strength, σ_U (MPa)	542
Total strain at failure, ε_U	0.043

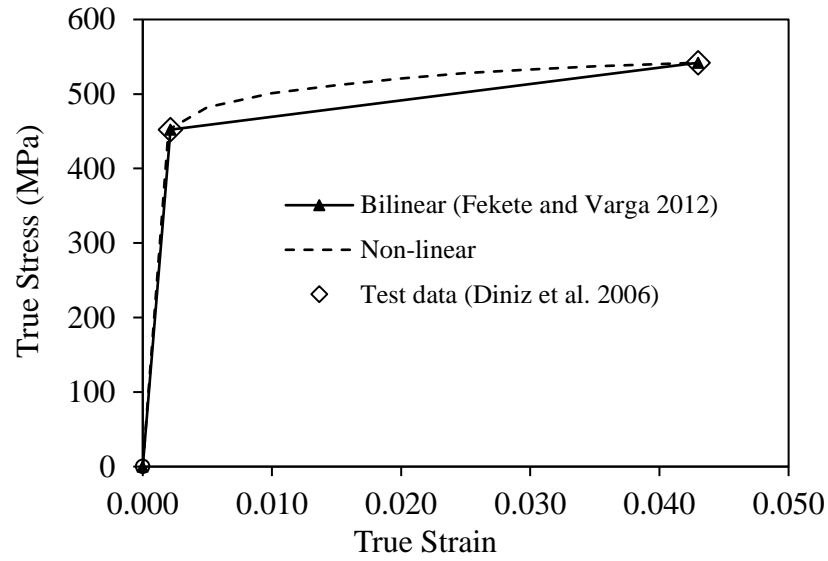


Figure 6.5: Stress-strain relation of pipe material (API 5L X60)

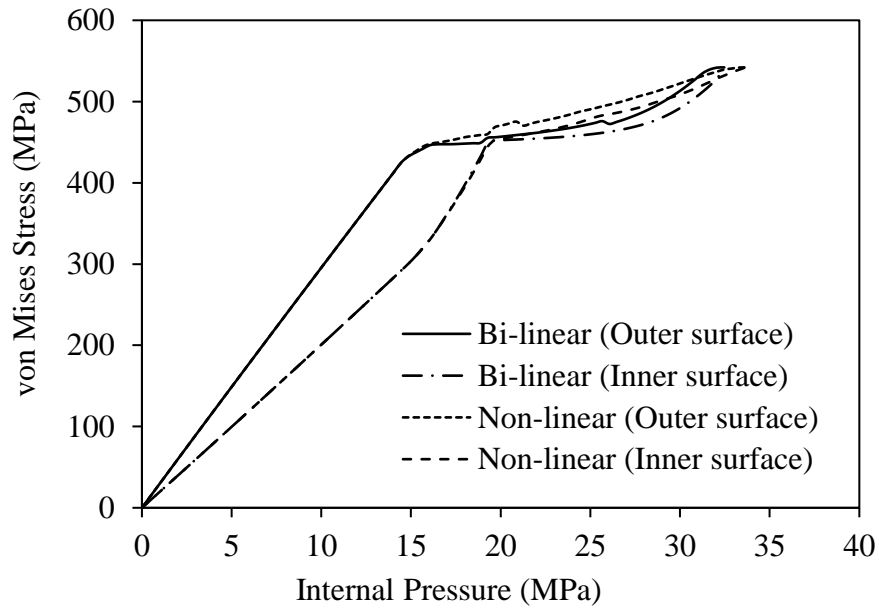


Figure 6.6: Effect of material model on burst pressure

A mesh sensitivity analysis is performed to determine the optimum mesh size. The fine mesh is applied within and around the corroded area where stress concentration is expected. The coarse mesh is applied where uniform stress is expected. An appropriate

gradient between coarse and fine mesh is also considered. A typical finite element mesh used in this study is shown in Figure 6.7.

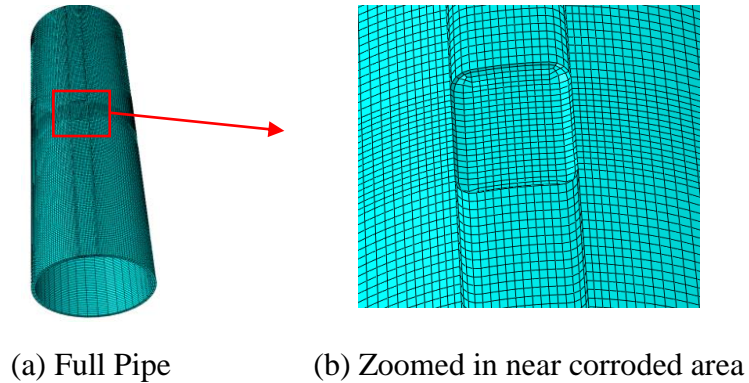


Figure 6.7: A typical finite element mesh

An automatic time increment is chosen for the solution process in Abaqus. Only pipelines under the loading of internal pressure are considered.

6.3.3 Validation of FE Model

The test results on the burst pressures of corroded pipelines with parameters for specific pipe materials are not available in the literature for a wide range of pipe dimensions considered in this study. Diniz et al. (2006) conducted burst test of a corroded pipeline and determined the parameters of the pipe material using laboratory tests. The burst test results and material parameters of Diniz et al. (2006) were used to validate the FE model for burst pressure prediction of the corroded pipeline (Mondal and Dhar 2016c). The validated FE model is used here to conduct a parametric study presented in this study. The burst pressures from FE models of un-corroded pipelines, developed in this study, are also

compared with the results those obtained from thin-wall pressure vessel theory. The results are in agreement within about 3.5%. Corrosion defects are then applied to the pipelines in the validated FE models. The burst pressures for un-corroded pipelines, calculated using FE analysis, are 40 MPa, 35.9 MPa and 40 MPa for 300 mm, 500 mm and 762 mm diameter pipes, respectively. These burst pressures are comparable to those obtained using the thin-walled pressure vessel theory (within about 3.5%). The thin-walled pressure vessel theory assumes a uniform stress distribution within the wall of the pipe, which might affect the burst pressure calculated using this theory.

The von Mises stress around the zone of corrosion for a corroded pipeline is also reviewed to examine the failure mechanism and compared with the test results available in the literature. Figure 6.8 plots the contour of the von Mises stress corresponding to the failure of a 300 mm diameter pipeline with corrosion dimensions (smooth-edged) of $l = 60$ mm, $w=20$ degree and d/t of 0.50. Figure 6.8 shows that the von Mises stress reaches to the true ultimate strength of pipe material (542 MPa) along a line almost parallel to the edge of the corrosion patch in longitudinal direction. This is similar to the failure mechanism observed in a full-scale pipe test with an artificial corrosion patch (Benjamin et al. 2005). Benjamin et al. (2005) conducted a burst test of a 458.8 mm diameter pipe with 8.10 mm wall thickness containing artificial corrosion of 39.6 mm length, 31.9 mm width and 0.665 d/t ratio. Figure 6.9 indicates the location of failure plane observed in Benjamin et al (2005), which is not at the centre of the corrosion patch. The finite element model thus reasonably simulates the failure plane observed. The analysis was also performed for the

test pipe with material parameters available in Andrade et al. (2006). Similar failure plane was predicted with the burst pressure within 0.3% of the test result.

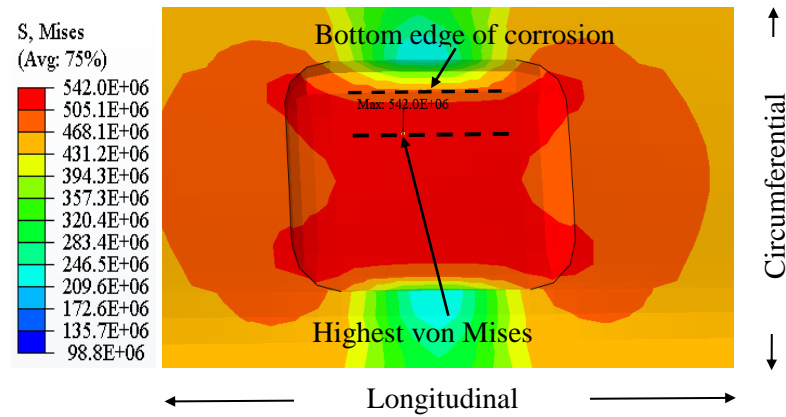


Figure 6.8: Failure location of pipe containing single corrosion defect

The von Mises stress along the failure plane is almost the same (the true ultimate strength) on the inner and the outer surface of the pipeline. A pipeline is assumed to burst when the von Mises equivalent stress throughout the thickness (the ligament) reaches the true ultimate strength of the pipe material.

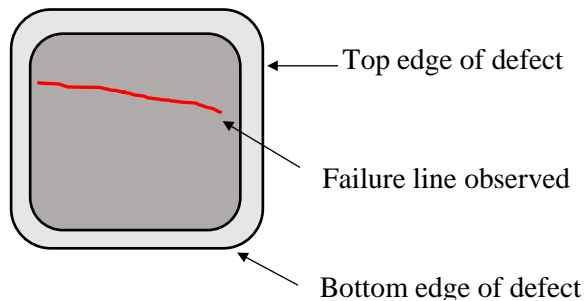


Figure 6.9: Location of failure observed in a full-scale pipe test (After Benjamin et al. 2005)

The effect of using sharp edge and smooth edge conditions (definitions are in Figure 6.4) of the corrosion patches are examined using FE analysis. The Table 6.4 compares the burst pressures for different sizes of pipelines with various corrosion dimensions. The last column of the table shows the percent difference of the calculated burst pressures using the two models (i.e., sharp edge and smooth edge). It shows that the difference in burst pressure is insignificant for using either of the smooth edge or the sharp edge. However, the development of FE models and the analysis considering the smooth edge of the corrosion defects are more complicated and time consuming than those based on the sharp edge. The sharp edge condition is, therefore, considered for the rest of the analysis.

6.4 Results and Discussions

6.4.1 Interaction of corrosion patches

Figures 6.10 and 6.11 plot the burst pressures of the corroded pipelines against the normalized spacing between successive corrosion patches. In these figures, Models C, D, E and F correspond to a 300 mm diameter pipe, Models H and I correspond to a 500 mm diameter pipe, and Models K and L correspond to a 762 mm diameter pipe. Models C, H and K consider the pipelines with corrosion patches on a same longitudinal line where the spacing between the patches are increased in the longitudinal direction ($S_c = 0$, $S_l = 0$ to $14t$ for Models C and H and $S_c = 0$, $S_l = 0$ to $16t$ for Model K, where “ t ” is the wall thickness). The Model D refers to a pipeline where the spacing (between the corrosion patches) in the longitudinal direction is equal to the spacing in the circumferential directions ($S_c = S_l = 0$ to $10t$). The patches are diagonally oriented. The Model E refers to a pipeline with a

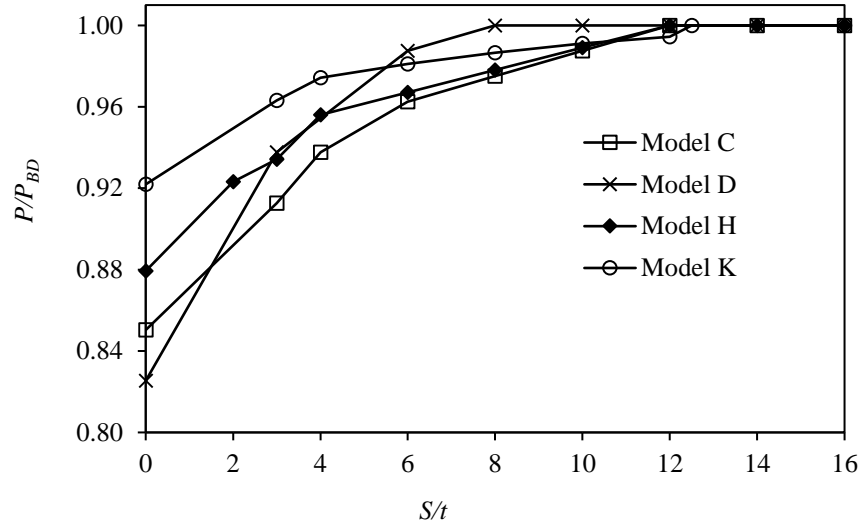
constant spacing (between the corrosion patches) in the longitudinal direction while the spacing is varied in the circumferential direction ($S_l=3t$ (overlap), $S_c = 0$ to $10t$). The Models F, I and L correspond to the pipelines where the spacing between corrosion patches are varied along circumferential direction of the pipelines (i.e. fully overlapped in the longitudinal direction). The size of the base defect is assumed to be the same in each of the pipelines with length, width and d/t ratio of 60 mm, 20 degree and 0.50, respectively.

Table 6.4: Burst pressures for different edge conditions

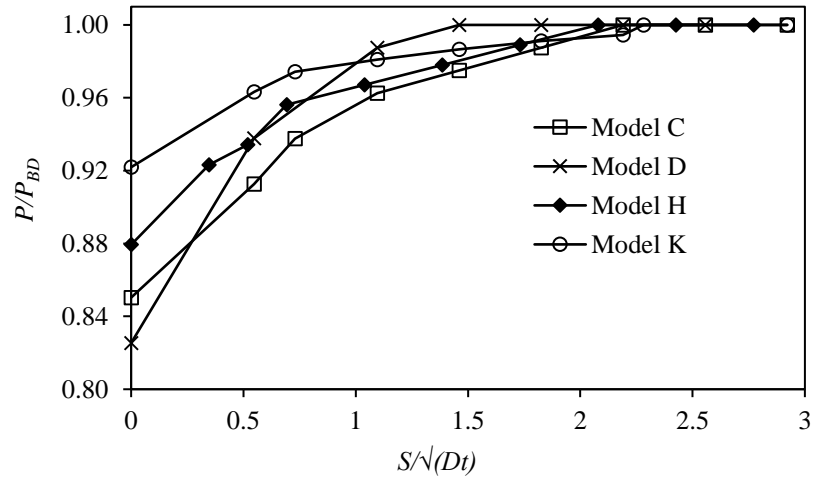
D (mm)	t (mm)	d/t	l (mm)	w (degree)	Edge condition	Burst pressure (MPa)	Variation (%)
300	10	0.50	60	20	Elliptical	33.00	2.82
300	10	0.50	60	20	Sharp	32.07	
300	10	0.50	120	20	Elliptical	27.27	0
300	10	0.50	120	20	Sharp	27.27	
500	15	0.50	60	20	Elliptical	31.91	1.10
500	15	0.50	60	20	Sharp	31.56	
500	15	0.50	120	20	Elliptical	27.89	1.90
500	15	0.50	120	20	Sharp	27.36	
762	25.4	0.50	60	20	Elliptical	35.85	1.20
762	25.4	0.50	60	20	Sharp	35.42	
762	25.4	0.50	120	20	Elliptical	34.25	2.14
762	25.4	0.50	120	20	Sharp	33.42	

In Figures 6.10 and 6.11, the burst pressures of the corroded pipelines (P) are normalized with the burst pressures of pipelines with the base defect (P_{BD}). The spacing are normalized using the pipe wall thickness and a dimensional parameter, \sqrt{Dt} , in Figure 6.10-6.11 (a) and 6.10-6.11 (b), respectively. In these figures, the normalized burst

pressures are less than unity (one) when interaction between the corrosion patches occurs.

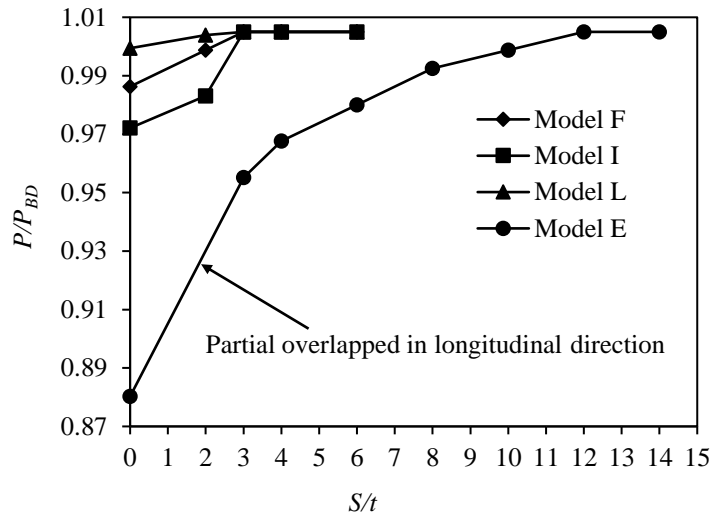


(a) Corrosion spacing in terms of pipe wall thickness

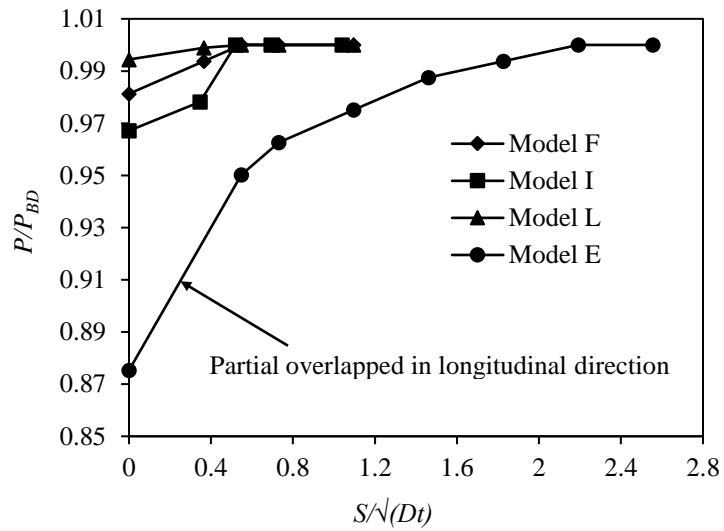


(b) Corrosion spacing in terms of pipe dimensions

Figure 6.10: Effect of interaction of longitudinally and diagonally spaced corrosion patches ($l=60\text{mm}$, $w=20^\circ$, $d/t=0.50$)



(a) Corrosion spacing in terms of pipe wall thickness



(b) Corrosion spacing in terms of pipe dimensions

Figure 6.11: Effect of interaction of circumferentially spaced corrosion patches ($l=60\text{mm}$, $w=20^\circ$, $d/t=0.50$)

6.4.1.1 Pipe Geometry

Figure 6.10 and 6.11 show that the burst pressure of the corroded pipeline increases with the increase of the spacing between the patches. The limit of interacting spacing depends on the pipe dimensions along with other factors. For 300 mm and 500 mm diameter pipelines with corrosion patches spaced along the longitudinal direction (Model C and H), the increase of the burst pressure is stabilized i.e. the normalized burst pressure becomes unity (one) at the spacing of $12t$ or about $2\sqrt{(Dt)}$. The spacing for 762 mm diameter pipeline (Model K) is $12.5t$ or $2.28\sqrt{(Dt)}$. Thus, the limiting spacing of interaction in general increases with the increase of pipe wall thickness. The spacing for the pipeline when the defects are spaced along diagonal direction ($S_c = S_l$) (Model D) is $8t$ or about $1.50\sqrt{(Dt)}$. It is to be noted that the interaction of defects in longitudinal direction is independent on pipe diameter for pipelines of 300 mm and 500 mm diameters. The spacing is about 4% longer for the 762 mm diameter pipeline. The longer spacing for the 762 mm diameter pipeline is due to the distribution of stress over a thicker wall for the larger diameter pipe having the same D/t ratio. The stress distribution within the pipe wall is discussed later in the chapter.

The limit of circumferential spacing is found to be independent of pipe diameter (Figure 6.11). The normalized burst pressure becomes unity for a circumferential spacing of $3t$ or $0.5\sqrt{(Dt)}$ when the defects are fully overlapped in the longitudinal direction (Models F, I and L). However, when the defects are partially overlapped in the longitudinal direction (Model E), the longitudinal limiting spacing is similar to the spacing for corrosion patches in the longitudinal direction (i.e., $12t$ or about $2\sqrt{(Dt)}$).

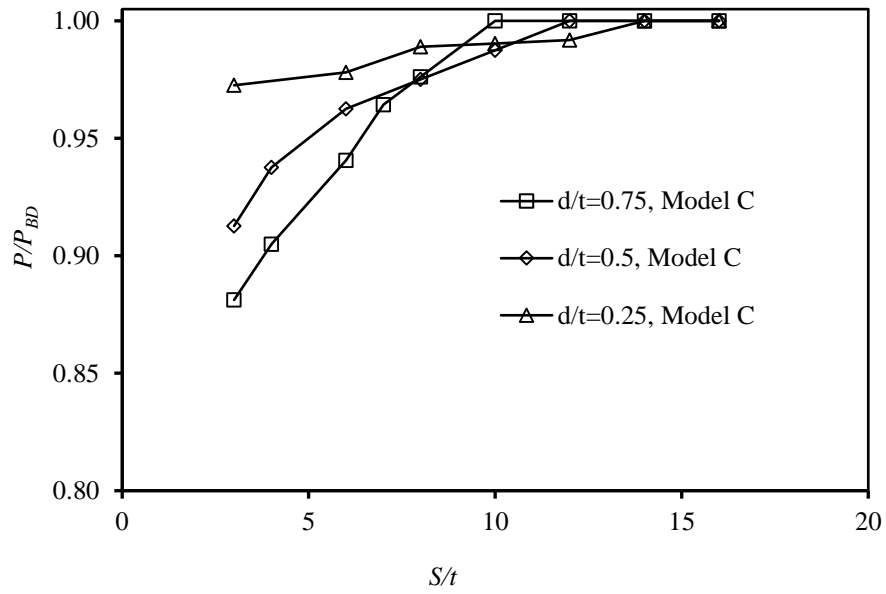
6.4.1.2 Locations of Corrosion Patches

The locations of the corrosion patches appear to influence the interaction of corrosion defects on the burst pressure and hence the limiting spacing (Figures 6.10 and 6.11). The corrosion defects spaced along longitudinal and diagonal directions reduce the burst pressure more significantly compared to the corrosion defects spaced along the circumferential direction. The limit of interacting space is the largest for the corrosion defects spaced along the longitudinal direction ($12t$ and $2\sqrt{Dt}$ for Model C and H, $12.5t$ and $2.28\sqrt{Dt}$ for Model K) followed by the spacing for defects spaced diagonally ($8t$ and $1.50\sqrt{Dt}$ for Model D) and defects spaced circumferentially ($3t$ and $0.52\sqrt{Dt}$ for Model I), respectively. The limiting spacing of the longitudinally spaced defects and the circumferentially spaced defects with overlapping in the longitudinal direction (overlap of $3t$ is considered, Model E) are almost the same. The limit of longitudinal spacing is higher by about 14% and 300% than those recommended in the DNV code (i.e., $2\sqrt{Dt}$) and ASME code (i.e. $3t$), respectively. The ASME code recommends a spacing of $3t$ for corrosion patched both in longitudinal direction and circumferential direction. The effects of using different interaction spacing rules are discussed later in this study.

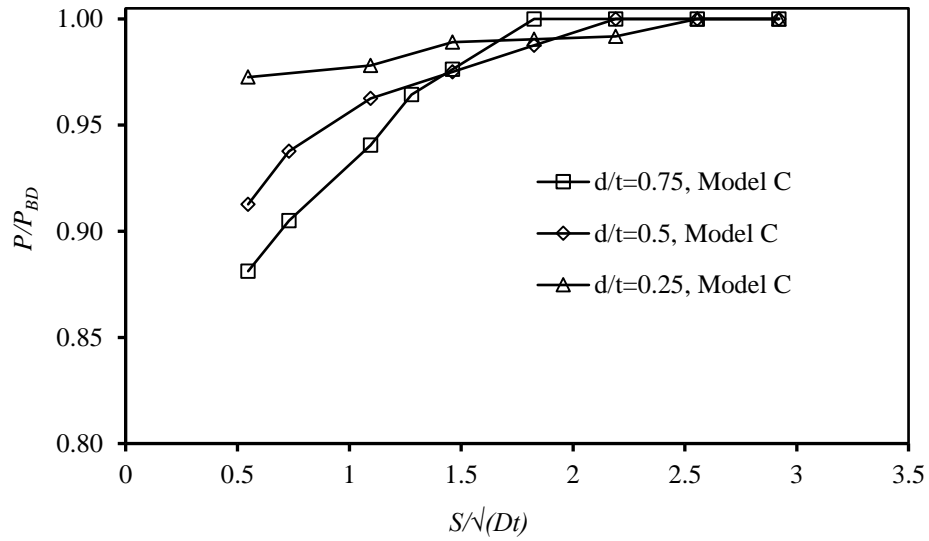
6.4.1.3 Depth of Corrosion Patches

Figure 6.12 plots the normalized burst pressure of pipe Model C against the spacing between the corrosion patches for different corrosion depths. To cover the lower and upper limits of corrosion depths considered in the current design code (i.e., ASME), three values of normalized corrosion depths of 0.25, 0.50 and 0.75 are considered. The length and width of corrosion defect are 60 mm and 20 degree, respectively. Figure 6.12 (a) represents the

spacing in terms of wall thickness (t) and Figure 6.12 (b) represents the spacing in terms of the dimensional parameter, \sqrt{Dt} . The limiting spacing of interaction appears to depend on the corrosion depth. For the normalized corrosion depths of 0.25, 0.50 and 0.75, the spacing are $14t$, $12t$ and $10t$ or $2.5\sqrt{Dt}$, $2.0\sqrt{Dt}$ and $1.8\sqrt{Dt}$, respectively. The effects of interaction are minimized within a shorter distance for higher corrosion depths and vice versa due to the distribution of stresses within the pipe wall. Figure 6.13 plots the distribution of von Mises stresses on the inner surface and outer surface of pipe wall from the centre to the centre of two corrosion defects for a 762 mm diameter pipeline with d/t ratio of 0.2 and 0.8. The defects are spaced at a distance of $6t$ or $1.1\sqrt{Dt}$. In this figure, the von Mises stress is high within the defects and at the space between the defects for $d/t = 0.8$ due to interaction of the defects. On the other hand, the von Mises stress between the defects is less for the pipeline with $d/t = 0.2$, indicating that the stress distribution within the defects are independent on each other for pipelines with a lower corrosion depth. However, the design codes do not consider the corrosion depth for calculating the spacing for the interaction of defects.



(a) Spacing in terms of pipe wall thickness



(b) Spacing in terms of pipe geometry

Figure 6.12: Effect of corrosion depth on interaction ($D=300$ mm, $l=60$ mm, $w=20$ degree)

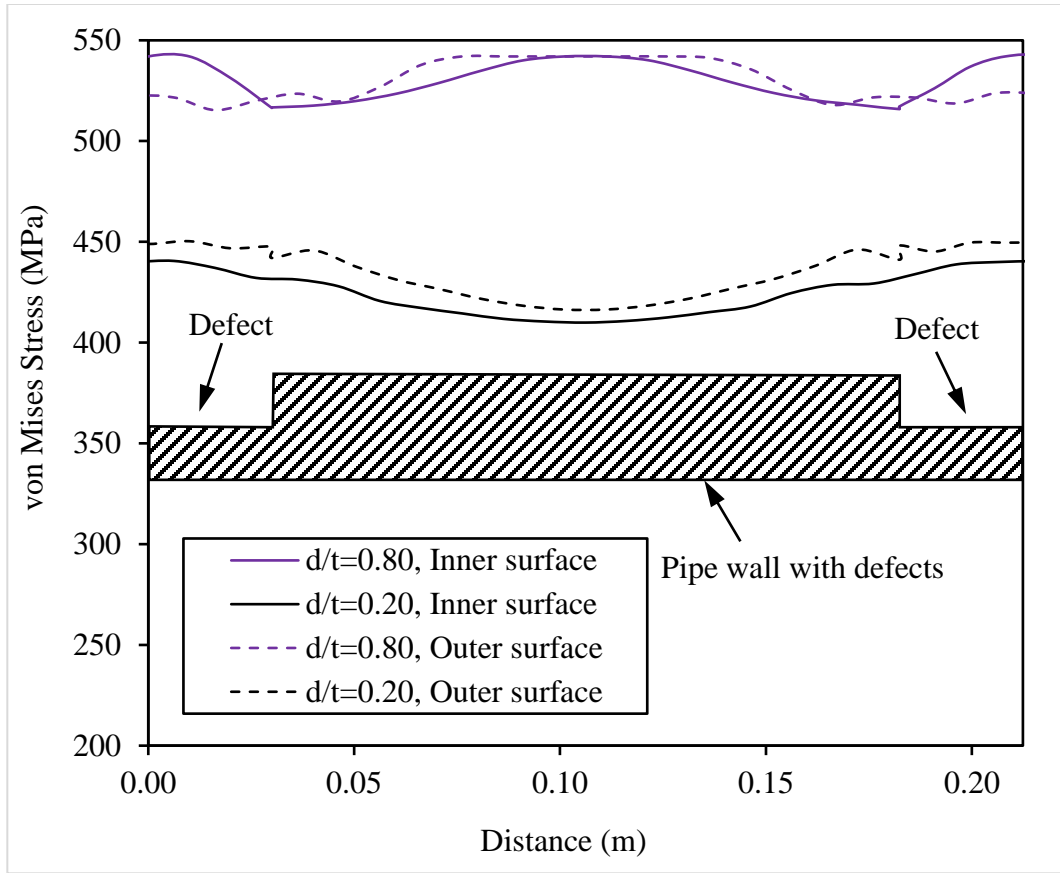


Figure 6.13: Distribution of von Mises stress through wall thickness

6.4.2 New Interaction Rule

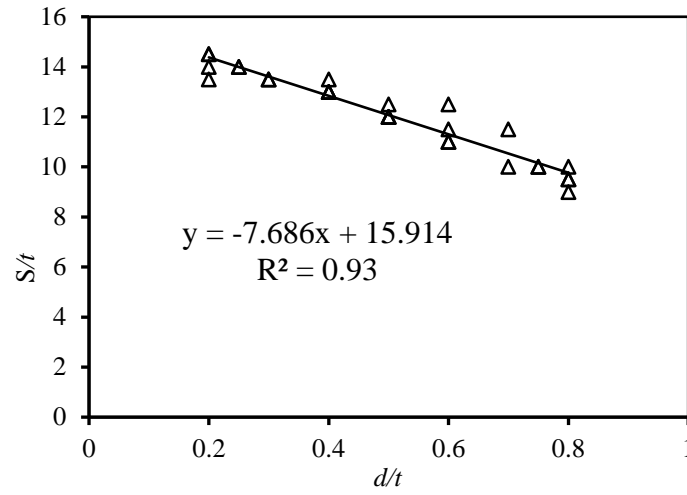
As discussed earlier, the spacing for interaction of corrosion patches in the longitudinal direction of the pipeline depends on the depth of corrosion along with pipe dimensions. However, the existing design codes do not incorporate the corrosion depth in defining the spacing for the interaction. A new interaction rule for longitudinal spacing is developed here to include the corrosion depth. For this purpose, a total of 154 FE models are developed with different pipe geometries and different corrosion depths. These 154 FE models include 39 of Model C with 10 mm wall thickness (with $d/t = 0.20, 0.25, 0.40, 0.50,$

0.60, 0.75 and 0.80), 38 of Model C with 15 mm wall thickness (with $d/t = 0.20, 0.30, 0.40, 0.50, 0.60, 0.70$ and 0.80), 39 of Model H (with $d/t = 0.20, 0.25, 0.40, 0.50, 0.60, 0.75$ and 0.80) and 38 of Model K (with $d/t = 0.20, 0.30, 0.40, 0.50, 0.60, 0.70$ and 0.80). The length and width of defects in all models are 60 mm and 20 degree, respectively. A total of 26 limiting interacting spacing are determined from these FE analysis. The interacting spacing are normalized with respect to pipe geometry (\sqrt{Dt}) and wall thickness (t) separately.

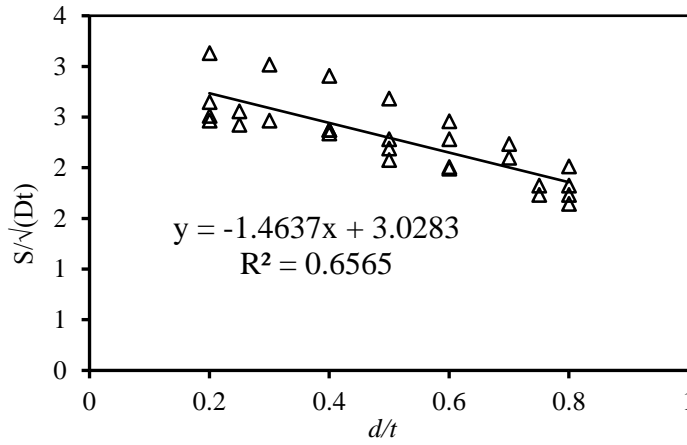
The normalized limits of interacting spacing are plotted with respect to the normalized depths of corrosion in Figure 6.14. Figure 6.14 (a) shows the spacing in terms of pipe wall thickness (t) and Figure 6.14 (b) shows the spacing in terms of pipe geometry (\sqrt{Dt}). The solid lines in the figures are the trend lines showing the linear relationship between the interacting spacing and the depth of corrosion. The linear regression analyses are performed with variables s/t and s/\sqrt{Dt} against d/t to develop new interaction rules. From regression analysis, the following interaction rules are obtained in terms of wall thickness and \sqrt{Dt} , respectively:

$$(S_l)_{lim} = \left(15.91 - 7.69 \frac{d}{t}\right) t \quad (6.2)$$

$$(S_l)_{lim} = \left(3 - 1.46 \frac{d}{t}\right) \sqrt{Dt} \quad (6.3)$$



(a) Spacing in terms of pipe wall thickness



(b) Spacing in terms of pipe geometry

Figure 6.14: New Interaction Rule

Figure 6.14 (b) shows that the points are highly scattered about the trend line when the interacting spacing is expressed in terms of \sqrt{Dt} . However, the deviation from the trend line is less when the spacing is expressed in terms of “ t ” (Figure 6.14 (a)). The points above the trend line in Figure 6.14 (a) correspond to the larger diameter pipeline (762 mm in this study) whereas those points in Figure 6.14 (b) correspond to the smaller diameter

pipeline (300 mm in this study). Figure 6.14 (a) indicates that the interacting spacing does not vary significantly with pipe diameter, if the distance is expressed in terms of t . It would, therefore, be reasonable to define the interacting rules using the pipe wall thickness. The limiting spacing of $3t$ in circumferential direction (recommended in ASME code) is found to be reasonable for the pipelines considered.

The burst pressure calculated based on different interaction rules for a 762 mm diameter pipe with two corrosion defects at a spacing of 300 mm apart (12 times the wall thickness) are compared in Figure 6.15 for d/t of 0.2, 0.4, 0.5, 0.6 and 0.8. According to the proposed interaction rules, the spacing between the defects are less than the limiting spacing for a d/t of up to 0.6 and greater than the limiting spacing for $d/t = 0.8$. However, the spacing is greater than the limiting spacing (i.e., $3t$) as per the ASME B31G recommendation, implying no interaction between the defects. As a results, the normalized burst pressure is over-predicted using the ASME B31G method with respect to the FE calculations (Figure 6.15). The burst pressure is normalized using a burst pressure of a pipeline with a single corrosion defect of the same size (called herein as “burst pressure for base defect, P_{BD} ”). Since no interaction between the defects exists, the normalized burst pressure of 1 is obtained using the ASME B31G method. On the other hand, the spacing between the defects is less the limiting spacing (i.e., $2\sqrt{Dt}$) as per DNV-RP-F101 recommendations. Thus, the DNV code provides similar results as those with the new interaction rule for a d/t of up to 0.6. The method under-predicts the burst pressure for $d/t = 0.8$, since no interaction between the defects are expected according to the new interaction rule.

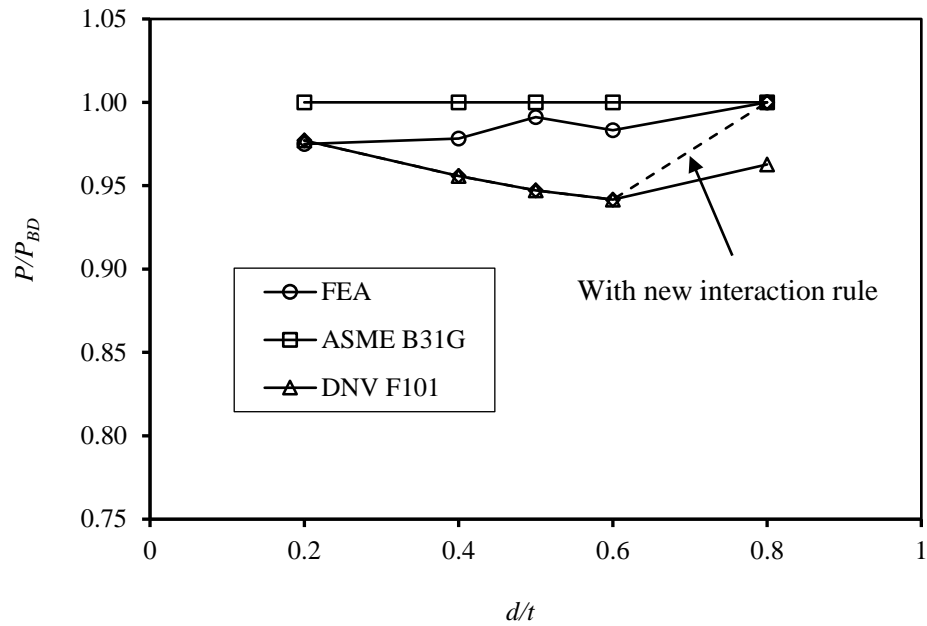


Figure 6.15: Comparison of burst pressures with various interaction rules

It is to be noted that the design codes recommend using an equivalent depth or full depth over the whole area between the corrosion defects for calculating the burst pressure. As a result, the burst pressure is underestimated even with the new interaction rule when interaction between the defects exists. Further research is required to determine the equivalent defect depth to be used for calculation of the burst pressure for interaction defects.

6.5 Summary

The burst pressures of corroded pipelines containing two corrosion patches are investigated in this study. The pipelines with different diameters are considered. Based on the study, the following conclusions can be drawn:

- The interaction between corrosion patches was found to depend on pipe dimensions and corrosion depth. The limiting spacing for interaction is higher for larger pipe dimensions. The spacing is independent of pipe diameter for pipe diameters of 300 mm and 500 mm, and is somewhat higher by about 14% for 762 mm diameter pipeline. The spacing is smaller for circumferentially spaced corrosion patches than the spacing for longitudinally spaced patches. The spacing for diagonal spaced patches is larger than circumferential spacing and smaller than longitudinal spacing.
- The limiting spacing also depends on the depth of corrosion. The new interaction rules for longitudinally spaced corrosion defects are developed incorporating the depth of corrosion. The limiting spacing is expressed in terms of ' t ' and $\sqrt{(Dt)}$. However, the spacing expressed in terms of ' t ' showed better performance. It is, therefore, reasonable to define the interaction rule using pipe wall thickness (t) rather than $\sqrt{(Dt)}$.
- For circumferentially spaced patches, the ASME (2012) recommendation (i.e., $3t$) is found to be reasonable.

The new interaction rules presented here are developed considering two base defects (i.e., 60 mm and 120 mm) for 300 mm, 500 mm and 762 mm diameter pipelines with D/t ratio of around 30. Further study is recommended to investigate the effects for pipelines with larger diameters with different D/t ratios and defect sizes.

CHAPTER 7

Burst Pressure of Corroded Pipelines Considering Combined Axial Forces and Bending Moments

7.1 Introduction

The offshore or onshore energy pipelines are generally designed for internal pressure only. However, the pipelines are often subjected to axial forces and bending moments due to external loads (Liu et al. 2009, Mondal and Dhar 2016b). For onshore pipelines, the external loads result from landslides, mining subsidence or seismic activities. For offshore pipelines, the loads could be the result of the formation of free spans, especially for unburied pipeline, and temperature difference as well as submarine landslides. The axial force and the bending moment may affect the internal pressure capacity (i.e., burst pressure) of the pipelines. Taylor et al. (2015) demonstrated through finite element (FE) analysis that the burst pressure of an intake pipeline is reduced under load imposed bending. Earlier, Lasebikan and Akisanya (2014) demonstrated using experimental investigation with minipipes that the burst pressure of an intake pipeline is also reduced under an axial tensile load. To the knowledge of the authors, the combined effects of axial forces and bending moments on the burst pressures of pipelines have not been reported in published literature. Studies on the burst pressures of corroded pipelines subjected to axial forces and bending moments are also very limited.

Oh et al. (2008) analytically developed plastic limit load solutions for pipelines subjected to combined internal pressure and bending moment for pipelines containing part-through surface cracks. They considered two shapes of defects, constant depth crack and circular crack. The solutions were validated for elastic-perfectly plastic material using finite element (FE) analysis. The solutions for part-through crack defects are found to provide lower bound plastic limit loads for pipelines with corrosion defects (Oh et al. 2009). This study is limited to elasto-plastic material for corroded pipelines with part-through surface cracks subjected to internal pressure and bending moments only.

Using FE analysis, Liu et al. (2009) examined the burst pressures of corroded pipelines subjected to internal pressure with either a bending moment or an axial compressive force. They developed some interaction diagrams for between the internal pressure and bending moment and between the internal pressure and axial force for some specific pipe sizes with specific materials. The combined effects of the axial force and bending moment on the burst pressure were not considered. The following failure criteria were considered in the development of an interaction diagram:

- i) The von Mises equivalent stress across the full remaining thickness reaches the true ultimate tensile strength of the pipe material.
- ii) The von Mises equivalent stress at a point 180° (i.e. diametrically opposite) from the corrosion defect reaches the yield strength of the pipe material.
- iii) The onset of local collapse or global instability/buckling.

The minimum pressure obtained from these criteria was considered as the failure pressure/burst pressure. As discussed in detail later in this chapter, it is observed that the

yield strength criterion governs the failure of the investigated pipeline. However, the ultimate strength criterion is preferably used for the assessment of burst pressure of an energy pipeline.

Chen et al. (2014) developed an analytical solution for the residual bending moment capacity of a corroded pipeline subjected to internal pressure and axial loading for infinitely long corrosion with three different corrosion patterns, i.e., constant depth, elliptical and parabolic corrosion considering elastic-perfectly plastic pipe material. This idealized analytical model also showed that the bending moment capacity reduces with internal pressure and axial force regardless of the state of axial force, i.e., tensile force or compressive force.

The DNV-RP-F101 (2015) recognized the effect of axial force and the bending moment on the burst pressure of corroded pipelines and accounted for the effect incorporating a factor, H_l , to the burst pressure model of the pipeline without the axial force and bending moment. The factor is defined in Equation 7.1, where ξ , γ_m , γ_d , σ_L , ε_d and $\text{StD}[d/t]$ indicate usage factor, partial safety factor for longitudinal corrosion, partial safety factor for corrosion depth, total longitudinal stress, fracture factor for corrosion depth and standard deviation of the measured corrosion depth, respectively. The effects of the bending moment and axial compressive force in the equation are accounted in terms of longitudinal stress. The ratio of hoop stress and longitudinal stress due to burst pressure is assumed as 2 during development of the equation (Bjornoy et al. 2001). Thus, the burst pressure model proposed in the DNV-RP-F101 code is applicable for the hoop stress to longitudinal stress ratio of 2. It is assumed that there is no effect of longitudinal tension on

the burst pressure, which is inconsistent with the findings reported in Lasebikan and Akisanya (2014) and Chen et al. (2014).

$$H_1 = \frac{1 + \frac{\sigma_L}{\xi \sigma_u A_r}}{1 - \frac{\gamma_m}{2\xi A_r} \frac{1 - \gamma_d \left(\frac{d}{t}\right)^*}{1 - \gamma_M \frac{1}{d_M} \left(\frac{d}{t}\right)^*}} \quad (7.1)$$

$$\text{where, } A_r = 1 - \frac{dw}{\pi D t} \text{ and } \left(\frac{d}{t}\right)^* = \frac{d}{t} + \varepsilon_d \text{StD} \left[\frac{d}{t}\right]$$

The objective of the present study is to revisit the burst pressures of corroded pipelines subjected to axial forces and bending moments. A parametric study has been conducted to develop interaction diagrams for the burst pressures with axial forces, bending moments and simultaneous effect of the axial forces and the bending moments. The ultimate strength criterion is used for the failure assessments of the pipelines.

7.2 FE Model

The Abaqus/Standard module is used in this study for calculating the burst pressures of corroded pipelines subjected to axial forces and bending moments. The pipe domain is modelled using eight-noded continuum elements (Abaqus element “C3D8R”). The corrosion defect with a smooth edge is applied on the outer surface of the pipeline, as shown in Figure 7.1 (after Mondal and Dhar 2017).

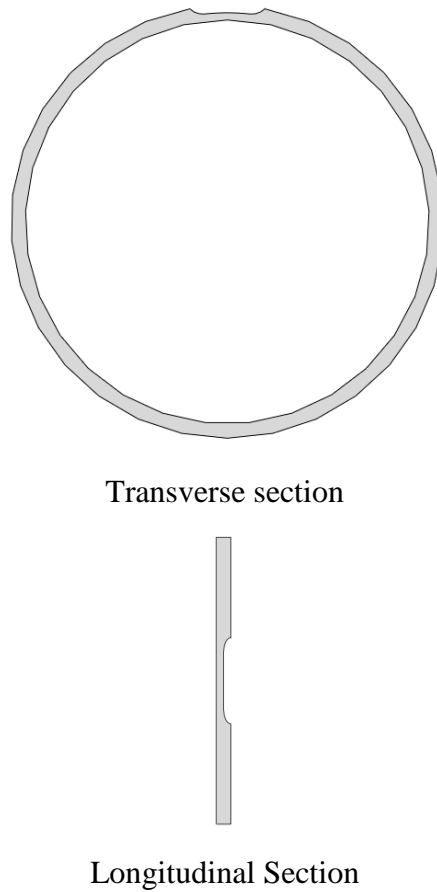


Figure 7.1: Typical sectional view of corrosion patch
(after Mondal and Dhar 2017b)

To save computation time, only a quarter of the full pipeline is modelled using the advantage of symmetry, as shown in Figure 7.2. The symmetric boundary conditions are applied at the plane of symmetry in the FE model. The top wall and bottom wall along the length of the pipeline are restrained to the X-direction and the left-end section is restrained to the Z-direction (Figure 7.2). The bottom point at the left end in Figure 7.2 is fully restrained to obtain the stability of the model.

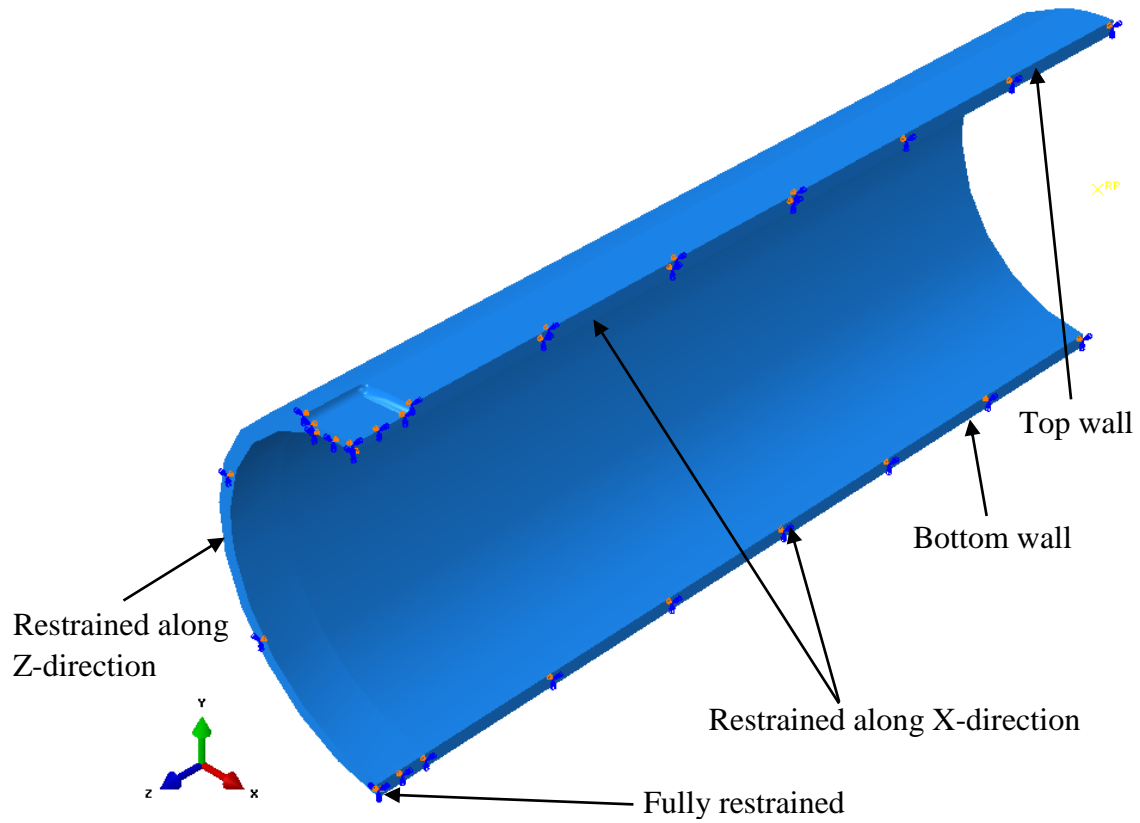


Figure 7.2: Quarter Model of Pipe with Boundary Conditions

In the FE model, the internal pressure is applied on the inner surface of the pipeline and axial force (tension or compression) is applied at the right-end cross-section of the pipeline, calculated using Equation 7.2, where σ_a , D_o and D_i indicate the applied axial stress, outer diameter and inner diameter of the pipeline, respectively. To apply the bending moment, a reference point is created at the centre point of the right-end cross-section. The right-end cross-section is connected to the reference point using the multi-point constraint option available in Abaqus. The bending moment is then applied to that reference point, as shown in Figure 7.3. Two types of bending moments are considered in this study: the opening bending moment when the corroded area is in tension under the bending moment

and the closing bending moment when the corroded area is in compression under the bending moment (Mohd et al. 2015).

$$F = \sigma_a \frac{\pi}{4} (D_o^2 - D_i^2) \quad (7.2)$$

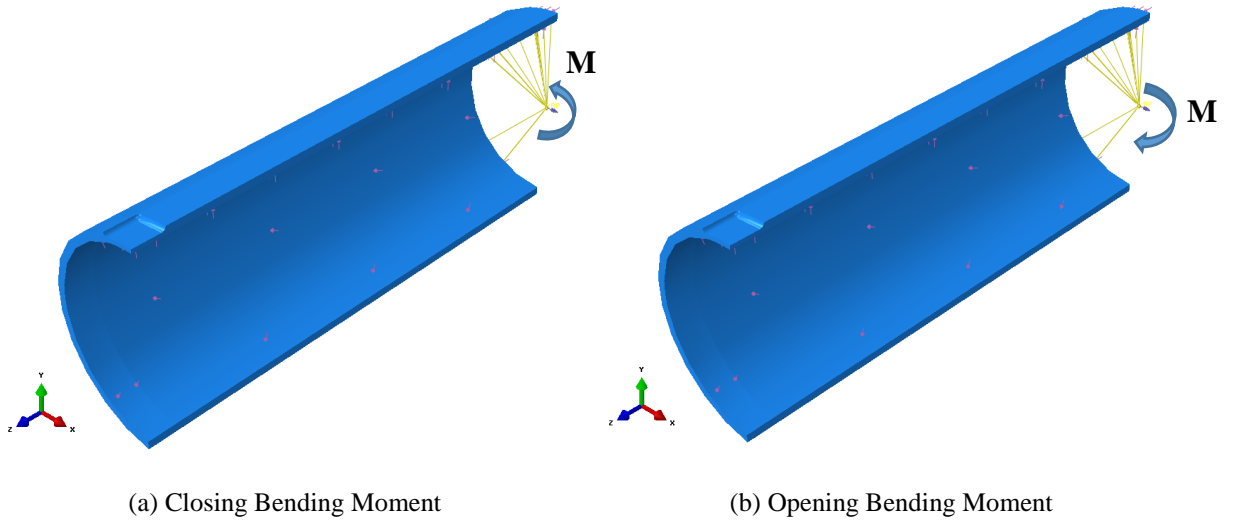


Figure 7.3: Application of loadings on FE model

During analysis, the stress concentration is expected around the corroded zone, whereas uniform stress is expected away from the corroded zone. Therefore, fine mesh is applied at and near the corroded zone and coarse mesh is applied away from the corroded zone. An appropriate gradient is applied in the transition zone of coarse to fine mesh that gives the mesh size with dimensions from 1.44 mm to 23 mm. After conducting a mesh sensitivity analysis for determining the optimum mesh size, six or five layers of element are applied over the thickness within the corroded zone. Figure 7.4 shows a typical finite-element mesh used in the analysis.

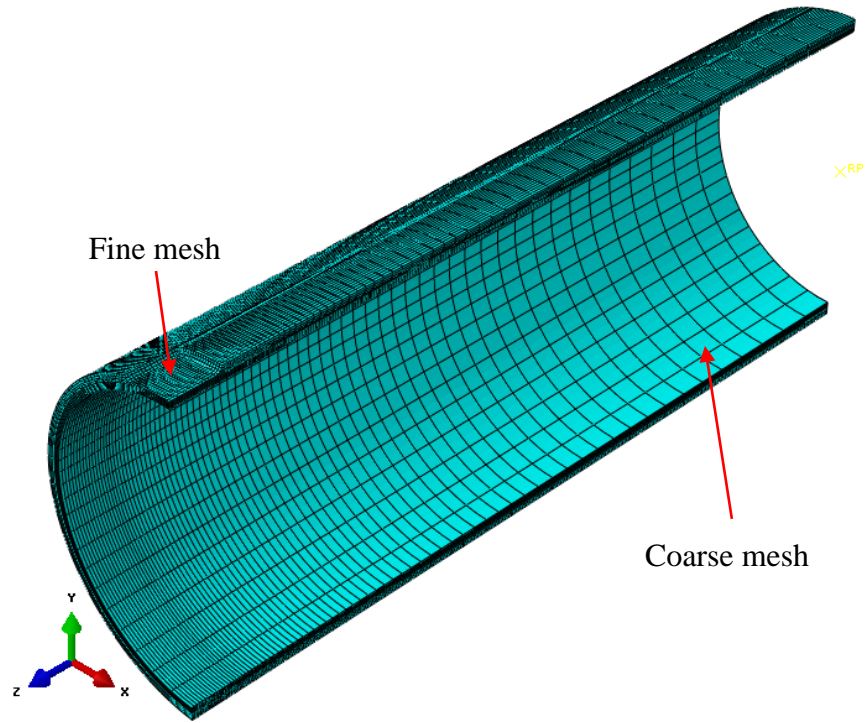


Figure 7.4: Typical meshing of FE model

7.2.1 Material Model

The nonlinear true stress–strain data of API X65 grade steel obtained from the published literature (Oh et al. 2007) are used in the FE model, as shown in Figure 7.5. The stress–strain data are inserted in the FE model using connected piecewise straight lines. Other properties of the steel pipe material are given in Table 7.1.

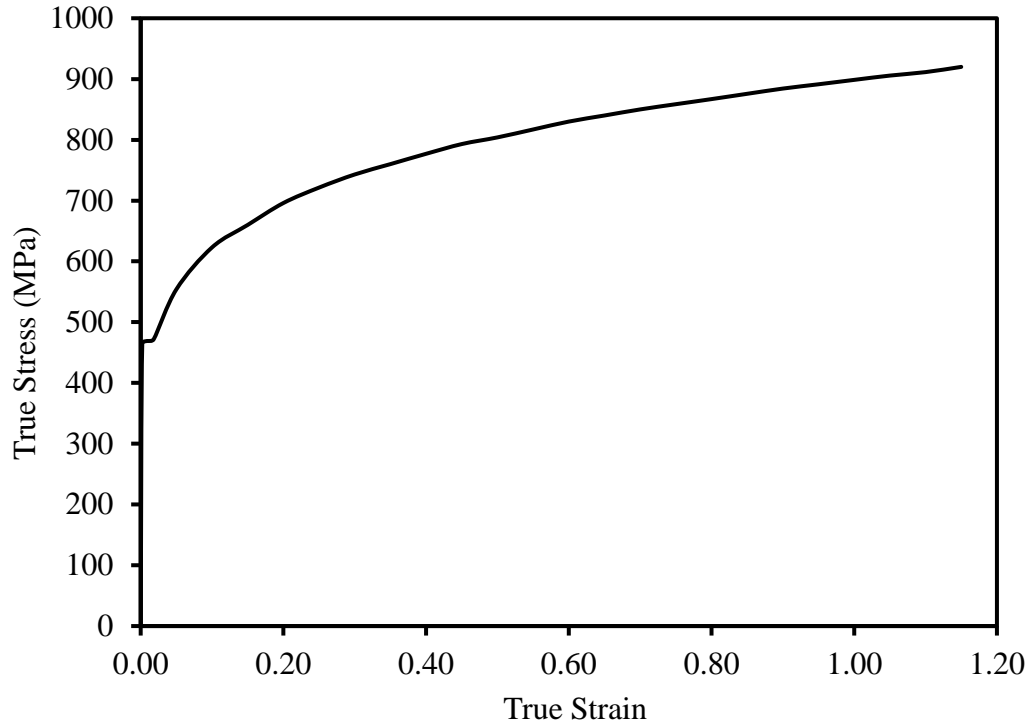


Figure 7.5: True stress–strain data for API X65 steel (Oh et al. 2007)

Table 7.1: Material parameters of API X65 Steel (Oh et al. 2007)

Property	Value
Density, ρ (kg/m ³)	7850
Modulus of Elasticity, E (GPa)	210.7
Poisson's Ratio, ν	0.30
Yield Strength, σ_Y (MPa)	464.5
Ultimate Tensile Strength, σ_U (Mpa)	563.8

7.2.2 Failure Criteria

In the conventional standard FE analysis, the node separation is not allowed. Hence, the crack initiation and its propagation in the pipeline cannot be simulated. The commonly

used approach for burst pressure assessment is to define failure when the von Mises equivalent stress throughout the thickness (the ligament) reaches the true ultimate strength of the pipe material (Li et al. 2016). This approach is employed in this study for the burst pressure assessment.

7.2.3 Validation of FE Model

The FE model is first validated through simulated burst pressure available in the literature (i.e., Oh et al. 2007). The pipe dimensions and corrosion dimensions given in Table 7.2 are obtained from Oh et al. (2007). The material properties given in Table 7.1 and in Figure 7.5 are used. During the burst pressure test of a corroded pipeline, the ends of the pipeline are capped to apply internal pressure. The applied internal pressure causes axial tensile stress in the pipe wall at the ends. To simulate this end cap effect during FE analysis, an axial tensile stress equivalent to the internal pressure is applied to the right-end section of the pipeline. The axial tensile stress, σ_t , equivalent to any internal pressure, P , is calculated using Equation 7.3. The burst pressure of the pipeline calculated using FE analysis is then compared with the test result available in Oh et al. (2007). The burst pressure of the corroded pipeline is reported as 24.3 MPa from the test.

$$\sigma_t = P \frac{D_i^2}{D_o^2 - D_i^2} \quad (7.3)$$

Figure 7.6 shows the average von Mises equivalent stresses calculated through the ligament under different internal pressures determined from the FE analysis. The average von Mises stress increases with the increase of internal pressure (Figure 7.6) and becomes

constant at an internal pressure of around 18 MPa. The corresponding von Mises stress is the yield strength of the material (i.e., 464.5 MPa). The von Mises stress remains constant at the yield strength up to a pressure of around 23 MPa, beyond which the stress increases up to failure of the pipeline. While the FE model continues calculating the stresses beyond failure, the internal pressure corresponding to the ultimate tensile strength is taken as the burst pressure. In Figure 7.6, the internal pressure corresponding to the average von Mises equivalent stress of 563.8 MPa (the ultimate tensile strength) is 24.47 MPa, which is within 0.69% of the test result of burst pressure (i.e., 24.30 MPa). Thus, the FE model reasonably represents the test condition.

Table 7.2: Dimensions of pipe and corrosion for FEM validation (Oh et al. 2007)

Parameter	Value
Pipe Diameter, D (mm)	762
Wall Thickness, t (mm)	17.5
Defect Depth, d (mm)	8.75
Defect Length, l (mm)	100
Defect Width, w (mm)	50

This FE modelling approach is used to investigate the burst pressure of corroded pipelines subjected to axial forces and/or bending moments. Pipe dimensions in Table 7.3 are considered for this investigation, after Liu et al. (2009).

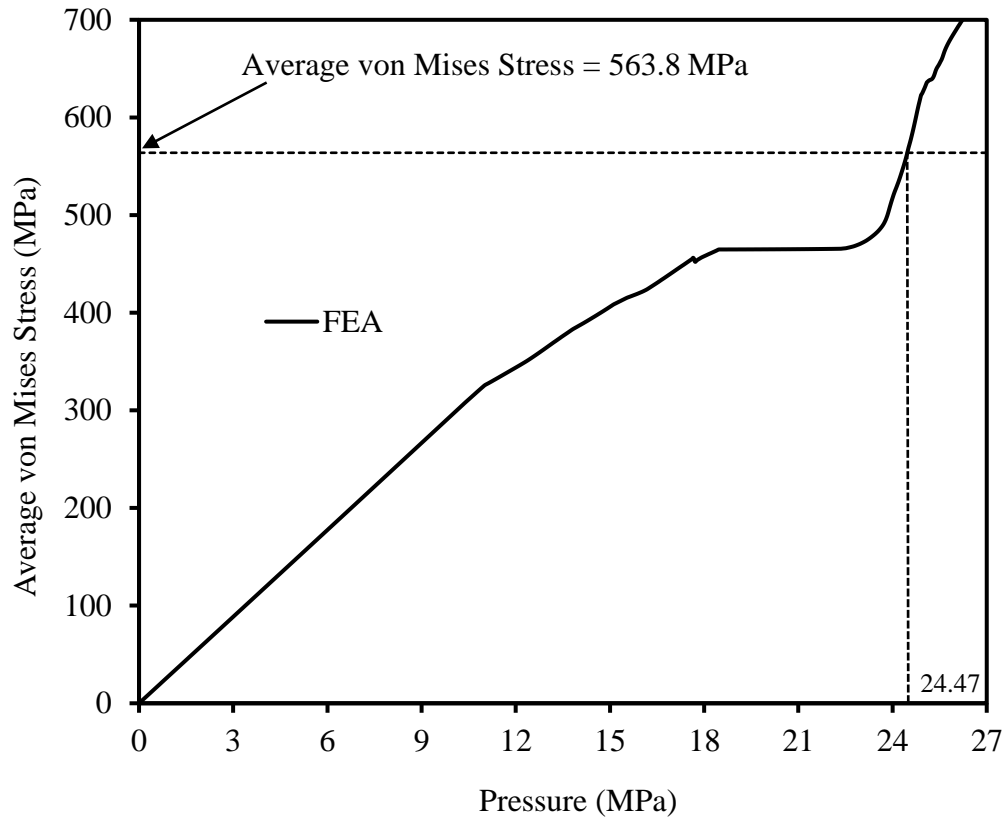


Figure 7.6: Burst Pressure Calculation Using FEA

7.3 Effects of Axial Force or Bending Moment

To investigate the effect of states of axial forces (i.e. compressive or tensile) and bending moments on the burst pressure of the corroded pipeline subjected to combined loadings, FE analyses are conducted with an increase of internal pressure and with independent application of 200 kN of axial tension, 200 kN of axial compression, 20 kN-m of opening bending moment and 20 kN-m of closing bending moment, respectively. Figure 7.7 shows the average von Mises equivalent stresses calculated through the ligament for different internal pressures. As seen in the figure, the average von Mises stresses are

higher for the pipelines with axial forces and bending moments than for the pipelines without these (i.e., internal pressure only), except during the yielding phase. The von Mises stress also reaches the yield strength and the ultimate strength at a lower internal pressure for the pipeline with axial forces and bending moments, indicating that the burst pressure is reduced due to the presence of an axial force and a bending moment. The ultimate tensile strength (i.e., 563.8 MPa) of the material is shown using a horizontal line and corresponding internal pressure is obtained as the burst pressure (Figure 7.7). The figure also reveals that the burst pressure reduction is higher for axial compression than for the axial tension. For the axial force and bending moment considered, the reduction of burst pressure for axial compression of 200 kN and closing bending moment of 20 kN-m is almost the same. Both the axial compressive force and closing bending moment cause compressive stress in the pipe wall in the corroded zone, which might be the reason for similar burst pressure reductions for these cases. The tensile axial force and opening bending moment cause tensile stress in the pipe wall at the corroded zone and provide similar burst pressure reductions (Figure 7.7), which is less than the burst pressure reduction due to compressive stress within the corroded area. The burst pressure reduction due to compressive stress within the corroded area is recognized in the DNV-RP-F101 (2015) design code, where no effect of tensile stress is assumed. However, the current study reveals that axial tensile stress also contributes to the reduction of burst pressure. Since the burst pressure reduction is higher for axial compressive stresses within the corroded area, the compressive axial force and closing bending moment are further investigated to develop the interaction diagram for burst pressure with various axial forces and bending

moments. The design method recommended in the DNV-RP-F101 (2015) is first evaluated using the FE results.

Table 7.3: Dimensions of pipe and corrosion defect after Liu et al. (2009)

Parameter	Value
Pipe Diameter, D (mm)	203.2
Wall Thickness, t (mm)	8.2
Defect Depth, d (mm)	4.1
Defect Length, l (mm)	65.6
Defect Width, w (mm)	65.6

As mentioned earlier, the DNV RP-F101 (2015) introduces a factor, H_I (Equation 7.1), to account for the axial compression and the bending moment in burst pressure calculation. An H_I value of less than one indicates that the axial force and bending moment reduce the burst pressure of a corroded pipeline and vice versa. The value of H_I depends on the resultant axial stress, σ_L , caused by the axial force and bending moment, expressed as a ratio of the ultimate strength of the material (Equation 7.1). The resultant axial stress can be calculated using elastic beam/column theories from the external axial force, F_z and the external bending moment, M .

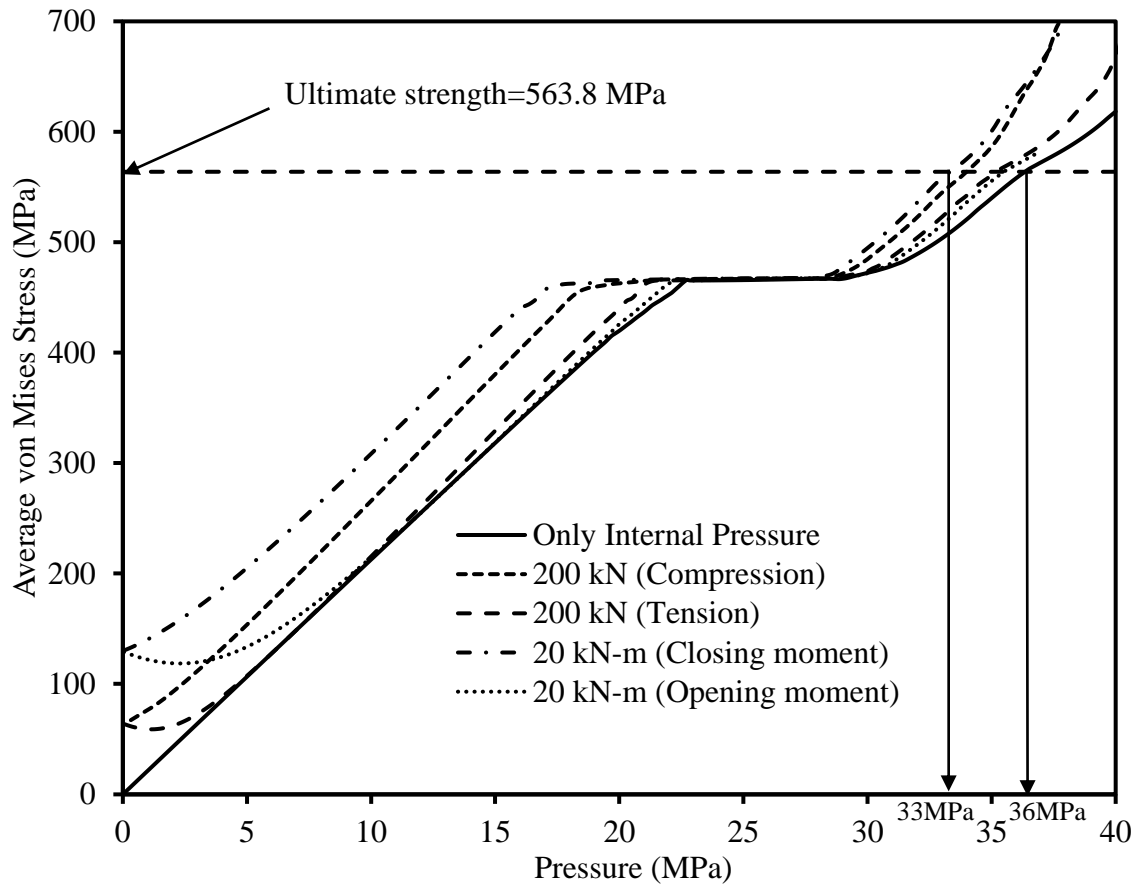


Figure 7.7: Effects of axial force and bending moment on burst pressure

The H_I from FE analysis is calculated as the ratio of burst pressure of the corroded pipeline with combined loadings, P_{com} , to the burst pressure of the same pipeline with internal pressure only, P , which is compared with the parameter calculated using Equation 7.1. The DNV-RP-F101 code, considers three safety classes (i.e., low, medium and high) with different values of usage factor and partial safety factor. The medium safety class with parameters listed in Table 7.4 is considered for comparison (Figure 7.8).

Table 7.4: Parameters for calculation of H_I

Parameter	Safety Class: Medium
Usage Factor, ζ	0.85
Partial Safety Factor, γ_m	0.88
Partial Safety Factor, γ_d	1.28
Standard Deviation, $\text{StD}[d/t]$	0.08
Fractile Value, ε_d	1.0

Figure 7.8 shows that when the resultant axial stress is less than about 25% of ultimate material strength, the DNV-RP-F101 code provides higher H_I values than one (unit), indicating that the burst pressure under axial compressive stress is higher than the burst pressure under internal pressure only. The H_I values from FE analysis are always less than one, indicating that the burst pressures under the load combinations are less. Thus, the DNV-RP-F101 code gives unconservative burst pressure at low compressive axial stress. However, for axial stress beyond 50% of the ultimate tensile strength, the DNV-RP-F101 code provides a reasonable estimation of the reduced burst pressure.

In the current study, a detailed investigation is conducted to develop failure loci of corroded pipelines subjected to internal pressure with an axial compressive and/or closing bending moment, as discussed below

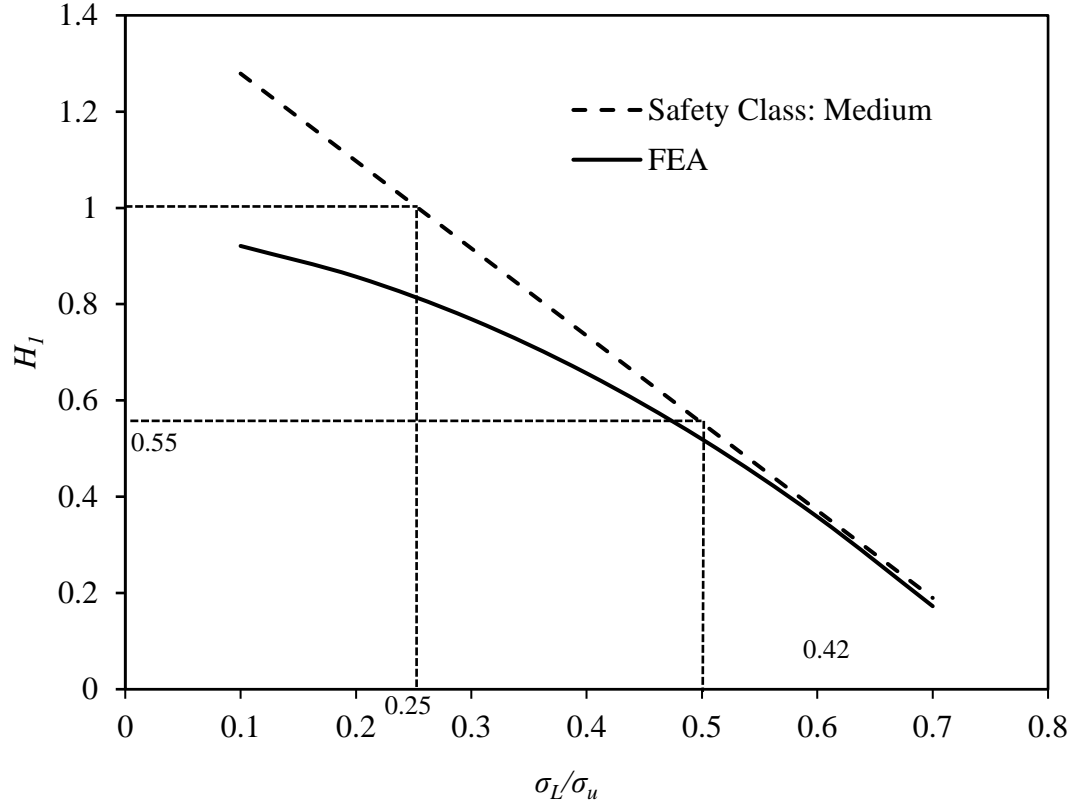


Figure 7.8: Evaluation of DNV-RP-F101 (2015)

7.4 Development of Failure Loci

Liu et al. (2009) used FE analysis to develop failure loci of corroded pipelines subjected to internal pressure with axial compressive force and internal pressure with bending moment. They considered three different pipe sizes, ($D=203.2$ mm with $t=8.2$ mm, $D=457.2$ mm with $t=5.6$ mm and $D=914.4$ mm with $t=12.7$ mm) with different corrosion depths ($d/t=0.20$ - 0.80). Two different material grades (X42 and X65) were used in the analysis. In this study, they employed three different failure criteria (discussed earlier); the minimum of these three criteria was used to determine the failure pressure. In the current

study, the ultimate strength criterion is used for the burst pressure assessment. The effects of using the failure criteria used in Liu et al. (2009) are first evaluated through comparison with the results of FE analysis conducted in this study. In the FE modelling, the yield strength at the bottom fibre (a criterion used in Liu et al. 2009) and ultimate strength over the whole thickness of the corroded area (ligament) are used as the failure criteria.

Figure 7.9 compares the failure locus obtained from the current FE analysis with the one obtained from Liu et al. (2009). The failure locus from the current study with the yield strength criterion matches the failure locus of Liu et al. (2009). Thus, the failure locus developed in Liu et al. (2009) is mostly governed by the yield strength criterion, for the pipeline investigated. However, the ultimate strength is commonly considered for the design of energy pipelines. As shown in Figure 7.9, the failure locus obtained based on the ultimate strength criterion provides significantly higher capacity of the pipelines compared to the one given in Liu et al. (2009). The ultimate strength based criterion is employed in the current study to develop the failure loci.

A parametric study is first conducted to identify the influencing parameters in the development of failure loci. The corrosion depth, corrosion length and pipe dimensions are considered for the parametric study.

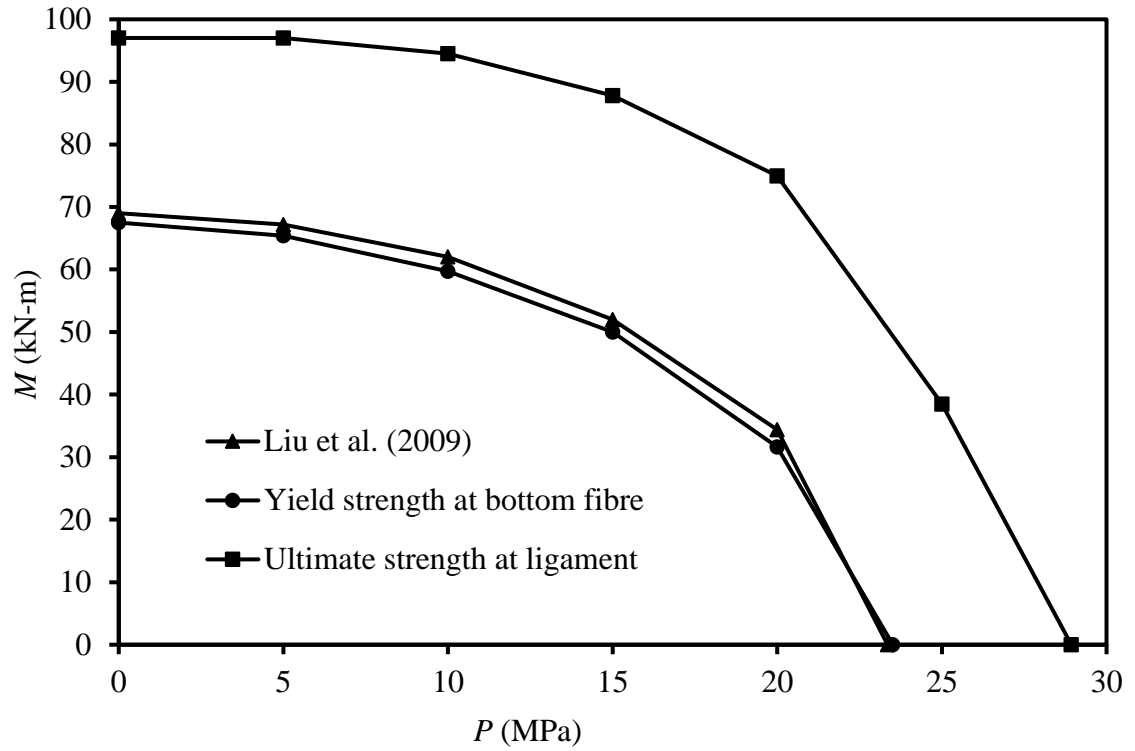


Figure 7.9: Comparison of failure locus developed by current study with Liu et al. (2009)

7.4.1 Corrosion Depth

To investigate the effect of corrosion depths on the failure locus for combined loadings, the FE models with two d/t ratios of 0.2 and 0.5 are developed. Other model parameters used are given in Table 7.3. Analyses are performed with varying closing bending moments and internal pressures for a constant compressive axial force of $F_z=200$ kN. The bending moments (M_{com}) and internal pressures (P_{com}) corresponding to failure under the combined loadings are calculated as discussed above. The bending moment and the internal pressure are normalized using the moment capacity (M_o) and burst pressure

(P_b) of the corroded pipeline without external loads, respectively. The M_o and P_b are obtained by performing FE analysis.

Figure 7.10 shows the failure loci for two defect depths with the preceding load combinations. The figure shows that the defect depth influences the burst pressure of the corroded pipeline subjected to a bending moment. The reduction of burst pressure is higher for the pipeline with higher corrosion depth. The defect depth is therefore considered for the development of failure loci of the corroded pipelines.

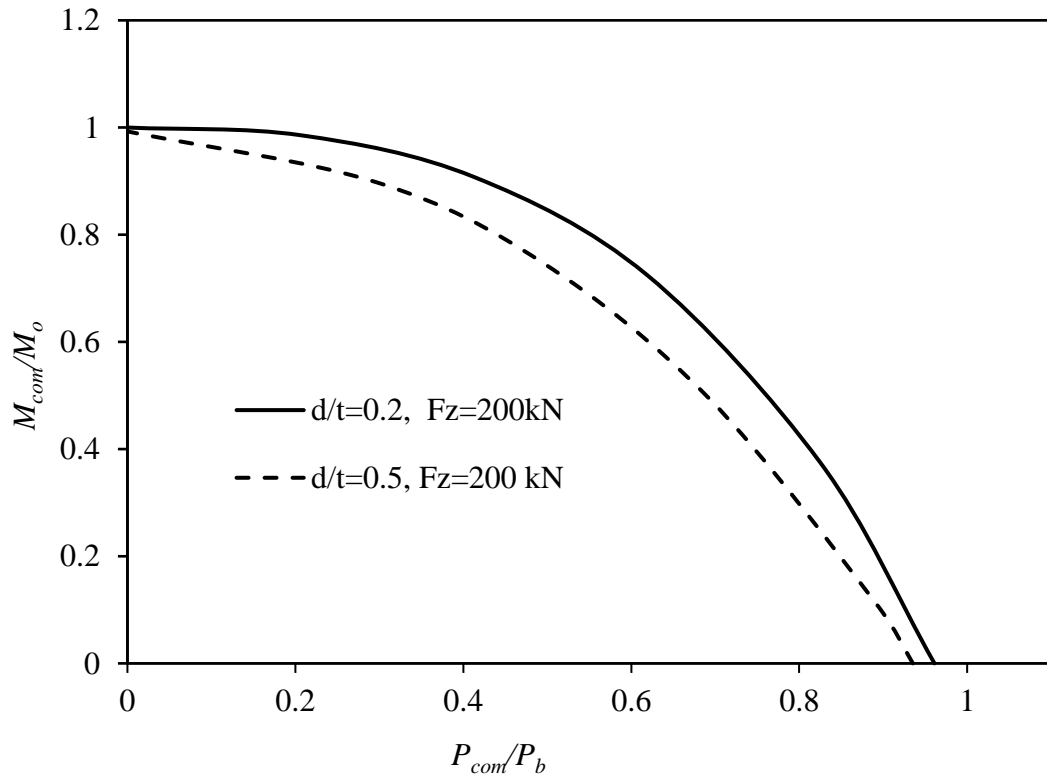


Figure 7.10: Effect of corrosion depth on failure locus

7.4.2 Corrosion Length

To investigate the effect of corrosion length on the failure loci, the FE models with two different defect lengths are developed. The defect lengths, l , are 8 times and 16 times the wall thickness, t ($l/t = 8$ and 16). Analyses are performed with varying closing bending moments and internal pressures for a constant compressive axial force of $F_z=200$ kN. The normalized bending moments (M_{com}/M_o) and internal pressures (P_{com}/P_b) corresponding to failure of the pipelines are compared in Figure 7.11. The comparison shows that the influence of corrosion length on the failure loci expressed in terms of normalized bending moment and normalized internal pressure is insignificant. A constant length is therefore considered for the development of failure loci.

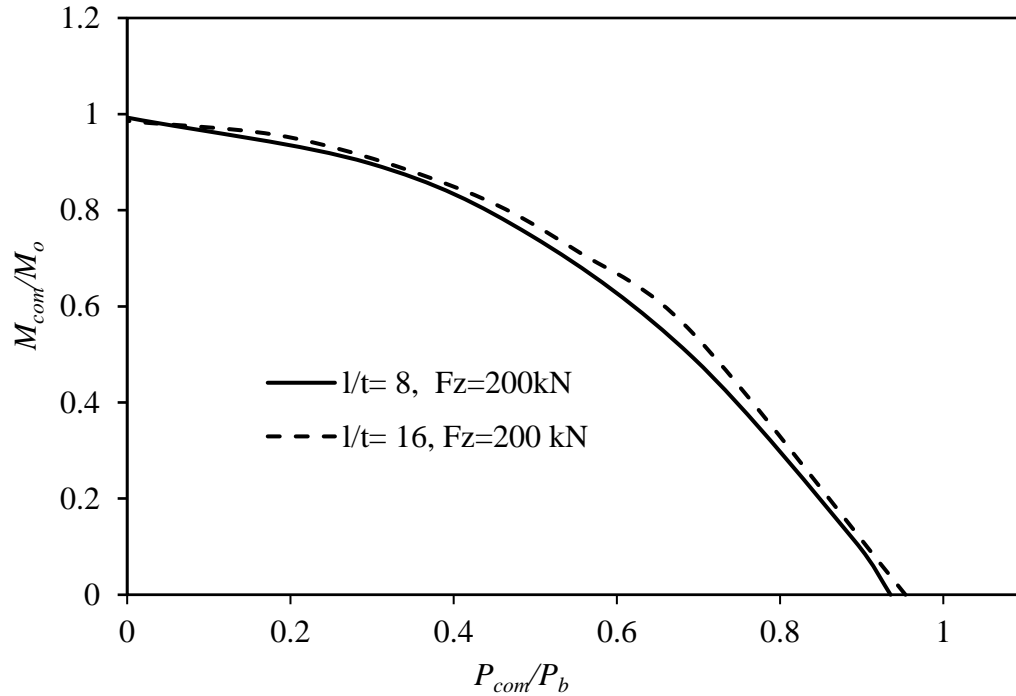


Figure 7.11: Effect of corrosion length on failure locus

7.4.3 Pipe Dimensions

The FE models with two different sets of pipe dimensions, shown in Table 7.4, are developed to investigate the effect of pipe dimensions on the failure locus. The dimensions of Pipe “A” are obtained from Liu et al. (2009) and those of Pipe “B” are obtained from Bedairi et al. (2012). The models are analyzed for the loading combinations considered in the investigation of corrosion depth and corrosion length, as mentioned above. The bending moments (M_{com}) and internal pressures (P_{com}) corresponding to failure of the pipelines under combined loadings are normalized using the moment capacity (M_o) and burst pressure (P_b) of the pipelines, respectively.

Figure 7.12 compares the failure loci for the two pipelines. The figure reveals that the pipe dimensions do not have significant effect on the failure loci. Although the strength of corroded pipelines with different pipe dimensions can be different, the failure loci expressed in terms of normalized strengths are not affected. Thus, a constant set of pipe dimensions is considered in the following study.

Table 7.4: Dimensions of Pipe “A” and Pipe “B”

Parameter	Pipe “A”	Pipe “B”
Pipe Diameter, D (mm)	203.2	508.0
Wall Thickness, t (mm)	8.2	5.7
d/t	0.5	0.5
l/t	8.0	8.0
w/t	8.0	8.0

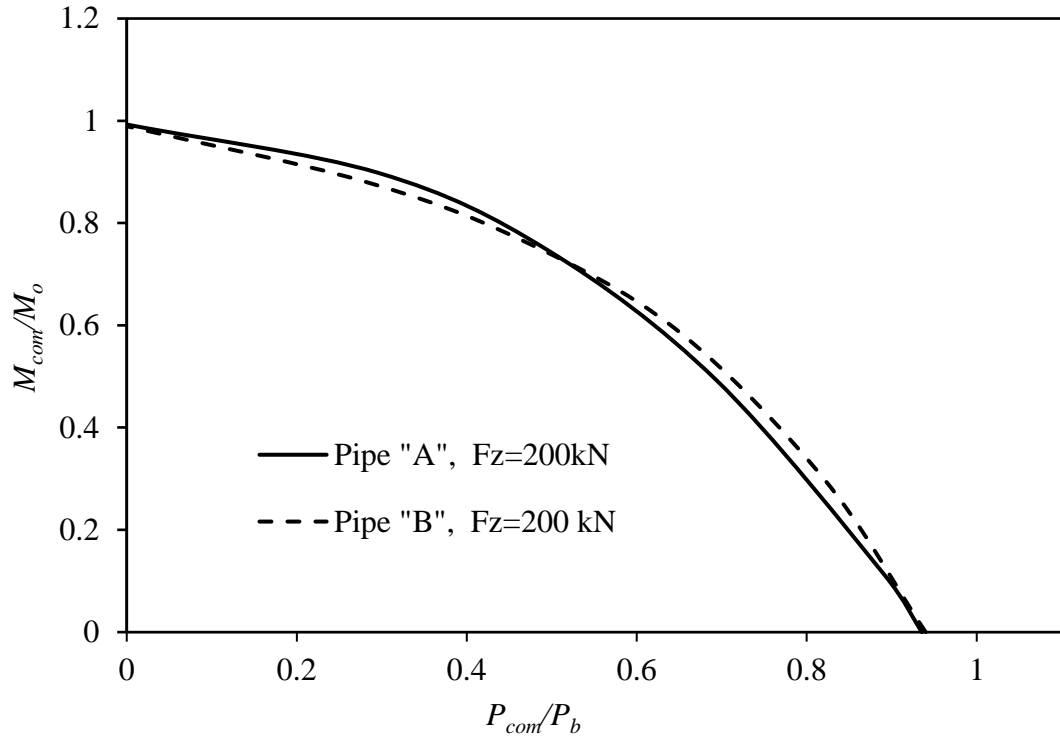


Figure 7.12: Effect of pipe dimensions on failure locus

7.5 Failure Loci

From these studies, it is observed that the failure locus of corroded pipelines subjected to axial forces and/or bending moments depends predominantly on the corrosion depth. The other parameters, such as corrosion length and pipe dimensions, have insignificant effects. Therefore, the failure loci are developed considering different depths of corrosion. Three different d/t ratios of 0.2, 0.5 and 0.8 that cover mild to severe corrosion for energy pipelines are considered. To account for the effects of both compressive axial force and closing bending moment on the burst pressure of corroded pipelines, the failure

loci of the combined bending moment and internal pressure are developed for different axial forces (Figure 7.13 to 7.15). The axial force (F_z), bending moment (M_{com}) and internal pressure (P_{com}) at failure under combined loadings are normalized using the strengths of the pipelines under each of the loads independently. For the development of the failure loci, the strengths of the pipelines under each of the loads are calculated using simplified equations to avoid the complexity of FE modelling during pipeline integrity assessment. The axial force capacity (F_o) and the bending moment capacity (M_o) of the intake pipeline are used, which are calculated using the classical failure of the short column and beam given by Equations 7.4 and 7.5, respectively. The burst pressure (P_b) of the corroded pipeline under internal pressure is obtained using the model proposed in Mondal and Dhar (2018) shown in Equation 7.6.

$$F_o = \frac{\pi}{4}(D_o^2 - D_i^2)SMYS \quad (7.4)$$

$$M_o = \frac{2I(SMYS)}{D_o} \quad (7.5)$$

where

I = moment of inertia of pipe cross-section

$SMYS$ = Specified minimum yield strength of pipe material

D_o = Outer diameter of pipe

D_i = Inner diameter of pipe

$$P_b = \frac{2t}{(D - 2t)} \sigma_u \left(\frac{1 - \frac{d}{t}}{1 - \frac{d}{tM}} \right) \quad (7.6)$$

where

$$M = \sqrt{1 + 0.278 \cdot \left(\frac{l^2}{Dt} \right)^{0.447} \times \left(\frac{d}{t} \right)^{-0.718} + 0.337 \cdot \left(\frac{l^4}{D^2 t^2} \right)^{0.717} \times \left(\frac{d^2}{t^2} \right)^{0.504}}$$

σ_u = Ultimate tensile strength of pipe material

Four normalized magnitudes of axial force, $F_z/F_o=0.086, 0.171, 0.343$ and 0.514 are considered for the development of failure loci. Each figure of Figure 7.13 to 7.15 contains four failure loci for four different axial forces and one failure locus for zero axial force. The figures reveal that the burst pressures and the moment capacities of the pipelines are reduced with the increase of axial compression. The burst pressure of the corroded pipeline subjected to a particular bending moment and/or an axial force can be predicted using the relevant failure locus shown in the figures.

7.7 Summary

The existing design codes, except the DNV-RP-F101, provide the models of burst pressure for corroded pipelines, assuming that the pipelines are subjected to internal pressure only. However, the pipelines are often subjected to different types of external loadings resulting in longitudinal bending moments and axial forces in addition to the internal pressure. The axial forces and the bending moments result in the reduction of burst pressure of the pipelines.

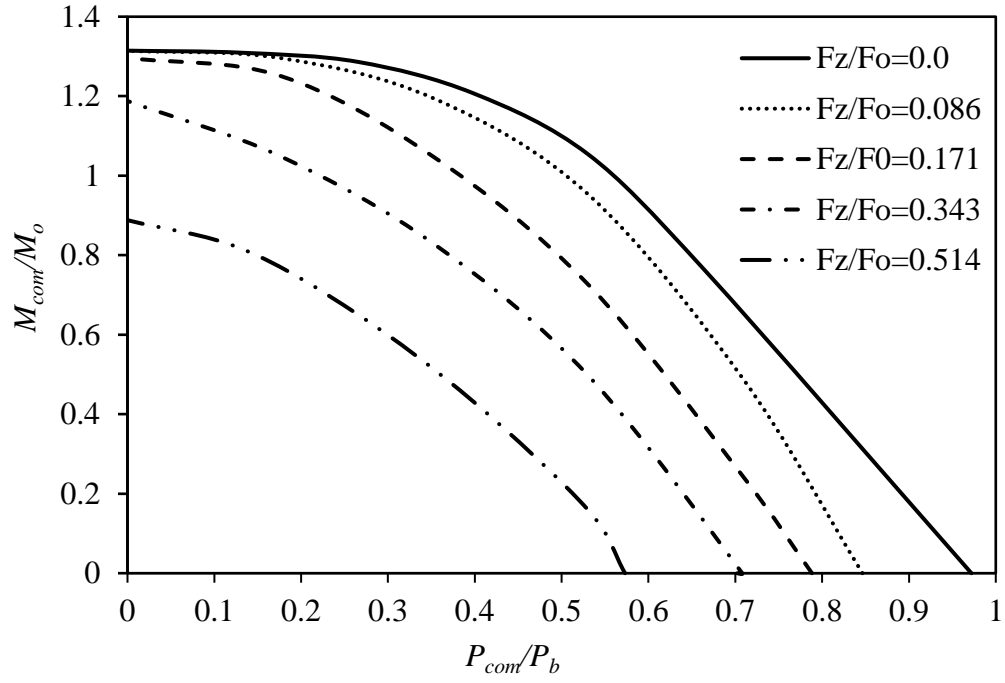


Figure 7.13: Failure Locus for d/t for 0.2

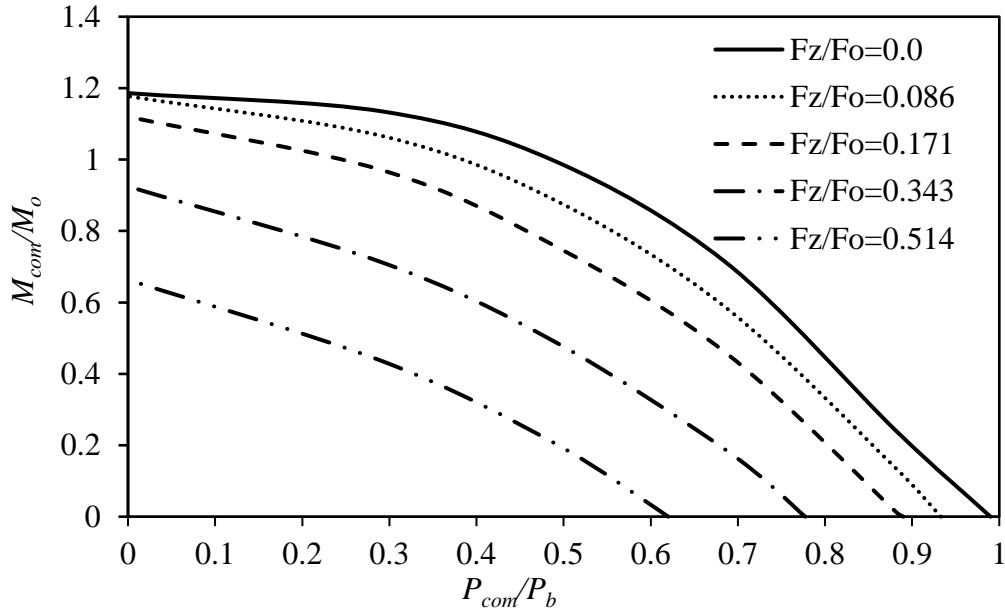


Figure 7.14: Failure Locus for d/t for 0.5

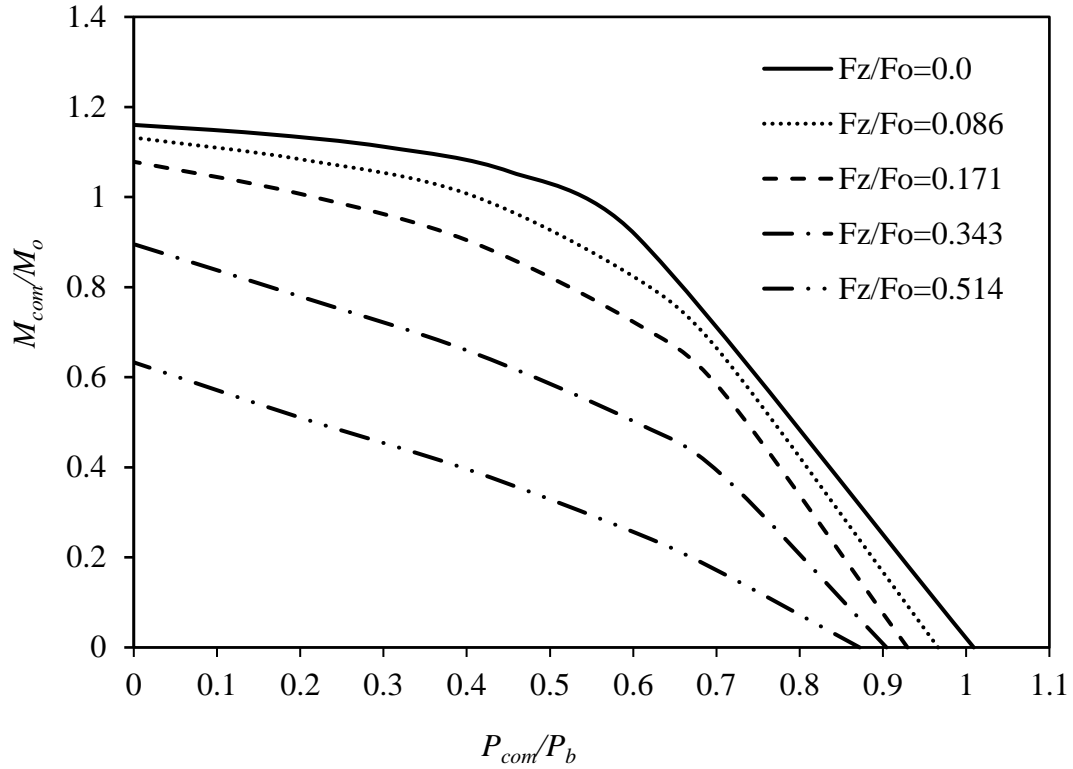


Figure 7.15: Failure Locus for d/t for 0.8

This research presents a detailed study on the effects of axial forces and bending moments on the burst pressure of corroded pipelines. The findings from this study are summarized below:

- The burst pressure of corroded pipelines is reduced due to the axial forces and bending moments acting on the pipelines.
- The axial compressive force and closing bending moment are found to reduce the burst pressure more significantly than the tensile axial force and opening bending moment. Therefore, the compressive axial force and closing bending

moment are considered to develop failure loci of corroded pipelines subjected to axial forces and bending moments.

- The DNV-RP-F101 (2015) design code recommends considering axial compressive stress for the assessment of burst pressure of corroded pipelines. However, the recommended method provides unconservative burst pressure when the ratio of the resultant axial compressive stress to the material ultimate strength is smaller than 0.25. The method is assumed to be applicable for the ratio of hoop stress to longitudinal stress of 2.
- The failure locus for corroded pipelines subjected to combined loadings significantly depends on corrosion depths and load combinations. The corrosion length and pipe dimensions have insignificant effects. Therefore, the failure loci are developed for different corrosion depths and load combinations.
- The developed failure loci can be used for assessing the burst pressure of corroded pipelines with known axial force and bending moment.

CHAPTER 8

Burst Pressure Assessment of Corroded Pipelines using Fracture

Mechanics Criterion

8.1 Introduction

The pipelines with corrosion defects are generally analyzed using the theory of continuum mechanics. In the continuum modelling approach, the von Mises equivalent stress is calculated and then compared with a limiting value. The most commonly used approach is to calculate the average von Mises equivalent stress throughout the thickness (ligament) of the pipeline and compare it with the ultimate strength of the pipe material (Li et al. 2016). The von Mises stress at the outer surface of the ligament reaches the ultimate strength first, particularly for a large depth of corrosion, which then extends to the inner surface (Liu et al. 2009, Mondal and Dhar 2018). When the von Mises stress on the outer surface reaches to the ultimate tensile strength, the stress is assumed to remain constant at this point while the stress increases at every other point in the pipe wall with the increase of internal pressure. However, when the von Mises stress at any point exceeds the ultimate strength, a crack might initiate at that point where the stress can be reduced to zero. The crack initiation and its propagation are not considered in continuum modelling. Thus, the continuum modelling approach may over-predict the pipe strength. The crack initiation and crack propagation during loading can be better modelled using fracture mechanics approach.

In fracture mechanics approach, the strength of a material against cracking is expressed using the fracture toughness of the material. The fracture toughness is defined in terms of four parameters, the stress intensity factor (K), strain energy release rate (G), J -integral (J) and crack tip opening displacement (δ) (Zhu and Joyce 2012). The critical values of these parameters corresponding to crack initiation are known as the fracture toughness (i.e., K_c , G_c , J_c and δ_c , respectively).

The stress intensity factor, K , is a measure of the stress field near a crack tip, which combines far field stress and crack dimensions. For an infinite plate with a crack length of ' $2a$ ' subjected to a far field stress of ' σ ', the stress intensity factor is defined as in Equation 8.1 (Irwin and de Wit 1983). The stress intensity factor, K , depends on crack geometries and loading conditions. The fracture toughness, K_c , is the critical value of K at which a crack initiates.

$$K_I = \sigma\sqrt{\pi a} \quad (8.1)$$

The strain energy release rate, G , is a measure of energy available for an increment of a crack. It is defined as in Equation 8.2, where π indicates the potential energy under the applied loading (Gdoutos 2005).

$$G = -\frac{\partial \pi}{\partial a} \quad (8.2)$$

The J -integral is a way of calculating the strain energy release rate and is equivalent to G for linear elastic material. The parameter is also applicable for non-linear elastic material. It is measured as the potential energy per unit fracture surface area over a region

bounded by an arbitrary surface extending from one face of the crack to the other face (as shown in Figure 8.1). The J -integral is given in Equation 8.3, where Γ is an arbitrary curve around the tip of a crack (Figure 8.1), w is the strain energy density, T_i is the components of the traction vector, u_i is the displacement vector components, ds is the length increment along the contour, and x and y are the rectangular coordinates with the y direction taken normal to the crack line and the origin at the crack tip (Zhu and Joyce 2012).

$$J = \oint_{\Gamma} \left(w dy - T_i \frac{\partial u_i}{\partial x} ds \right) \quad (8.3)$$

The crack tip opening displacement, δ , is the gap between the crack-surfaces measured at a distance equal to the radius of the plastic zone, r_y , behind the crack tip (Irwin and de Wit 1983). Due to the plastic property of the material, the crack tip deforms and makes a blunt notch before extending the crack further. Then, the crack tip opening displacement is determined by the distance between the intercepts of two 45° lines, drawn back from the crack tip to the deformed crack profile, as shown in Figure 8.2 (Zhang et al. 2015).

The stress intensity based fracture toughness, K_c , is generally used for brittle materials that follow linear elastic fracture mechanics principles. The non-linear fracture mechanics with the J -integral is used for ductile materials where the critical point of the structure undergoes significant yielding before the stress intensity factor reaches K_c . For nonlinear elasto-plastic material, the total J -integral comprises two components: an elastic

component, J_{el} , and a plastic component, J_{pl} , corresponding to elastic deformation and plastic deformation, respectively.

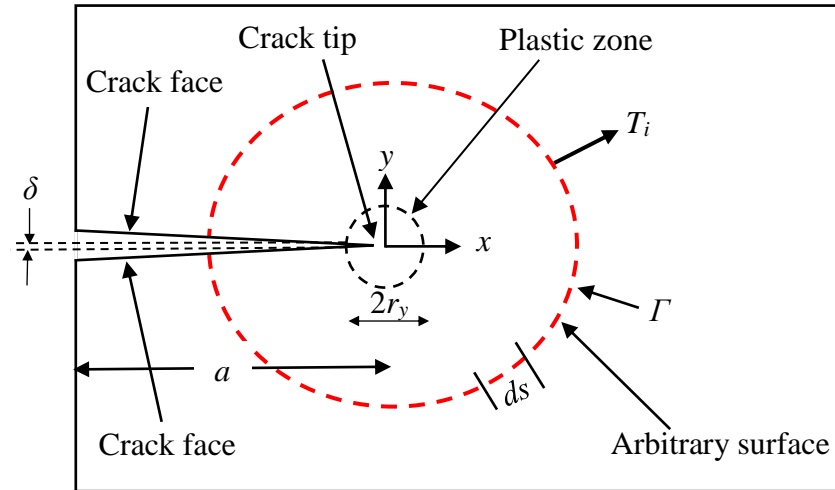


Figure 8.1: Arbitrary contour for the definition of J -integral

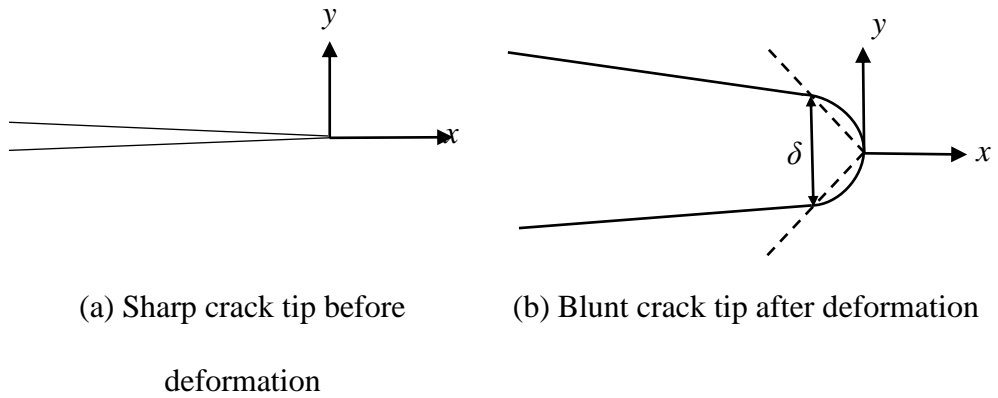


Figure 8.2: Measurement of crack tip opening displacement, δ

However, the existing design practices for crack assessment in pipelines are based on the stress intensity factor, likely due to the simplicity of the design (e.g., Yan et al. 2014, BS 7910 2013). The stress intensity factor, K , relates to the elastic component, J_{el} , using Equation 8.4, where $E' = E$ for the plane stress condition and $E' = E/(1-\nu^2)$ for the plane strain condition (Zhu and Joyce 2012).

$$J_{el} = \frac{K^2}{E'} \quad (8.4)$$

Using the failure assessment curve (*FAC*) in Milne et al. (1988), Yang et al. (2016) developed an analytical model for the elastic fracture toughness by quantifying the K_c of ductile pipeline material.

Determination of the stress intensity factor and /or the J -integral for pipelines containing corrosion defects is the major challenge in applying fracture mechanics for a failure assessment of the pipelines. In FE model (such as Abaqus), the J -integral for a crack is generally calculated using the contour integral method (Gdoutos 2005). For the analysis, a crack is defined at the element boundary where the J -integral is calculated. Thus, modelling of a crack using conventional FEM requires the conformance of the mesh to the geometry of the crack. However, for a corroded pipeline, the location of the crack and the direction of crack propagation are often unknown in advance during developing the FE model. In this study, Extended Finite Element Method (XFEM) using Abaqus is first performed to identify the location of crack initiation and the direction of crack propagation.

The XFEM in Abaqus employs maximum principal stress criteria to determine the initiation and propagation of a crack. The use of a local enrichment function in XFEM to the nodal degree of freedom avoids the mesh conformance of the crack geometry. The enrichment function consists of a near-tip asymptotic function that captures singularity around the crack tip and a discontinuous function that represents the jump in the displacements across the crack surface.

Through identification of the location of crack initiation from XFEM, the FE model is developed to calculate the J -integral at the location of the crack using the contour integral method to assess the burst pressure of the corroded pipeline. The pipelines containing corrosion defects and corrosion with a crack-like defects are considered in this study. For corrosion with a crack defect, a predefined location of a crack is considered. A parametric study is conducted to investigate the effects of corrosion geometries, crack geometries and pipe dimensions on the J -integral of the pipeline.

Bedairi et al. (2012) used the J -integral method for assessing the burst pressure of a crack-in-corrosion (CIC) defect of a pipeline. They reported a higher burst pressure using the J -integral method than the one obtained from the experiment or calculated using the ultimate tensile strength of the material. In calculating the burst pressure using the J -integral, Bedairi et al. (2012) estimated the fracture toughness of the material as 197 kJ/m^2 based on a specimen test, while the fracture toughness of the actual tested pipe material was unknown. In the current study, the fracture toughness of the pipe material is back-calculated from the burst test results for failure assessment of pipelines.

8.2 FE Model Development

8.2.1 Pipe Geometry

The Abaqus/Standard module is used in this study for calculating the fracture parameters for pipelines containing a corrosion defect (C) and a crack-in-corrosion (CIC) defect subjected to internal pressure. For the development of FE modelling with validation, analyses and test conditions reported in Bedairi et al. (2012) are first simulated. Bedairi et al. (2012) reported an analysis and the results of a full scale rupture test of a pipeline with an artificial crack-in-corrosion defect, where a flat bottom and a uniform depth crack were applied at the centre of the corrosion. Dimensions of the pipeline and defects used in Bedairi et al. (2012) are modelled as shown in Figure 8.3. The crack width is uniform throughout the depth (Figure 8.3 c) except at the bottom where an arc of a circle with a radius of 0.0022 mm is fitted, (after Bedairi et al. 2012). This type of crack is called herein ‘blunt tip’ crack. The corroded pipeline without the crack is also analyzed, as shown in Figure 8.4. In both cases, the corrosion is applied on the outer surface of the pipeline with smooth edges (Figure 8.3 and 8.4). Pipe dimensions and defect dimensions are summarized in Table 8.1.

To save computation time and to take the advantage of symmetry, only half of the full pipeline is modelled, as shown in Figure 8.5. The advantage of symmetry of the cross-section is not considered, to allow calculating the J -integral at unsymmetric crack locations. The symmetric boundary conditions are applied to one end (the left end in Figure

8.5) of the model. The bottom point at the left end is fully restrained to ensure stability of the model under the applied loading. The pipe domain is modelled using the eight-noded continuum element (Abaqus element “C3D8R”).

Internal pressure is applied at the inner surface of the pipeline during analysis. For simulation of the test results reported in Bedairi et al. (2012), the end cap effect is simulated by applying an equivalent axial load at the other end of the FE model (right end in Figure 8.5).

The equivalent axial load is calculated using the axial tensile stress, as given in Equation 8.5:

$$\sigma_t = P \frac{D_i^2}{D_o^2 - D_i^2} \quad (8.5)$$

where

P : internal pressure

D_o : outer diameter of pipe

D_i : inner diameter of pipe

During analysis, the internal pressure and the axial tensile stress are increased linearly until failure.

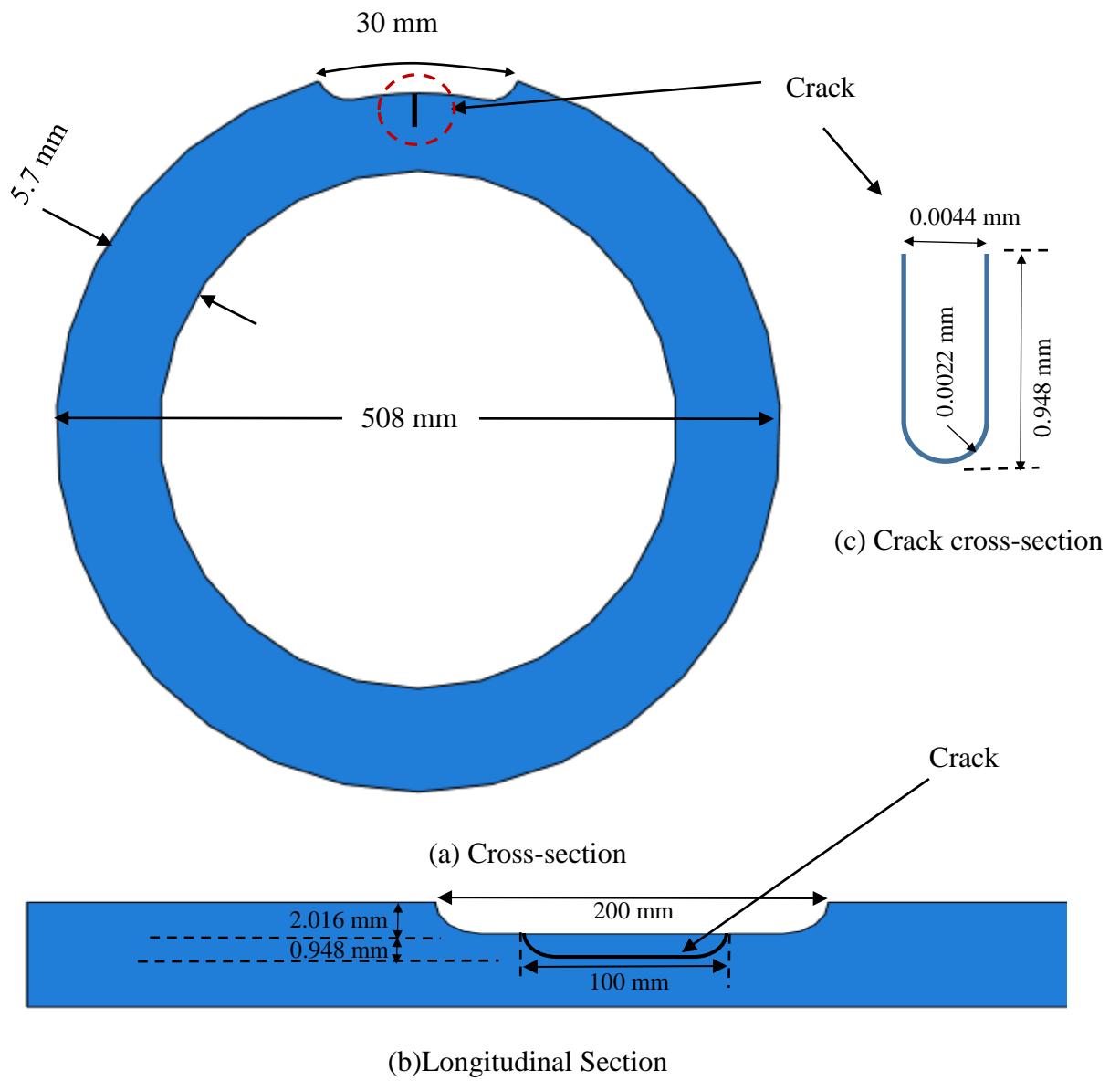


Figure 8.3: Sectional view of pipe with crack-in-corrosion (CIC) defect (Not to scale)

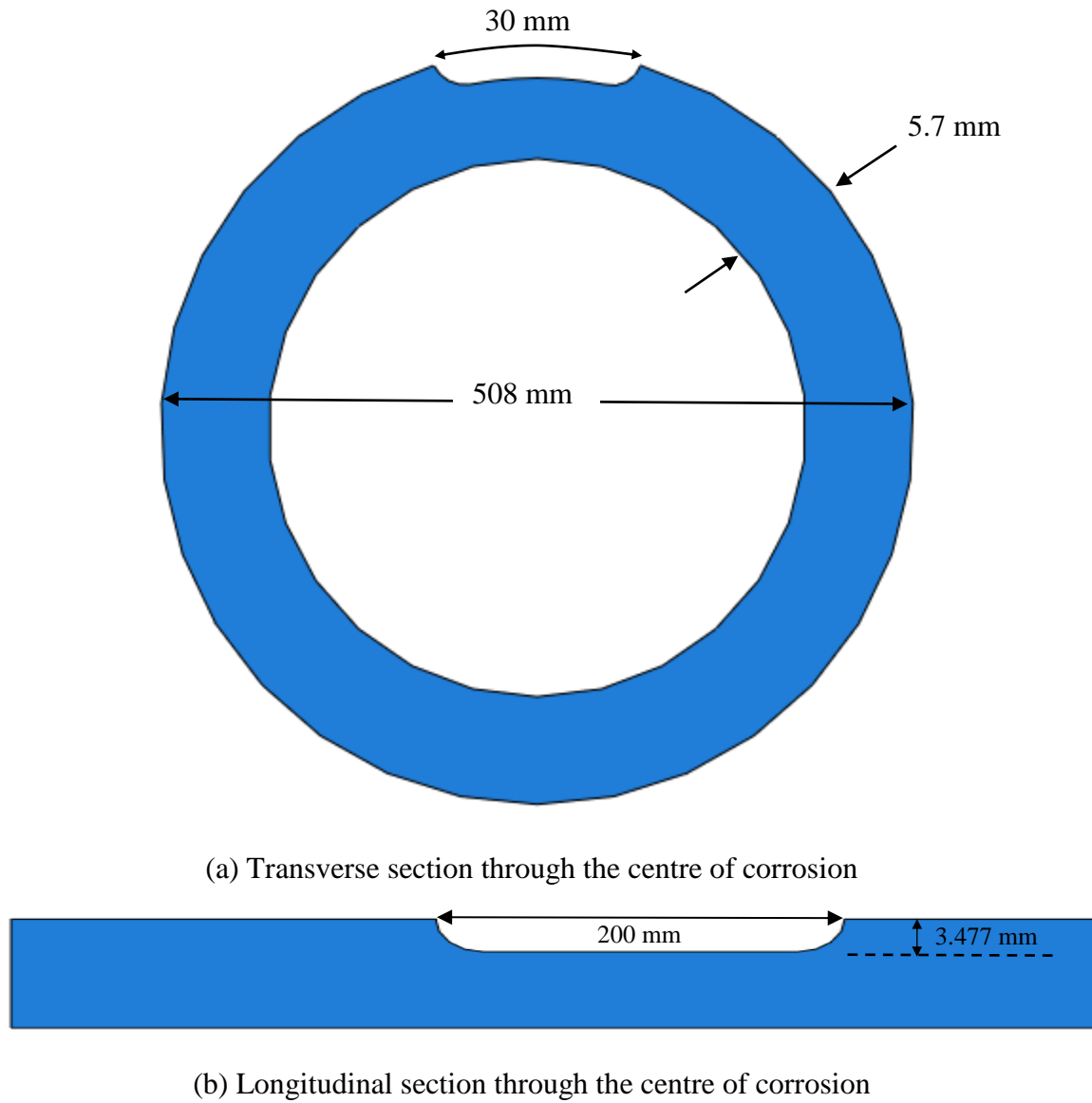


Figure 8.4: Sectional view of pipe with corrosion defect (Not to scale)

Table 8.1: Pipe dimensions and defect geometries

Geometries	Values
Pipe diameter, D (mm)	508
Wall thickness, t (mm)	5.7
Corrosion depth, d (mm)	2.016
Corrosion length, l (mm)	200
Corrosion width, w (mm)	30
Crack depth, d_c (mm)	0.948
Crack length, l_c (mm)	100
Crack shape	Smooth

Since stress concentration is expected near the defect zone, fine mesh is applied at and near the corroded zone. The coarse mesh is applied away from the corroded zone where uniform stress is expected. An appropriate gradient is used in the transition zone of coarse to fine mesh. A mesh sensitivity analysis is conducted for determining the optimum mesh size. Five or six layers of elements are applied over the thickness of the pipeline (i.e., the ligament). Figure 8.6 shows a typical finite-element mesh used in the analysis. The lengths (L) of the pipe models are selected in such a way that the applied boundary conditions do not affect the stress and strain at and near the corroded zone and thereby do not affect the failure pressure of the pipelines. The lengths are greater than the minimum length (L_{min}) recommended in Fekete and Varga (2012) (Equation 8.6).

$$L_{min} = \frac{l}{2} + \frac{d}{t} \sqrt{D \cdot t \cdot l} \quad (8.6)$$

where,

l : length of corrosion

d : depth of corrosion

t : thickness of pipe wall

D : diameter of pipe

8.2.2 Material Model

The true stress–strain behaviour of a pipe material from Bedairi et al. (2012) is incorporated in the FE analysis. The true stress–strain data are obtained using the Ramberg-Osgood equation (Equation 8.7) from the engineering stress–strain data of test specimens.

$$\varepsilon = \frac{\sigma}{E} + \beta \left(\frac{\sigma}{\sigma_y} \right)^{n-1} \left(\frac{\sigma}{E} \right) \quad (8.7)$$

Bedairi et al. (2012) employed $\beta = 1.75$ and $n = 9$. The true stress–strain curve obtained using Equation 8.7 is shown in Figure 8.7. The true stress–strain curve is inserted in the FE models using a linear connection method for the pieces. Other material parameters used in the analysis are presented in Table 8.2.

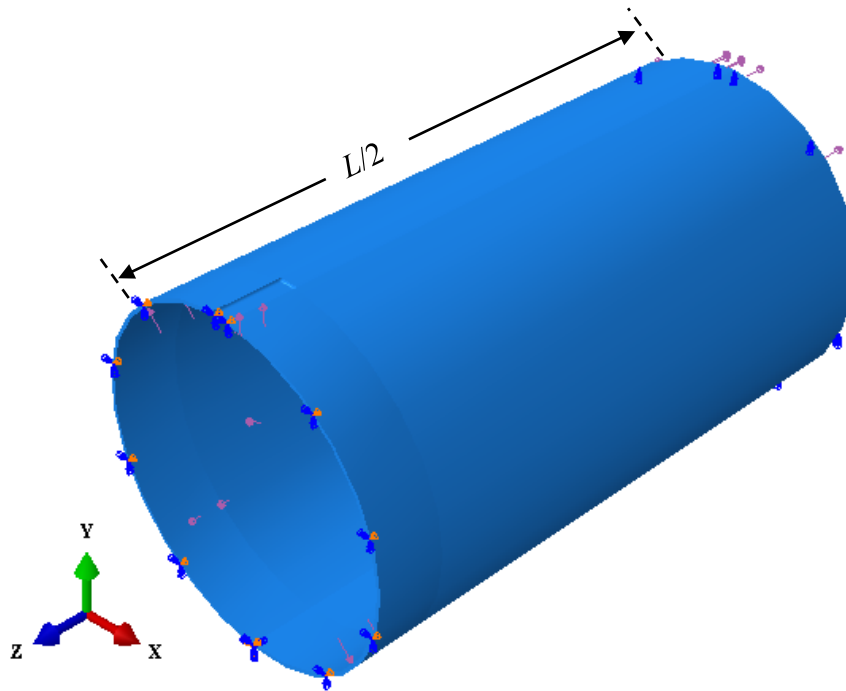


Figure 8.5: Half model of full pipeline with boundary conditions and loading

Table 8.2: Properties of Pipe Steel (Bedairi et al. 2012)

Property	Value
Density, ρ (kg/m ³)	7850
Modulus of Elasticity, E (GPa)	207
Poisson's Ratio, ν	0.30
Yield Strength, σ_Y (MPa)	435
Ultimate Tensile Strength, σ_U (Mpa)	631

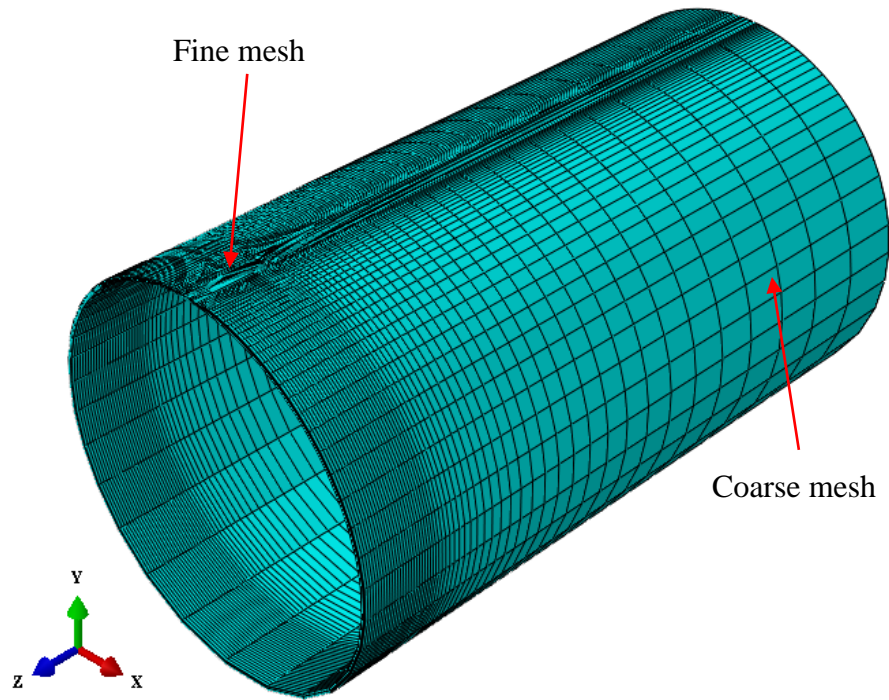


Figure 8.6: Typical meshing of FE model

8.3 J -integral based Burst Pressure Assessment

8.3.1 Crack-in-corrosion (CIC) defect

For validation of the FE model in calculating the J -integral, the J -integral calculated in Bedairi et al. (2012) is simulated and compared. Bedairi et al. (2012) conducted an FE analysis to calculate the J -integral of a pipeline containing a CIC defect tested to failure under internal pressure. The test result of the J -integral for a corroded pipeline subjected to internal pressure loading is not available in the literature.

In the current study, an FE model is developed using the dimensions of the pipeline and the CIC defect like those used by Bedairi et al. (2012). The material properties are also similar to those in Bedairi et al. (2012). The maximum J -integrals at the deepest point of the crack are calculated using the contour integral method, available in the Abaqus. The calculated J -integrals are compared with those from Bedairi et al. (2012) in Figure 8.8. The figure shows that the J -integral obtained from the current study matches closely with those from Bedairi et al. (2012).

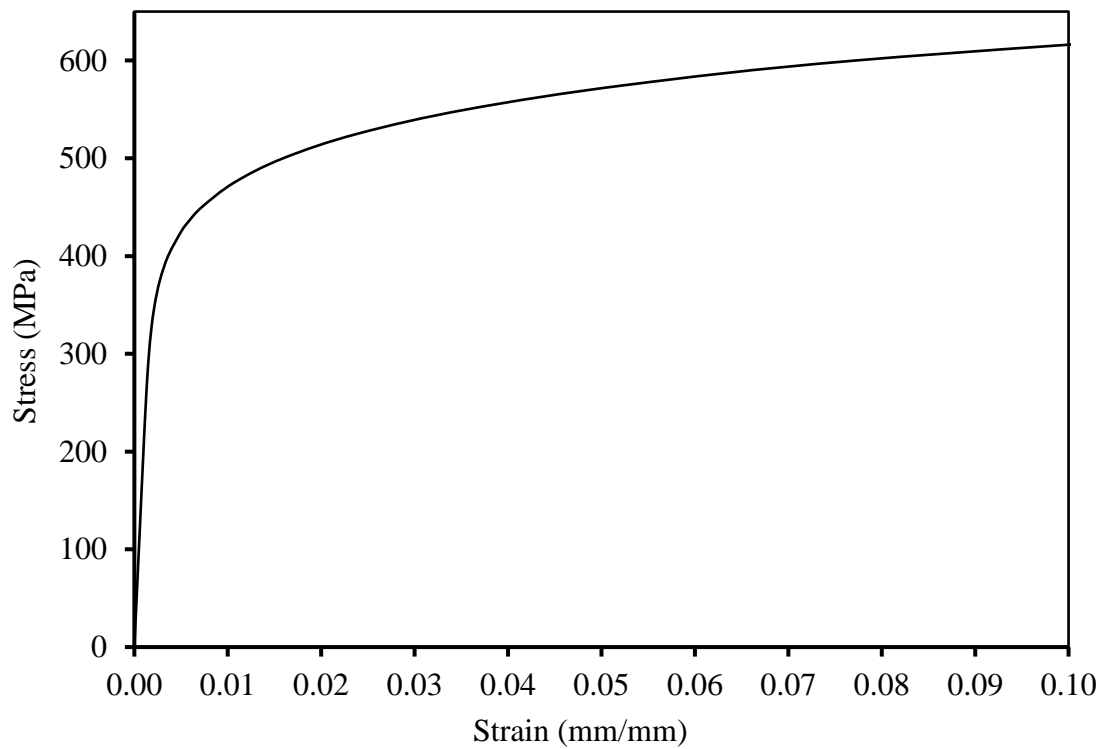


Figure 8.7: True stress–strain curve of pipe steel, after Bedairi et al. (2012)

Figure 8.8 demonstrates that the J -integral increases non-linearly with the increase of internal pressure of the pipeline, due to the use of a non-linear stress–strain relation. A crack starts to propagate if the J -integral is equal to or greater than the fracture toughness of the material, leading to failure. The pipeline with a CIC defect failed at an internal pressure of 7.74 MPa during the rupture test (Bedairi et al. 2012). The J -integral corresponding to the failure pressure is 87 kJ/m² (Figure 8.8). Thus, the critical J -integral at the failure of the pipeline appears to be 87 kJ/m². However, Bedairi et al. (2012) estimated the fracture toughness of 197 kJ/m² for the pipe material from a single edge bend test corresponding to a 0.2 mm crack extension. The 0.2 mm crack extension criterion thus provides a higher J -integral at the failure of the pipeline than the one back-calculated from the burst pressure. Nevertheless, the burst pressure for the pipeline with a CIC can be obtained as the internal pressure corresponding to the critical J -integral.

8.3.2 Corrosion only defect

As mentioned earlier, the J -integral, using the contour integral method, is calculated at the crack tip or crack line. The crack location (a point or a line) has to be assigned for determination of the J -integral. For a pipeline with a corrosion only defect, the crack location is not known. The XFEM is used to identify the crack location in the pipeline with the corrosion only defect. In XFEM, the material discontinuity due to cracking is modelled using a displacement jump function, $H(x)$, where the nodal displacement vector is defined using $H(x)$, as shown in Equation 8.8 (Belytschko and Black 1999).

$$\mathbf{u} = \sum_{I=1}^N N_I(x) \left[u_I + H(x) a_I + \sum_{\alpha=1}^4 F_{\alpha}(x) b_I^{\alpha} \right] \quad (8.8)$$

where $N_I(x)$ = nodal shape function

u_I = usual nodal displacement vector

a_I = nodal enriched degree of freedom vector

$H(x)$ = displacement jump function across the crack surface

$$= \begin{cases} 1 & \text{if } (x - x^*) \cdot n \geq 0 \\ -1 & \text{otherwise} \end{cases}$$

$F_{\alpha}(x)$ = elastic asymptotic crack-tip function

$$= \left[\sqrt{r} \sin \frac{\theta}{2}, \sqrt{r} \cos \frac{\theta}{2}, \sqrt{r} \sin \theta \sin \frac{\theta}{2}, \sqrt{r} \sin \theta \cos \frac{\theta}{2} \right]$$

b_I^{α} = nodal enriched degree of freedom vector

x = sample (Gauss) point

x^* = point on the crack closest to x

n = unit outward normal to the crack at x^*

r, θ = polar coordinate system with its origin at the crack tip

Analyses are performed for the same pipeline as discussed above, but with the corrosion only defect; the corrosion dimensions are shown in Figure 8.4. The XFEM uses the maximum principal stress criterion for the assessment of crack initiation and its propagation. The ultimate tensile strength of 631 MPa (Table 8.2) is used for the crack analysis using XFEM.

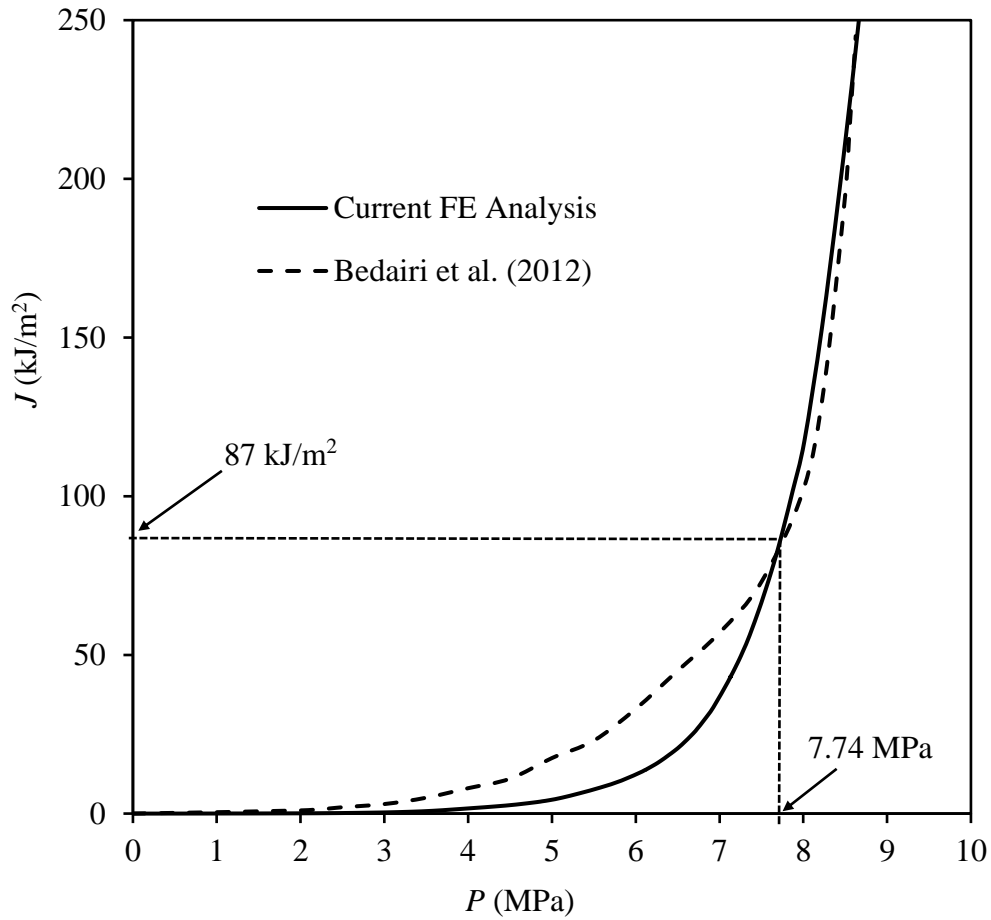


Figure 8.8: Comparison of J -integral obtained from the current study and those from Bedairi et al. (2012)

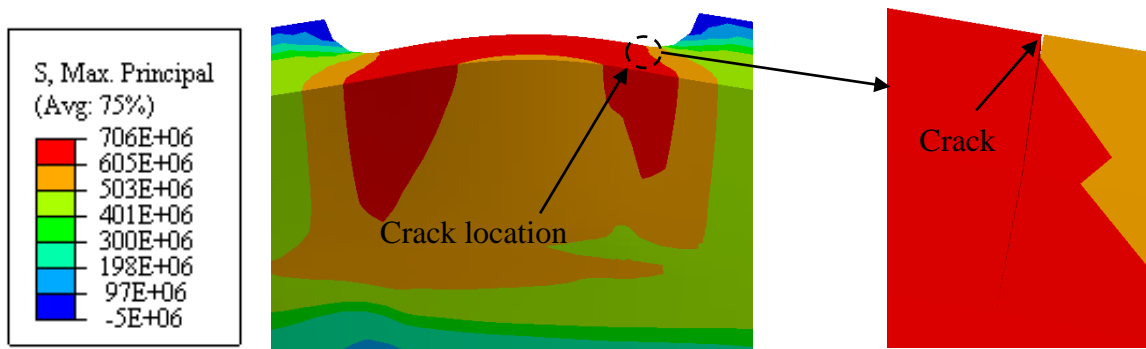
Figure 8.9 shows the crack growths obtained from the XFEM analysis for three different levels of internal pressures. The internal pressure of 6.53 MPa corresponds to the initiation of the crack, where the internal pressure of 6.64 MPa corresponds to the crack growth throughout the ligament. Figure 8.9 demonstrates that the crack is not located at the centre of the corrosion defect but close to the defect edge. Similar observations were reported from a burst test of a corroded pipeline (Benjamin et al. 2005) and FE analysis (Mondal and Dhar 2017b). A crack near the edge of the corrosion is therefore assigned for

calculation of the J -integral for a pipeline with a corrosion only defect using the contour integral method.

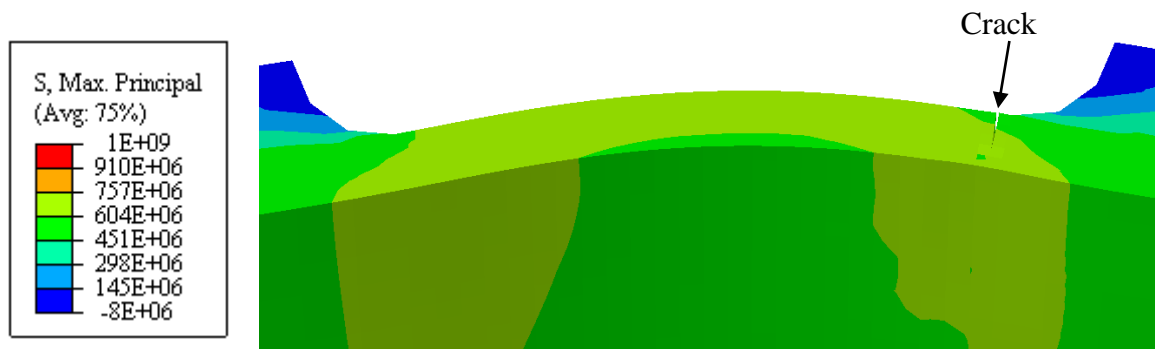
Figure 8.10 shows the J -integral values against internal pressure calculated using FE analysis. The internal pressure corresponding to the critical J -integral, J_c of 197 kJ/m² (Bedairi et al. 2012) is 9.33 MPa. The burst pressure for the pipeline from the test is reported to be 7.58 MPa (Bedairi et al. 2012), which is less than the internal pressure corresponding to $J_c=197$ kJ/m². Bedairi et al. (2012) stated that $J_c=197$ kJ/m² gives higher burst pressure for the pipeline, with respect to test results. The value of J -integral corresponding to the test burst pressure of 7.58 MPa of the pipeline is 51 kJ/m² (Figure 8.10). Thus, $J_c=51$ kJ/m² is assumed to provide better estimation of the critical J -integral for the burst pressure assessment. This criterion is used for the assessment of different burst test results of corroded pipelines available in Bedairi et al. (2012). Table 8.3 gives the dimensions of four pipelines along with the defects which were tested to failure under internal pressure (Bedairi et al. 2012). These pipe tests are simulated using FE analysis to calculate the J -integrals against internal pressure.

Table 8.3: Dimensions of pipe and corrosion geometries used (after Bedairi et al. 2012)

Geometries	Pipe C1	Pipe C2	Pipe C3	Pipe C4
Pipe Diameter, D (mm)	508	508	508	508
Wall thickness, t (mm)	5.7	5.7	5.7	5.7
Corrosion depth, d (mm)	1.254	2.565	3.762	3.990
Corrosion length, l (mm)	200	200	200	200
Corrosion width, w (mm)	30	30	30	30



(a) Internal Pressure, $P_i = 6.53\text{MPa}$



(b) Internal Pressure, $P_i = 6.60\text{MPa}$



(c) Internal Pressure, $P_i = 6.64\text{MPa}$

Figure 8.9: Crack growth in corrosion only defect from XFEM

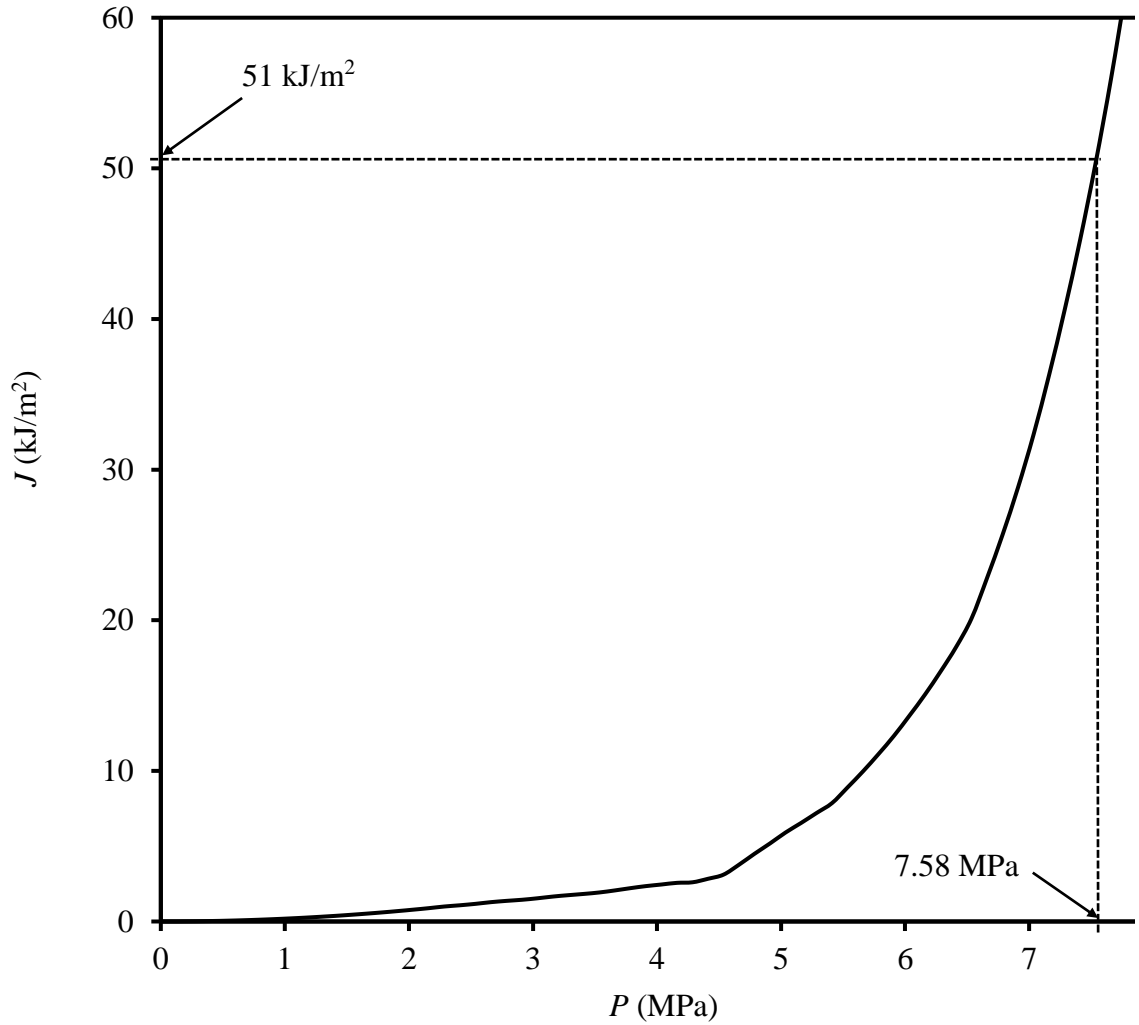


Figure 8.10: J -integral for pipe with corrosion only defect under internal pressure

For application of the contour integral method, the assigned locations are obtained from the XFEM, as discussed above. Figure 8.11 plots the J -integrals against internal pressures for each of the four pipelines. The internal pressures corresponding to $J_c=51$ kJ/m² are 13.40 MPa, 9.60 MPa, 6.96 MPa and 6.04 MPa for pipe C1, C2, C3 and C4, respectively. The burst pressures from the tests for these pipes are 12.80 MPa, 9.59 MPa, 6.63 MPa and 6.12 MPa, respectively (Bedairi et al. 2012). These deviations of the

calculated internal pressures corresponding to $J_c = 51 \text{ kJ/m}^2$ (i.e., burst pressure) are 4.69%, 1.04%, 4.98% and 1.31%, respectively, from the test burst pressures (Table 8.4). Thus, the fracture mechanics approach with $J_c = 51 \text{ kJ/m}^2$ provides a reasonable estimation of the burst pressures measured during the tests.

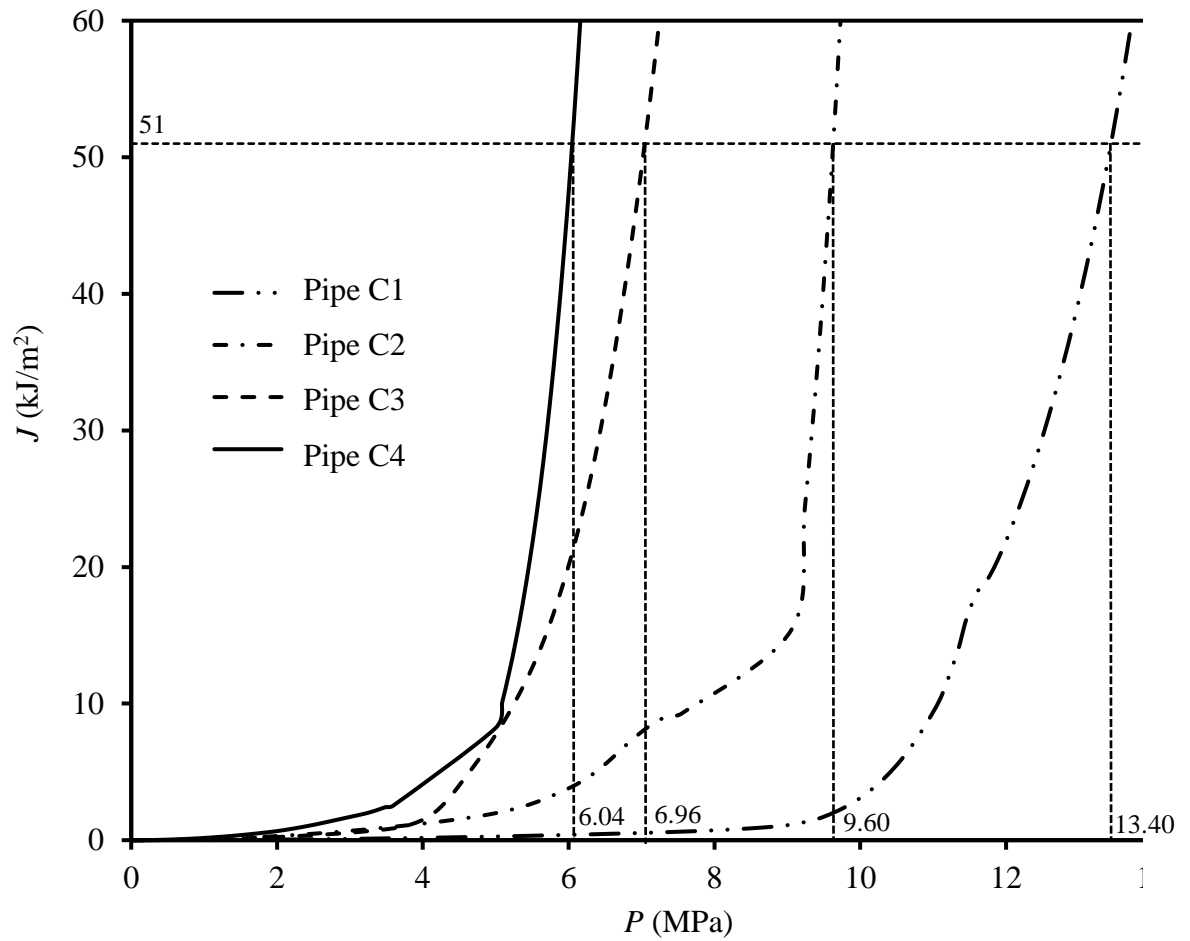


Figure 8.11: Burst pressure estimation based on $J=51 \text{ kJ/m}^2$ criterion

Table 8.4: Comparison of Burst Pressures

Model ID	P_{FEA} (MPa) (at $J=51$ kJ/m²)	P_{Test} (MPa) (Bedairi et al. 2012)	Deviation from test result (%)
Model C1	13.40	12.80	4.69
Model C2	9.60	9.59	1.04
Model C3	6.96	6.63	4.98
Model C4	6.04	6.12	1.31

8.3.3 Comparison with Existing Burst Pressure Models

The study presented above reveals that the fracture mechanics approach with the appropriate value of the fracture parameter (i.e., J -integral) could be used to assess the remaining strengths of corroded pipelines. However, the existing models for burst pressure were developed based on yield strength or ultimate strength of the pipe material. The existing models of burst pressure for corroded pipelines developed for corrosion only defects are compared here with the burst pressure determined using J -integral based fracture mechanics considering $J_c=51$ kJ/m². For the comparison, four pipelines, discussed above in Table 8.3, and four additional pipelines, described in Table 8.5, are considered. The burst pressures calculated using the modified ASME B31G (2012) and DNV-RP-F101 (2015) codes and the one proposed in Mondal and Dhar (2018) are compared with burst pressures predicted using the fracture mechanics approach. Figure 8.12 shows the comparisons of burst pressures where the burst pressure predicted using design equations and those from the tests discussed above are plotted against the burst pressure from FE

analysis with the fracture criterion. The solid line (i.e., 1:1 Line) in Figure 8.12 corresponds to the equality line. Figure 8.12 shows that burst pressures from the tests lie almost on the equality line, indicating that the fracture mechanics based predictions of burst pressure are most accurate with respect to the experimental results. The burst pressures predicted using the DNV-RP-F101 model are higher than the experimental burst pressures and lie above the equality line. The DNV-RP-F101 method thus provides unconservative estimation of the burst pressure. The burst pressures calculated using the modified ASME B31G method are less than the experimental burst pressure and those from FE calculations, implying that the calculated burst pressures are conservative. The burst pressures predicted using the model proposed in Mondal and Dhar (2018) are less conservative, as shown in Figure 8.12. Figure 8.12 reveals that among different models the burst pressures calculated using FE analysis considering the J -integral provide the best match with the test results. While the fracture mechanics approach provides a better prediction of burst pressure, some of the existing models can be used for conservatively predicting the burst pressure of pipelines with corrosion only defects. However, care should be taken in assessing pipelines with crack-like defects using existing models; when the crack propagation can be better modelled using fracture mechanics.

8.3.4 Pipeline containing Crack-Like Defect

Note that the existing models for burst pressure prediction of a corroded pipeline employ the length and depth of corrosion in the calculation. Width of the corrosion is not used, since conventional FE analysis performed in developing the models showed no effects of defect width (Chiodo and Ruggieri 2009). However, the models may not be

applicable for crack-like defects, as the J -integrals for a crack-like defect and a corrosion defect are expected to be different. The J -integrals for a pipeline with a corrosion defect, presented in section 8.2, are calculated here considering a crack-like defect to examine the effect of the defect type on the fracture parameter (i.e., J -integral). The depth and length of the crack are the same as the depth and length of the corrosion for the pipeline (Figure 8.4), i.e., 3.477 mm and 200 mm, respectively. The crack-like defect is modeled using a sharp V-notch to avoid the complexity of modelling a uniform crack with a bottom arc, discussed earlier (Figure 8.3). The opening of the notch at the pipe surface is 0.01 mm.

Table 8.5: Dimensions of pipe and corrosion geometries

Geometries	Pipe C5	Pipe C6	Pipe C7	Pipe C8
Pipe Diameter, D (mm)	508	508	508	508
Wall thickness, t (mm)	5.7	5.7	5.7	5.7
Corrosion depth, d (mm)	2.565	3.477	3.762	3.990
Corrosion length, l (mm)	100	100	100	100
Corrosion width, w (mm)	30	30	30	30

Figure 8.14 shows a comparison of the maximum J -integrals for a corrosion defect and crack-like defect for different internal pressures. It is observed that the J -integral is significantly higher for the pipe with a crack-like defect. Thus, although both defects have same defect depth and defect length, the pipeline with the crack-like defect is weaker than the pipeline with a corrosion defect under internal pressure. The internal pressures corresponding to 51 kJ/m² for (i.e., burst pressure) the corroded pipeline and the cracked

pipeline are 7.55 MPa and 4.58 Mpa, respectively. The burst pressure calculated using the existing design equation available in the DNV-RP-F101 (2015) is 7.98 MPa. Thus, the existing design equation overestimates the burst pressure. Use of the J -integral is therefore recommended for the remaining strength assessment of a pipeline with crack-like defects. However, calculation of the J -integral remains the major challenge in applying the method for the assessment of pipelines. The following section presents a parametric study for calculation of the J -integral for different crack-like defects.

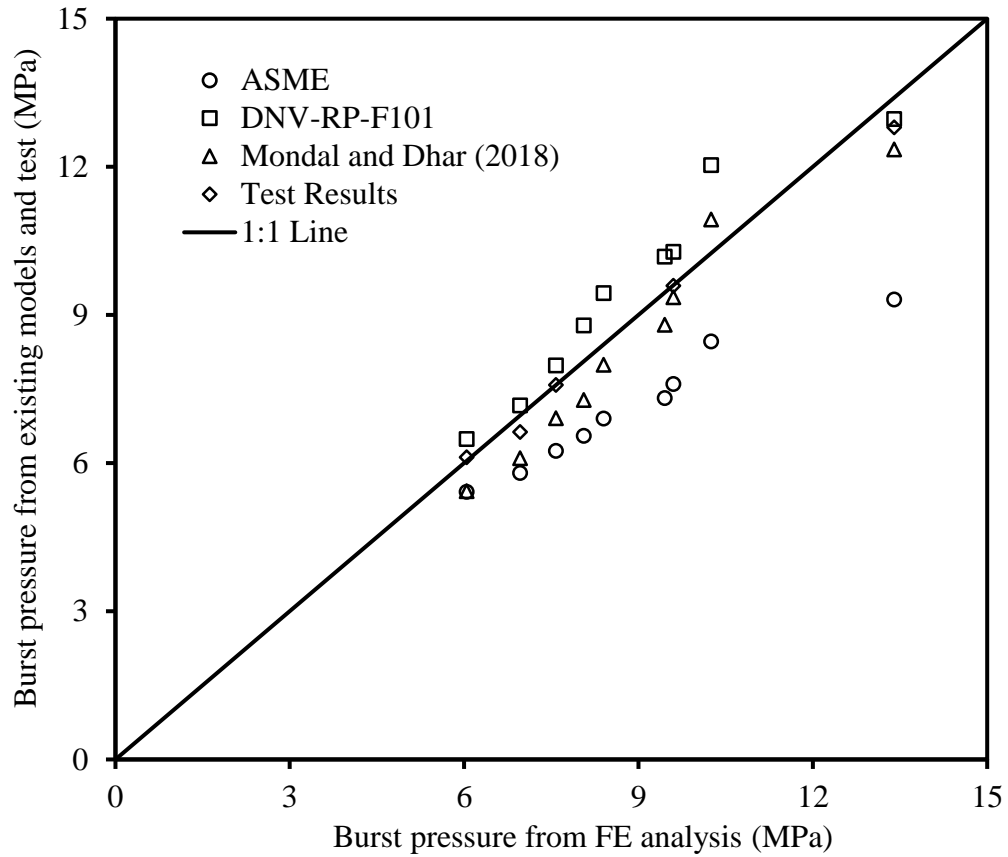


Figure 8.12: Comparison of Burst Pressures

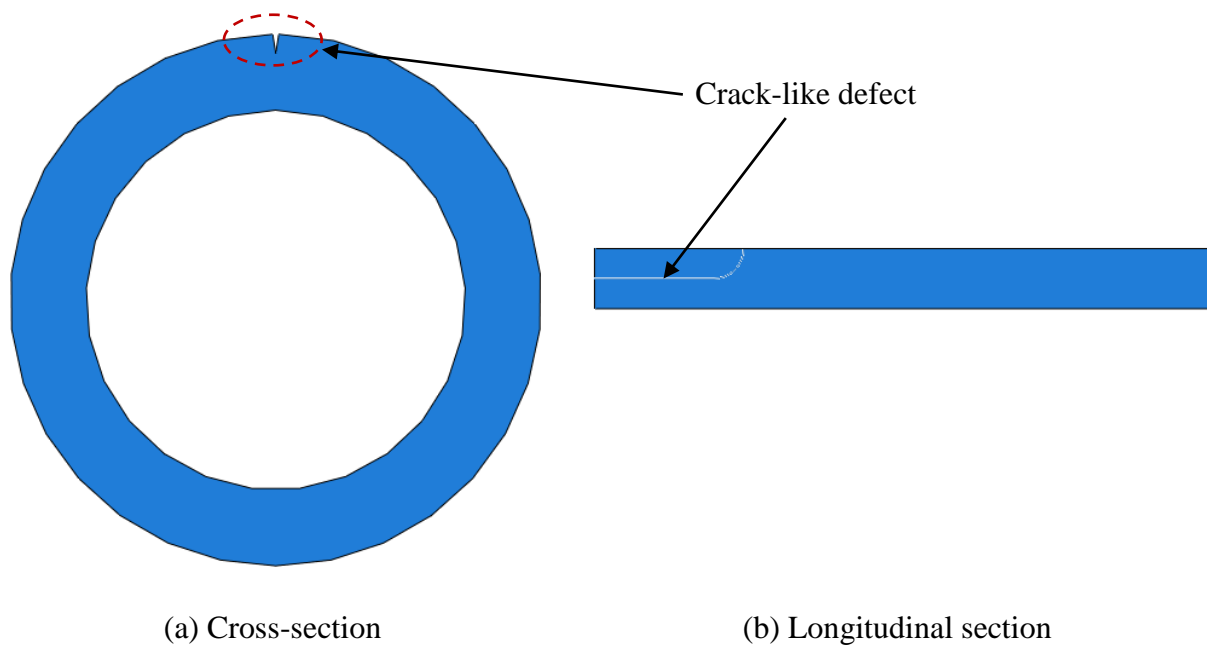


Figure 8.13: Schematic diagram of crack-like defect

8.4 Parametric Study on CIC pipe

As discussed in section 8.3.2, the FE modelling using the J -integral can successfully simulate the experimental burst pressure for a pipe with a CIC defect. The FE analysis is extended here to conduct a parametric study with various crack dimensions. However, a V-notch shaped crack is considered for simplicity in modelling the crack (Figure 8.15). The effect of considering a V-notch shaped crack is first examined through simulation of a CIC pipe, discussed in section 8.2.2.

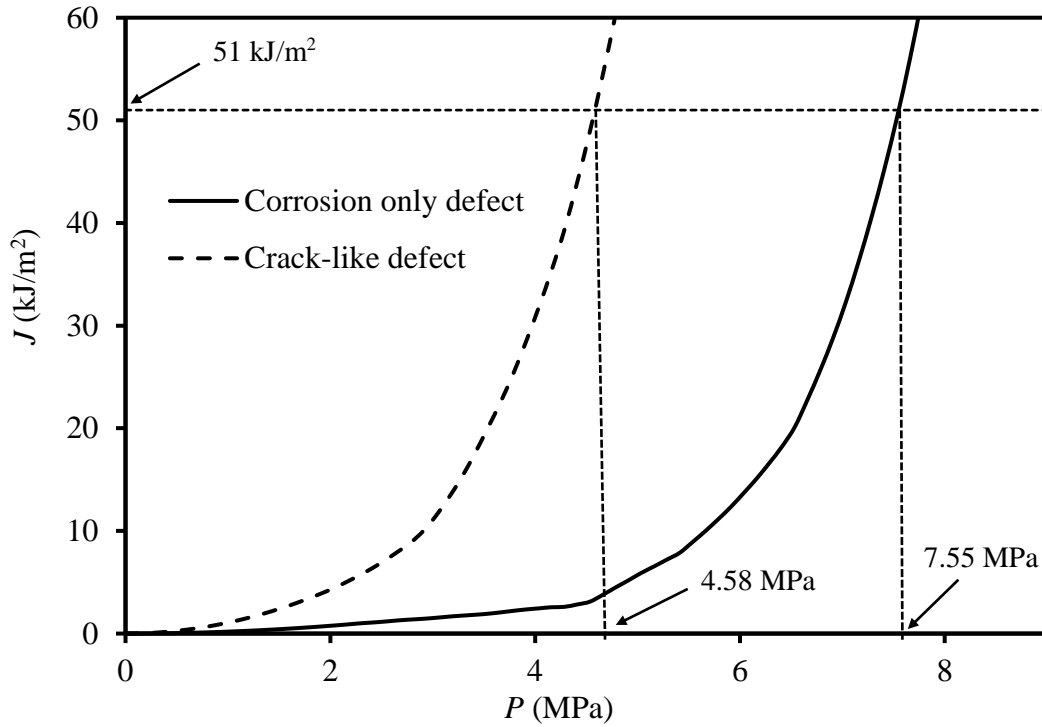
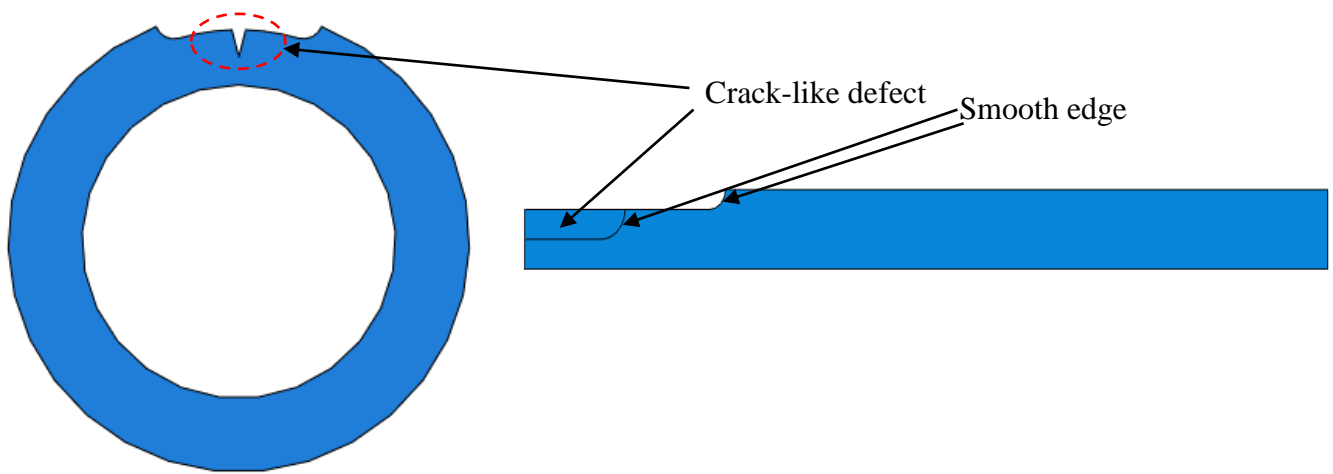


Figure 8.14: Comparison of J -integral for corrosion defect and crack-like defect

Figure 8.16 compares the J -integrals obtained from the V-notch shaped crack and blunt tip crack with the same crack depth and crack width. As seen in Figure 8.16, the J -integrals for the two shapes of cracks are not significantly different at a low stress level (i.e., lower internal pressure). However, at high stress levels, the integral for a blunt tip crack is much higher. The estimated burst pressures based on $J_c=51 \text{ kJ/m}^2$ are 7.28 MPa and 7.94 MPa, for the blunt tip crack and V-notch crack, respectively. Thus, the burst pressure for the blunt tip crack is around 9% less than the burst pressure for the V-notch crack.



(a) Transverse section

(b) Longitudinal section

Figure 8.15: Cross-section of pipe with CIC defect

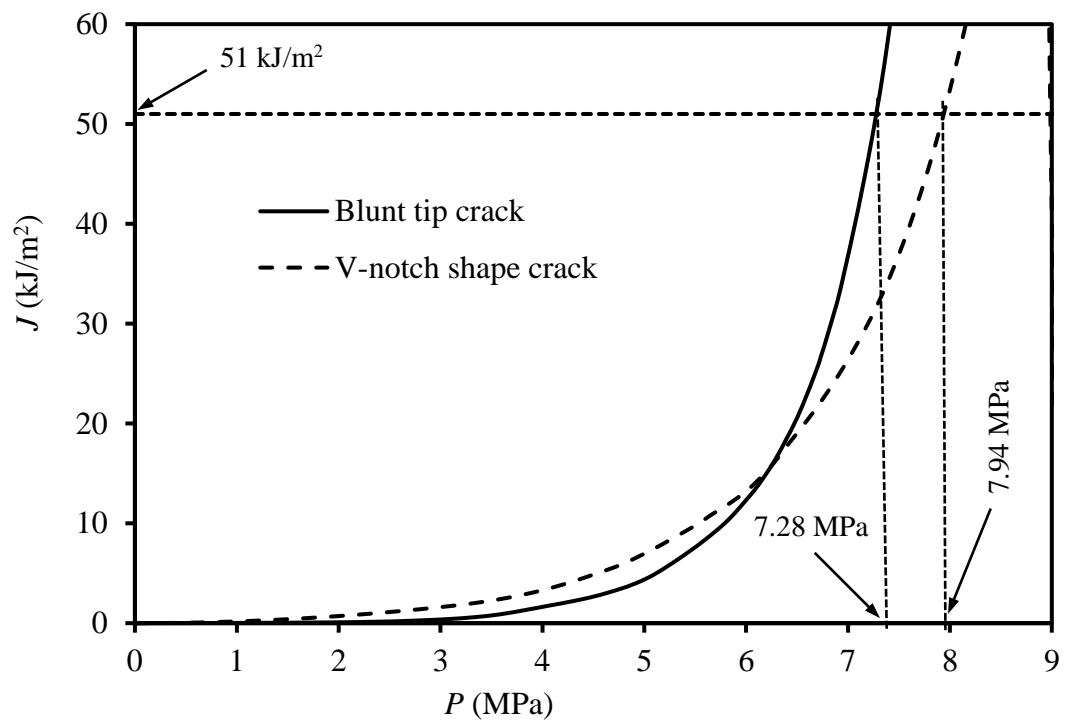


Figure 8.16: Comparison of blunt crack and V-notch crack in CIC defect

The effect of a smooth edge (Figure 8.15) and a sharp edge (Figure 8.17) of the crack on the J -integral is also investigated. The modelling of a smooth edged crack is complicated and requires a longer time to complete the analysis. However, as shown in Figure 8.18, J -integrals calculated using a smooth edged crack and sharp edged crack are very close to each other. The calculated burst pressures based on $J_c=51 \text{ kJ/m}^2$ for two edge shapes of the crack (7.94 MPa and 8.16 MPa, respectively) are within around 2.5% for this case. Thus, to account for the simplicity in modeling and less analysis time, the cracks with sharp edges are used in the parametric study.

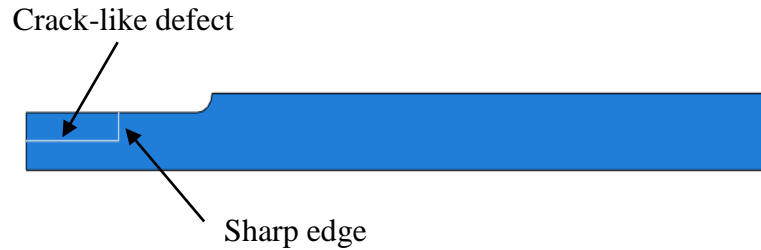


Figure 8.17: Crack-like defect with sharp edge

8.4.1 Effect of Crack Depth

To investigate the effect of crack depth (d_c) on the burst pressure of a pipeline containing a CIC defect, FE models are developed with different crack depths ranging from 0.50 mm to 2.00 mm. The length of crack (l_c), depth of corrosion (d) and length of corrosion (l) are kept constant with a magnitude of 100 mm, 2.0155 mm and 200 mm, respectively. Figure 8.19 shows the variation of J -integrals with internal pressure for different crack

depths. The figure indicates that the J -integral increases with the increase of crack depth. The increase of the J -integral with the increase of internal pressure is non-linear. Due to the increase of the J -integral, a pipeline with a deeper crack reaches the critical value ($J_c=51$ kJ/m²) at a lower internal pressure. Thus, the burst pressure for the pipeline with a deeper crack is less.

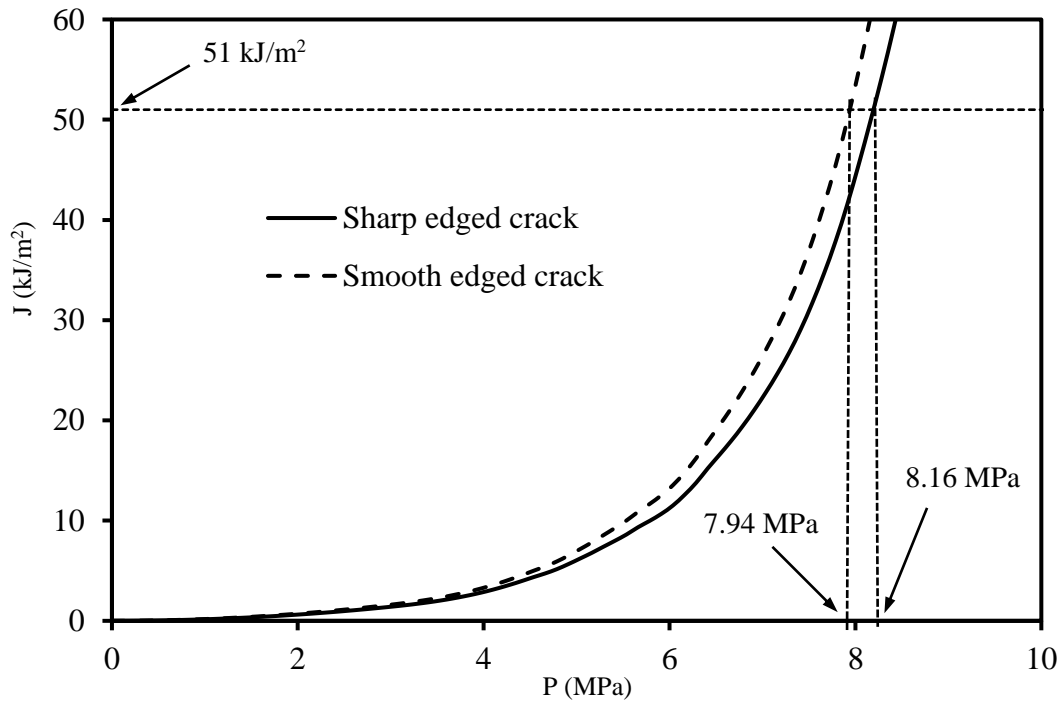


Figure 8.18: J -integral of CIC defect with sharp crack edge and smooth crack edge

To demonstrate the increase of the J -integral with crack depth, the parameter corresponding to two particular internal pressures is examined. In Figure 8.20, the J -integrals at burst pressure, normalized by the corresponding burst pressure of the pipeline (i.e., internal pressure corresponding to $J_c=51$ kJ/m²), are plotted against crack depths. The J -integral corresponding to the initiation of yielding in the pipe wall, normalized using

corresponding internal pressure is also plotted in the figure. The internal pressures developed on the pipe wall are calculated using FE analysis.

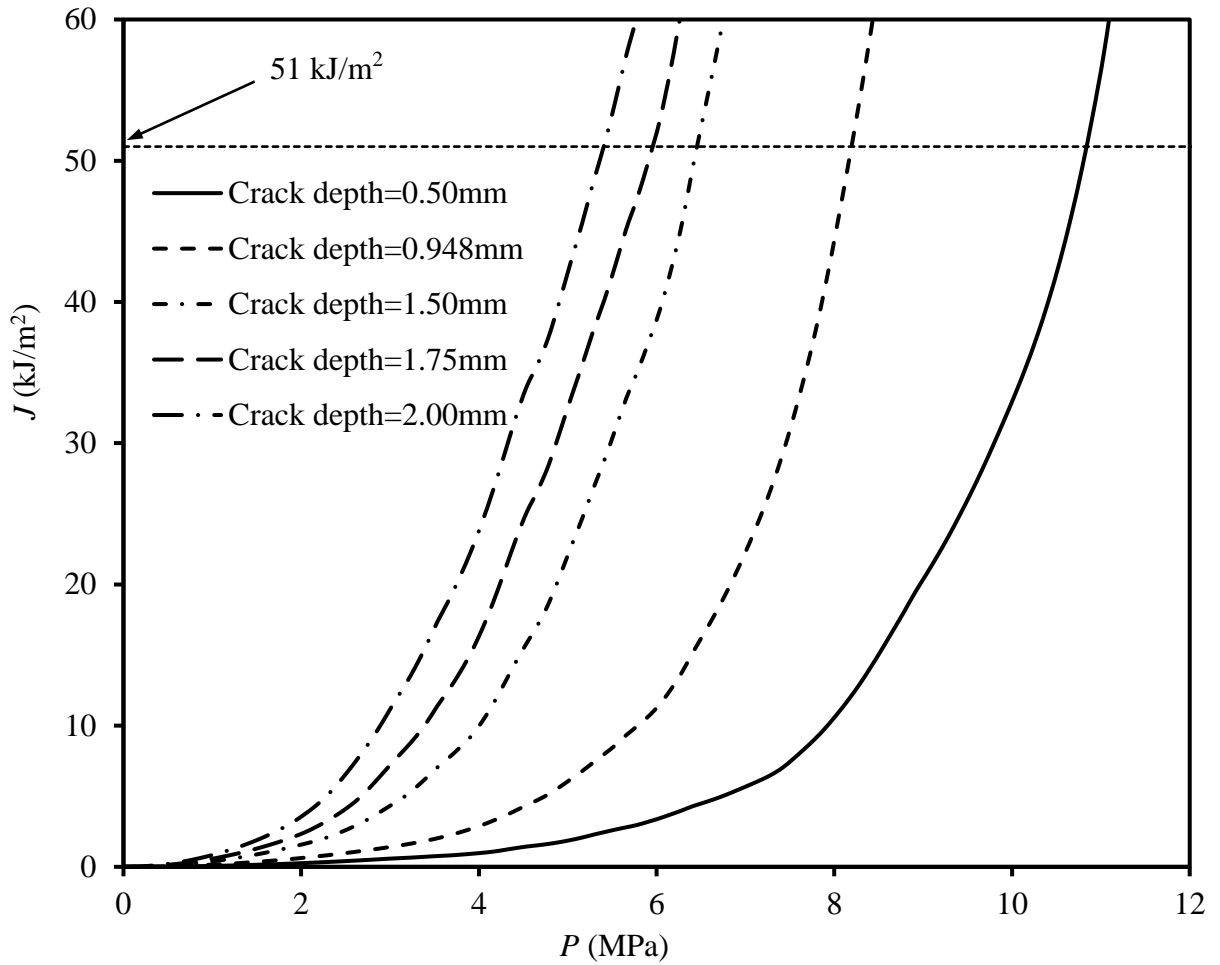


Figure 8.19: J -integral for pipe with CIC defect of different crack depths

Figure 8.20 shows that the ratio of J/P increases almost linearly with the increase of crack depth. The increase of the normalized J -integral is higher at the burst pressure than the increase of the parameter J at the yielding of the pipe.

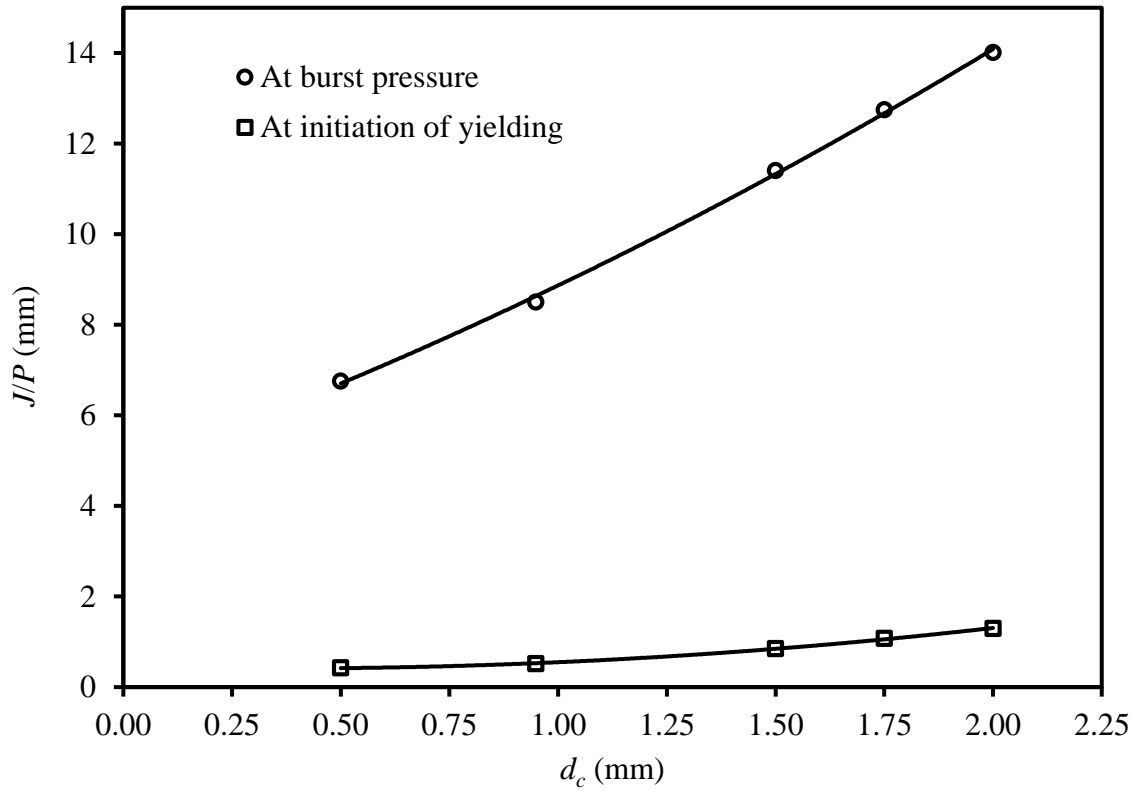


Figure 8.20: Variation of J -integrals with crack depths of pipe with CIC defect

In order to examine the effects of crack depths on the burst pressures, the burst pressures of the pipelines, described above, are predicted considering both the fracture criterion (i.e., $J_c=51 \text{ kJ/m}^2$) and von Mises criterion (i.e., average von Mises stress=631 MPa). The normalized burst pressures are plotted against normalized crack depths in Figure 8.21. The burst pressures (P) are normalized using the burst pressure of the pipeline with a corrosion only defect (P_b). The burst pressures of pipelines with a corrosion only defect are calculated using the equation proposed in Mondal and Dhar (2018) (Equation 8.9). The crack depths are normalized by the wall thickness of the pipe. Figure 8.21 shows that the burst pressure decreases nonlinearly with the increase of crack depth for both approaches.

The burst pressures calculated using the von Mises criterion are higher than the burst pressures calculated using the fracture criterion. The differences are greater for higher crack depths. Thus, the errors in burst pressure calculations using the von Mises criterion are higher for pipes with deeper cracks.

$$P_b = \frac{2t}{(D - 2t)} \sigma_u \left(\frac{1 - \frac{d}{t}}{1 - \frac{d}{tM}} \right) \quad (8.9)$$

where

$$M = \sqrt{1 + 0.278 \cdot \left(\frac{l^2}{Dt} \right)^{0.447} \times \left(\frac{d}{t} \right)^{-0.718} + 0.337 \cdot \left(\frac{l^4}{D^2 t^2} \right)^{0.717} \times \left(\frac{d^2}{t^2} \right)^{0.504}}$$

σ_u = Ultimate tensile strength of pipe material

8.4.2 Effect of Crack Length

Similar to the investigation of the effects of crack depths, to investigate the effect of crack lengths on the burst pressure of a pipeline containing a CIC defect, four FE models are developed with different crack lengths ranging from 50 mm to 190 mm. The depth of the crack, depth of corrosion and length of corrosion are assumed to be 0.948 mm, 2.016 mm and 200 mm, respectively.

Figure 8.22 shows the variation of J -integrals with internal pressure for different crack lengths. The figure indicates that the calculated J -integral is higher for a longer crack. However, the effect of crack lengths on the J -integral is not significant, particularly for a crack length greater than 150 mm for the considered corrosion dimensions and crack depth.

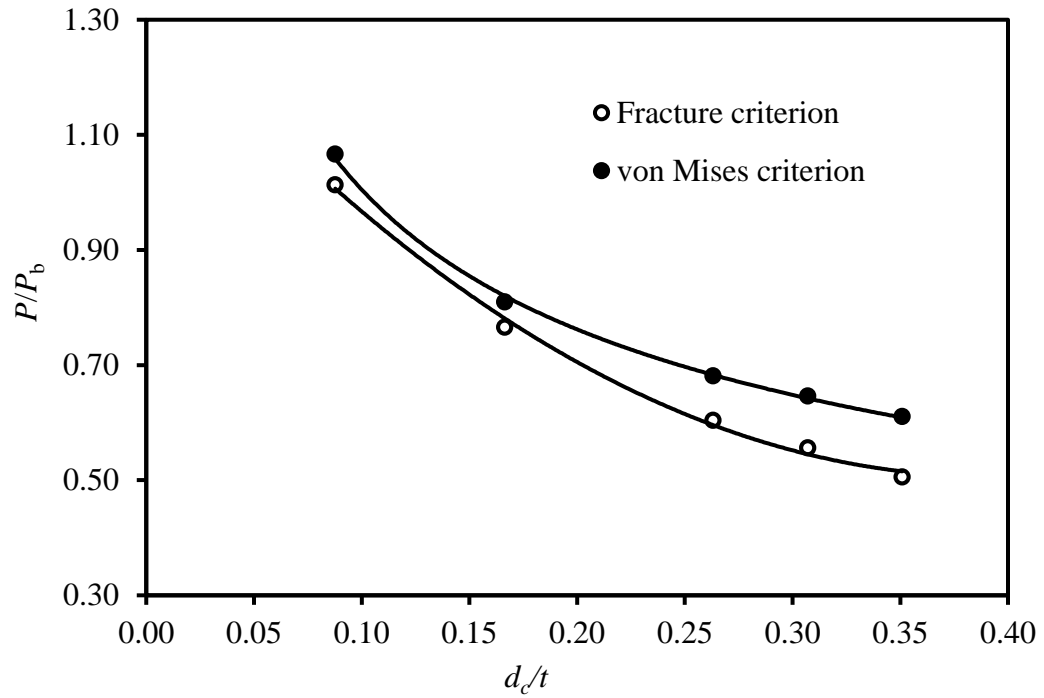


Figure 8.21: Effect of crack depth on burst pressure of pipe with CIC defects

Figure 8.23 plots non-dimensional burst pressure of the pipeline with a CIC defect against the crack depth to crack length ratio (i.e., d_c / l_c). The burst pressure of the pipeline with a CIC defect is normalized by the burst pressure of the pipeline with a corrosion only defect (Equation 8.9). The burst pressures calculated using the fracture criterion as well as von Mises criterion are compared in the figure. It reveals that the burst pressure decreases with the increase of d_c / l_c ratio. As before, the von Mises criterion provides higher burst pressure compared to the fracture criterion.

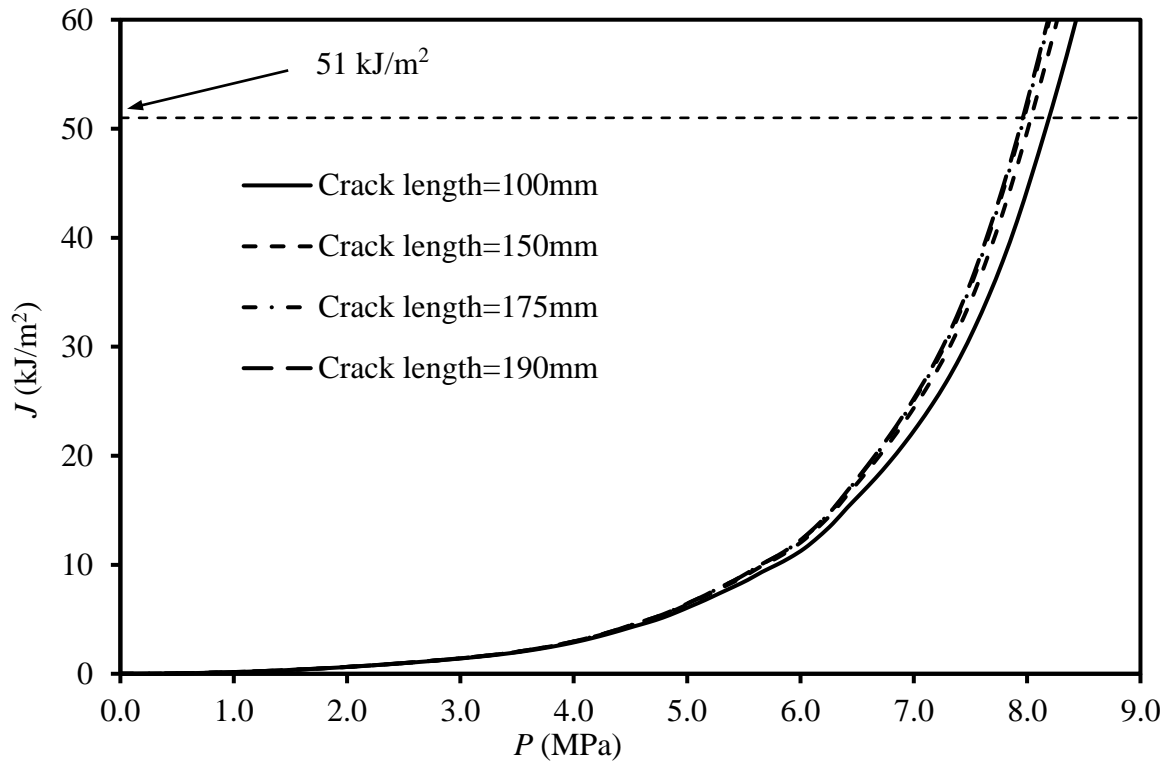


Figure 8.22: J -integral of pipe with CIC defect with different crack lengths

8.9 Summary

In the conventional method of FE analysis for the remaining strength assessment of a corroded pipeline, the von Mises failure criterion is used. This continuum based modelling approach is unable to assess the cracking of the pipeline. In this study, a fracture mechanics approach is used for the assessment of burst pressure of pipelines with corrosion only defects, pipelines with crack-like defects and pipelines with crack-in-corrosion defects. The findings from this study are summarized below:

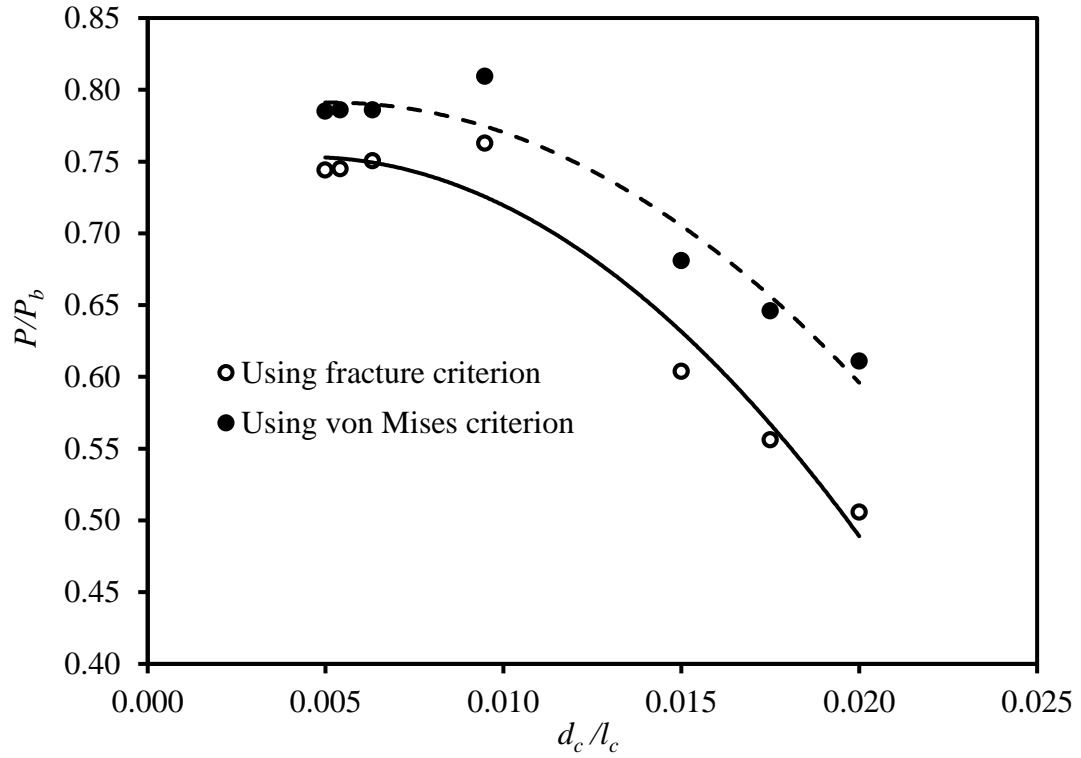


Figure 8.23: Effect of crack dimensions on burst pressure of a pipe with CIC defect

- The J -integral based fracture criterion can successfully be used for the assessment of burst pressure of pipelines with wall defects. The FE analysis using the contour integral method is employed in this study to calculate the J -integrals. To apply the contour integral method, the location of the crack needs to be identified, which is usually not known for pipelines with corrosion only defects. The XFEM technique is effectively used to identify the crack location.
- Careful determination of the critical J -integral, J_c (i.e., fracture toughness), is required for assessment of burst pressure using the fracture criterion. The J_c , back calculated from a burst pressure test is used in this study. Using the back calculated

value of J_c , several other results of burst pressure tests have been successfully simulated. The calculated J_c value for X60 steel pipeline is found to be 51 kJ/m², which is significantly less than the value reported in the literature.

- The study reveals that the fracture mechanics approach used here provides a better estimation of the burst pressure observed in the rupture test. However, the conventional design equations can reasonably be used for the remaining strength assessment of corrosion only defects. Fracture mechanics should be used for pipelines containing crack-like defects and crack-in-corrosion defects.
- The continuum based modelling with the von Mises criterion provides higher burst pressure than the J -integral based fracture mechanics criterion. The difference is higher for deeper cracks. Thus, the von Mises criterion may not be suitable for analysis of a pipe with deeper corrosion.
- A parametric study with various crack depths and crack lengths indicates that a deeper crack significantly reduces the burst pressure. The effect of crack length on the burst pressure is found to be insignificant.

CHAPTER 9

Conclusion and Future Work

9.1 Overview

The remaining strength assessment of a deteriorating pipeline is required to maintain structural integrity of the pipeline in service. The pipelines are often exposed to a corrosive environment, leading to wall corrosion during the service life. The remaining strength of the corroded pipeline is generally assessed in terms of burst pressure, which is the internal pressure at which the pipeline fails. The design codes (i.e., DNV-RP-F101, modified ASME etc.) have adopted equations for calculating the burst pressure of corroded pipelines. Researchers have identified the limitations of the design equations in the codes and are working toward developing the improved models for rationally assessing the burst pressure of deteriorating pipelines. Furthermore, the equations for burst pressure account only for the internal pressure of pipelines. However, the pipelines are often subjected to axial forces and bending moments resulting from external loading and boundary conditions. In this research, the improved models for burst pressure prediction for deteriorating pipelines are developed including consideration of axial forces and bending moments based on extensive finite element analysis using Abaqus. The axial forces and bending moments experienced by offshore pipelines are first examined. The burst pressure models are then developed for deteriorating pipelines under internal pressure only and with axial force and bending moment. The findings from the relevant chapters of the thesis are summarized in the following sections.

9.1.1 Forces Experienced by Surface-Laid Offshore Pipelines

The Chapter 3 of the thesis presents a study on the internal forces experienced by an offshore energy pipeline. The study is conducted for a seabed condition observed offshore from Newfoundland and then a parametric study is conducted. The major conclusions from this study include:

- The offshore energy pipelines laid on the imperfect/undulated seabed have different shapes, initial imperfections, depending on the shapes of the seabed profiles and material properties. During the development of the initial imperfection, the axial forces and/or bending moments develop in the pipe wall.
- The axial compressive forces and/or bending moments are also developed in the pipe wall during operation at a high temperature and high pressure. These axial forces and/or bending moments along with internal pressure should be considered for structural integrity assessment of the pipelines.

9.1.2 Existing Burst Pressure Models

An evaluation of the existing burst pressure models such as the modified ASME, CSA Z662-15, DNV-RP-F101, LPC-1, Shell 92 etc. using detailed FE analysis is presented in Chapter 4. The major findings from this study are:

- The DNV-RP-F101 design code provides unconservative burst pressure with respect to FE results. The modified ASME code provides both conservative and unconservative burst pressure with respect to FE calculation. The CSA and Shell 92 codes provide overly conservative estimation of the burst pressures. The LPC-1

method appears to provide the most reasonable calculation of the burst pressures among the methods discussed herein for the ranges of pipelines investigated.

- The discrepancies in the burst pressures provided by different methods are mainly due to the different definitions of the flow stress and the burst pressure reduction factor. The flow stress depends on the material strength and the burst pressure reduction factor depends on the geometric parameter.
- The geometric parameter in the burst pressure reduction factor is defined in terms of the Folias factor, M , which is expressed in terms of corrosion length (l), pipe diameter (D) and wall thickness (t). However, the FE evaluation revealed that the Folias factor also depends on the defect depths. Therefore, further research is recommended to develop an improved model of the Folias factor.

9.1.3 Improved Burst Pressure Models

The Chapter 5 includes an improved burst pressure model developed for pipelines with a single corrosion defect under the load of internal pressure only.

- The study reveals that the Folias factor decreases with pipe size, increases with defect length and decreases with defect depth. An improved equation of the Folias factor is developed as the function of pipe dimensions, corrosion length and corrosion depth, capturing the effects of the parameters influencing the Folias factor.
- The revised burst pressure model is developed using the theory of thick walled cylinder and the Folias factor proposed in the current study. The evaluation of the

proposed burst pressure model shows that the proposed model provides reasonable lower bound estimations of the burst pressures obtained from FE analyses.

- The proposed burst pressure model has been evaluated using test burst pressures obtained from published literature and was found to provide a reasonable lower bound estimation of the test burst pressures.

9.1.4 Interaction of multiple corrosion defects

Corrosion in a pipeline often occurs in multiple patches those sometimes act as a single defect or as separate independent defects depending on the distance between the defects. The Chapter 6 presents an evaluation of existing codes of practice for multiple defects and proposes new interaction rules.

- The existing design standards define interaction rules depending on the pipe dimensions and corrosion lengths. However, the FE evaluation of the interaction rules shows that the interacting distance depends not only on pipe dimensions and corrosion length but also on corrosion depth. Two new interaction rules have been developed including the effect of pipe dimensions and corrosion depth.
- The new interaction rules are expressed in terms of wall thickness, ' t ', and (\sqrt{Dt}) . However, the spacing expressed in terms of ' t ' showed better performance. It is, therefore, reasonable to define the interaction rule using pipe wall thickness (t) rather than \sqrt{Dt} .

- The new interaction rules presented here are developed considering two base defects (i.e., 60 mm and 120 mm) for 300 mm, 500 mm and 762 mm diameter pipes with a D/t ratio of around 30.

9.1.5 Effects of Axial Forces and Bending Moments

As mentioned earlier, offshore energy pipelines are subjected to axial forces and bending moments in addition to internal pressure. The burst pressure of a corroded pipeline is affected by the axial force and bending moment acting on the pipeline. The Chapter 7 presents an investigation of the effects of axial force and the bending moment on the burst pressure of corroded pipelines using FE analysis.

- The study shows that the axial compressive force and closing bending moment reduce the burst pressure more significantly than the tensile axial force and opening bending moment. Therefore, the compressive axial force and closing bending moment are considered to develop failure loci of corroded pipelines subjected to axial forces and bending moments.
- The DNV-RP-F101 design standard recommends considering the effect of axial force and/or the bending moment for the prediction of burst pressure of a corroded pipeline. However, the recommended method provides unconservative burst pressure when the ratio of the resultant axial compressive stress to the material ultimate tensile strength is smaller than 0.25. The method is applicable for the ratio of hoop stress to the longitudinal stress of 2.

- A parametric study conducted here reveals that the normalized burst pressure of corroded pipelines depends on corrosion depths and load combinations. The corrosion length and pipe dimensions have insignificant effects. Therefore, the failure loci have been developed for different corrosion depths and load combinations.
- The developed failure loci can be used for assessing the burst pressure of corroded pipelines with known axial force and bending moment.

9.1.6 Application of Fracture Criterion

In the conventional method of FE modelling for the assessment of burst pressure of corroded pipelines, the von Mises stress along the pipe thickness is examined. However, this approach is unable to capture the effects of cracking of the pipe wall. In order to better model the cracking of a pipe wall, fracture mechanics is employed, which is discussed in the Chapter 8.

- A J -integral based failure criterion considered is suitable for fracture assessment of corroded pipelines. The J -integral at a crack location is calculated using the contour integral method. The XFEM technique is used to determine the crack location.
- The critical J -integral, J_c , (i.e., fracture toughness) back-calculated from the burst test result is found to be reasonable for the failure assessment of the corroded pipeline with a corrosion only defect, crack-in-corrosion defect and crack-like defect.

- The von Mises failure criterion provides a higher burst pressure of defected pipelines compared to the fracture mechanics criterion. The difference is greater for increased crack depth.
- The study indicates that the fracture criterion should be a useful tool for the failure assessment of a corroded pipeline.

9.2 Recommendations for Future Work

9.2.1 Effect of Loads

- In the current research, the effect of axial force and the bending moment on the burst pressure of corroded pipelines have been investigated using FE analysis. The FE model was validated using test burst pressure obtained from the published literature. Using that validated FE model, the failure loci for combined loading have been developed. The burst pressure of a corroded pipeline subjected to an axial force and a bending moment is not available in the literature. Therefore, laboratory tests are recommended to evaluate the developed failure loci using the test results.

9.2.2 Interacting Defects

- The proposed new interaction rules for pipelines containing multiple interacting defects have been developed considering one pipe material, two different corrosion lengths and one corrosion width. Further study is recommended to investigate the effect of material properties on the limiting interacting distance. A comprehensive investigation is recommended using different corrosion lengths and corrosion widths.

- Similar to the investigation of the effects of loading, the new interaction rules have been developed using FE analysis. Experimental investigation is recommended to validate the proposed interaction rules for predicting the burst pressure.

9.2.3 Application of Fracture Mechanics

- In the current research, pipelines containing crack-like defects have been investigated using the J -based fracture mechanics criterion. It was observed that the J -based fracture toughness determined by a single edge bent test is not same as the J -integral at failure of the pipelines subjected to internal pressure. The research is required to determine the fracture toughness of the pipe material.
- This research introduces fracture parameters for the remaining strength assessment of pipelines. The fracture mechanics approach could extensively employed for failure assessment of pipelines. Particularly, the pipeline containing a crack-like defect or CIC defect are also subjected to combined loads of internal pressure, axial force and/or bending moment during operation. A study is required to develop the failure loci for pipelines with a crack-like defect or CIC defect subjected to combined loads of internal pressure, axial force and a bending moment.

9.2.4 Study on Buried Pipelines

- The current study has focused on the remaining strength of surface-laid pipelines. In reality, the pipelines are not always laid on the surface, but often buried in the ground. The remaining strength assessment for buried pipelines would be within the scope of future research.

REFERENCES

- Al-Owaisi, S.S., Becker, A.A. and Sun, W., 2016, “Analysis of shape and location effects of closely spaced metal loss defects in pressurised pipes”, *Journal of Engineering Failure Analysis*, Elsevier, 68(October 2016): 172-186.
- Andrade, E.Q. d., Benjamin, A.C., Machado Jr., P.R.S., Pereira, L.C., Jacob, B.P., Carneiro, E.G., Guerreiro, J.N.C., Silva, R.C.C. and Noronha Jr., D.B. 2006. “Finite element modeling of the failure behavior of pipelines containing interacting corrosion defects”, *In Proceedings of OMAE2006 25th International Conference on Offshore Mechanics and Arctic Engineering*, 4-9 June 2006, Hamburg, Germany.
- ASME B31G 2012, “Manual for Determining the Remaining Strength of Corroded pipelines”, Supplement to the ASME B31 Code for Pressure Piping.
- Bedairi, B., Cronin, D., Hosseini, A. and Plumtree, A. 2012, “Failure prediction for Crack-in Corrosion defects in natural gas transmission Pipelines”, *International Journal of Pressure Vessels and Piping*, Elsevier, 96-97(August-September 2012): 90-99.
- Belytschko, T. and T. Black, T., 1999, “Elastic Crack Growth in Finite Elements with Minimal Remeshing”, *International Journal for Numerical Methods in Engineering*, 45(5): 601–620.
- Benjamin, A.C., Freire, J.L.F., Vieira, R.D and Cunha, D.J.S., 2016, “Interaction of corrosion defects in pipelines- Part 2: MTI JIP database of corroded pipe tests”, *International Journal of Pressure Vessels and Piping*, Elsevier, 145(September 2016): 41-59.

Benjamin, A.C., Freire, J.L.F., Vieira, R.D., Diniz, J.L.C. de and Andrade, E.Q. d., 2005, "Burst tests on pipeline containing interacting corrosion defects," *In Proceedings of OMAE2005 24th International Conference on Offshore Mechanics and Arctic Engineering*, 12-17 June 2005, Halkidiki, Greece, pp.1-15.

BjØrnoy, O. H., Sigurdsson, G. and Marley, M. J., 2001, "Background and Development of DNV-RP-F101 "Corroded Pipelines"", *In Proceedings of the Eleventh (2001) International Offshore and Polar Engineering Conference Stavanger, Norway*, June 17-22, 2001: 102-109.

BS 7910, 2013, "Guide to methods for assessing the acceptability of flaws in metallic structure," British Standard Institution.

Canadian Standard Association, 2015, "Oil and gas pipeline systems", CSA standard Z662-15, Mississauga, Ontario, Canada.

Canadian Energy Pipeline Association (CEPA), 2017, "2017 Transmission pipeline industry performance report-Performance data", Calgary, Alberta.

Chauhan, V. and Swankie, T., 2010, "Guidance for Assessing the Remaining Strength of Corroded Pipelines", Project # 153M, GL Noble Denton.

Chen, Y., Zhang, H., Zhang, J., Liu, X., Li, X. and Zhou, J., 2014, "Residual Bending Capacity for Pipelines with Corrosion Defects", *Journal of Loss Prevention in the Process Industries*, ELSEVIER, 32 (November 2014): 70-77.

Chen, Y., Zhang, H., Zhang, J., Li, X. and Zhou, J., 2015, "Failure Analysis of High Strength Pipeline with Single and Multiple Corrosions", *Journal of Materials and Design*, ELSEVIER, 67(February 2015): 552-557.

Chiodo, M.S.G. and Ruggieri, C., 2009, “Failure assessments of corroded pipelines with axial defects using stress-based criteria: Numerical studies and verification analyses”, *International Journal of Pressure Vessels and Piping*, Elsevier, 86(February-March 2009): 164-176.

Craveiro, M.V. and Neto, A.G., 2016, “Buckling Of Pipelines Due To Internal Pressure”, *Proceedings of the XXXVII Iberian Latin-American Congress on Computational Methods in Engineering*, ABMEC, DF, Brazil, November 6-9, 2016: 1-20.

Cronin, D.S. and Pick, R.J., 2000, “Experimental Database for Corroded Pipe: Evaluation Of RSTRENG and B31G,” *In Proceedings of 2000 International Pipeline Conference*,” Volume-2, ASME, IPC2000-190: 757-767.

Dhar, A.S. and Mondal, B.C., 2015, “FE Modelling of Corroded Pipelines under Internal Pressure”, *IBC Energy 6th annual conference*, Artic Oil and Gas, North America, 14-15 April, St. John’s, Newfoundland and Labrador, Canada.

Diniz, J.L.C., Vieira, R.D., Castro, J.T., Benjamin, A.C. and Freire, J.L.F., 2006, “Stress and strain analysis of pipelines with localized metal loss”, *Experimental Mechanics*, 46(6): 765–775.

DNV-RP-F101, 2007, “Global Buckling of Submarine Pipelines”, Det Norske Veritas, Norway.

DNV-RP-F101, 2015, “Corroded Pipeline”, Det Norske Veritas, Norway.

Fekete, G. and Varga, L., 2012, “The effect of the width to length ratios of corrosion defects on the burst pressures of transmission pipelines”, *Engineering Failure Analysis*, Elsevier, 21(April 2012): 21-30.

Folias, E. S., 1964, “The Stresses in a Cylindrical Shell Containing an Axial Crack,” ARL 64-174, Aerospace Research Laboratories.

Folias, E.S., 1973, “Fracture in Pressure Vessels,” Chapter 21, *Thin Shell Structures*, edited by Y.C. Fung & E.E. Schler, Prentice-Hall, pp. 483-518.

Freire, J.L.F., Vieira, R.D., Castro, J.T.P. and Benjamin, A.C., 2006, “A series on Applications of Experimental Techniques in the Field of Pipeline Integrity”, Part 3: Burst Tests of Pipeline with Extensive Longitudinal Metal Loss, *Experimental Techniques*, 11(August 2006): 60-65.

Fu, B., and Batte, D., 1999, “An overview of advanced methods for the assessment of corrosion in linepipe”, *Offshore Technology Report—OTO 51*.

Gdoutos, E.E., 2005, “Fracture Mechanics: An Introduction”, Second Edition, Springer, 3300 AA Dordrecht, The Netherlands.

Guo, B., Song, S., Ghalambor, A. and Lin, T.R., 2014, “Offshore Pipelines: Design Installation, and Maintenance”, Second Edition, Gulf Professional Publishing, Elsevier.

Hasan, M., Khan, F. and Kenny, S., 2011, “Identification of the Cause of Variability of Probability of Failure for Burst Models Recommended by Codes/Standards”, *Journal of Pressure Vessel Technology*, ASME, 133(4): 1-9.

Hearn, E.J., 1997, "Mechanics of Materials, Volume 1: An Introduction to the Mechanics of Elastic and Plastic Deformation of Solids and Structural Materials," 3rd Edition, Elsevier: 215-221.

Hobbs, R. E., 1984, "In-service buckling of heated pipelines", *Journal of Transportation Engineering*, 110(2): 175–189.

Irwin, G. and de Wit, R., 1983, "A Summary of Fracture Mechanics Concepts", *Journal of Testing and Evaluation*, 11(1): 56-65.

Karampour, H., Albermani, F. and Gross, J., 2013, "On lateral and upheaval buckling of subsea pipelines", *Engineering Structures*, Elsevier, 52(July 2013): 317-330.

Kiefner, J.F. and Vieth, P.H., 1989, "A Modified Criteria for Evaluating the Remaining Strength of Corroded Pipe," Final Report on Project PR 3-805.

Kiefner, J. F. and Vieth, P. H., 1990, "Evaluating pipe Conclusion: PC program speeds new criterion for evaluating corroded pipe", *Oil & Gas Journal*, 88 (34): 91-93.

Kim, Y.P., Lee, Y.K., Kim, W.S. and Oh, K.H., 2004, "The Evaluation of Failure Pressure for Corrosion Defects within Girth or Seam Weld in Transmission Pipelines," *In Proceedings of IPC2004 International Pipeline Conference*, October 4-8, 2004, Calgary, Alberta, Canada, IPC2004-216: 1-9.

Lasebikan, B. A. and Akisanya, A. R., 2014, "Burst pressure of super duplex stainless steel pipes subject to combined axial tension, internal pressure and elevated temperature", *International Journal of Pressure Vessels and Piping*, 119(July 2014): 62-68.

- Li, X., Bai, Y., Su, C. and Li, M., 2016, “Effect of interaction between corrosion defects on failure pressure of thin wall steel pipeline”, *International Journal of Pressure Vessels and Piping*, Elsevier, 138(February 2016): 8-18.
- Liu, J., Chauhan, V., Ng, P., Wheat, S. and Hughes, C., 2009, “Remaining Strength of Corroded Pipe Under Secondary (Biaxial) Loading”, Project # 153J, GL Operating 24/7.
- Liu, R., Basu, P. and Xiong. H., 2015, “Laboratory tests and thermal buckling analysis for pipes buried in Bohai soft clay”, *Marine Structures*, Elsevier, 43(October 2015): 44-60.
- Liu, R., Wang, W., Yan, S. and Wu, X., 2012, “Engineering measures for preventing upheaval buckling of buried submarine pipelines”, *Applied Mathematics and Mechanics (English Edition)*, Shanghai University and Springer-Verlag; 33(6): 781-796.
- Liu, R., Xiong, H., Wu, X. and Yan, S., 2014, “Numerical studies on global buckling of subsea pipelines”, *Ocean Engineering*, Elsevier, 78(1 March 2014): 62–72.
- Liu, R. and Yan, S., 2013, “Brief history of upheaval buckling studies for subsea buried pipeline”, *Journal of Pipeline System Engineering and Practice*, 4 (3): 170-183.
- Ma, B., Shuai, J., Liu, D. and Xu, K., 2013, “Assessment on Failure Pressure of High Strength Pipeline with Corrosion Defects,” *Engineering Failure Analysis*, 32(September 2013): 209–219.
- Milne, I., Ainsworth, R.A., Dowling, A.R. and Stewart, A.T., 1988, “Assessment of the integrity of structures containing defects”, *Int. J. Pres. Ves. & Piping*, 32(1-4): 3–104.

- Mohd, M.H., Lee, B.J., Cui, Y. and Paik, J.K., 2015, “Residual strength of corroded subsea pipelines subject to combined internal pressure and bending moment”, *Ships and Offshore Structures*, Taylor & Francis, 10(5): 554–564.
- Mohitpour, M., Golshan, H. and Murray, A., 2003, “Pipeline Design and Construction: A Practical Approach”, ASME Press, New York, NY 10016.
- Mondal, B.C. and Dhar, A.S., 2015, “Corrosion Effects on the Strength of Steel Pipes Using FEA”, OMAE15, Proceedings of the ASME 34th International Conference on Ocean, Offshore and Arctic Engineering, May 31 – June 5, 2015, St. John’s, NL, Canada.
- Mondal, B.C. and Dhar, A.S., 2016a, “Finite-Element Evaluation of Burst Pressure Models for Corroded Pipelines,” *Journal of Pressure Vessel Technology*, ASME, 139(2): 021702-1.
- Mondal, B. C. and Dhar, A.S., 2016b, “Upheaval Buckling Behavior of Offshore Oil Pipeline”, *In Proceedings of Geo Vancouver Conference 2016*, 2-5 October, Vancouver, BC, Canada.
- Mondal, B.C. and Dhar, A.S, 2016c, “Burst pressure assessment for pipelines with multiple corrosion defects”, 5th International Structural Specialty Conference, Canadian Society for Civil Engineering, 1-4 June 2016, London, ON, Canada.
- Mondal, B. C. and Dhar, A.S., 2017a, “Upheaval buckling of surface-laid offshore pipeline”, *Applied Ocean Research*, Elsevier, 66(June 2017): 146-155.
- Mondal, B.C. and Dhar, A., 2017b, “Interaction of Multiple Corrosion Defects on Burst Pressure of Pipelines,” *Canadian Journal of Civil Engineering*, 44(8): 589-597.

- Mondal, B.C. and Dhar, A.S., 2018, “Improved Folias Factor and Burst Pressure Models for Corroded Pipelines,” *Journal of Pressure Vessel Technology*, ASME, 140(1): 011702-1.
- Oh, C.K., Kim, Y.J., Baek, J.H., Kim, Y.P. and Kim, W.S., 2007, “Ductile failure analysis of API X65 pipes with notch-type defects using a local fracture criterion”, *Journal of Pressure Vessels and Piping*, Elsevier, 84(8): 512–525.
- Oh, C. K., Kim, Y. J. and Park, C. Y., 2009, “Effects of local wall thinning on net-section limit loads for pipes under combined pressure and bending”, *Nuclear Engineering and Design*, 239(2): 261-273.
- Oh, C. K., Kim, Y. J., Kim, J. S. and Jin, T. E., 2008, “Yield locus for circumferential part-through surface cracked pipes under combined pressure and bending”, *Engineering Fracture Mechanics*, 75(8): 2175-2190.
- Palmer, A.C. and King, R.A. 2008. *Subsea Pipeline Engineering*, 2nd Edition, PennWell Corporation, Tulsa, Oklahoma, USA.
- Phan, H., Dhar, A. and Mondal, B.C., 2017, “Revisiting Burst Pressure Models for Corroded Pipelines,” *Canadian Journal Civil Engineering*, 44(7): 485-494.
- Pipeline Operator Forum Document, 2005, “Specifications and requirements for intelligent pig inspection of pipelines”, Version 3.2, January (2005).
- Run, L., Wu-gang, W. and Shu-wang, Y., 2013, “Finite element analysis on thermal upheaval buckling of submarine burial pipelines with initial imperfection”, *J. Cent. South Univ*, Springer, 20(1): 236-245.

Sadasue, T., Kubo, T., Glover, A., Ishikawa, N., Horsley, D., Igi, S., Endo, S. and Toyoda, M., 2004, "Ductile Cracking Evaluation of X80/X100 High Strength Linepipes," *In Proceedings of International Pipeline Conference*, October 4-8, 2004, Calgary, Alberta, Canada, IPC2004-249: 1-9.

Shi, R., Wang, L., Guo, Z. and Yuan, F., 2013, "Upheaval buckling of a pipeline with prop imperfection on a plastic soft seabed", *Thin-Walled Structures*, Elsevier, 65(April 2013): 1-6.

Silva, R.C.C., Guerreiro, J.N.C. and Loula, A.F.D, 2007, "A study of pipe interacting corrosion defects using the FEM and neural networks", *Journal of Advances in Engineering Software*, Elsevier, 38(11-12): 868–875.

"Soil friction angle", 2013. Retrieved from:

<http://www.geotechdata.info/parameter/angle-of-friction.html>

Storn, R., and Price. K., 1997, "Differential Evolution – A simple and efficient heuristic for global optimization over continuous spaces", *Journal of Global Optimization*, 11(4): 341-359.

Swankie, T., Owen, R., Bood, R., Chauhan, V., and Gilbert, G., 2012, "Assessment of the remaining strength of corroded small diameter (below 6") pipelines and pipework", *Proceedings of the 2012 9th International Pipeline Conference, IPC2012*, September 24-28, 2012, Calgary, Alberta, Canada.

Sykes, J., 2012, "Metallurgical Failures in Oil and Gas Pipelines", *Asia Offshore Energy Conference*, September 2012, Jimbaran, Indonesia.

"Table of ultimate friction factors for dissimilar materials" 2017. Retrieved from:

<https://www.finesoftware.eu/help/geo5/en/table-of-ultimate-friction-factors-for-dissimilar-materials-01/>

Taylor, N., Clubb, G. and Atkins, I.M, 2015, “The effect of bending and axial compression on pipeline burst capacity”, *In* Proceedings of SPE Offshore Europe Conference, SPE-175464-MS, 8-11 September, Aberdeen, Scotland, UK.

Taylor, N. and Gan, A. B., 1986, “Submarine pipeline buckling-imperfection studies”, *Thin-Walled Structures*, 4(4): 295-323.

Taylor, N. and Tran, V., 1996, “Experimental and Theoretical Studies in Subsea Pipeline Buckling”, *Marine Structures*, Elsevier, 9(2): 211-257.

Vincenzi, L., Roeck, G. D., and Savoia, M., 2013, “Comparison between coupled local minimizers method and differential evolution algorithm in dynamic damage detection problems”, *Advances in Engineering Software*, 65 (November 2013): 90–100.

Wang, H.P., Li, X. and Zhou, J., 2016, “Ultimate bending capacities of steel pipelines under combined loadings”, *Advances in Structural Engineering*, 19(4): 642-659.

Wang, L., Shi, R., Yuan, F., Guo, Z. and Yu, L., 2011, “Global buckling of pipelines in the vertical plane with a soft seabed”, *Applied Ocean Research*, Elsevier, 33(2): 130-136.

Wang, Z., Huachen, Z., Liu, H. and Yidu Bu, Y., 2015, “Static and dynamic analysis on upheaval buckling of unburied subsea pipelines”, *Ocean Engineering*, Elsevier, 104(1 August 2015): 249-256.

Wilson, B., 2016, “Pipeline metallurgical failure analysis”, 16TAN License 802177-001, Acuren Project No.: 306-0087829-1-R1, Calgary, Canada.

- Woodson, R.D., 1990, "Offshore Pipeline Failures", A thesis for Master of Engineering, Department of Civil Engineering, University of California, USA.
- Yang, S., Li, C.Q. and Yang, W., 2016, "Analytical model of elastic fracture toughness for steel pipes with internal cracks", *Engineering Fracture Mechanics*, 153 (March 2016): 50-60.
- Yan, Z., Zhang, S. and Zhou, W., 2014, "Model error assessment of burst capacity models for energy pipelines containing surface cracks", *International Journal of Pressure Vessels and Piping*, ELSEVIER, 120-121(August–September 2014): 80-92.
- Ye, H., Yan, S. and Jin, Z., 2016, "Collapse of Corroded Pipelines under Combined Tension and External Pressure", *PloS ONE*, 11(4): e0154314.
- Zeng, X., Duan, M. and Che, X., 2014, "Critical upheaval buckling forces of imperfect pipelines", *Applied Ocean Research*, Elsevier, 45(March 2014): 33-39.
- Zhang, X. and Duan, M., 2015, "Prediction of the upheaval buckling critical force for imperfect submarine pipelines", *Ocean Engineering*, Elsevier, 109(15 November 2015): 330-343.
- Zhang, Y.M., Yi, D.K., Xiao, Z.M. and Huang, Z.H., 2015, "Engineering critical assessment for offshore pipelines with 3-D elliptical embedded cracks", *Engineering Failure Analysis*, ELSEVIER, 51(May 2015): 37-54.
- Zhou, W. and Huang, G.X., 2012, "Model error assessments of burst capacity models for corroded pipelines", *International Journal of Pressure Vessels and Piping*, ELSEVIER, 99-100(November-December 2012): 1-8.

Zhou, W., and Zhang, S., 2015, “Impact of model errors of burst capacity models on the reliability evaluation of corroding pipelines”, *Journal of Pipeline Systems Engineering and Practice*, ASCE, 7(1): 1-11.

Zhu, X.K. and Joyce, J.A., 2012, “Review of fracture toughness (G, K, J, CTOD, CTOA) testing and standardization”, *Engineering Fracture Mechanics*, 85(May 2012): 1-46.

Zhu, X.K. and Leis, B.N., 2012, “Evaluation of burst pressure prediction models for line pipes”, *International Journal of Pressure Vessels and Piping*, Elsevier, 89(January 2012): 85–97.

Appendix I

Proceedings of the ASME 2015 34th International Conference on Ocean, Offshore and Arctic Engineering
OMAE2015
May 31 – June 5, 2015, St. John's, Newfoundland, Canada

OMAE2015-42003

CORROSION EFFECTS ON THE STRENGTH OF STEEL PIPES USING FEA

Bipul Chandra Mondal
Memorial University of Newfoundland
St. John's, NL, Canada

Ashutosh Sutra Dhar
Memorial University of Newfoundland
St. John's, NL, Canada

ABSTRACT

This paper presents a finite element investigation on the strength and deformation characteristics of corroded steel pipes with corrosion on the exterior and interior surfaces of the pipes considering different corrosion parameters such as circumferential extent (width) of corrosion, ratio of corrosion width to pipe diameter and the locations of corrosion. The finite element analysis was performed using a commercially available general purpose finite element program, ABAQUS/Explicit. The study reveals that localized bending develops on the pipe wall within the corroded zone that extent up to a certain distance (1 to 1.5 times the corrosion dimension) in the non-corroded area. The localized bending causes stress concentration in the vicinity of the corroded area that is not well captured in the current design standards (i.e. modified ASME B31G). As a result, the modified ASME B31G method overestimated the pipe capacity comparing to the capacity calculated based on the finite element analysis. A pipe designed using the modified ASME B31G method is expected to provide a factor of safety less than the design factor of safety. The effects of circumferential extent of corrosion appears to be less compared to the effects of longitudinal extent of corrosion. The exterior corrosion was found to be more detrimental in comparison with the interior corrosion.

INTRODUCTION

The application of steel pipe is progressively increasing worldwide, specially in the arctic region, due to its better performance than concrete pipe in terms of durability and strength. Hundreds of thousands of kilometers of steel pipelines cross over the land and ocean to transport oil, gas and other petroleum products. The steel pipes are subjected to corrosion. Besides, many of the steel pipes around the world are close to or

have exceeded their design life and may require replacement and/or rehabilitation mostly due to corrosion deterioration. The performance of the pipelines is greatly influenced by the corrosion deterioration.

Three common types of corrosion that occurs in the steel pipelines include local, general, and pitting corruptions. The corrosion results in different types of corrosion patterns on the pipe wall. The types and the patterns of the corrosion significantly affect the performance of corroded pipelines. Regular monitoring is often used to maintain the integrity of the pipelines in service against corrosion defects. In this regards, the assessment of remaining life of the pipeline would be beneficial to determine the monitoring schedule by estimating the time when a failure mechanism may be detected. Any repair/maintenance work could also be completed efficiently if the residual strength of the pipe could be predicted precisely. The prediction of the residual strength and the remaining service life of pipeline require a better understanding of the strength of the corroded pipelines.

Currently, there are a number of design practices [1-4] to predict remaining strength of corroded pipelines considering different corrosion related parameters. Table 1 summarizes a few of them.

Table 1. INTERNAL PRESSURE CAPACITY MODEL OF CORRODED PIPES [1-4]

Source	Prediction Model
DNV RP-F101 [1]	$P = 1.05 \cdot \frac{2t}{D-t} \cdot \sigma_u \cdot \frac{1-\frac{d}{t}}{1-\frac{d}{tQ}}$ $Q = \sqrt{1 + 0.31 \cdot \left(\frac{t}{\sqrt{Dt}}\right)^2}$
BS 7910 [2]	$P = \frac{2t}{D-t} \cdot \sigma_{ref} \cdot \frac{1-\frac{d}{t}}{1-\frac{d}{tQ}}$

	σ_{ref} = reference stress used for creep and plastic collapse consideration
ABS [3]	$P = \frac{2t}{D-t} \cdot 0.5 \cdot (SMYS + SMTS) \cdot \frac{1-\frac{d}{t}}{1-\frac{d}{tQ}}$
Modified ASME B31G [4]	$P_F = \frac{2tS_F}{D}$ $S_F = S_{flow} \cdot \left[\frac{1-0.85\frac{d}{t}}{1-0.85\frac{d}{tM}} \right]$ <p>For $\frac{l^2}{D-t} \leq 50$</p> $M = \sqrt{1 + 0.6275 \cdot \frac{l^2}{D-t} - 0.003375 \cdot \frac{l^4}{D^2t^2}}$ <p>For $\frac{l^2}{D-t} > 50$</p> $M = 0.032 \cdot \frac{l^2}{D-t} + 3.30$ $P_S = \frac{P_F}{SF}$

In the equations in Tab. 1, D , t , d and l represent pipe outer diameter, non-corroded wall thickness, depth of corrosion, longitudinal length of corrosion of the corroded pipe, respectively, in meter. P and P_F are failure pressure or burst pressure in MPa. $SMTS$ and $SMYS$ are specified minimum ultimate tensile strength and specified minimum yield strength, respectively, in MPa.

In modified ASME B31G, failure stress level, S_F is estimated based on corrosion dimensions and flow stress, S_{flow} . Then pipe failure pressure, P_F is estimated using the calculated failure stress. The safe operating pressure, P_S is then obtained from the failure pressure using a factor of safety, SF .

Chen *et al* [5] revealed that most of the design standards for estimating the remaining strength underestimate the actual failure pressure of the corroded pipes. However, the current design method including modified ASME B31G was found to overestimate the failure pressure by other researchers. Swankie *et al.* [6] reported the result of burst tests for a number of pipes with diameters ranging from 88.9 mm to 168.3 mm where the modified ASME B31G method provided un-conservative estimation for 30% of the pipes tested. The modified ASME B31G method was also found to provide overestimation of failure pressure for 324 mm diameter pipe [7].

The design models typically do not consider the effects of the circumferential extent of corrosion, as seen in Tab. 1. Although the contribution of circumferential extent of corrosion is not as significant as the contribution of the longitudinal corrosion, the effect is not negligible [8]. It was therefore recommended to

incorporate the circumferential effect on the prediction of the remaining strength of corroded pipe.

In this paper, the effects of different patterns of corrosion on the strength and deformation characteristics of steel pipes and its failure mechanism are investigated using finite element analysis. Different corrosion parameters such as circumferential extent (width) of corrosion, ratio of corrosion width to pipe outer diameter (OD), locations of corrosion (inner or outer side of pipe) are investigated.

FINITE ELEMENT MODELING

The commercially available finite element (FE) software ABAQUS/Explicit was used for analysis of the corroded pipes which is effective in modelling problem with large non-linearity. Large non-linear stress distribution is expected for the corrosion shape considered in this study. Pipe domain was modelled using eight-node continuum element (ABAQUS element "C3D8R"). Corrosion geometry was simulated as a rectangular groove on the pipe wall (Fig. 1). A total of 30 FE models were developed to perform a parametric study.

The FE model was first developed for a non-corroded pipe and the burst pressure was calculated, which was compared with the burst pressure obtained from thin walled pressure vessel theory for validation. Corrosion geometry was then introduced into the validated finite element model.

This study is limited to rectangular corrosion geometries with sharp edges. Research is currently underway to investigate different shapes of corrosion geometry and edge shapes.

Geometry and Boundary Conditions

Pipe length was sufficiently long with respect to the dimension of the corrosion patch to avoid localized effects. For example, the pipe length is 6.67 times the length of the corrosion patch in the longitudinal direction. The single rectangular corrosion patch was applied at the middle of the pipe specimen. Pipe deformation along the length of the pipe was restrained.

The following presents the pipe and the corrosion parameters considered:

- Outer Diameter of the pipe, OD = 1.0m
- Wall thickness of the pipe, t = 0.02m
- Length of pipe, L = 1.0m
- Corrosion length to OD ratio, W_p/OD = 0.15
- Depth of corrosion, d = 0.01m
- The ratios of corrosion width along the perimeter to OD were W_p/OD = 0.175 (20°), 0.3 (34.38°), 0.34 (40°), 0.52 (60°), 0.785 (90°) and 3.14 ((360°)

For the finite element mesh, fine mesh was used within the zone where stress concentration was expected and coarse mesh was used where uniform stress was expected. Stress concentration is generally expected in and around the corroded area of the pipes. Thus, fine mesh was applied within and in the vicinity of the corroded zone and coarse mesh was applied away from the corroded area. A mesh sensitivity analysis was performed to identify the optimum mesh size, however, not included in this paper for brevity. The finite element mesh shown in Fig. 2 was used for analysis of pipes with internal and external corrosion. Automatic time increment was chosen for the solution process in ABAQUS.

Material and Failure Mechanism Modeling

The material has been selected as homogeneous and isotropic steel. Elastic perfectly plastic model was used with the material parameters as below:

Density = 8050 kg/m^3
 Modulus of elasticity = 200 GPa
 Yield strength = 500 MPa
 Strain at yield point = 0.20% and
 Poisson's ratio = 0.30 .

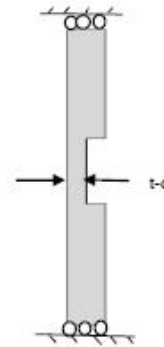
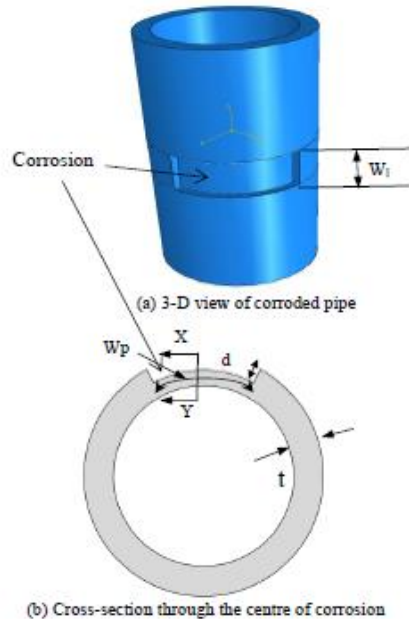


Figure 1. IDEALIZATION OF PIPE WALL CORROSION

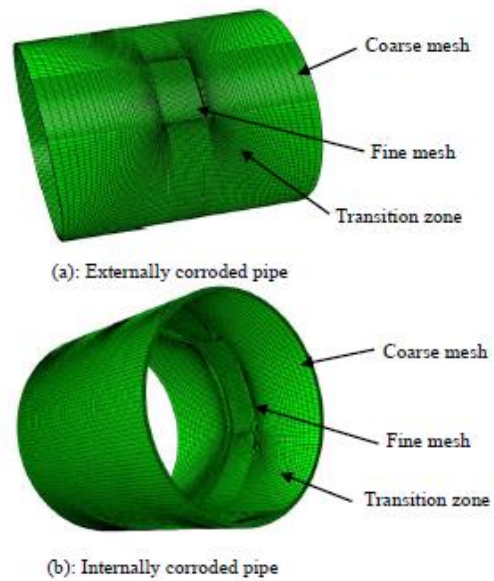


Figure 2. FE MESH FOR CORRODED PIPE SPECIMEN

The von Mises yield theory was used as the failure criteria. The internal pressure was increased gradually up to failure which was defined by von Mises criteria. The external pressure generally developed by the surrounding material was assumed to be negligible compared to the internally applied failure bursting pressure and therefore not considered in the analysis.

CORROSION EFFECTS

Pipe wall deformations and wall stresses are investigated for the corroded pipes under internal pressures. Figure 3 shows the pipe deformations of a corroded pipe with corrosion on the exterior surface. Corrosion dimensions were 150 mm along the pipe length (W_l) and 520 mm and 3140 mm (full circumference) along the pipe circumference (W_p). The circumferential dimension provides its ratio with pipe outer diameter (OD) as 0.52 and 3.14, respectively. The pipe deformations are plotted under an internal pressure of 10.3 MPa. At this internal pressure, the pipe wall stress reached the von Mises failure criteria, indicating that this internal pressure is the maximum capacity of the pipe (i.e. the burst pressure). Burst pressure for this pipe was calculated using Modified ASME method. The calculated burst pressure was 17.0 MPa for a factor of safety of unity, which is the case for finite element analysis. The modified ASME method is thus overestimating the burst pressure with respect to FE analysis. This is in contrary to the observation of Chen et al [5], who demonstrated that the failure pressure is underestimated by most design standards. Burst pressure for non-corroded pipe is calculated to be 20 MPa, which is about 17% higher than the burst pressure for the corroded pipe.

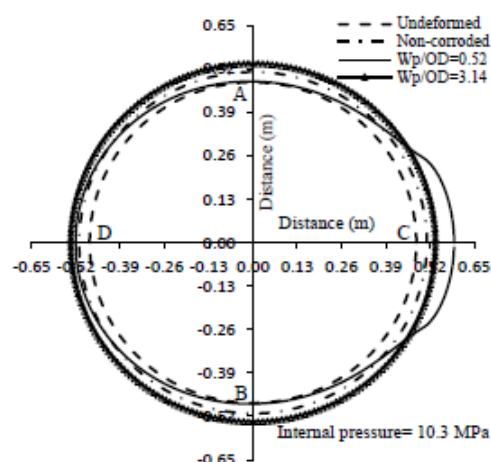


Figure 3. GEOMETRY OF INNER SURFACE ALONG THE CENTRE OF CORROSION [Deformation is exaggerated by 50 times]

Figure 3 shows deformation of the pipe circumference for corroded and non-corroded pipes. The corroded zone of the pipe wall has undergone outward bending that is associated with non-uniform pipe stresses as discussed further below. Pipe diameter change in the direct of corrosion (along CD in Fig. 3) is larger compared to the diameter change along AB for the pipe with corrosion over a part of the circumference, while pipe diameter change is uniform throughout the pipe circumference for non-

corroded pipe and for the pipe with corrosion over the full-circumference (Fig. 3).

The stress was found to be localized within the corroded zone. Figure 4 shows the contour of von Mises stresses on the pipe wall. It is evident that the maximum von Mises stresses occur within the corroded zone.

The distributions of pipe wall stresses on the pipe inner surface are plotted in Fig. 5. Figure 5(a) plots the stresses along the axial length of the pipe. It indicates that the longitudinal stress is less at the centre of the corroded zone and becomes the maximum at the interface of the corroded and non-corroded zone. The maximum circumferential stress and hence the von Mises stress occur at the centre of the corroded zone. The failure due to bursting would thus initiate at the middle of the corroded area.

The circumferential stress decreases from the corroded zone toward the non-corroded area gradually [Fig. 5(a)]. After a certain distance (about 1 to 1.5 times the length of corrosion) the stress becomes uniform. The uniform stress is close to the circumferential stress of non-corroded pipe (i.e. 250 MPa) for the same internal pressure. This implies that the corrosion has its effect on the structural performance of pipeline up to 1.5 times of corrosion length along the length of pipe on either sides of corroded area. Beyond that distance, the effects of corrosion is insignificant.

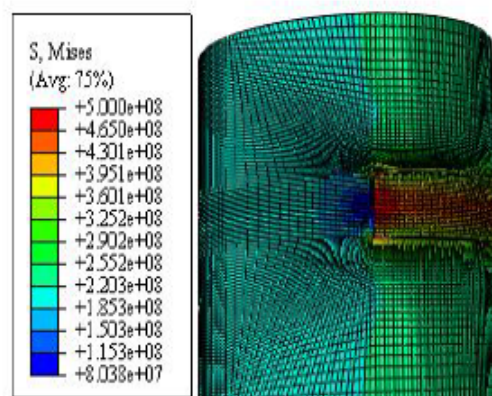


Figure 4. CONTOUR OF VON MISES STRESSES ($W_p/OD=0.52$, Pressure=10.3MPa)

Along the circumferential distance, the stress pattern is similar as that along the length except at the interface of corroded and non-corroded area where a jump is observed due to abrupt change of wall thickness [Fig. 5(b)]. The uniform

circumferential stress that occurs at around 90° apart from the centre of corrosion is almost same as the circumferential stress of non-corroded pipe. This implies that the influence of corrosion is only significant within 90° from the corrosion centre for this case.

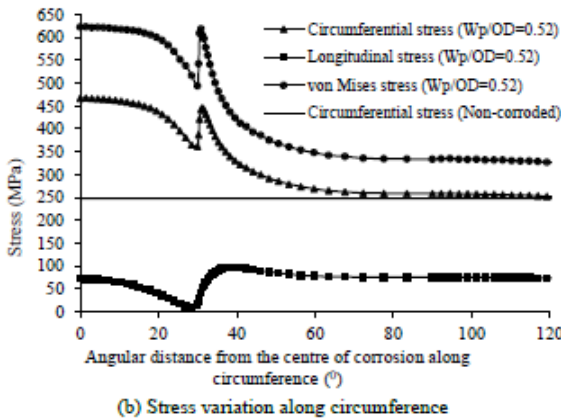
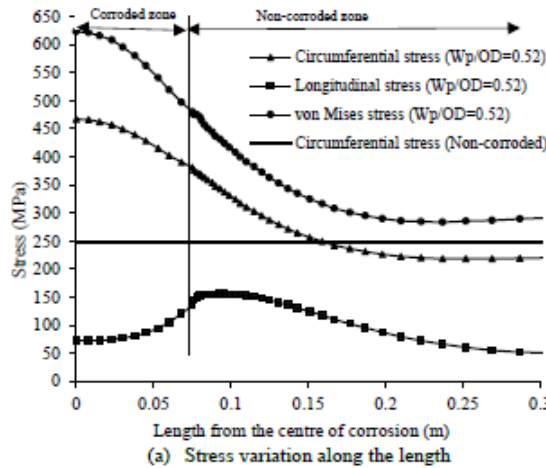


Figure 5. WALL STRESS VARIATION (Internal pressure =10.3MPa)

Circumferential stress on the inner surface and outer surface for the pipe is plotted in Fig. 6. Stresses on the inner surface and the outer surface are unequal within the corrosion zone and beyond the corrosion zone up to a distance. The unequal stresses are an indication of bending on the wall. Outer surface stresses

are higher than the inner surface stresses within the corroded area, indicating outward bending and lower than the inner surface stresses beyond the corroded area, indicating inward bending. Stress concentration observed in Fig. 5 is attributed to these bending. Beyond certain distance, the bending effect is minimized and therefore inner surface stress and outer surface stress merges, resulting in the uniform stress in the pipe wall.

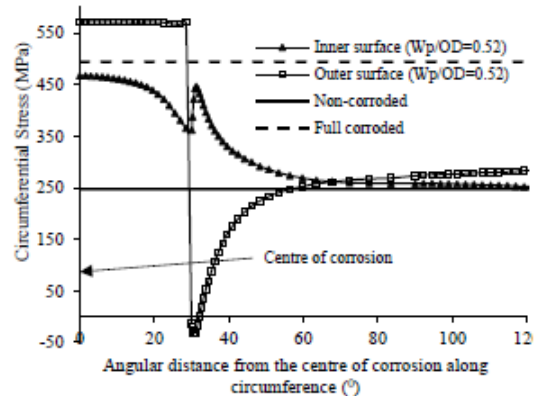
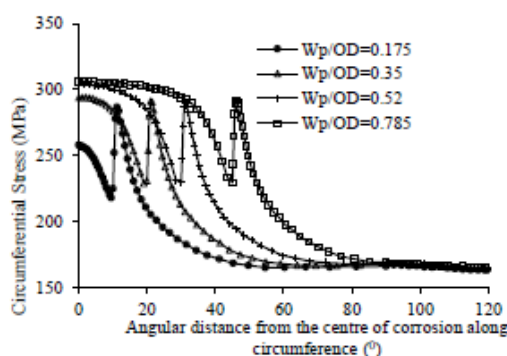


Figure 6. STRESSES ON INNER AND OUTER WALLS [Wp/OD=0.52, Internal pressure =10.3MPa]

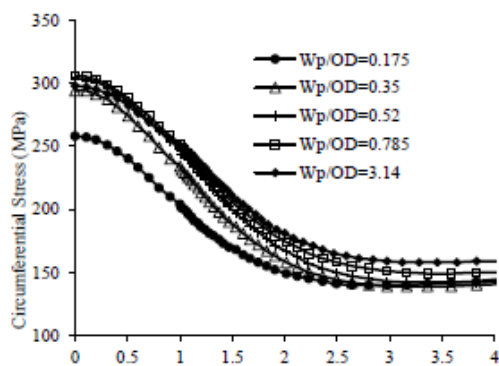
CIRCUMFERENTIAL EXTENT OF CORROSION

Most of the earlier studies on the effects of circumferential extent of corrosion focused on the effect on the overall burst pressure. Mustaffa and Gelder (2010) revealed that the circumferential extent of corrosion does not influence the failure pressure (i.e. burst pressure) of the corroded pipes significantly. According to them, the failure pressure is affected when the depth of corrosion is higher than 50% of the thickness of the parent pipe. The overall burst pressure calculated in this research corresponds to the finding of the earlier research. However, the finite element calculation of the burst pressure was less than the burst pressure calculated using ASME B31G method. In the current research, stress localization was investigated to demonstrate how the high localized stress development corresponds to the overall burst pressure.

Figure 7 shows the variation of circumferential stress at the inner surface along the perimeter [Fig. 7(a)] and along the longitudinal axis [Fig. 7(b)] of the corroded pipe with the variation of the ratio of corrosion width (Wp) to the outer diameter (OD) of the non-corroded pipe. It is seen that the stress influencing zone along the perimeter increases with the Wp/OD ratio.



(a) Along pipe circumference



(b) Along pipe length

Figure 7. EFFECT OF W_p ON THE CIRCUMFERENTIAL STRESSES [Internal pressure of 6.70 MPa]

Concentration of stress appears to depend on the circumferential extent of the corrosion zone. The stress concentration is not considered in the current pipe design codes. As seen in Tab. 1, the design codes recommend to calculate the overall burst pressure based on Specified Minimum Yield Strength (SMYS). The factor of safety of the pipe obtained using this overall burst pressure may be different from the actual factor of safety that depend on the concentration of stresses.

It is thus revealed that the current design standards (i.e. Modified ASME B31G) do not account properly for the stress concentration and the resulting higher stresses within the corroded area. As a result, the pipe capacity estimated using the design code may not provide required level of factor of safety to the pipe.

To investigate the actual factor of safety of a corroded pipe designed using ASME B31G method, the ratio of the failure stress to the maximum stress (i.e. factor of safety) on the pipe wall from finite element analysis is plotted against the pipe internal pressure in Fig. 8. The safe internal pressure for the pipe was then estimated using ASME B31G method considering a factor of safety of 2. The calculation of safe internal pressures is shown below:

$$D = 1.00\text{m}$$

$$l = 0.15\text{m}$$

$$t = 0.02\text{m}$$

$$d = 0.01\text{m}$$

$$SMYS = 500\text{ MPa}$$

$$S_{flow} = SMYS = 500\text{ MPa},$$

for considering elastic perfectly plastic material.

$$\frac{l^2}{Dt} = 1.125 < 50$$

$$M = 1.3045,$$

$$\frac{l^2}{Dt} = 1.125 < 50$$

$$M = 1.3045,$$

$$S_F = 426.4\text{ MPa}$$

$$P_F = 17.0\text{ MPa}$$

$$FS = 2.0$$

$$\text{Thus, } P_S = \frac{P_F}{FS} = 8.5\text{ MPa}$$

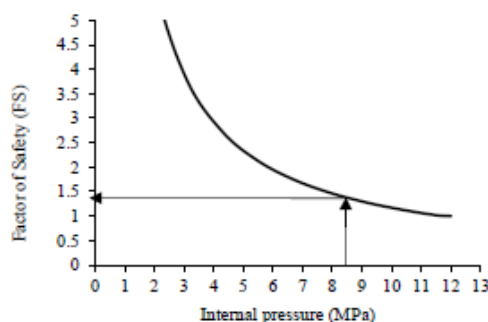


Figure 8. INTERNAL PRESSURE FOR DIFFERENT FACTOR OF SAFETY [$W_p/OD=0.52$]

An internal pressure of 8.5 MPa for the pipe corresponds to an actual factor of safety of 1.37 (from Fig. 8), which is less than the design factor of safety of 2. This reveals that the design standard for corroded pipe may provide un-conservative design of the pipe with a factor of safety less than the desired factor of safety. Research is currently underway to investigate the effects of stress concentration for different pipes with various corrosion geometries and loading conditions.

EFFECT OF THE LOCATIONS OF CORROSION

Corrosion on the outer surface of the pipe was generally considered for investigation by the researchers. However, pipe may transport aggressive material which may lead to the corrosion of pipeline at the inner surface as well. The models for failure pressure prediction provided in Tab. 1 are considered applicable for corrosion on both the internal surface and the external surface of the pipe.

The effect of corrosion on the interior surface and the exterior surface of the pipe was investigated using finite element analysis. Figure 9 compares the pipe wall stresses for a pipe with corrosion on the interior and on the exterior surface. The figure shows similar patterns of bending for the both cases under the internal pressure. Outward bending is observed within the corroded zone and inward bending is observed beyond the corroded zone. However, the magnitude of circumferential stress is higher for the pipe with corrosion on the outer surface. Thus, the exterior corrosion is more detrimental to the pipe than the interior corrosion.

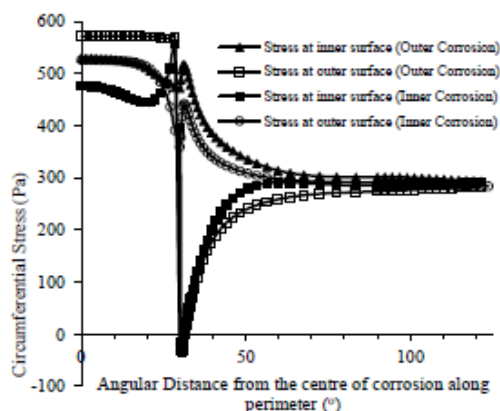


Figure 9. EFFECT OF LOCATION OF CORROSION ON CIRCUMFERENTIAL STRESS [$W_p/OD=0.52$]

CONCLUSION

The finite element investigation of the corroded pipe reveals that current design code for the corroded pipe may provide un-conservative design of the pipes. Pipe capacity calculated using ASME B31G method was higher in comparison with the capacity of the pipe calculated using finite element analysis.

Localized bending develops on the pipe wall within the corroded zone that extent up to a certain distance (1 to 1.5 times the corrosion dimension) in the non-corroded area. The localized

bending causes stress concentration in the vicinity of the corroded area that is not well captured in the current design standards (i.e. modified ASME B31G). It was also demonstrated that the factor of safety of a corroded pipe designed using modified ASME B31G method would be less than the actual design factor of safety. The circumferential extent of corrosion appears not to affect the capacity of the corroded pipe significantly like longitudinal corrosion. Exterior corrosion was found to be more affective comparing to the interior corrosion.

ACKNOWLEDGMENTS

The financial support for the study is provided by Research and Development Corporation of Newfoundland and Labrador, which is gratefully acknowledged.

REFERENCES

- [1] DNV RP-F101, 2010. *Corroded Pipeline*, Det Norske Veritas, Norway.
- [2] BS 7910, 2013. *Guide to methods for assessing the acceptability of flaws in metallic structure*, British Standard Institution.
- [3] ABS, 2005. *Submarine Pipeline Systems*, American Bureau of Shipping, USA.
- [4] ASME B31G, 2012. *Manual for Determining the Remaining Strength of Corroded pipelines*, Supplement to the ASME B31 Code for Pressure Piping.
- [5] Chen, Y., Zhang, H., Zhang, J., Li, X., and Zhou, J., 2014. "Failure Analysis of High Strength Pipeline with Single and Multiple Corrosions", *Journal of Materials and Design*, ELSEVIER.
- [6] Swankie, T., Owen, R., Bood, R., Chauhan, V., and Gilbert, G., 2012. "Assessment of the remaining strength of corroded small diameter (below 6") pipelines and pipework", *Proceedings of the 2012 9th International Pipeline Conference, IPC2012*, September 24-28, 2012, Calgary, Alberta, Canada.
- [7] Fekete, G., and Varga, L., 2012. "The effect of the width to length ratios of corrosion defects on the burst pressures of transmission pipelines", *Engineering Failure Analysis*, 21, Elsevier, pp.21-30.
- [8] Mustafa, Z., and Gelder, P. V., 2010. "A Review and Probabilistic Analysis of Limit State Functions of Corroded Pipelines". *Proceedings of the Twentieth (2010) International Offshore*

Appendix II



RESILIENT INFRASTRUCTURE

June 1–4, 2016



BURST PRESSURE ASSESSMENT FOR PIPELINES WITH MULTIPLE CORROSION DEFECTS

Bipul Chandra, B.C. Mondal
Graduate Student, Memorial University of Newfoundland, NL Canada

Ashutosh Sutra Dhar
Memorial University of Newfoundland, NL Canada

ABSTRACT

Pipeline with multiple corrosion defects are often observed in the field. The strength of pipe with multiple corrosion patches depends on the corrosion patch intensity, their locations along longitudinal and circumferential directions of the pipe, in addition to the parameters influencing the strength of pipe with single corrosion defect. The existing design codes recommend the spacing between the corrosion patches when the interacting corrosion patches can be considered as a single patch for calculating the burst pressure of the defected pipe. In this paper, the strength and deformation characteristics of corroded pipe are investigated using finite element analysis. The parameters considered in the analysis are pipe geometries, number of corrosion patches, spacing between multiple corruptions, edge conditions (e.g. sharp and elliptical edges) and the locations of the corrosion patches. The spacing of the corrosion patches are varied along the pipe length and pipe circumference with both symmetrical and unsymmetrical orientations. The study reveals that the effect of the interaction of adjacent corrosion patches exists if the patches are located within a distance of $8t$ and $1.5\sqrt{Dt}$, where D is the pipe diameter and t is the pipe wall thickness. This distance is similar to the distance recommended in DNV-RP-F101 code. The distances recommended in ASME B31G and CSA Z662-15 codes appear to be un-conservative. The finite element results are compared with different burst pressure prediction models for corroded pipelines.

Keywords: Burst pressure, Corroded pipe, Multiple corrosion patches, Interaction, Stress intensity factor

1. INTRODUCTION

Pipelines are used for transporting hydrocarbons, municipal water and waste water, and for other industrial applications. The pipes often carry corrosive substance and/or are buried in corrosive environment that causes wall corrosion. The corrosion reduces the strength of the pipeline significantly and may lead to failure. A prediction of the remaining strength of corroded pipeline is required to assess the structural integrity of the pipe.

Corrosion in pipeline may occur in a single patch or in multiple patches. Researchers extensively investigated the effects of single corrosion patch on the strength of pipelines (e.g. Mondal and Dhar 2015, Chen et al. 2015a, Swankie et al. 2012, Zhou and Huang 2012, Li et al. 2012, Fekete and Varga 2012). The pipe strength is generally expressed in term of the burst pressure, which is the internal pressure at the plastic collapse of the pipe. The researchers are still contributing to the improvement of the burst pressure model for determining the remaining strength of corroded pipeline. Studies on the strength of pipeline with multiple corrosion patches are also available in the literature (e.g. Dhar and Mondal 2015, Chen et al. 2015b, Andrade et al. 2006, Benjamin et al. 2006, Li et al. 2011, Silva et al. 2007, Peng et al. 2011). In most of the studies, the identical sizes of corrosion patches were applied symmetrically about either a longitudinal line or a circumferential line. The effects of the spacing of the patches are however not investigated extensively. However, for multiple corrosion patches, the defects may interactively contribute to the reduction of the pipeline strength that requires additional research attention.

Design codes such as CSA Z662-15 2015, DNV RP-F101 2015, BS 7910 2013, ASME B31G 2012 codes incorporate design procedure for calculating the strength of corroded pipeline with single or multiple patches of corrosion. The

STR-953-1

models used in the codes are however found to provide conservative and un-conservative estimations of the burst pressure (Swankie et al. 2012). Further evaluation of these design models is therefore required to calculate the burst pressure correctly.

The current paper presents a finite element (FE) investigation of the remaining strength of corroded pipe containing multiple corrosion patches. The strength of the pipe is evaluated for different orientation of the corrosion patches. The results of FE analysis are compared with those obtained using existing pipe design codes.

2. INTERACTION RULE

An interaction rule is employed to account for the interaction of multiple corrosion patches in the calculation of the burst pressure. The interaction rule states about the limiting distances along the circumferential and longitudinal directions, $(S_c)_{lim}$ and $(S_l)_{lim}$, respectively, between two successive corrosion patches beyond which the effect of interaction of the adjacent patches is negligible. Three basic types of interacting corrosion defects are generally considered, which are termed as Type 1, Type 2 and Type 3, respectively (Kiefner and Vieth 1990). In Type 1 interaction, the projections of two or more corrosion patches overlap in the longitudinal direction when projected onto a longitudinal plane passing through the wall thickness, as shown in Figure 1. The corrosion patches are separated in the circumferential direction (at distances of S_{c1} , S_{c2} ... S_{cn} etc.). In Type 2, the corrosion patches are separated in longitudinal direction (at distances of S_{l1} , S_{l2} ... S_{ln} etc.) as shown in Figure 2. Type 3 corresponds to a larger corroded area with localized deeper zones. The following parameters are consistently used within this paper.

D : Outer diameter of the pipe
 t : wall thickness
 d : maximum depth of corrosion patch
 l : longitudinal extent of corrosion patch
 w : circumferential extent of corrosion patch
 S_l : longitudinal spacing between adjacent corrosion patches
 S_c : circumferential spacing between adjacent corrosion patches

The effect of interaction of adjacent corrosion patches depends on the distance between the defects. Design codes (e.g. DNV, ASME, CSA) recommend the limiting distances (spacing), $(S_c)_{lim}$ and $(S_l)_{lim}$, in terms of different parameters. DNV code expresses the spacing in terms of pipe dimensions (diameter and thickness). ASME B31G and CSA Z662-15 codes express the spacing in terms of pipe wall thickness and the dimension of corrosion patches, respectively. Table 1 provides a summary of different recommendations for the spacing and the criteria for interaction between the patches. The effect of interaction between the defects exists when $S_l \leq (S_l)_{lim}$ or $S_c \leq (S_c)_{lim}$.

The interacting corruptions are treated as a single corrosion for calculating the burst pressure. ASME B31G (2012) code recommends using a length equals to the total length of corrosion group, l_{mn} and a depth equals to the maximum depth in the group, d_{mn} . The width of the corrosion defect is not included in the ASME B31G model. DNV code (DNV-RP-F101-2015) also uses the length similar to that recommended in ASME method. The depth for corrosion group in the DNV code is calculated using Equation 1.

$$[1] \quad d_{mn} = \frac{\sum_{i=1}^{mn} d_i l_i}{l_{mn}}$$

Here, d_i and l_i are the maximum depth and length, respectively, of i^{th} corrosion of the interacting corrosion group as shown in Figure 1.

3. FE ANALYSIS

The FE analysis provides a powerful tool for modelling complex problems with non-linear material responses. Among the commercially available software for FE analysis, ABAQUS is most commonly used for analysis of pipeline. ABAQUS has the capability of modelling the non-linear deformation during yielding of corroded pipeline under high pressure. ABAQUS/Explicit module is used in this study for calculation of burst pressure of corroded pipes with multiple corrosion defects.

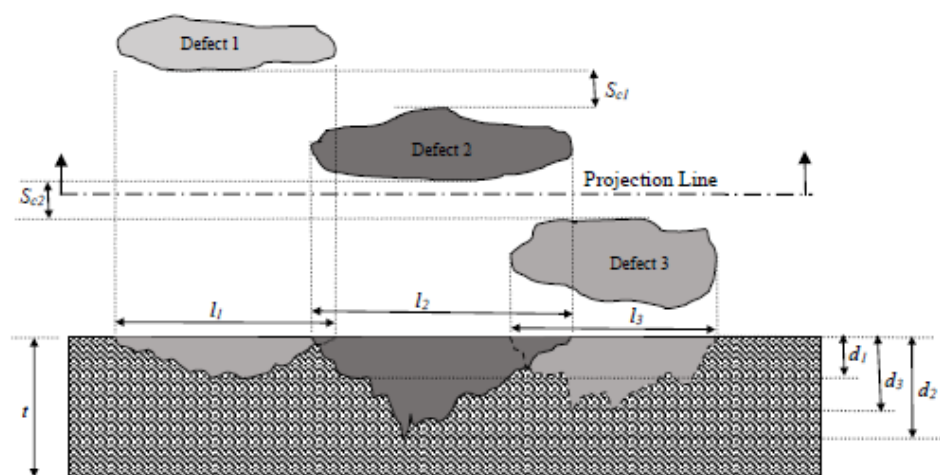


Figure 1: Type 1 Interaction (DNV RP-F101 2015)

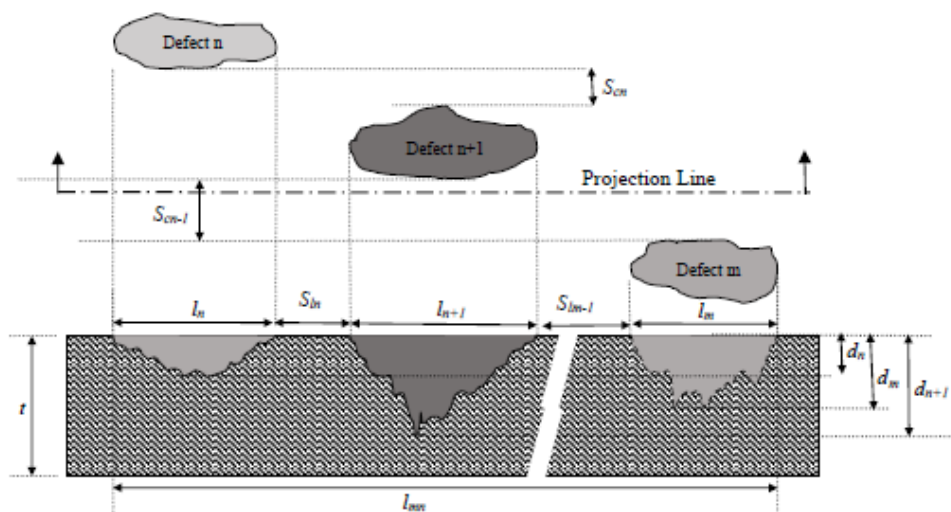


Figure 2: Type 2 Interaction (DNV RP-F101 2015)

3.1 FE Model

Although the actual geometry of corrosion patch is very complex, existing literature reveals that the failure behavior of corroded pipeline mainly depends on the maximum depth and the longitudinal extent of the corroded area. A rectangular area with constant depth (flat at the bottom) is therefore considered for idealization of the corrosion patch. The corrosion defects are created on the external surface of the pipe wall as shown in Figure 3. Sharp and smooth (curved) edges (Figure 3) are considered to investigate the effects of the edge conditions of corrosion patch on the burst pressure. An ellipse with a ratio of the major to minor axis of 2 is fitted to produce the curved edge.

STR-953-3








To investigate the interaction of different corrosion patches, 35 numbers of 3D Finite Element Models are developed and analyzed using ABAQUS/Explicit module. The spacing between the patches is varied independently along the longitudinal, circumferential and oblique directions. The depth of corrosion as 50% of the wall thickness is considered. The dimensions of the corrosion defects and the pipes considered in FE analysis are summarized in Table 2.

Table 1: Interaction Rule

Source	Longitudinal limit, $(S_l)_{lim}$	Circumferential limit, $(S_c)_{lim}$	Criteria for interaction
DNV RP-F101 (2015)	$2\sqrt{D}t$	$360 \sqrt{\frac{t}{D}}$ (degree)	$S_l \leq (S_l)_{lim}$ $S_c \leq (S_c)_{lim}$
ASME B31G (2012)	$3t$	$3t$	$S_l \leq (S_l)_{lim}$ $S_c \leq (S_c)_{lim}$
CSA Z662-15 (2015)	Minimum(l_m to l_n)	Minimum(l_m to l_n)	$S_l \leq (S_l)_{lim}$ $S_c \leq (S_c)_{lim}$
Kiefner and Vieth (1990)	Minimum($6t, l_m$ to l_n)	Minimum($6t, w_m$ to w_n)	$S_l \leq (S_l)_{lim}$ $S_c \leq (S_c)_{lim}$
Pipeline Operator Forum (2005)	25.4 mm (1 inch)	$6t$	$S_l \leq (S_l)_{lim}$ $S_c \leq (S_c)_{lim}$

The efficiency of FE analysis could be achieved by applying simplified boundary condition (such as symmetric condition) to the model. It is however difficult to apply simplified boundary condition to the pipes containing unsymmetric corrosion patches such as Model D and E in Table 2. For this reason, fully restraint boundary conditions at the end of the pipes are applied. To avoid the effect of boundary conditions within the corroded zone, the length of the pipes is chosen to be sufficiently long (longer than minimum length as determined by Fekete and Varga 2012).

Table 2: Pipes dimensions and corrosion geometries

Model ID	Corrosion arrangement	D (mm)	t (mm)	d/t	l (mm)	w (degree)	S_l (times t)	S_c (times t)
A	Un-corroded	300	10	-	-	-	-	-
B		300	10	0.50	60	20	-	-
C		300	10	0.50	60	20	0-10	-
D		300	10	0.50	60	20	0-10	0-10
E		300	10	0.50	60	20	3 (overlap)	0-10
F	Un-corroded	500	15	-	-	-	-	-
G		500	15	0.50	60	20	-	-
H		500	15	0.50	60	20	0-10	-
I		500	15	0.50	60	20	-	0-6

A mesh sensitivity analysis was performed to determine the optimum mesh size. Fine mesh is applied within and around the corroded area where stress concentration is expected. Coarse mesh is applied where uniform stress is expected. Appropriate gradient between coarse and fine mesh is also considered. A typical finite element mesh used in this study is shown in Figure 4.

The pipe domain is modelled using eight-node continuum element (ABAQUS element "C3D8R"). The bilinear elastic material is considered. The material properties used in the analysis are shown in Table 3. The von Mises failure criterion is used for the pipe material. The failure is thus assumed when the minimum equivalent von Mises stress on

the pipe wall reaches or exceeds the ultimate tensile strength of the pipe material. Automatic time increment is chosen for the solution process in ABAQUS. The pipes under the loading of internal pressure are only considered.

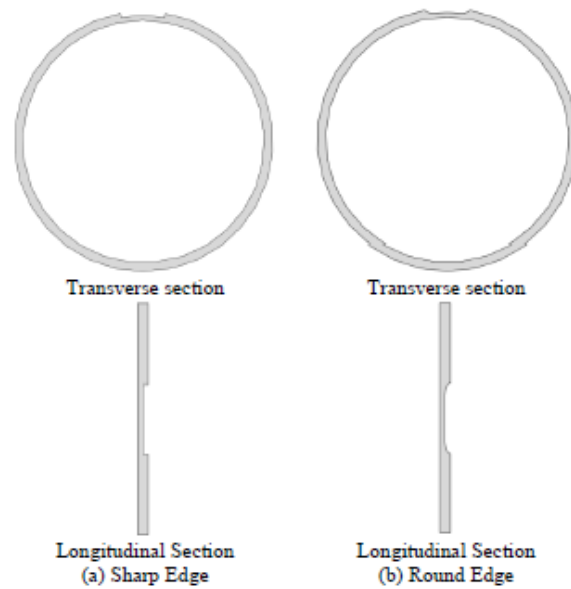


Figure 3: Edge condition of corrosion patch

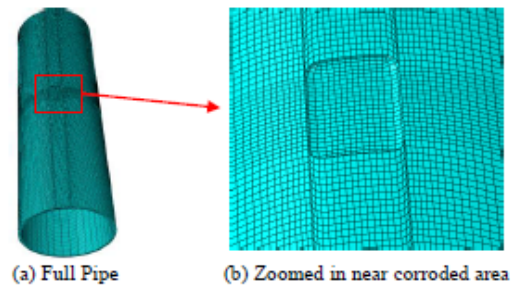


Figure 4: A typical finite element mesh

3.2 Validation of FE Model

Adequate test results on the burst pressures of corroded pipes are not available in the literature for validation of FE models for different pipe dimensions and corrosion geometries. To this end, FE models for un-corroded pipes are first validated through comparison with the results from thin-wall pressure vessel theory. Corrosions are then applied to the pipes in the validated FE models. The burst pressures for un-corroded pipes, calculated using FE analysis, are 35.91 MPa and 40.01 MPa for 300 mm and 500 mm diameter pipes, respectively. These burst pressures are comparable to those obtained using the thin-walled pressure vessel theory (within 3.25% for 300 mm diameter pipe and within 3.65% for 500mm diameter pipe). The thin-walled pressure vessel theory assumes uniform stress distribution within in the wall of the pipe, which may affect the burst pressure calculated using this theory.

Table 3: Material Properties

Property	Value
Density, ρ (kg/m ³)	7080
Young's Modulus, E (GPa)	210
Poisson's Ratio, ν	0.30
Yield Strength, σ_Y (MPa)	452
Ultimate Strength, σ_U (MPa)	542
Total strain at failure, ϵ_U	0.043

4. RESULTS AND DISCUSSION

4.1 Edge condition of corrosion patch

Table 4 shows the burst pressures calculated considering smooth (elliptical) and sharp edges of the corrosion patches. The last column of the table shows the percent difference of the burst pressure calculated using the two models (sharp edge and smooth edge). It reveals that the difference of the burst pressure is insignificant for using the smooth edge and the sharp edge. However, the development of models and the analysis considering the smooth edge of the corrosion defects are complicated and time consuming compared to those of pipe modelled using sharp edge. Sharp edge condition is therefore considered for the rest of the analysis.

Table 4: Burst pressure for different edge conditions

D (mm)	t (mm)	d/t	l (mm)	w (degree)	Edge condition	Burst pressure (MPa)	Variation (%)
300	10	0.50	60	20	Elliptical	33.07	0.60
300	10	0.50	60	20	Sharp	32.87	
300	10	0.50	120	20	Elliptical	27.27	0
300	10	0.50	120	20	Sharp	27.27	
500	15	0.50	60	20	Elliptical	31.91	1.10
500	15	0.50	60	20	Sharp	31.56	
500	15	0.50	120	20	Elliptical	27.89	1.90
500	15	0.50	120	20	Sharp	27.36	

4.2 Interaction of corrosion patches

Figure 5 plots the burst pressure of the corroded pipe against the spacing between successive corrosion patches. The burst pressure of the corroded pipe (P) is normalized with the burst pressures of a un-corroded pipe (P_0) and plotted in the figure. The spacing are normalized using the pipe wall thickness and a dimensional parameter, \sqrt{Dt} , as shown in Figure 5 (a) and 5 (b), respectively. In Figure 5, the burst pressure of the corroded pipe increases with the increase of the spacing between the patches. At a spacing of $8t$ and $1.5\sqrt{Dt}$, the increase of burst pressure is stabilized. It can thus be concluded that for the corrosion length (i.e., 60 mm) and the pipe conditions considered, the effect of interaction of the adjacent corrosion defects is minimized if the defects are spaced at a distance of $8t$ (and $1.5\sqrt{Dt}$) or greater. This spacing is similar to the limiting spacing (S_{lim}) recommended in DNV code (i.e. $2\sqrt{Dt}$), indicating the DNV recommendation to be applicable for the investigated pipes. However, the values recommended in the other codes in Table 1 are un-conservative (the recommended spacing is less) with respect to the value obtained from this study.

The location of the corrosion patches appears to influence the effect of interacting corrosion defects on the burst pressure. Models C, D and E provide different burst pressures for the same pipe (300 mm diameter), as seen in Figure 5. Here, Model C corresponds to a pipe with corrosion patches on a same longitudinal line where the spacing between the patches is increased in the longitudinal direction ($S_c = 0$, $S_l = 0$ to $10t$ where t is the wall thickness). Model D corresponds to a pipe where the spacing (between the corrosion patches) in the longitudinal is equal to the spacing in the circumferential directions ($S_c = S_l = 0$ to $10t$). Model E corresponds to a pipe with a constant spacing (between the corrosion patches) in the longitudinal direction while the spacing is varied in the circumferential direction ($S_l = 3t$ (overlap), $S_c = 0$ to $10t$).

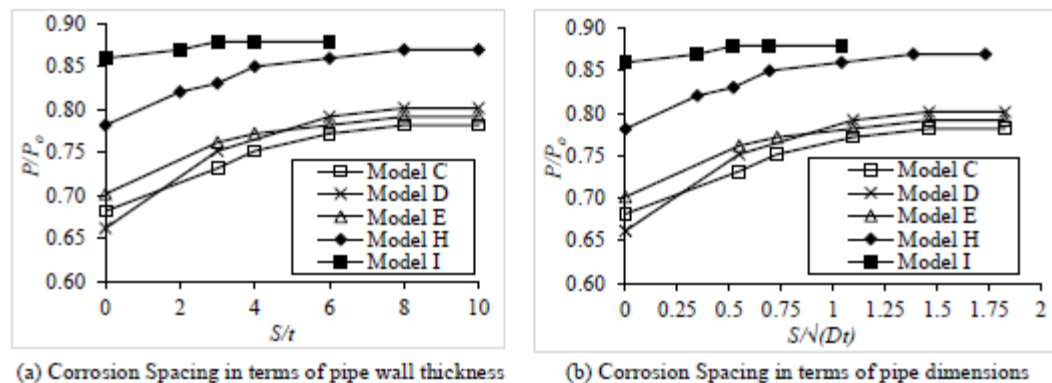


Figure 5: Effect of interaction of corrosion patches

Similar results are obtained for 500 mm diameter pipe. Model H corresponds to a pipe with corrosion patches on a same longitudinal line where the spacing between the patches is increased in the longitudinal direction ($S_c = 0$, $S_l = 0$ to $10t$). The normalized burst pressure for Model C and Model H are almost parallel, reaching the maximum value at a distance of $8t$ and $1.5\sqrt{Dt}$.

For the pipe with the corrosion patches spaced in the circumferential direction (Model I in Figure 5), the variation of the burst pressure with the spacing of the defects is less. This is due to the fact that the effect of circumferential extent of the corrosion on the burst pressure is not significant.

4.3 Stress and Deformation

This section investigates the influence of interacting corrosion patches on the stress in the pipe wall. The stress is expressed in terms of stress intensity factor (SIF), which is defined as the ratio of stress in the corroded pipe to that of an un-corroded pipe subjected to the same internal pressure. Figure 6 (a) represents the SIF along the longitudinal direction of pipe passing through the centre of corrosion patches. The pipes contained two identical corrosions spaced at a distance of $8t$ with each other. The SIFs have been calculated at the outer surface and inner surface of pipes under the internal pressure of 25.27 MPa.

Figure 6 (a) indicates that the von Mises stress is increased significantly within the corroded zone. The stress between the corroded zones is also increased. For larger diameter pipe (Model H), the stress within the corroded zone and between the corroded zones (un-corroded area) is almost the same. This indicates that the effect of interaction between the corrosion patches exists for the large diameter pipe.

Figure 6 (b) shows the pipe wall deformation along the length of the pipe along the centreline of the corrosion patches. The figure reveals that the localized outward bending is developed within the corroded zone due to internal pressure which leads to stress redistribution within that zone.

4.4 Comparison with Design Models

The results of FE analysis are compared with design models (Modified ASME, DNV RP-F101 and CSA Z662-15) for evaluation. The results of burst pressures calculated using different codes and the FE model are included in

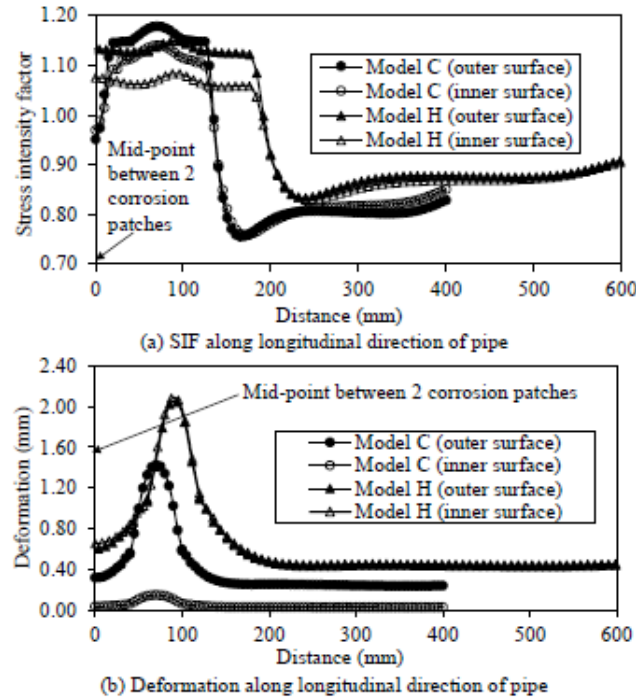


Figure 6: Stress Intensity Factor and deformation [$l/t=8$, $P=25.27$ MPa]

Table 5 along with percent deviation of design code predictions from the FE predictions. The deviations have been calculated using the Equation 2. Five corrosion configurations (Models C, D, E, H and I in Table 1) and three spacing ($l/t = 3, 6$ and 8) between two identical corrosion patches are considered for the comparison.

$$[2] \quad \delta = \frac{(P_{\text{predicted}} - P_{\text{FEA}})}{P_{\text{FEA}}} \times 100$$

Figure 7 plots the variation of the burst pressure calculated using three different codes with respect to the FE calculations for a 300 mm diameter pipe (Model C3 in Table 5) and a 500 mm diameter pipe (Model H3 in Table 5). The figure indicates that CSA and ASME codes are highly conservative while DNV code is less conservative in calculating the burst pressure of the corroded pipe.

5. CONCLUSIONS

This paper investigates the burst pressure of corroded pipes containing two corrosion patches located with different orientation. The following present the findings from this research:

- FE model can be developed for corroded pipes through applying localized wall thinning. A study with a sharp and rounded edge for the corrosion patches has indicated that the effect of rounding the edges on the burst pressure of the pipeline is not significant. Corrosion patches with sharp edges can therefore be used avoiding the complexity associated with rounding the edge (smooth edge).
- For the corrosion length (i.e., 60 mm) and the pipe conditions considered, the effect of the interaction of adjacent corrosion defects is minimized when the defects are spaced at a distance of $8t$ (and $1.5\sqrt{Dt}$) or

greater. This distance (spacing) is similar to the value recommended in DNV code (i.e., $2\sqrt{Dt}$). The ASME and the CSA codes however provide a shorter distance and thus might be un-conservative.

- The burst pressure of corroded pipe determined using different codes varies significantly from each other. Among the codes studied, the CSA and the ASME codes are found to be highly conservative while the DNV code is found to be less conservative.

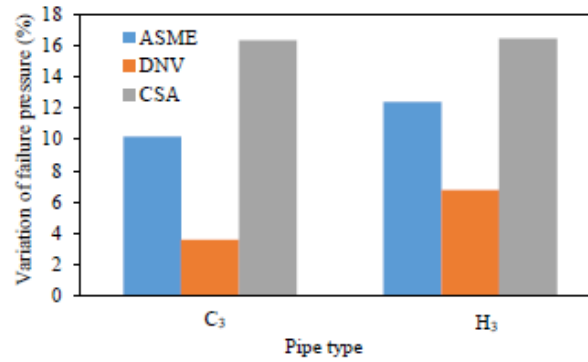


Figure 7: Deviation of burst pressure of corroded pipes [$l/t=8$]

Table 5: Burst pressure determined using different codes and their deviation

Model ID	l (mm)	S_l (mm)	S_c (mm)	l_{mn} (mm)	d_{mn} (mm)	P_{FEA} (MPa)	P_{ASME} (MPa)	P_{DNV} (MPa)	P_{CSA} (MPa)	Deviation, δ (%)		
										ASME	DNV	CSA
C1	60	30	-	150	4.00	29.27	23.27	28.73	20.66	-20.50	-1.84	-29.42
C2	60	60	-	180	3.33	30.87	28.09	29.67	26.15	-9.01	-3.89	-15.29
C3	60	80	-	200	3.00	31.27	28.09	30.16	26.15	-10.17	-3.55	-16.37
D1	60	30	30	150	4.00	30.07	23.27	28.73	20.66	-22.61	-4.46	-31.29
D2	60	60	60	180	3.33	31.67	28.09	29.67	26.15	-11.30	-6.32	-17.43
D3	60	80	80	200	3.00	32.07	28.09	30.16	26.15	-12.41	-5.96	-18.46
E1	60	-30	30	90	6.67	30.47	25.76	24.51	23.43	-15.46	-19.56	-23.10
E2	60	-30	60	90	6.67	31.27	28.09	24.51	26.15	-10.17	-21.62	-16.37
E3	60	-30	80	90	6.67	31.67	28.09	24.51	26.15	-11.30	-22.61	-17.43
H1	60	45	-	165	5.45	29.81	22.46	28.43	20.27	-24.66	-4.63	-32.00
H2	60	90	-	210	4.29	30.86	27.34	28.85	26.06	-11.41	-6.51	-15.55
H3	60	120	-	240	3.75	31.21	27.34	29.10	26.06	-12.40	-6.76	-16.50
I1	60	-	45	60	-	31.56	27.34	31.42	26.06	-13.37	-0.44	-17.43
I2	60	-	90	60	-	31.56	27.34	31.42	26.06	-13.37	-0.44	-17.43
I3	60	-	120	60	-	31.56	27.34	31.42	26.06	-13.37	-0.44	-17.43

6. ACKNOWLEDGEMENTS

The financial support for the study is provided by Research and Development Corporation of Newfoundland and Labrador, which is gratefully acknowledged.

7. REFERENCES

- Andrade, E.Q. d., Benjamin, A.C., Machado Jr., P.R.S., Pereira, L.C., Jacob, B.P., Carneiro, E.G., Guerreiro, J.N.C., Silva, R.C.C. and Noronha Jr., D.B. 2006. Finite element modeling of the failure behavior of pipelines containing interacting corrosion defects. *Proceedings of OMAE2006 25th International Conference on Offshore Mechanics and Arctic Engineering* Hamburg, Germany.
- ASME B31G. 2012. Manual for Determining the Remaining Strength of Corroded pipelines. Supplement to the ASME B31 Code for Pressure Piping.
- Benjamin, A.C., Vieira, R.D., Freire, J.L.F. and Andrade, E.Q. d. 2006. Burst tests on pipeline containing closely spaced corrosion defects. *Proceedings of OMAE2006 25th International Conference on Offshore Mechanics and Arctic Engineering* Hamburg, Germany.
- BS 7910. 2013. Guide to methods for assessing the acceptability of flaws in metallic structure. British Standard Institution.
- Canadian Standard Association. 2015. Oil and gas pipeline systems. CSA standard Z662-15, Mississauga, Ontario, Canada.
- Chen, Y., Zhang, H., Zhang, J., Li, X. and Zhou, J. 2015a. Failure analysis of high strength pipeline with single and multiple corrosion defects. *Journal of Materials and Design*, Elsevier, 67: 552–557.
- Chen, Y., Zhang, H., Zhang, J., Liu, X., Li, X. and Zhou, J. 2015b. Failure assessment of X80 pipeline with interacting corrosion defects. *Journal of Engineering Failure Analysis*, Elsevier, 47: 67–76.
- Dhar, A.S. and Mondal, B.C. 2015. FE Modelling of Corroded Pipelines under Internal Pressure. *IBC Energy 6th annual conference, Arctic Oil and Gas*, North America, St. John's, Newfoundland and Labrador, Canada.
- DNV-RP-F101. 2015. Corroded Pipelines. Det Norske Veritas, Norway.
- Fekete, G. and Varga, L. 2012. The effect of the width to length ratios of corrosion defects on the burst pressures of transmission pipelines. *Journal of Engineering Failure Analysis*, Elsevier, 21:21–30.
- Kiefner, J. F. and Vieth, P. H. 1990. Evaluating pipe Conclusion: PC program speeds new criterion for evaluating corroded pipe. *Oil & Gas Journal*, 88 (34):91–93.
- Li, X., Bai, Y. and Wang, A. 2012. Study on residual strength estimation methods of corroded pipelines under internal pressure. *Proceedings of the ASME 2012 31st International Conference on Ocean, Offshore and Arctic Engineering*, OMAE2012, Rio de Janeiro, Brazil.
- Li, X., Chen, Y. and Su, C. 2011. Burst capacity estimation of pipeline with colonies of interacting corrosion defects. *Proceedings of the ASME 2011 30th International Conference on Ocean, Offshore and Arctic Engineering OMAE2011*, Rotterdam, The Netherlands.
- Mondal, B.C. and Dhar, A.S. 2015. Corrosion Effects on the Strength of Steel Pipes Using FEA. *OMAE15, Proceedings of the ASME 34th International Conference on Ocean, Offshore and Arctic Engineering*, St. John's, NL, Canada.
- Peng, J., Zhou, C.Y., Xue, J.L., Dai, Q. and He, X.H. 2011. Safety assessment of pipes with multiple local wall thinning defects under pressure and bending moment. *Nuclear Engineering and Design*, Elsevier, 241: 2758– 2765.
- Pipeline Operator Forum Document. 2005. Specifications and requirements for intelligent pig inspection of pipelines, Version 3.2, January (2005).
- Silva, R.C.C., Guerreiro, J.N.C. and Loula, A.F.D. 2007. A study of pipe interacting corrosion defects using the FEM and neural networks. *Advances in Engineering Software*, Elsevier, 38: 868–875.
- Swankie, T., Owen, R., Bood, R., Chauhan, V., and Gilbert, G. 2012. Assessment of the remaining strength of corroded small diameter (below 6") pipelines and pipework. *Proceedings of the 2012 9th International Pipeline Conference*, IPC2012, Calgary, Alberta, Canada.
- Zhou, W. and Huang, G.H. 2012. Model error assessments of burst capacity models for corroded pipelines. *International Journal of Pressure Vessels and Piping*, Elsevier, 99–100: 1–8.

Appendix III

Upheaval Buckling Behavior of Offshore Oil Pipeline

Bipul Chandra Mondal & Ashutosh Sutra Dhar

Department of Civil Engineering – Memorial University of Newfoundland
St. John's, NL, Canada, A1B 3X5



GEOVANCOUVER
2016

ABSTRACT

Offshore oil pipelines generally operate under very high pressure and temperature in order to maintain flow assurance. The high pressure and temperature could significantly increase the longitudinal forces in the pipeline resulting in upheaval buckling, which is one of the key design considerations. Prediction of the upheaval buckling of offshore pipelines is challenging because of number of factors involved including seabed sediment behavior, cover depth, pipe material, and the operating conditions. Different models currently exist in the literature to predict the critical buckling loads that are based on assumed shapes of pipeline imperfection, soil loading, and boundary conditions. However, researchers have demonstrated that the critical load is very sensitive to the imperfection geometry, soil resistance, and end boundary conditions, which are very difficult to be predicted for subsea pipelines. One possible way to deal with the problem is to model the possible scenarios numerically. Numerical modelling of upheaval buckling of subsea pipeline using finite element (FE) method is being used over the past several years to address this issue. Current research progress in this area is mostly limited to simplified imperfection geometries, use of elastic spring for uplift resistance, and fixed end conditions. This paper presents an investigation of upheaval buckling under a realistic imperfection geometries using FE modelling. A parametric study is conducted to investigate the effects of initial shape of imperfection and the pipe cross-sectional property on the upheaval buckling. The universal design curve used to design preventive measure against upheaval buckling is evaluated using FE analysis.

RÉSUMÉ

Offshore oléoducs fonctionnent généralement sous très haute pression et température afin de maintenir l'assurance de la circulation. La haute pression et la température pourraient augmenter significativement les forces longitudinales dans le pipeline entraînant bouleversement à contre-courant, qui est l'un des facteurs clés de la conception. Prédiction de la déformation de bouleversement de pipelines offshore est difficile en raison de nombreux facteurs impliqués, y compris le comportement des sédiments des fonds marins, la profondeur de la couverture, matériau de la conduite et les conditions de fonctionnement. Différents modèles existent actuellement dans la littérature pour prévoir les charges critiques de flambement qui reposent sur des formes supposées de pipeline imperfection, chargement de sol et conditions aux limites. Toutefois, les chercheurs ont démontré que la charge critique est très sensible à la géométrie de l'imperfection, résistance du sol et fin des conditions aux limites, qui sont très difficiles à prévoir pour pipelines sous-marins. Une façon possible de régler le problème est de modéliser les scénarios possibles numériquement. Numérique, modélisation des bouleversements flambage du pipeline sous-marin à l'aide d'éléments finis (FE) méthode est utilisée au cours des dernières années pour régler ce problème. Progrès de la recherche actuelle dans ce domaine sont principalement limité aux géométries imperfection simplifiée, utilisation d'un ressort élastique de résistance dynamique et les conditions de l'extrémité fixe. Cet article présente une étude de bouleversements flambage sous un géométries d'imperfection réaliste grâce à la modélisation de FE. Une étude paramétrique est menée afin d'étudier les effets de la forme initiale de l'imperfection et la propriété transversale de la pipe sur le flambement de bouleversement. La courbe de la conception universelle utilisée pour la conception de mesure préventive contre des bouleversements flambage est évaluée en utilisant l'analyse FE.

1 INTRODUCTION

Offshore oil and gas development activities have grown rapidly over the past few decades to meet the global energy demand. Pipelines, as the most viable mean for transporting oil and gas, is being used worldwide for transporting offshore oil and gas. However, offshore pipeline design faces a number of engineering challenges, which require proper understanding of the behavior of the pipelines on and in the seabed under various operating conditions. Upheaval buckling was recognized as an important design consideration for offshore pipelines in the early 1980s when a few upheaval buckling incidents occurred in the North Sea (Liu and Yan 2013).

Upheaval buckling is a mode of pipeline deformation (upward) that overstresses the pipe wall and may lead to

fracture (DNV-RP-F101 2007). Such fracture damage in pipelines should be prevented not only to avoid the huge economic loss associated with a system shut-down, repair, and the loss of products, but also to safeguard the environment from the escaping contaminants. Therefore, the prediction of upheaval buckling and protective measures against this phenomenon is very important for offshore pipelines (Liu et al. 2015).

The offshore pipeline transporting oil with high internal pressure and high temperature (HP/HT) experiences high compressive force normal to the pipe cross-section when the pipe is constrained along longitudinal direction. The pipe buckles laterally, vertically or obliquely when this compressive force exceeds the critical buckling force. Theory and laboratory-scale experiments demonstrate that the high internal pressure alone can cause upheaval

buckling (Palmar and King 2008). The surrounding soil offers resistance to buckling of the pipeline. The soil resistance is generally greater against lateral buckling than the upheaval buckling (Run et al. 2013, Wang et al. 2011, DNV-RP-F101 2007).

In addition to the operating conditions (high pressure and high temperature), the upheaval buckling of subsea pipelines is greatly affected by initial imperfection (out-of-straightness) of the pipelines (Zeng et al. 2014, Wang et al. 2011, Shi et al. 2013, Karampour et al. 2013, Liu et al. 2012). The initial imperfection may be due to the imperfection of the existing seabed, manufacturing defect, and installation of the pipelines. The imperfection of the seabed may occur during trenching for buried pipelines. The behavior of the pipeline during buckling is influenced by the amplitude (Run et al. 2013, Karampour et al. 2013, Liu et al. 2015, Liu et al. 2012) and the shape (Zeng et al. 2014, Karampour et al. 2013, DNV-RP-F101 2007) of the imperfection.

For the structural stability assessment of pipelines subjected to upheaval buckling, several analytical solutions were developed for critical buckling forces using beam formulations with assumed shapes of localized imperfections (e.g., Hobbs 1984, Palmar and King 2008, Zeng et al. 2014, Zhang and Duan 2015, Liu et al. 2012). For simplicity in analysis, different idealized shapes of initial imperfection were used in the development of the analytical solutions. The idealized shapes include those of Taylor and Tran (1996), who developed empathetic models from mathematical reasoning for three different types of imperfections such as "basic contact undulation", "isolated prop" and "infill prop". Palmer et al. (2008) employed sinusoidal imperfection shape for a pipeline, and defined it using two parameters such as imperfection height and length. However, researchers have demonstrated that the imperfection geometry of pipeline in the seabed is much more complex than the idealized shapes, which has significant effect on the critical buckling load. Zeng et al. (2014) investigated the pipelines with sinusoidal and other polynomial shaped imperfections using finite element analysis and showed that the imperfection shapes significantly influence the critical buckling force. The study implies the necessity of considering realistic imperfection shapes for the assessment of upheaval buckling for subsea pipeline.

In this paper, the initial shape of unburred pipeline laid on imperfect seabed is developed using finite element (FE) modeling techniques. The developed shape is compared with the existing models for initial imperfection (Taylor and Tran 1996, Karampour et al. 2013). The upheaval buckling behavior of the pipeline subjected to pressure and temperature is then investigated. A parametric study is conducted to investigate the effects of imperfection geometry and pipe cross-sectional property on the upheaval buckling. The design method proposed in Palmer et al. (1990) is evaluated using FE modelling for upheaval buckling.

2 SEABED PROFILE

A real seabed profile of offshore Newfoundland in Canada has been considered for this study. Seabed profile and the

geotechnical information of the subsea soil along a potential pipeline project was obtained. A length of 500 m along the pipeline route is considered. Figure 1 shows the seabed profile over the length of 500 m from a reference point. Figure 1 represents profile with respect to the depth of water. The figure also shows elevation of the seabed profile with respect to an arbitrary datum located at 76m below the water surface. The figure reveals that seabed is irregular and have an upward prop of about 2.2 m height between the distance of 250 m and 350 m. Pipe laid on this seabed will develop an initial shape of imperfection that will be governed by the shape of the seabed and the flexural rigidity of the pipeline.

3 SHAPE OF INITIAL IMPERFECTION

Several different idealized profiles for subsea pipeline exist in the literature to represent the initial shape of pipeline imperfection. Taylor and Tran (1996) proposed the shape of initial imperfection for an isolated prop of seabed imperfection (Eq. 1).

$$y = \frac{q}{72EI} \left[2L_o \left(\frac{L_o}{2} - x \right)^3 - 3 \left(\frac{L_o}{2} - x \right)^4 \right] \quad [1]$$

Where,

y = height above the lowest point

H = maximum height of imperfection

L_o = wave length of imperfection = $5.8259 \left(H \frac{EI}{q} \right)^{\frac{1}{4}}$

x = distance measured from the symmetric point of imperfection

q = submerged otherwise self-weight of pipeline per unit length

I = moment of inertia of pipe section

E = modulus of elasticity of pipe material

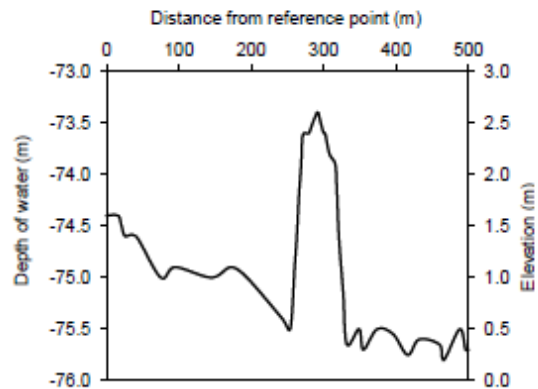


Figure 1. Seabed profile

For infilled prop imperfection where the pipeline is perfectly fitting with the seabed, the proposed shape of imperfection is (Taylor and Tran 1996):

$$y = H \left[0.707 - 0.26176 \frac{\pi^2 x^2}{L_o^2} + 0.293 \cos \left(\frac{2.86\pi x}{L_o} \right) \right] \quad [2]$$

Palmer and King (2008) employed sinusoidal profile of imperfection (Eq. 3) to develop universal design curve for upheaval buckling.

$$y = \frac{H}{2} \left[1 - \cos \left(\frac{2\pi x}{L_o} \right) \right] \quad [3]$$

Karampour et al. (2013) used two other imperfection shapes (Eq. 4 and Eq. 5) to account for possible undulations of the seabed.

$$y = H \left(8 \frac{x}{L_o} + 1 \right) \left(\frac{2x}{L_o} - 1 \right)^4 \quad [4]$$

$$y = H \left[\frac{32}{3} \left(\frac{x}{L_o} \right)^2 + 6 \left(\frac{x}{L_o} \right) + 1 \right] \left(1 - \frac{2x}{L_o} \right) \quad [5]$$

The shape of the seabed considered in this study corresponds to an isolated prop type imperfection (Figure 1). The shape given in Eq. (1) would thus represent the idealized initial shape with imperfection. The initial shape given in Eq. (1) as well as those given in Eq.(2) to Eq. (5) are investigated here for comparison.

In the above idealized imperfection shapes, only Eq. (1) includes a term for flexural rigidity (EI) of the pipeline. The effects of soil stiffness are not incorporated in any of the equations above. A FE modelling technique is used in this research to investigate the effect of pipe flexural rigidity and seabed soil stiffness on the shape of initial imperfection. FE method employed in this study is discussed below.

4 FE ANALYSIS

The purpose of the FE analysis presented in this paper is three-folds. In step 1, the initial shape of imperfection of pipeline is investigated. A pipe is allowed to fall on a flexible seabed under gravity to obtain the initial shape of imperfection. In step 2, upheaval buckling associated with pipe temperature increase under a constant pressure is investigated. The effects of upheaval buckling on pipeline with an initial shape of imperfection obtained from the FE analysis and those obtained from idealized imperfection shapes are compared. It is to be noted that upheaval buckling prediction using the idealized imperfection shape neglect the residual stress in the pipe resulting from pipeline installation. The effect of residual stress resulting from falling of pipeline to the seabed under the gravity load is included in the analysis. In step 3, soil load for resisting upheaval buckling is investigated.

A commercially available FE software "Abaqus" is used in this study. The pipeline is modeled using 1m long 2D pipe element (Abaqus element type PIPE21H). The outer diameter of the pipe is 324 mm. Two wall thicknesses (e.g., 9.74 mm and 25 mm) are considered to evaluate the effects of the flexural rigidity of the pipeline. The seabed is modeled using plane strain element (Abaqus element type CPE8R). The node-to-surface interaction with frictional coefficient of 0.40 is applied between the pipeline and seabed. Linear elastic model is used for the seabed soil anticipating that the effect of soil nonlinearity would be

insignificant since the upward movement of the pipe may not induce significantly large deformation to the soil. However, research is currently underway to investigate the effects of soil non-linearity on the pipe behaviour. The bilinear elastic material model is used for the steel pipe material. However, the effects of bilinear material model is expected to be negligible for the study presented here, since the pipe stress during upheaval buckling is not significantly higher than the yield strength. The material properties used in the model are listed in Table 1.

Table 1: Material Properties

Property	Steel	Soil
Density, ρ (kg/m ³)	7850	1800
Modulus of Elasticity, E (MPa)	210000	20
Poisson's Ratio, ν	0.30	0.25
Yield strength, σ_y (MPa)	452	---
Ultimate strength, σ_U (MPa)	542	---
Total strain at ultimate strength, ϵ_U	0.043	---
Thermal expansion coefficient, α (m/m/°C)	1.3×10^{-5}	---

Analysis is performed in different steps using automatic time increment in each step. Dynamic implicit method is considered for the analysis. The modelling approach used in each step of analysis is further elaborated below.

Step 1: The pipe is first placed horizontally at the crest level of the upward prop on the seabed (Figure 2). The pipe is then allowed to deform under gravity load. At this level of analysis, pipe deformation at the crest of the prop is restrained. The nonlinearities in geometry and material is included in the analysis.

Step 2: Temperature of the pipe having an initial shape with imperfections is increased to investigate upheaval buckling. The initial shape obtained from FE analysis in step 1 is first investigated. Pipe with idealized imperfection (Eq. 1) is also considered. As the pipe is modeled using 2D element, the internal pressure could not be applied directly during the FE analysis. The effect of the internal pressure is incorporated indirectly through increasing an equivalent amount of pipe temperature calculated using Equation 6 (Karampour et al. 2013).

$$\Delta T_p = \frac{pD(1-2\nu)}{4tE\alpha} \quad [6]$$

Where ΔT_p is the temperature change required to result in the same effect as that of an internal pressure of p . The other parameters in the equation such as D , t , E , α and ν represent pipe outer diameter, pipe wall thickness, modulus of elasticity, coefficient of thermal expansion and Poisson's ratio of steel, respectively. The internal pressure considered in this study is 10 MPa.

Pipe operating temperature (in addition to the temperature corresponding to the internal pressure) is applied to the pipe. For this simulation, the pipe ends are fully restrained. The pipe between the ends is set free to move and/or rotate. The dynamic implicit method is used for the analysis, which is computationally efficient (less time required) with respect to the dynamic explicit method. The implicit and explicit methods were found to provide similar results for 2D analysis (Liu et al. 2014).

Step 3: In this step, downward force required for resisting upheaval buckling is investigated. To simulate the required soil resistance (from the soil above the pipe for buried pipe), the pipe is subjected to downward line load and the temperature is increased after applying the line load to develop upheaval buckling.

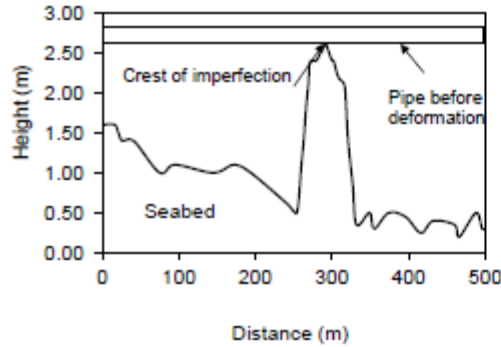


Figure 2: Pipeline placed at the crest of the seabed prop

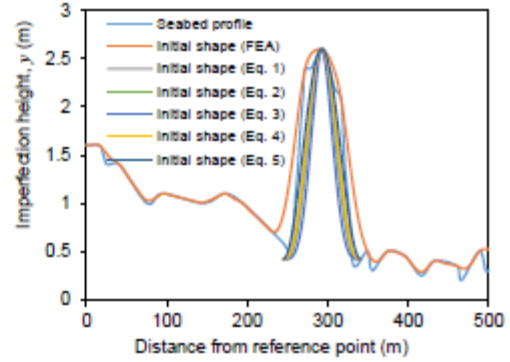
5 RESULTS AND DISCUSSION

5.1 Shape of Initial Imperfection

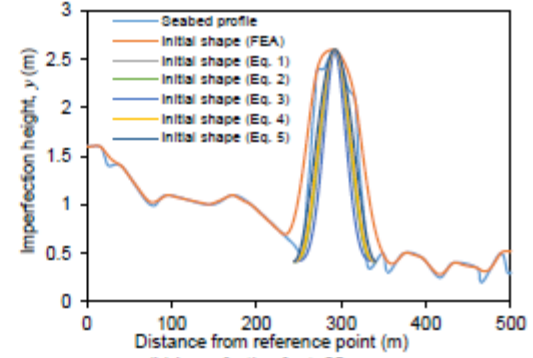
Figure 3 compares the shapes of initial imperfection derived using the idealized shapes (Eq. 1 to 5) and from FE analysis. For the idealized shapes, the value of wave length, L_0 is calculated to be 96 m for a pipe with a wall thickness of 9.74 mm, according to Taylor and Tran (1996). The wave length is calculated for $H = 2.2$ m and $q = 740.52$ N/m. The wave length for the same pipe with wall thickness of 25 mm is calculated to be 94 m. The values of L_0 obtained by FEA with the actual seabed profile are 119.5 m and 117.5 m for 9.74 mm and 25 mm pipe wall thicknesses, respectively. The wave length of imperfection from the idealized shapes is about 20% less than that calculated using the FE analysis.

The comparison in Figure 3 indicates that the differences of the initial shapes given by Eqs. 1 to 5 are not significant. However, the idealized initial profiles differ from that obtained from FE analysis. The FE analysis accounts for the real shape of the seabed. The shapes from the FE analysis matches the shape of the seabed except around the prop. The effects of these shapes on the pipe response to upheaval buckling is discussed in the following sections.

The flexural stiffness of the pipe is found to affect the initial shape of the pipeline. The initial shapes of pipes having wall thickness of 9.74 mm and 25 mm are plotted in Figure 4. The seabed profile is also included in the figure. The figure indicates that the shape of profile is somewhat different for two different stiffness of the pipe.



(a) Imperfection for $t=9.74$ mm



(b) Imperfection for $t=25$ mm

Figure 3. Comparison of initial shapes of pipe

Figure 5 includes the results for a pipe with 9.74 mm wall thickness and with an idealized initial shape (Eq. 1). It indicates that the temperature required to initiate upheaval buckling with idealized initial shape is higher (i.e., around 18°C). The idealized profile thus provides an unconservative estimation for the initiation of the buckling. At very high temperature (beyond 150°C), all curves merges, indicating the pipe deformation is independent on the initial shape or the pipe stiffness.

The undulations observed in Figure 5 between the temperatures of 20°C to 50°C are due to the fact that the location of maximum deflection varies. The location of maximum deflection is found to vary around the crest and is not always at the crest of initial shape. This movement is caused by the seabed features, which are not symmetric about the crest. For analysis with an idealized initial shape, the profile is assumed symmetric about the crest. Therefore, no undulation is observed for the analysis based on the idealized imperfection shape (Figure 5). Again, at very high temperature the effect of unsymmetric seabed shape is insignificant on the buckling amplitude.

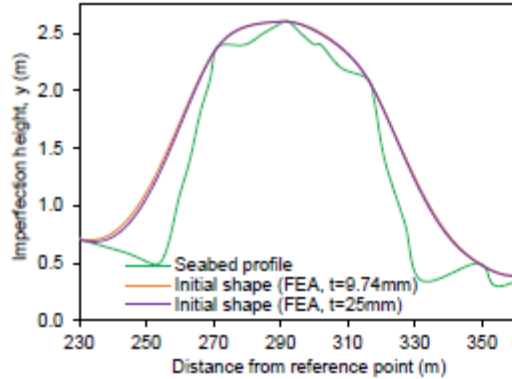


Figure 4. Effect of pipe stiffness on the initial shape

5.2 Bending moments

Due to upheaval buckling, bending moments develop at the pipe cross sections. Figure 6 plots the bending moments along the length of the pipe at two different temperatures (i.e., 12°C and 152°C). As discussed earlier, the pipe undergoes instability at the temperature around 12°C. The upheaval buckling is fully developed at the temperature of 152°C when all curves in Figure 5 merge. Figure 6 reveals that the bending moment is the maximum at the centre (crest) of the imperfection at the higher temperature (i.e., 152°C). However, before the instability, bending moment on the pipe wall is governed by local imperfection of the seabed. As a result, pipe bending moments are higher near the edge of the seabed prop.

The bending moments at the crest are plotted against temperature increase in Figure 7. Bending moments calculated using the initial shape obtained from the current study are compared with those calculated based on the idealized initial shape (Eq. 1). To investigate the upheaval buckling for pipes with idealized initial shape, FE model is developed with an initial shape of the pipe given by Eq. (1). The pipe was then subjected to temperature increase.

It is to be noted that FE model developed using the initial shape given in Eq. (1) does not account for the initial stress condition of the pipeline resulting from installation. In order to account for the initial stress condition, an idealized seabed is first developed using Eq. (1). The pipe is then laid on the seabed under gravity, as discussed in section 4. The resulting initial shape of the pipeline was found to match with shape of the idealized seabed. Temperature load was then applied to the pipe.

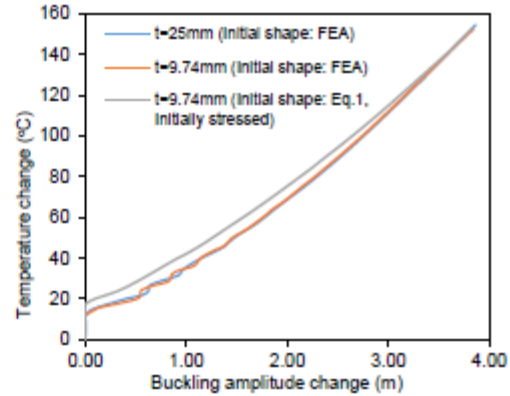


Figure 5. Buckling amplitude against temperature

Figure 7 reveals that pipe bending moment is significantly underestimated if the initial stress condition is not considered for the idealized shape of initial imperfection. When the initial stress of the pipe is considered, bending moments calculated using the idealized profile match with the bending moments calculated using a more realistic profile (from this study) at very high temperature (beyond 152°C). However at lower temperatures, bending moments calculated based on the idealized profile are higher, indicating conservative estimations of the bending moments.

The thick pipe experiences significantly larger moments than the thin pipe in Figure 7. This indicates that the effect of upheaval buckling is more significant on thick wall pipe than on thin wall pipe. Palmer and King (2008) also indicated earlier that the thick pipe is highly prone to upheaval buckling.

5.3 Axial force

Figure 8(a) plots the axial forces along the length of the pipe. As expected, the axial force is the minimum around the zone of pipeline buckling. Pipe axial force increases linearly due to soil friction and reach the maximum value near the boundary where the longitudinal displacement is restrained. Negative sign of the axial force in the figure indicates compression.

Axial forces at the crest of initial imperfection are plotted with the temperature changes in Figure 8 (b). The axial force initially increases with the increase in temperature and then decreases. As in the case of bending moment, axial force also depends on the initial stress condition of the pipeline. Axial forces are less for the pipes with idealized initial shape (Eq. 1) when the initial stress conditions are not considered. However, when the initial stress is considered, the idealized profile provides over-estimation of the axial force at lower temperatures. At higher temperatures, the axial forces calculated based on the idealized profile are the same as those calculated based on a more realistic profile obtained from this study.

Axial force is also significantly higher for the pipe with higher wall thickness (Figure 8b).

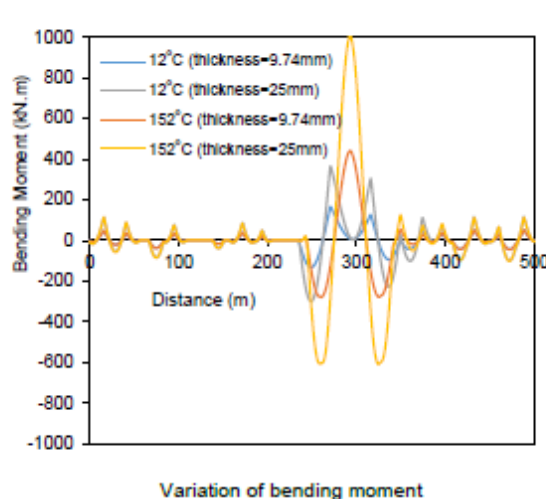


Figure 6. Variation of moment along the length of pipe

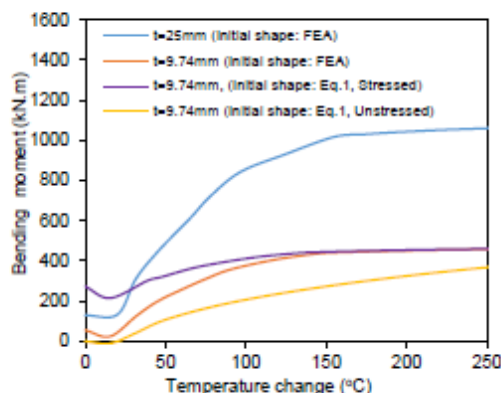
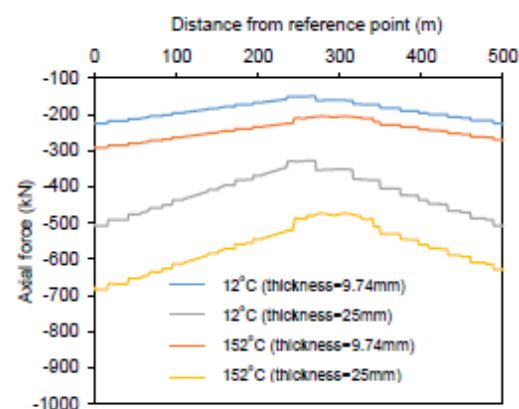


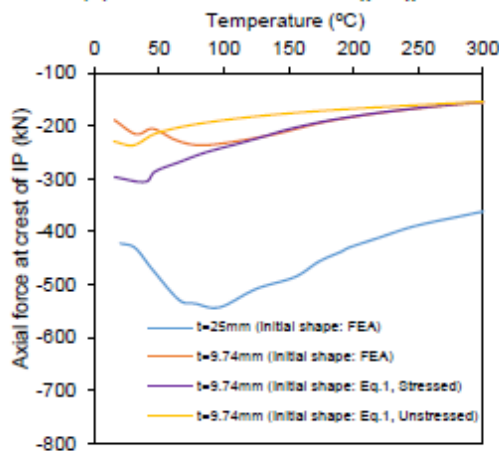
Figure 7. Variation of moment with temperature [At the crest of initial imperfection]

6 EVALUATION OF DESIGN CURVE

A widely accepted preventive measure for upheaval buckling is providing sufficient soil cover over the pipeline. The soil cover exerts download to the pipe and thus resist upward movement associated with upheaval buckling. Palmer et al. (1990) developed the universal design curve to calculate the download (W) required for maintaining the equilibrium of the pipeline subjected to upheaval buckling. The design curve is based on a simple sinusoidal shape of imperfection and linear elastic material. Download required to resist upheaval buckling is calculated here based on finite element analysis and compared with those obtained from the universal design curve of Palmer et al. (1990).



(a) Variation of axial force along length



(b) Variation of axial force along length

Figure 8. Variation of axial forces

The steps involved in the finite element analysis are discussed earlier in section 4. The download, W (in N/m), is calculated to keep the pipeline stable against upheaval buckling for different level of pipeline temperatures. Pipe with initial shape of imperfection obtained from the current study and the idealized imperfection shape (given in Eq. 1) is employed. Initial stress condition of the pipe is considered that is obtained through allowing deformation of the pipe under gravity load, as discussed earlier.

Figure 9 compares the download requirement from various methods against the pipeline temperature. The figure indicates that the download determined by FEA does not match closely with the design curve. In the figure, the download requirement based on the universal design curve increases linearly with the increase of temperature. However, FE calculation shows non-linear relation of the download requirement with the temperature. At lower temperature (temperature $<130^{\circ}\text{C}$), the downloads calculated using the universal design curve provide upper bound values with respect to the calculation based on the

initial imperfection shape obtained from FE analysis. Beyond 130°C, the universal design curve is found to provide un-conservative values. The download requirement calculated based on the idealized shape of initial imperfection is generally conservative up to a temperature of 130°C (in Figure 9) beyond which the calculated download is un-conservative. Special attention is thus required for the calculation of download requirement to stabilize pipeline against upheaval buckling. Use of finite element analysis based on a realistic initial shape would provide rational estimation of the download.

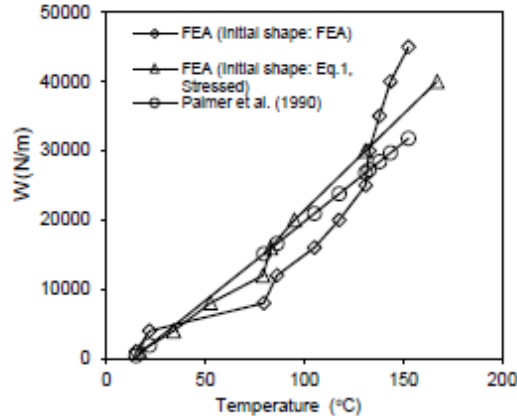


Figure 9. Variation of minimum download with temperature

Figure 10 plots the downloads calculated based on the universal design curve (Palmer et al. 1990) against those obtained from FE calculation. The figure reveals that the universal design curve based estimations provide conservative values up to a download requirement of 25000 N/m, beyond which the universal design curve provides un-conservative values of the downloads.

The axial force and bending moment of pipeline subjected to download are revealed in Figures 11 and 12, respectively. Pipe under a download of 18000 N/m is presented in the figures. This download is required to stabilize the pipeline against a temperature increase of 127.5°C.

Figure 11 reveals that the axial compression on the pipe is increased significantly from the axial force in Figure 8 due to stabilizing the pipeline using download. However, the bending moments on the pipe wall are reduced (Figure 12) with respect to the bending moments in Figure 6. Pipe stress under the high compressive load and the moments need to be investigated in order to assess the structural condition of the pipeline.

7 CONCLUSION

This paper investigates the initial shape of imperfection of subsea pipeline using FE analysis. Upheaval buckling behavior of the pipeline with the initial imperfection is analysed under high temperature loading. The design

method proposed in Palmer et al. (1990) is evaluated using FE modelling.

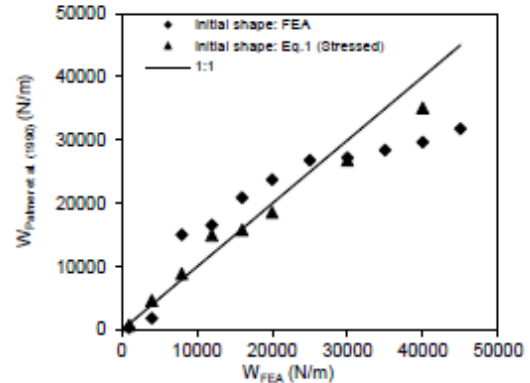


Figure 10. Comparison of the downloads from Palmer et al. (1990) and from FEA

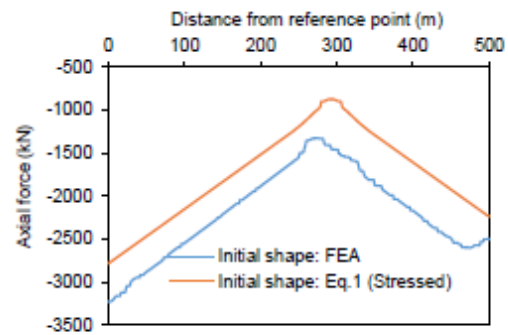


Figure 11. Axial force with 18000 N/m of download (Temperature: 127.5°C)

Initial shape of the pipe is found to be significantly governed by the seabed profile. The initial shapes from the FE analysis match the shape of the seabed except around the prop on the seabed. The flexural stiffness of the pipe also contributes to the shape of initial imperfection of subsea pipeline, particularly around the prop.

The critical condition of buckling for the pipe considered is reached at the temperature increase of around 12°C. Beyond this temperatures, the amplitude increases at a higher rate. However, no snap-through instability is observed for pipe with high amplitude of initial imperfection (i.e., 2.2 m for the pipe investigated). This finding is consistent with the observations reported in the literature.

Before the initiation of upheaval buckling (pipe temperature up to 12°C), pipe bending moment is governed by local imperfection of the seabed. However, the bending moment is the maximum at the crest of the seabed prop at high temperatures.

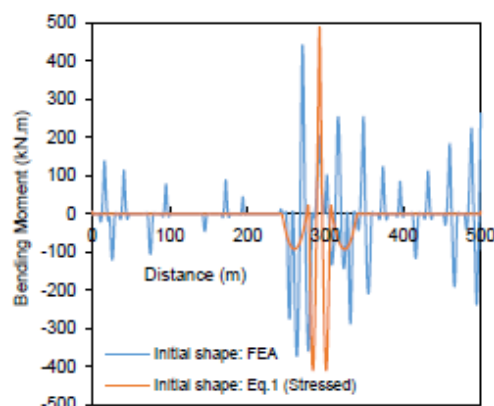


Figure 12. Bending moment with 16000 N/m of download (Temperature: 127.5°C)

The study reveals that the initial stress condition of the pipe should be considered for investigating the pipe under upheaval buckling. Without consideration for the initial stress condition, pipe axial force and bending moment can be significantly underestimated. With consideration of the initial stress, the axial force and bending moments calculated using the idealized profile match with the bending moments calculated using a more realistic profile (from this study) at very high temperatures. However at lower temperatures, the axial force and the bending moment calculated based on the idealized profile are higher, indicating conservative estimations of the internal forces.

The download requirement to resist upheaval buckling increases with the increase of pipe temperature. The download requirement according to the universal design curve, increases linearly with the increase of temperature. However, FE calculation shows non-linear relation of the download requirement against the temperature increment. At lower temperatures, the downloads calculated using the universal design curve provide upper bound values with respect to the calculation based on the initial imperfection shape obtained from FE analysis. The download requirement calculated based on the idealized shape of initial imperfection is generally conservative up to a temperature of about 130°C beyond which the calculated downloads are un-conservative. Special attention is thus required for the calculation of the download requirement to stabilize pipeline against upheaval buckling at high temperature. Use of finite element analysis based on a realistic initial shape would provide rational estimation of the download.

Axial compression on the pipe is increased significantly due to stabilizing the pipeline using downloads. The bending moments on the pipe wall are however reduced. Pipe stress under the high compressive load and the moments should be investigated in order to assess the structural condition of the pipeline.

ACKNOWLEDGEMENTS

The financial support for the research is provided by Mitacs through its Accelerate program. The financial support is gratefully acknowledged. The author would like to acknowledge the contribution of Husky Energy through providing necessary information and supporting the project.

REFERENCES

- DNV-RP-F101. 2007. *Global Buckling of Submarine Pipelines*, Det Norske Veritas, Norway.
- Karampour, H., Albermani, F. and Gross, J. 2013. On lateral and upheaval buckling of subsea pipelines, *Engineering Structures*, Elsevier, 52: 317-330.
- Liu, R. and Yan, S. 2013. Brief history of upheaval buckling studies for subsea buried pipeline, *Journal of Pipeline System Engineering and Practice*, ASCE, 4(3): 170-183.
- Liu, R., Basu, P. and Xiong, H. 2015. Laboratory tests and thermal buckling analysis for pipes buried in Bohai soft clay, *Marine Structures*, Elsevier, 43: 44-60.
- Liu, R., Wang, W., Yan, S. and Wu, X. 2012. Engineering measures for preventing upheaval buckling of buried submarine pipelines, *Applied Mathematics and Mechanics (English Edition)*, Shanghai University and Springer-Verlag, 33(8): 781-796.
- Liu, R., Xiong, H., Wu, X. and Yan, S. 2014. Numerical studies on global buckling of subsea pipelines, *Ocean Engineering*, Elsevier, 78: 62-72.
- Palmer, A.C. and King, R.A. 2008. *Subsea Pipeline Engineering*, 2nd Edition, PennWell Corporation, Tulsa, Oklahoma, USA.
- Palmer, A.C., Ellinas, C.P., Richards, D.M. and Guijt, J. 1990. Design of submarine pipelines against upheaval buckling, *22nd Annual Offshore Technology Conference*, OTC 6335, Houston, Texas, 551-560.
- Run, L., Wu-gang, W. and Shu-wang, Y. 2013. Finite element analysis on thermal upheaval buckling of submarine burial pipelines with initial imperfection, *J. Cent. South Univ*, Springer, 20: 236-245.
- Shi, R., Wang, L., Guo, Z. and Yuan, F. 2013. Upheaval buckling of a pipeline with prop imperfection on a plastic soft seabed, *Thin-Walled Structures*, Elsevier, 65: 1-6.
- Taylor, N. and Tran, V. 1996. Experimental and Theoretical Studies in Subsea Pipeline Buckling, *Marine Structures*, Elsevier, 9: 211-257.
- Wang, L., Shi, R., Yuan, F., Guo, Z. and Yu, L. 2011. Global buckling of pipelines in the vertical plane with a soft seabed, *Applied Ocean Research*, Elsevier, 33: 130-136.
- Zeng, X., Duan, M. and Che, X. 2014. Critical upheaval buckling forces of imperfect pipelines, *Applied Ocean Research*, Elsevier, 45: 33-39.
- Zhang, X. and Duan, M. 2015. Prediction of the upheaval buckling critical force for imperfect submarine pipelines, *Ocean Engineering*, Elsevier, 109:330-343.